

BEHAVIOUR OF REINFORCED CONCRETE FRAMES
WITH LIGHTWEIGHT BLOCKWORK INFILL PANELS

by

MOHAMMED-LAID SAMAI

Ingenieur en genie civil (Algiers)

Thesis submitted to the University of Sheffield for the Degree of
Doctor of Philosophy in the Faculty of Engineering

Department of Civil and Structural Engineering

January, 1984.

To my father and mother

To the memory of my brother Mokhtar

To my family

To my friends

TABLE OF CONTENTS

	Page
LIST OF FIGURES	ix
LIST OF TABLES	xiii
LIST OF NOTATIONS	xv
ACKNOWLEDGEMENTS	xxi
SUMMARY	xxii
CHAPTER 1 INTRODUCTION	1
1.1 General	1
1.2 Economical Aspect	2
1.3 Aims of the Research	3
1.4 Introduction to the Experimental Programme Performed	5
1.5 Structure of the Thesis	6
CHAPTER 2 LITERATURE REVIEW	7
2.1 Introduction	7
2.1.1 General	7
2.1.2 Classification of methods	8
2.2 Purely Experimental Investigations	9
2.2.1 Full scale tests	9
2.2.2 Model tests	11
2.3 Empirical Predictions	14
2.3.1 Benjamin and Williams	14
2.3.2 Holmes	17
2.3.3 Fiorato et al	18
2.3.4 Mainstone et al	20
2.3.5 Kadir and Hendry	22
2.3.6 S.K.Mallick and Barua	26
2.4 Theoretical Investigations	27
2.4.1 Sachanski and Barua and Mallick, S.K.	27
2.4.2 Stafford Smith et al	29
2.4.3 S.V.Mallick and Severn	39

	Page
2.4.4 Liauw	40
2.4.5 Wood	43
2.4.6 P. A. C. Sims	47
2.4.7 May	47
2.5 Summary of Previous Work	49
2.5.1 Test methods	49
2.5.2 General behaviour of infilled frames	49
2.5.3 Stiffness predictions	51
2.5.4 Strength predictions	53
2.5.4.1 Tensile failure strength	53
2.5.4.2 Shear failure strength	53
2.5.4.3 Ultimate strength	54
2.5.5 Conclusions	56
CHAPTER 3 CONSTRUCTION AND TESTING OF INFILLED AND OPEN FRAMES	58
3.1 Choice of the Model-Scale	58
3.2 Terminology	59
3.3 Reinforced Concrete Frames	60
3.3.1 General description	60
3.3.2 Concrete	61
3.3.3 Reinforcement properties	63
3.3.4 Reinforcement details	63
3.4 Infill Panels	65
3.4.1 General description	65
3.4.2 Mortar	65
3.4.3 Blocks	68
3.4.4 Blockwork compressive strength	69
3.4.5 Static modulus of blockwork	73
3.4.6 Shear strength of blockwork assemblies	73
3.5 Construction of the Infilled Frame	76

	Page
3.5.1 Reinforced concrete frame	76
3.5.2 Infill panel	77
3.6 Testing of Infilled and Open Frames	78
3.6.1 Test arrangement	78
3.6.2 Instrumentation	80
3.6.2.1 Loads	80
3.6.2.2 Deflections	82
3.6.2.3 Photography	82
3.6.2.4 Strain measurements	82
3.6.3 Setting up and test procedure	84
CHAPTER 4 PRESENTATION AND DISCUSSION OF TEST RESULTS	86
4.1 General Observations	86
4.2 Load-Deflection Graphs	87
4.3 General Response of Infilled Frames	88
4.3.1 Response prior to cracking of infill	88
4.3.2 Post cracking response	89
4.4 Mode of Failure of Infilled Frames	92
4.4.1 General	92
4.4.2 Normal collapse mechanisms, involving flexural failure of frames	92
4.4.3 Special cases	96
4.5 Principal Parameters from Tests	98
4.5.1 Load causing the first cracks in the frame	98
4.5.2 Load causing the first cracks in the infill	99
4.5.3 Ultimate carrying capacity	99
4.5.4 Plastic load	99
4.5.5 Racking stiffness values	100
4.6 Effect of the Different Variables	100
4.6.1 Effect of the infill	100

	Page
4.6.2	Effect of the infill thickness 103
4.6.3	Effect of the vertical loads 105
4.6.4	Effect of the amount of reinforcement .. 105
4.6.5	Effect of the beam stiffness and strength .. 105
4.6.6	Effect of the column stiffness and strength 108
4.7	Discussion of Test Results 108
4.7.1	General 108
4.7.2	Stiffness comparison 108
4.7.3	Ultimate strength comparison 109
4.7.4	Duplicate specimens 111
CHAPTER 5	COMPARISON OF TEST RESULTS WITH THEORETICAL AND EMPIRICAL PREDICTIONS FROM EARLIER WORK 114
5.1	Physical Properties of Reinforced Concrete Frames .. 114
5.1.1	Estimated ultimate resistance moments of frame members 114
5.1.2	Shear resistance of frame members 114
5.1.3	Ultimate resistance moments from tests .. 118
5.1.4	Ultimate resistance moments from the analysis of open frame test results 118
5.1.5	Flexural stiffnesses of frame members .. 123
5.2	Physical Properties of Infill Panels 123
5.3	Physical Properties of Infilled Frames 125
5.3.1	Relative stiffness parameters 125
5.3.2	Relative strength parameter 128
5.3.3	Moment of inertia of transformed frame- infill section 129
5.3.4	Moments of inertia of equivalent frame members 129
5.4	Principal Parameters from Theoretical and Empirical Predictions from Previous Work 130

	Page
5.4.1	Introduction 130
5.4.2	Horizontal racking stiffness 131
5.4.3	Infill cracking load 137
5.4.3.1	Tensile failing load 137
5.4.3.2	Shear failing load 137
5.4.4	Ultimate load 137
5.5	Wood's Method 139
5.5.1	General 139
5.5.2	Separate contributions of infill and frame for Wood's method 139
5.5.3	Penalty factor for infilled frames tested, γ_{pe} 145
5.6	May's Method 147
CHAPTER 6	ANALYSIS OF THE TWO IDENTIFIED PLASTIC COLLAPSE MECHANISMS 152
6.1	General 152
6.2	Analysis of Mechanism 1 152
6.2.1	Determination of angles of rotation 152
6.2.2	Dissipation of energy in infilled frame .. . 153
6.2.3	Minimization of H_p 155
6.2.4	Comments 159
6.2.5	Numerical procedure for mechanism 1 160
6.3	Analysis of Mechanism 2 162
6.3.1	Determination of angles of rotation 162
6.3.2	Dissipation of energy in infilled frame .. . 163
6.3.3	Minimization of H_p 165
6.3.4	Numerical procedure for mechanism 2 166
6.4	Comparison With Test Results 167

	Page
CHAPTER 7 CONCLUSIONS	171
7.1 Overall Behaviour of Reinforced Concrete Frames With Blockwork Infills	171
7.1.1 General influence of infill panels	171
7.1.2 Load/deflection response	171
7.1.3 Modes of collapse	172
7.1.4 Comparison with steel frames	173
7.2 Parameters Affecting Behaviour	173
7.2.1 Vertical loads on columns	173
7.2.2 Infill thickness	173
7.2.3 Workmanship	174
7.2.4 Frame member sizes and reinforcement	174
7.2.5 Reinforcement detailing	174
7.3 Methods of Analysis	175
7.3.1 Initial racking stiffness	175
7.3.2 Cracking load of the infill	175
7.3.3 Ultimate load	175
7.4 Further Work	175
APPENDIX A SCHEDULE OF REINFORCEMENT	177
APPENDIX B ACCURACY OF READINGS	178
B.1 Accuracy of Instruments	178
B.2 Accuracy of Strain Measurements from Photogrammetry	179
APPENDIX C LOAD-DEFLECTION GRAPHS IN THE INITIAL STAGES AT AN ENLARGED SCALE	181
APPENDIX D STRAIN DISTRIBUTION OVER THE INFILL	182
APPENDIX E NUMERICAL ANALYSIS	183
E.1 Mechanism 1	183
E.2 Mechanism 2	186
REFERENCES	187

LIST OF FIGURES

Figure

2.1	Idealized representation of the diagonal strut concept								
2.2	Knee-braced shear rotation mode identified by Fiorato et al [18]
2.3	Characteristic width after Mainstone [19]					
2.4	Diagonal strut width after Kadir [22]				
2.5	Approximation of masonry infilled frame at cracking load after Kadir [22]
2.6	Load carried by the infill after Kadir [22]					
2.7	Dimensions of equivalent brickwork frame after Kadir [22]								
2.8	Load carried by the infill after S. Smith [31]						
2.9	Force systems for laterally and diagonally loaded infilled frames
2.10	Load carried by the infill after S. Smith [32]						
2.11	Assumed panel loading after S. Smith [33]					
2.12	Loading arrangement in reference [35]				
2.13	Equivalent frame after Liauw [41]			
2.14	Collapse modes identified by Liauw [43]				
2.15	Assumed stress distribution by Liauw [43]					
2.16	Collapse modes identified by Wood [44]				
2.17	Different test arrangements from previous work						
2.18	Idealized load-deflection response for steel infilled frames
3.1	Geometrical characteristics of frames 1 to 3					
3.2	Geometrical characteristics of frames 4 and 5						
3.3	Grading curves for sand and gravel				
3.4	Typical stress-strain curves for high tensile steel bars
3.5	Typical stress-strain curve for wire					
3.6	Reinforcement details for frame 5				
3.7	Grading curve for building sand				

Figure

3.8	Methods of cutting blocks
3.9	Specimens used for compression tests
3.10	Typical stress-strain curve for blockwork
3.11	Specimen and shear test equipment
3.12	Shear test relationship
3.13	Moulds for the frames
3.14	Test rig
3.15	Left hand support
3.16	Right hand support
3.17	Stabilizer details
3.18	Pivot details
3.19	Demec disc disposition for infilled frames
4.1	Failure sequence for a typical 'IH' specimen
4.2	Sequence of failure for a typical 'IC' specimen
4.3	Load-deflection diagrams for weak infill and horizontal loading
4.4	Load-deflection diagrams for medium strength infill and horizontal loading
4.5	Load-deflection diagrams for strong infill
4.6	Load-deflection diagrams for medium strength infill and combined loading
4.7	Load-deflection diagrams for frames with deep beams or deep columns
4.8	Idealized load-deflection diagrams for 'IH' specimens
4.9	Idealized load-deflection diagrams for 'IC' specimens
4.10	Idealized load-deflection diagrams for open frames
4.11	Different load-deflection responses prior to cracking of the infill
4.12	'IH' specimens at peak load
4.13	'ICM' specimens at peak load
4.14	'IC' specimens at peak load

Figure

4.15	'IH' specimens at large deflection or after failure	..
4.16	'ICM' specimens at large deflection or after failure	..
4.17	'IC' specimens at large deflection or after failure	..
4.18	Typical illustration of mechanism 1
4.19	Idealized representation of mechanism 1
4.20	Specimens developing mechanism 1
4.21	Typical illustration of mechanism 2
4.22	Idealized representation of mechanism 2
4.23	Specimens developing mechanism 2
4.24	Specimen developing a combination of mechanism 1 and 2	
4.25	Illustration of failure involving other failure modes (special cases (a - c))
4.26	Illustration of failure involving other failure modes (special cases (d and e))
5.1a	Arrangements of supports for testing frame elements	..
5.1b	Typical load-deflection graph for frame member tested in flexure
5.2	Load-deflection diagrams for open frames
5.3	Comparison of stiffness test results with previous work	
5.4	Comparison of infill cracking load test results with tensile strength from previous work
5.5	Comparison of infill cracking load test results with shear strength from previous work
5.6	Penalty factor from test for f_{ci}
5.7	Penalty factor from test for $0.8f_{ci}$
5.8	Comparison of ultimate and plastic load test results for 'IH' specimens with previous work for f_{ci}
5.9	Comparison of ultimate and plastic load test results for 'IH' specimens with previous work for $0.8f_{ci}$
5.10	Comparison of ultimate and plastic load test results for 'IC' specimens with previous work for f_{ci}
5.11	Comparison of ultimate and plastic load test results for 'IC' specimens with previous work for $0.8f_{ci}$

Figure

6.1	Geometry of collapse mechanisms
6.2	Instantaneous centre for mechanism 1
6.3	'Plastic' diagonal strut for mechanism 1
6.4	Graphical representation of left hand side of equation (11a)
6.5	'Plastic' diagonal strut for mechanism 2
6.6	Graphical representation of left hand side of equation (31a)
A.1	Reinforcement details for frames 1, 2 and 3
A.2	Reinforcement details for early frames 2
A.3	Reinforcement details for IHM3 and ICM3
A.4	Reinforcement details for frame 4
C.1	Load-deflection diagrams for weak infills at an enlarged scale
C.2	Load-deflection diagrams for medium strength infill at an enlarged scale
C.3	Load-deflection diagrams for strong infill and for frames with deep beams or deep columns at an enlarged scale
D.1	Strain distribution over the infill for IHW1 at a load of 17.3KN
D.2	Strain distribution over the infill for IHM1 at a load of 23.5KN
D.3	Strain distribution over the infill for ICML after application of vertical loads
D.4	Strain distribution over the infill for IHS1 at a load of 27.1KN
D.5	Strain distribution over the infill for ICS1 after application of vertical loads
E.1	Predicted plastic load for IHW1 for different values of a

LIST OF TABLES

Table	Page
3.1 Concrete control test results	62
3.2 Steel bar and wire test results	64
3.3 Mortar control test results	67
3.4 Block compressive strength	70
3.5 Compressive strength and static modulus of blockwork ..	71
3.6 Shear test results	75
3.7 Calibration factors and accuracy of readings	81
4.1 Principal parameters from tests	101
4.2 Effect of the infill	102
4.3 Effect of the infill thickness	104
4.4 Effect of the vertical loads	106
4.5 Effect of the amount of reinforcement	107
5.1 Geometrical characteristics of frame members	115
5.2 Estimated ultimate moments of resistance by three methods	116
5.3 Shear strength of frame members	117
5.4 Ultimate resistance moments and shear strengths from tests	119
5.5 Moments of resistance of open frame members	121
5.6 Flexural stiffnesses of frame members	123
5.7 Physical properties of infill panels	124
5.8 Physical properties of infilled frames	127
5.9 Prediction equations from previous work	132-135
5.10 Lateral racking stiffness from previous work	136
5.11 Cracking load from previous work	138
5.12 Ultimate load from previous work	140
5.13 Ultimate load by Wood's method	141

Table	Page
5.14 Ultimate load by May's method for $k = 0.50, 0.75$ and 1.0 and f_{ci}	148
5.15 Ultimate load by May's method for $k = 0.50, 0.75$ and 1.0 and $0.8f_{ci}$	149
6.1 Comparison of plastic load test results with analysis	169
E.1 H_p for test panel IHWL for $a = 1$	184
E.2 Predicted plastic load for test panel IHWL for different values of a	185
E.3 H_p for test panel ICML	186

LIST OF NOTATIONS

A_s	: area of tension reinforcement for frame members
A'_s	: area of compression reinforcement for frame members
A_{sv}	: Cross-sectional area of the two legs of a link
a	: ratio of X to Y
b	: width of frame section
C	: ratio of horizontal wall stress to crushing stress in reference [44]
c	: workmanship factor in reference [14]
d	: frame diagonal between centre-lines
d'	: depth to compression reinforcement
d_1	: = $d_t - d' - z$
d'_1	: depth to compression reinforcement at corner level
d_i	: infill diagonal
d_t	: depth of frame section
E	: static modulus of elasticity
E_{bw}	: static modulus of elasticity of assemblies of blockwork
E_c	: static modulus of elasticity of concrete
E_{di}	: static modulus of infill for diagonal loading
E_i	: static modulus of infill for vertical loading
E_f	: static modulus of frame
E_s	: static modulus of steel
EI_b	: flexural stiffness of beam
EI_c	: flexural stiffness of column
f	: shear strength of infill
f_b	: concrete flexural strength
f_{bs}	: bond shear strength
f_{cb}	: block compressive strength
f_{cbw}	: assemblies of blockwork compressive strength

f_{ci} : infill compressive strength for vertical loading
 f_{cm} : mortar compressive strength
 f_{cu} : concrete cube strength
 f_{dci} : infill compressive strength for diagonal loading
 f_{dti} : infill tensile strength for diagonal loading
 f_f : non dimensional parameter to determine the frame contribution in reference [44]
 f_i : non dimensional parameter to determine the infill contribution in reference [44]
 f_s : non dimensional parameter to determine the ultimate load in reference [44]
 f_t : concrete tensile strength
 f_{ti} : infill tensile strength for vertical loading
 f_{tm} : mortar tensile strength
 f_u : steel ultimate strength
 f_{y1} : 0.2% proof stress
 f_{y2} : yield stress determined from a 0.5% total elongation in accordance with BS 18 Part 2 [56]
 f_{yv} : yield strength of link reinforcement
 G : shearing modulus of infill
 H : horizontal racking load
 H_{CF} : frame cracking load
 $H_{CF(G)}$: frame cracking load obtained from the graph
 $H_{CF(O)}$: frame cracking load observed
 H_{CI} : infill cracking load
 $H_{CI(G)}$: infill cracking load obtained from the graph
 $H_{CI(O)}$: infill cracking load observed
 H_{cr} : cracking load in reference [22]
 H_F : load carried by the frame in reference [22]
 H_{fe} : load carried by the frame in the elastic range in reference [24]
 H_{fa} : load carried by the frame from analysis
 H_{ia} : load carried by the infill from analysis

H_p : plastic load
 H_{pa} : plastic load from analysis
 H_{pe} : plastic load from experiment
 H_{O1} : recorded load when the structure starts to behave elastically
 H_s : shear load
 H_{si} : shear load carried by the infill
 H_{st} : total shear load
 H_t : tensile load
 H_u : ultimate load
 H_{u1} : ultimate load for mode 1 in reference [43]
 H_{u2} : ultimate load for mode 2 in reference [43]
 H_{u3} : ultimate load for mode 3 in reference [43]
 H_{ue} : ultimate (peak) load from experiment
 H_{uf} : ultimate load carried by the frame in reference [44]
 H_{ui} : ultimate load carried by the infill in reference [44]
 H_{us} : ultimate load by S. Smith's method [36]
 H_{ut} : total ultimate load
 H_{uw} : ultimate load by Wood's method [44]
 h : height of frame between centre lines of beams
 h' : location of hinge in windward column as defined in figure 6.1(a)
 h'' : location of hinge in leeward column as defined in figure 6.3
 h_i : height of infill
 I_b : second moment of area of beam
 I_c : second moment of area of column
 I_{eb} : second moment of equivalent beam in reference [41]
 I_{ec} : second moment of equivalent column in reference [41]
 I_t : second moment of transformed frame-infill section as defined in section 5.5.3
 K : shape factor as defined in reference [18]
 K_h : non dimensional parameter as defined in Table 5.7

- k : ratio of ultimate moment of joint to ultimate moment of beam or column
- l : length of frame between centre-lines of columns
- l' : hinge location in top beam as defined in figure 6.1
- l'' : hinge location in lower beam as defined in figure 6.1
- l_{brace} : length of braced columns in reference [18] as defined in figure 2.2
- l_{ce} : $= l_i - l_{\text{brace}}$
- M_e : beam end moment if not plastic in reference [44]
- M_{p1} }
 M_{p2} } : plastic moments as defined in figure 6.1
 M_{p3} }
 M_{p4} }
 M_{p5} }
- M_{pj} : smaller of M_{pb} and M_{pc}
- M_u : ultimate moment of resistance
- M_{ub} : ultimate moment of beam section
- M_{ubc} : ultimate moment of beam at corner level
- M_{uc} : ultimate moment of column section
- M_{ucc} : ultimate moment of column at corner level
- M_{cuL} : moment in leeward column
- M_{ucw} : moment in windward column
- M_{ues} : estimated ultimate moment of frame members
- M_{ut} : ultimate moment of frame members from tests
- m : non dimensional ratio for frame/infill strength as defined by Wood [44]
- m_b : non dimensional ratio for beam/infill strength as defined by Wood [44]
- m_c : non dimensional ratio for column/infill strength as defined by Wood [44]
- m_e : effective relative strength parameter as defined in reference [44]
- m_n : nominal relative strength parameter as defined in reference [44]
- n : ratio of E_s to E_c

R : diagonal load
 R_c : diagonal load to cause crushing of the infill in reference [36]
 S_H : initial racking stiffness
 S_{He} : initial racking stiffness from experiment
 s_v : spacing of links along the member
 t : infill thickness
 V : shear strength of frame member
 V_{es} : estimated shear strength of frame member
 V_t : shear strength of frame member from test
 v : shear stress in frame member
 v_c : ultimate shear stress in concrete
 W' : characteristic width after Mainstone as defined in figure 2.2
 W'_{ec} } effective width of infill considered as a single diagonal strut
 W'_{ek} } in reference [20] suffixes c, k and t denote values appropriate
 W'_{et} } to ultimate strength, stiffness and first-crack strength
 } respectively
 W_f : work done on frame
 W_i : work done on various parts of the strut
 W_{it} : total strut work
 w : width of the diagonal strut
 X : location of hinge in top beam as defined in figure 6.1(a)
 X_1 : location of hinge in top beam as defined in figure 6.1(b)
 X_2 : location of hinge in lower beam as defined in figure 6.1(b)
 Y : location of hinge in windward column as defined in figure 6.1(a)
 z : lever arm
 α : length of contact against frame members
 α_h : length of contact against columns
 α_l : length of contact against beams
 γ_f : partial safety factor for loads
 γ_m : partial safety factor for materials
 γ_{mv} : partial safety factor for stresses

- γ_p : penalty factor to allow for idealization of plasticity introduced by Wood [44]
- γ_{pa} : penalty factor obtained from analysis
- γ_{pe} : penalty factor obtained from experiment by equating H_{uw} and H_{ue} or H_{uw} and H_{pe} as determined in section 5.5.3
- γ_{pf} : penalty factor introduced to allow for the limited ductility of the frame
- γ_{pi1} : penalty factor for infill in mechanism 1
- γ_{pi2} : penalty factor for infill in mechanism 2
- δ_H : horizontal displacement of infilled frame
- δ_i : horizontal displacement of infill alone
- δ_f : horizontal displacement of frame alone
- θ : slope of the infill diagonal
- λ_h :
$$= \sqrt[4]{\frac{E_i t \sin 2\theta}{4EI_c h}}$$
- λ_l :
$$= \sqrt[4]{\frac{E_i t \sin 2\theta}{4EI_b l}}$$
- μ : apparent coefficient of friction
- ν : Poisson's ratio
- ρ : geometrical ratio of reinforcement
- σ_n : normal compressive stress

ACKNOWLEDGEMENTS

Foremost I would like to express my gratitude to the Algerian Ministry of Higher Education who sponsored my studies and to the Department of Civil and Structural Engineering of the University of Sheffield.

I wish to express my wholehearted thanks to my supervisor Mr. B. Hobbs for his help, guidance and encouragement throughout the project and his assistance during the presentation of this thesis.

Special thanks are extended to the technical staff of the light and heavy structures laboratories for their valuable help in the experimental work.

I also acknowledge the assistance of Mr. D. Thomson for initiating me to the photogrammetry equipment and Mr. L. Ward for his guidance on blocklaying.

I would also like to thank the workshop and photography staff for their assistance.

My final thanks are to Mrs. A. Crawshaw for her careful typing of this thesis.

I remain grateful and much indebted to my father for his incessant support and encouragement.

SUMMARY

The current investigation concerns the behaviour of lightweight blockwork infill panels bounded by reinforced concrete frames. A detailed and comprehensive review of the literature on different frame-infill combinations is presented. Details are given of tests on sixteen third-scale infilled frames and four open frames. These were tested under two types of loading: horizontal racking loading only and combined vertical loads on columns and racking loading. The complete load-deflection response is considered in detail including initial elastic behaviour, influence of cracking and the formation of collapse mechanisms after the attainment of peak load. The variables investigated include the overall effects of the infill, the infill thickness, the vertical loads, the amount of reinforcement, the change in stiffness and strength of beams and of columns and the effect of reinforcement detailing. Those found to have a major influence are the vertical loads, the infill thickness, the reinforcement detailing particularly in the opening corners of the frame, and the workmanship.

The principal parameters obtained from the tests are the initial racking stiffness, the infill cracking strength, the ultimate load and the plastic collapse load. Their values are compared to the available empirical and theoretical methods. None of these methods is found to safely predict the initial racking stiffness and the ultimate carrying capacity of this type of structure. A plastic analysis is presented to predict the two plastic collapse mechanisms identified in the tests. The penalty factor to allow for idealization of plasticity of the infill is found as part of the solution. A second penalty factor is introduced to allow for the limited ductility of the frame. The proposed method is found to yield satisfactory and safe predictions

for the plastic resistance of these infilled frames. In conclusion some design recommendations are proposed for the initial racking stiffness and the cracking infill strength.

CHAPTER 1

INTRODUCTION

1.1 GENERAL

The high cost of land in urban areas has led to a rapid increase in the numbers of tall buildings constructed during the last decades. The necessity for these tall buildings to be designed as safely and as economically as possible has led to extensive research programmes throughout the world. The vertical load-resisting capability of a building is its reason for existence, and many methods of designing buildings to support vertical loads have been developed. Large horizontal forces must also be resisted, however, and this has necessitated the development of methods of analysis capable of solving the problem of providing the required lateral strength and stiffness. These may be achieved in various ways. For a framed structure they may be obtained by the provision of bracing members, by the rigidity of the joints, by the provision of complete shear truss assemblies acting in conjunction with the frame, or by the provision of shear resistant panels. The use of bracing or shear panels becomes more important as the height of the building increases. In the case of unbraced reinforced concrete frames, for instance, the dimensions of frame elements and amounts of reinforcement become so large that this might lead to practical impossibilities in construction.

In reinforced concrete structures, the most convenient way of ensuring lateral stability is generally by the use of shear walls. Three types of shear wall structures may be envisaged:

a) Shear walls: structures which consist entirely of wall and floor slab elements in which the load-bearing walls resist all lateral forces.

b) Shear walls combined with frames: modern forms of construction have resulted in the use of the shear wall as the principal lateral-load-resisting member and designed as a vertical cantilever.

c) Infilled frames: structures with two heterogeneous materials, frame and infill, working jointly to resist the lateral load.

The last type of shear wall structures is of a great interest when the infilling panel is made of brickwork or blockwork masonry. This type of infill which has long been used as a partition or a separator for fire protection and sound insulation purposes in a building, has generally not been taken into consideration in the structural design. Only its geometrical and physical properties have been exploited to fulfil the requirements mentioned above. The main reason for this has been a reluctance to rely on the structural performance of such masonry panels due to the need for strict control of workmanship and the large scatter in results from tests on elements of masonry. During the last decades, however, the interest shown in brickwork and blockwork construction has led to extensive theoretical and experimental work in this field. The aim of this work has been the development of more rigorous methods so that the physical properties of the masonry may be fully exploited. Thus, the use of masonry as a bracing element in multistorey buildings has been encouraged.

1.2 ECONOMICAL ASPECT

By considering the infill to be a non-structural element and by ignoring its interaction with the frame in design, a significant portion of the strength of the system is wasted. The structures may be over designed and the full capacity of the components forming the

structures is not exploited. All tests conducted on actual buildings which were to be demolished and on laboratory specimens at various scales have shown the important influence of the infilling on both stiffness and strength. It has also been shown from tests performed by many investigators that the composite strength and stiffness of infilled frames are greater than the sum of the two components taken separately. Even when the infill material contains an opening, which may be the case in practice, it has been shown that the infilled frame is stronger and stiffer than the corresponding open frame.

The inclusion of the infill in structural design should lead to using less material in the case of steel frames or less reinforcement in the case of reinforced concrete frames. In this latter case, the interaction of infill and frame could lead to problems due to shear or tension in the frame but the strength still remains higher than that of the open frame. Thus, taking into account the infill and exploiting its full capacity for resisting lateral load could be expected to lower the cost of construction of many buildings, since the whole sidesway movement is reduced and the gain in strength and stiffness is considerable.

1.3 AIMS OF THE RESEARCH

Since most of the work done in this field has concerned steel frames infilled with brickwork or plain concrete and since most of the available theoretical methods have been based on tests carried out on steel frames, it was decided to test reinforced concrete frames infilled with lightweight aggregate concrete blockwork. This frame/infill combination has been chosen for the following reasons:

(i) The infill shrinks with the frame. Thus, the infill and the frame remain bonded together, and therefore some of the long term

problems occurring with other frame/infill combinations, such as the long term expansion of clay brickwork and the shrinkage of concrete in a steel frame, may be avoided. In effect, the expansion of brickwork causes additional stresses with steel frames and especially with reinforced concrete frames that shrink. The shrinkage of concrete infills in steel frames leads to lack of fit problems.

(ii) The infill is light, cheap and a good insulator, thus it may be used as an external wall.

(iii) This type of infilled frame is commonly used in a large number of countries.

(iv) Finally, the fact that very little previous work has covered modern types of lightweight blockwork justifies its use for the current investigation.

The analysis of a full three-dimensional frame and the masonry under lateral loading is not an easy task. Because of the high in-plane stiffness of the floor slabs, it is generally assumed that the shear walls may be considered as two-dimensional structures subjected to lateral loads at each floor level. All previous investigations have therefore dealt with free standing infilled frames subjected to horizontal racking loads simulating the effect of earthquake, blast or wind. The horizontal loads due to these phenomena are actually of a dynamic nature. However, the different national codes treat the last type as a static loading, and since behaviour under static loading must be fully understood before dynamic loads are considered, this investigation has been restricted to the consideration of statically applied loads.

The objectives of the present work are:

(i) To investigate complete load/deflection behaviour from initial elastic response through peak load and following post-peak behaviour through to final collapse.

(ii) To identify modes of behaviour and, in particular, modes of structural collapse.

(iii) To evaluate critical structural parameters such as initial racking stiffness, loads at which cracks form in the frame and the infill, peak loads and 'plastic' collapse loads.

(iv) To investigate the influence on these parameters of various likely design variables such as;

- frame member dimensions and reinforcement
- infill thickness
- effect of vertical loads on columns.

(v) To compare these parameters with the predictions obtained from existing empirical and theoretical methods.

(vi) To consider the results in relation to the limit state approach and to develop suitable analytical techniques and recommendations for design.

1.4 INTRODUCTION TO THE EXPERIMENTAL PROGRAMME PERFORMED

Because of the high cost of any research, and because full-scale structures are time consuming and necessitate a lot of space in laboratory, it was decided that a scale of approximately 1 : 3 should be adopted. Three square infill panels made of lightweight aggregate concrete blockwork of three different thicknesses have been used in combination with five different reinforced concrete frames with square and rectangular sections, to investigate the

effect of the different parameters selected for the purpose of this research. The lightweight aggregate blocks used here may be taken as being representative of the general range of building blocks in use.

A total of four open frames and sixteen infilled frames have been tested. Two open frames and eight infilled frames have been tested under static horizontal racking loading applied in the plane of the frame. The other two open frames and eight infilled frames have been tested under combined loading (vertical loads on the columns plus horizontal racking load applied in the plane of the frame). Two of the infilled frames in each group have been made identical to check the repeatability of the test results. The full details of this experimental programme are given in Chapter 3.

1.5 STRUCTURE OF THE THESIS

Chapter 2 contains a review of previous experimental and theoretical work in relation to infilled frames or shear walls built inside a frame. The experimental work carried out for this project is described in Chapter 3, which gives details of the specimens tested, the materials used, the methods of construction and curing and the terminology adopted for the specimens. The instrumentation used, the setting up and testing procedures and the control and subsidiary tests carried out are also described in detail. The presenting and discussing of the results and consideration of the effect of the different variables are given in Chapter 4. The comparison of the principal parameters obtained from the tests with the predictions obtained from existing empirical and theoretical methods is made in Chapter 5. The analysis for the plastic collapse mechanisms identified for the infilled frames tested is presented in Chapter 6. Finally, the general conclusions are presented in the last chapter.

CHAPTER 2

LITERATURE REVIEW

2.1 INTROUDCTION

2.1.1 General

Since 1948 the topic of the contribution of the infill to the horizontal racking stiffness and strength of an infilled frame has been the subject of separate investigations at various institutions throughout the world. The first major investigation was started by a team of engineers led by Polyakov [1, 2] in the U.S.S.R. Many investigators have followed the path since then. The different researchers who have dealt with the behaviour of such composite structures have admitted the complexities and the difficulties encountered when trying to formulate either theoretical or empirical solutions. The variables affecting the behaviour of such structures are numerous and complex to formulate in mathematical form. Theoretical and empirical methods have been proposed to predict the behaviour of infilled frames both in the pre-cracking and post-cracking stages. In the pre-cracking stage, emphasis has been placed on predicting the lateral stiffness and the load causing the first crack in the infill. In the post-cracking stage, efforts have been made to predict the strength of the infill and the ultimate carrying capacity of the structure.

It was Polyakov [1, 2] and his team who first introduced one of the most widely adopted idealizations of infilled frame behaviour, the concept of the diagonal strut. Observations of tests showed that the infill tends to separate from the bounding frame in the region of the unloaded corners as indicated in figure 2.1 and this led to the proposal that the action of the infill panel could be represented by diagonal band of material acting in compression between the loaded corners, as also shown in figure 2.1.

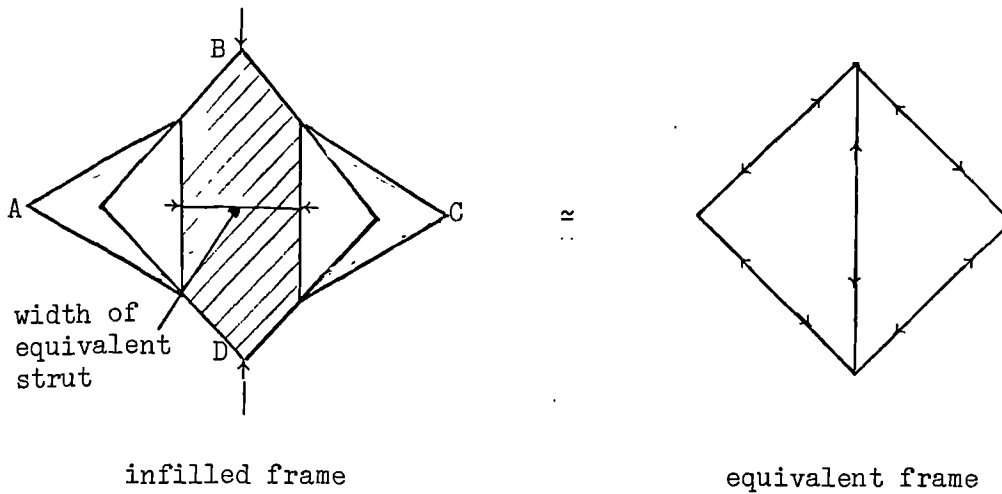


Figure 2.1 Idealized representation of the diagonal strut concept

2.1.2 Classification of Methods

The method of tackling this complex problem differed from one author to another. Basically, the work published up to 1983 may be split into three categories:

- (i) purely experimental investigations;
- (ii) experimental investigations leading to empirical predictions;
- (iii) theoretical investigations.

The first category concerns tests carried out both on actual buildings which were to be demolished and laboratory work on models at various scales up to full size. Results have generally been presented in the form of load-deflection curves of infilled frames and similar open frames. These showed that the infill greatly enhanced both the initial horizontal racking stiffness and the horizontal racking strength. No attempts to produce theoretical analyses or empirical formulae were made. The main reason for this was that the number of tests was small. Some authors, however, compared their test results with the predictions of various existing analytical methods. The second category concerns experimental investigations which produced empirical predictions for lateral racking stiffness and strength of infilled frames. To produce these

empirical equations a large number of tests on models and/or full size structures were needed. The third category comprises investigations whose primary aim was to develop a theoretical approach to predict the behaviour of the composite structure consisting of the infill and frame working jointly. These theoretical investigations were usually checked against experimental test results, either produced by the author concerned or resulting from previous investigations.

2.2 PURELY EXPERIMENTAL INVESTIGATIONS

2.2.1 Full Scale Tests

Early work on full scale concrete encased steel frames infilled with brickwork and blockwork (both hollow clay blocks and clinker blocks) with and without openings was carried out by Thomas [3]. The specimens were subjected to a horizontal racking load and were restrained at the top of the windward column. Only the measured load-deflection graphs were reported. One open frame was tested for comparison. The maximum racking load sustained with a 114 mm brick infilling was 2.6 times that of the open frame. The 76 mm clinker block and hollow clay block infillings increased the strength respectively by factors of 1.75 and 1.5.

Further full scale tests were carried out by Ockleston [4] on two three storey single bay reinforced concrete frames with brick infill walls. These frames formed part of the old dental hospital in Johannesburg which was being demolished in 1952 after ten years of service. They were subjected to a horizontal load applied at the corner of the top beam of the top floor. The load-deflection curves showed that the infilled frame was 5 times stronger and 3 times stiffer than the corresponding open frame.

In 1965, a small power station building was to be demolished. During the demolition, two reinforced concrete portal frames were tested by Read [6] to failure by applying a horizontal load at the roof level. The infill consisted of concrete-block masonry, windows, and a secondary system of concrete beams and columns which were not continuous with the main frame. The frame with infill was 7 times stronger and 8.6 times stiffer than the corresponding open frame.

L. G. Simms [7] continued the experimental investigation started at the B.R.S. (Building Research Station) by Thomas [3]. Results of tests carried out on full-scale single storey reinforced concrete frames infilled with no fines concrete were reported. Two infilled frames were tested under combined loading. A small uniform loading (29KN/m) was applied on the top beam by means of four hydraulic jacks and maintained constant during the subsequent application of the racking load. The windward column was restrained at the top. One frame had its columns prestressed prior to testing. An open frame was tested for comparison. The presence of the infill was found to change the position of the plastic hinges (away from the junction of the beams with the columns) and therefore increased the theoretical strength of the frame by 23%. This was defined as the strength of the frame acting compositely. The strength of the infill acting compositely was estimated by the difference between the strength of the composite and that of the frame acting compositely. The modes of failure of the frames and the infill were not discussed. Only the propagation and the widths of the cracks were described. The specimen with prestressed columns was 3.4 times stronger than the open frame, and the other 2.7 times stronger. The only effect of prestress commented on concerned the increase in strength.

2.2.2 Model Tests

Test results of 26 tenth-scale model steel frames infilled with concrete, with and without openings, were reported by Coull [8] in 1966. The frame members were 25 mm wide and 10 mm deep mild steel bars and were constructed on the back to back principle. They were tested as a beam, simply supported at its ends, and carrying a central point load. Details about different testing procedures are given in section 2.5.1. The prediction of the ultimate strength by Holmes' method [15] (see section 2.3.2) were found to be roughly double the test results. A relatively good agreement was, however, found between theoretical predictions using S. Smith's theory [30] (see section 2.4.2) and the test results. The ratio of the two loads varied from 0.6 to 1.1. However, the stiffnesses predicted by S. Smith's approach were found to be much higher. The ratio of the experimental values to the theoretical ones varied from 0.46 to 0.56. For the range of infilled frames tested, the only mode of failure observed was due to crushing of the infill at the end of the compression diagonal, either simultaneously at each end, or else at the loaded end. The increase in strength and stiffness of the open frame, due to the infilling, varied from about 4 to 15, and about 40 to 70 times respectively. It was concluded that the simple equivalent strut technique was a reasonable tool for the predictions of strength and stiffness, although high degrees of accuracy could not be expected.

Using larger scale models (1 : 3) and adopting the same testing procedure as Coull [8], Mallick et al [9] reported test results on nine reinforced concrete frames infilled with brickwork. The variables studied were the mortar mix and the panel proportions ($l_1/h_1 = 1, 1.25$ and 1.5). The mortar mixes used were 1 : 3, 1 : 4 and 1 : 6 (cement : sand). Two modes of infill failure, bond shear

failure and tensile failure, were observed depending on the mortar mix. The first mode was observed for a mix of low cement content (1 : 6). Very little agreement was witnessed between the test results of strength and stiffness and those obtained according to the theories of Smith [36] and Mainstone [20] (see sections 2.3.4 and 2.4.2). The first theory overestimated the strength except for specimens which failed by bond shearing. The range of discrepancies varied from 105 to 203%. The second was found to overestimate the strength for 1 : 6 brickwork, which failed in the tests due to bond shear, whereas it predicted failure in the tensile and compressive modes only. S. Smith's predictions for the lateral stiffness were found consistently higher than those obtained experimentally to the extent of 1.29 to 1.59 times. On the other hand, the values obtained by Mainstone's approach were very much smaller ranging between 46 to 61% of that measured in the tests.

The infill was found to increase both lateral stiffness (4.6 to 11.5 times) and lateral strength (2.7 to 6.9 times) of the corresponding open frame. The overall strength and lateral stiffness were also found to increase with the lengths of the panels. For instance the increases observed between a square panel and a rectangular panel ($l_1/h_1 = 1.5$) were of the order of 59% for stiffness and 29% for strength. It was concluded that the separation between the frame and the infill did not take place for 1 : 3 and 1 : 4 brickwork and that for 1 : 6 brickwork this separation was confined to relatively small lengths. The final conclusion was that slip at the interface, for which the maximum recorded value was of the order of 0.18 mm inclusive of the deformations within the gauge length, was not likely to have any appreciable influence on the behaviour under service load.

A discussion by T. P. Ganesan and M. Mohideen [10] pointed out that the stiffness calculated by Mainstone's corrected relationship [21] (section 2.3.4) agreed within reasonable limits of experimental

scatter with these authors' test results.

A scale of 1 : 3 was also used by Irwin and Afshar [11] in their tests on six identical reinforced concrete frames each infilled with a different combination of materials. The infills comprised combinations of lightweight concrete block and expanded polystyrene with coverings of plain micro-concrete, micro-concrete reinforced cement and steel fibre reinforced micro-concrete. The specimens were subjected to in-plane cyclic loading. The lower beam was anchored to the test rig. The column adjacent to the application of the horizontal loading was prevented from lifting by application of a vertical load acting through machined bearing plates and rollers. On reversal of the horizontal loading, the vertical loading system was moved to act on the other column and with each reversal the test units were forced to display greater ductility than the previous loading. The relative ductilities, strengths and elasto-plastic cyclic load capacities of the units were compared.

It was concluded that the best unit tested was that in which the cladding was reinforced by two layers of steel mesh each side in 15 mm of micro-concrete. That unit was found to retain its geometry even after having been damaged. It was also concluded that the cladding applied to an infill radically affected the strength, stiffness and ductility of the unit. The increase in strength brought by the cladding varied from 41 to 127%. The failure modes for the frame and the infill were not discussed. Only the shapes of frame distortions and crackings in frame and infill were schematically represented.

Using the same scale (1/10) and the same type of frames (steel frames made of flat bars) as did Coull [8], but adopting a different type of loading (diagonal), Saneinejad [12] carried out a large number of tests on square steel frames infilled with micro-concrete and a sand/browning plaster mix. The reason for using the second type of infill was to enable him to cover the full range of the relative stiffness parameter, $\lambda_h h$, from 3.1 to 15.2 and the relative strength

parameter, m_n , from 0.009 to 1.190. These parameters were first introduced by S. Smith [30] (see section 2.4.2) and Wood [44] (see section 2.4.5) respectively. The frames were fabricated using rigid welded connections. Two open frames were tested for comparison. The test results were compared to the predictions formulated by S. Smith [36], Mainstone [20] (see section 2.3.4) and Wood [44].

The graphical comparison showed that the experimental compressive load agreed with the predicted one using S. Smith's method for $\lambda_n h$ ranging between 6 and 10. For higher values of $\lambda_n h$, the experimental load was 10% higher and for lower values of $\lambda_n h$, it was 17% lower. Mainstone's method gave higher values (28% for $\lambda_n h = 7$ and about 14% for $\lambda_n h = 4$). A good agreement was found using Wood's method for values of m_n between 0.05 and 0.35. The predictions were, however, 12% lower for strong infill ($m_n = 0.05$). The agreement for lateral stiffness was found to be less satisfactory. For $\lambda_n h$ between 3 and 8 the test results laid between S. Smith's curve and Mainstone's. The first being higher because the width of the diagonal strut was approximately 3 times that of Mainstone's. It was concluded that the infill increased the lateral stiffness by a factor of 7 to 300 and the strength by approximately 1 to 25.

2.3 EMPIRICAL PREDICTIONS

2.3.1 Benjamin and Williams

Benjamin and Williams [13] carried out extensive experimental work on large and model scale reinforced concrete frames infilled with plain and reinforced concrete. The geometrical scale varied from $\frac{1}{8}$ to $\frac{3}{8}$. The specimens were tested as vertical beams (fixed base and racking load applied at the top corner of the surrounding frame). Although theoretical investigations were conducted based on a simplification of a lattice analogy method during the experimental

programme, it was concluded that the results were no more accurate than those given by a simpler strength of materials approach. The parameters investigated were the scale effect, the panel proportions, the column strength and the panel reinforcement. No scale effect was observed from the test results. It was concluded that if this latter were present, it was hidden by the general scatter of results. The observed modes of failure were by tension in the windward column, shearing of the leeward column, cracking around the perimeter of the infill, and cracking along, and parallel to, the compression diagonal of the infill.

The width to height ratio of the panel was found to have a pronounced influence on the ultimate strength and stiffness. As this ratio increased, the load at first crack or at a major break in the load-deflection graph approached the ultimate load. For the specimens tested, the two loads agreed approximately at an l_i/h_i of three with unreinforced panels, and approximately at four for the reinforced walls. The lateral stiffness was predicted by using the simple strength of materials approach. The shear wall being considered as a vertical cantilever and the shear distortions were assumed to be taken by the wall only. It was suggested that the load causing first crack in the panel should be taken as the failure load of the wall neglecting steel and columns. As for the ultimate load and deflection, these were predicted empirically.

In 1958, they [14] reported results from a further series of tests carried out on large size and model brick walls bounded by steel and reinforced concrete frames. The same testing procedure was adopted as for the previous series of tests. The bounding frames were designed to have a higher strength than the masonry panel. That is, the tension column steel was not placed in yield by the largest

load attained in these tests. The infill panel cracked before the compression column sheared off at the foundation. A total of twenty shear walls having a brick panel and a reinforced concrete frame were tested together with two full size brick walls enclosed by a steel frame, and two model scale brick walls without bounding frames. The various parameters investigated, in addition to scale effect, were length to height ratio, brick size, frame effect (variable concrete area and variable steel area). The following conclusions were drawn from these tests. The length to height ratio was, as previously, found to have an important influence on both strength and stiffness. The brick size was reported to be unimportant. The variations in column steel and concrete area did not influence the stiffness in the uncracked range insofar as could be determined experimentally.

As in the investigation of concrete infills, the lateral stiffness of the system was related to that of the infill panel only and the calculation was based on the simple strength of materials approach where only shear deformations in the panel were considered. Unlike the concrete infill, the brickwork panel was found to fail in shear. The cracking strength was determined from tests on couplets of bricks with the angle between the line of application of the load and the mortar joint, varying from 0 (pure tension) to 135° (compression and shear). The limited investigation of bond strength in combined stress indicated that a 120° test gave a good index of the quality of a particular couplet of masonry. The shear strength of the couplet was then used for the whole panel with a reduction factor, termed the workmanship factor. This latter was found to vary between 0.6 and 1. In determining the shear strength of the infill, the contribution of the frame was neglected. It was concluded that test results depended to a great extent on the quality of workmanship.

2.3.2 Holmes

Taking up Polyakov's proposal [1, 2] of the diagonal strut concept, Holmes [15] carried out four tests on one-sixth welded steel frames infilled with concrete. Although the specimens were subjected to horizontal loading, the analysis was conducted for diagonal loading. The width of the strut was suggested to be taken equal to one-third the diagonal length of the infill. This "one-third" rule was suggested as being applicable irrespective of the relative stiffness of the frame and the infill. Only compressive mode of infill failure was considered. The deformation and strength were then predicted by an elastic analysis of the equivalent frame. The prediction of the strength was based on the assumption that the infill was to fail at a predetermined average diagonal strain depending upon the material. The strength of the composite was taken as the sum of the strength of the frame and that of the diagonal strut.

In addition to the tests carried out by the author, test results of eight full-scale concrete encased steel frames infilled with brickwork reported by Wood [16] and one full-scale steel frame infilled with brickwork reported by Benjamin and Williams [14], were checked against theoretical predictions. Good agreement was found between theoretical and experimental results. The maximum variation between theoretical and experimental failing loads was 14% with the majority of values well below this figure. It was concluded that the theoretical deflection at ultimate load was generally much lower than the experimental deflection. The theoretical deflection seemed to correspond to the measured deflection at some point between 90 and 100% of the ultimate load. This is hardly surprising, since the analysis assumed a linear elastic response up to failure.

In 1963, Holmes [17] proposed a semi-empirical method to predict

the deformation and strength of single storey infilled frames subjected to vertical loading applied to the middle of the top beam. Two specimens were subjected to combined loading (vertical load on the top beam plus horizontal racking load). The ultimate strength was found to be smaller (-13%) when the two loads were applied simultaneously. In the same paper, he also presented a method for predicting the behaviour of two storey infilled frames subjected to horizontal loading. This was based on his previously used concept of the equivalent diagonal strut.

2.3.3 Fiorato et al

Fiorato et al [18] described in their report a total of twenty-seven tests using eighth-scale models of reinforced concrete frames infilled with masonry walls (small scale clay-bricks and mortar). Eight single-storey single-bay, twelve five-storey single-bay and six two-storey three-bay infilled panels were tested. One five-storey single-bay frame was tested with no filler walls. The single-storey specimens were subjected to lateral load at the mid-span of the top beam to simulate the transmission of the load through floor slabs of a building. In the five-storey specimens equal loads were applied at the third point of each beam. In the two-storey specimens 80% of the total load was applied at the mid-span of the top beam, 10% was applied at the mid-span of the middle first-storey beam and 10% was applied at the mid-span of the outside first-storey beam (on the tension side of the specimens). They claimed that the particular application of loading was justified and realistic to simulate the earthquake effects. The specimens had fixed bases. Because of the method of fabrication of the test specimens, no gaps between the wall and the frame were expected. Both frame and wall were assumed to

participate in transmitting the load through the structure. It was assumed that the wall carried most of the shear as in the web of an I section.

Two modes of infill failure were observed, flexural failure mechanism and shear failure mechanism. The load causing flexural cracking was calculated based on the elastic flexure formula assuming a linear distribution of strains throughout the cross-section. An identical modulus of elasticity was assumed for the frame and the infill. The infilled frame was, thus, considered as a vertical cantilever with the critical section at the base. The calculation of the shear cracking load was governed by the shear capacity of the masonry. The panels were assumed to act as isolated elements loaded diagonally. The bond shear strength and the coefficient of friction found from tests were respectively 0.48N/mm^2 and 0.46 . Using the same procedure as Benjamin and Williams [14], the shear strength was assumed to follow Coulomb's law $f = f_{bs} + \mu\sigma_n$ where f is the shear strength, f_{bs} the bond shear strength, σ_n the normal stress and μ the coefficient of friction. Then the horizontal and vertical reactions resulting from the diagonal loading were used to express the average shear and normal stresses at the centre of the panel. These stresses were substituted in the basic relationship to derive the shear strength of the masonry.

The initial response was found to be that of a vertical cantilever. The system behaved, essentially, as a beam until the wall developed shearing cracks which were idealized as horizontal. When these cracks did not form, the capacity of the frame-wall system developed as a beam failing in flexure. Following the initiation of shearing cracks, the load-deflection characteristics of the frame-wall system were calculated using the knee-braced-frame concept as

shown in figure 2.2. The calculation of ultimate load was reduced to determine the load necessary to develop the yield capacity of the braced columns. In addition to the height (number of storeys) and width (number of bays) the controlled variables were the amount of reinforcement in frame members (1.1%, 2.2% and 3.4%), vertical loads on the columns, which were maintained constant during the test while the racking loads were increased, and the presence of wall openings.

The increase of amount of reinforcement in the columns resulted in an increase in strength and stiffness of the structures (a maximum increase in strength of 135% was observed for the five-storey specimens). The application of vertical loads on the columns not only stiffened and strengthened the columns, but also increased the shearing capacity of the walls and increased the ultimate load (45% for the two-bay specimens). Openings in the walls decreased the strength and the stiffness of the structure and affected the location of the brace length. The amount of reinforcement in the columns was seen to affect to a great extent the sequence of failure. Specimens with larger amounts of reinforcement were more likely to develop the shearing capacity of the wall prior to yielding of the frame reinforcement. The ratio of observed to ultimate loads calculated using the knee-braced-frame concept varied from 0.91 to 1.80. The agreement between observed and calculated cracking loads was good for the single-storey single-bay specimens, but the ratio of observed to calculated loads varied from 0.75 to 1.0 for the five-storey specimens and from 0.58 to 1.28 for the two-storey two-bay specimens.

2.3.4 Mainstone et al

Further tests on model scale structures were carried out by Mainstone et al [19 - 21]. The investigation was conducted for

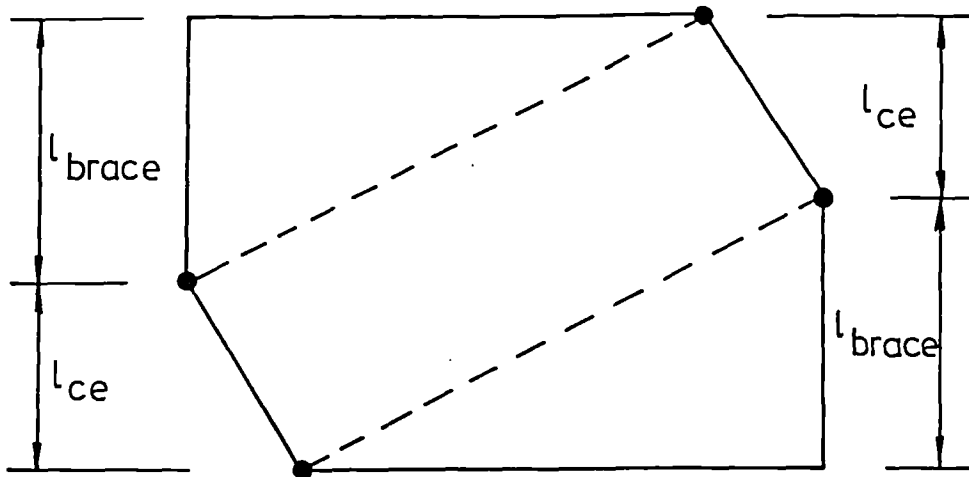


FIG. 2-2 KNEE - BRACED SHEAR ROTATION MODE
IDENTIFIED BY FIORATO et al [18]

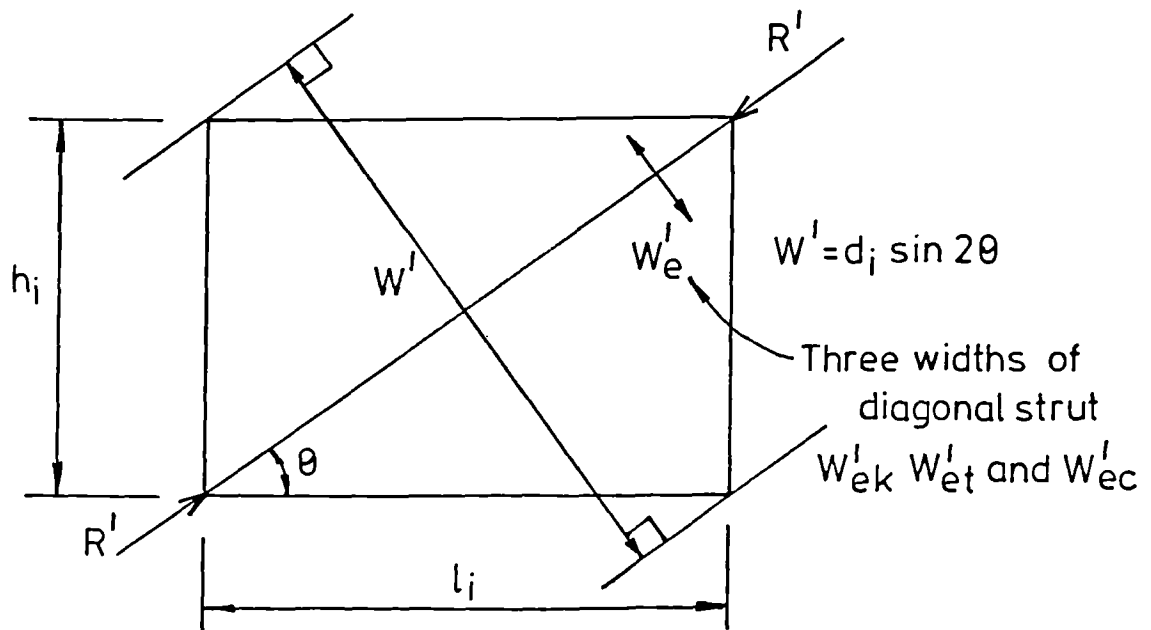


FIG. 2-3 CHARACTERISTIC WIDTH AFTER MAINSTONE [19]

infilled frames under full range of restraint offered to an infill by different types of surrounding frames. These were made of steel with square and I sections, light and heavy concrete encased steel and steel with stiffening plates to simulate the action of adjacent infills. The infill panels consisted of model brickwork and micro-concrete with and without reinforcement. The geometrical scale of the infilled frames tested was 1 : 6. Some unframed walls, two-bay single-storey and two-bay two-storey were also tested. The specimens were loaded within a stiff outer frame in such a way as to give, in effect, a diagonal compression. Early full-scale tests conducted at the B.R.S. [3, 16] and one more full-scale with stiffened plates added to the frame served as control. The variables investigated were numerous and included the reinforcement of the infills made of micro-concrete, repeated loading, a gap of 1.5 mm left deliberately along the top of model brickwork infills, the strength of the joints, which were riveted or welded, the frame stiffness and the panel proportions.

The parameter found to have the greatest influence on the behaviour of such structures was the relative stiffness of the columns to the infill, defined by the parameter $\lambda_n h$. The approach to the analysis of the strength and stiffness was based on the concept of the diagonal strut as originally suggested by Polyakov [1, 2]. The effective width of the diagonal strut was not constant, as suggested by Holmes [15], but varied with the level of loading. Three distinct widths were defined as illustrated in figure 2.3. The first, w'_{ek} , was defined in the initial linear part of the load-deflection graph to predict the lateral stiffness. The second, $w'_{e\bar{c}}$, for predicting the cracking strength of the infill (only tensile failure load was considered) and the third, w'_{ec} , for predicting the

compressive strength of the infill. From test results, design charts and empirical equations were derived to give the effective width of the diagonal strut in relation to $\lambda_h h$ for the three stages of loading. These empirical relationships were altered a first time in 1974 [21] and their definitive forms were published in the discussion to Wood's paper [46] (section 2.4.5) after correcting an arithmetical error in the conversion to S.I units of the stiffness of the columns and beams of the stiffest frames. .

A very big scatter was observed between identical specimens or specimens with approximately the same relative stiffness, $\lambda_h h$. For model brickwork infilled frames, for instance, the maximum variation was of the order of 900% for stiffness, 1100% for cracking strength and 280% for compressive strength. The design charts were, however, drawn towards the conservative side and passed through the regions where there was a concentration and a relatively smaller scatter of the test results. It was suggested that for design purposes, the horizontal racking stiffness and the composite strength up to first crack could be taken as those of the infill alone, because the load carried by the frame at the deflection which produced the first crack was usually small. Similarly it was suggested that the frame contribution could be ignored when estimating the composite ultimate strength. For brickwork infill, it was suggested that a conservative value for the effective width ($w = 0.1 d_i$, where d_i is infill diagonal) should be used to predict the cracking and compressive strengths of the infill.

2.3.5 Kadir and Hendry

This work included the development of an approximate analytical method but since this is based on empirically determined values for the lengths of contact, the work has been included in this section

rather than in section 2.4. Using a scale of approximately $\frac{1}{6}$ to $\frac{1}{8}$ and adopting the back to back testing procedure as used by Coull [8] and Mallick et al [9], Kadir [22] carried out a large number of tests on square and rectangular brickwork panels bounded by mild steel frames. The test results were also reported in a paper published with Hendry [23] and a summary of Kadir's simplified theory was also reported by Hendry [24]. One-third-scale model bricks were used for the construction of the walls. Two types of mortar were used for laying the bricks. The first was 1 : 3 by weight, the second was a modified mortar, obtained by adding 40% of revinex 29Y40 on the cement weight, to give high bond strength. The frames were made of mild steel rectangular section of 38.1 mm width with varying thicknesses ranging between 12.7 mm and 25.4 mm. The infill was built inside the frame with and without a gap at the top of the wall.

The parameters, found to have a direct influence, were the height to length ratio of the panel, the frame stiffness, the lack of fit and the rigidity of the joints. Separation of the infill from the frame, except in the vicinity of the loaded corners, was observed only for the infills laid in 1 : 3 mortar, and was found to occur at a load of about 10 to 20% of the load causing the first shear crack inside the infill. Sliding of the infill along the frame members was observed in some walls. Two modes of infill failure were observed, diagonal shear crack and crushing of brickwork at the loaded corners. In the case of rectangular panels, the crack was almost horizontal.

In the analytical approach, the infill was considered to behave as a diagonal bracing member in compression after the separation had occurred and up to the occurrence of the first shear crack. The width of the diagonal strut was related to the experimental lengths of contact against the beams, α_λ , and the columns, α_h . These were

found to be close to the curves $\alpha_h/h = \pi/2\lambda_h h$ and $\alpha_l/l = \pi/\lambda_l l$. The effective width was then defined as $w = \frac{1}{2}\sqrt{\alpha_l^2 + \alpha_h^2}$ as shown in figure 2.4. The use of the diagonal strut concept was suggested as being suitable to estimate the lateral stiffness of the equivalent structure. The diagonal strut was assumed to be pin-jointed at the corners and under uniform compressive stress over the effective width, w . The reactions exerted by the infill upon the frame along the lengths of contact, and the consequent change in mode of frame deformation were neglected. The width of the diagonal strut was in fact related to both relative stiffnesses of beams and columns and the infill, whereas Mainstone [19] related it only to $\lambda_h h$ and Holmes [15] had ignored the importance of the relative stiffness and suggested a constant width of $0.33d_c$.

The cracking strength of the infill was estimated by expressing approximately the average shear and normal stresses at the centre of the panel and using the basic relationship for shear strength $f = f_{bs} + \mu\sigma_n$ as did Benjamin and Williams [14] and Fiorato et al [18]. Kadir did, however, take into account the frame infill interaction by considering the equivalent frame shown in figure 2.5 and using earlier work by Seddon [25] on partially loaded concrete walls to express the stresses at the centre of the panel. These stresses were substituted in the basic relationship $f = f_{bs} + \mu\sigma_n$ to derive the cracking strength of the infill. After cracking, the assumption was made that crushing failure of the equivalent diagonal strut took place over the effective width, w . The load carried by the infill was obtained by assuming a linear distribution of contact stresses over a length of column equal to $w \cos\theta$ as shown in figure 2.6. The maximum stress occurring at the edge was taken equal to the

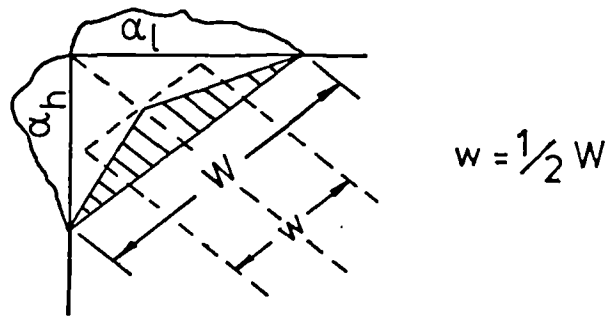


FIG.2.4 DIAGONAL STRUT WIDTH AFTER KADIR [22]

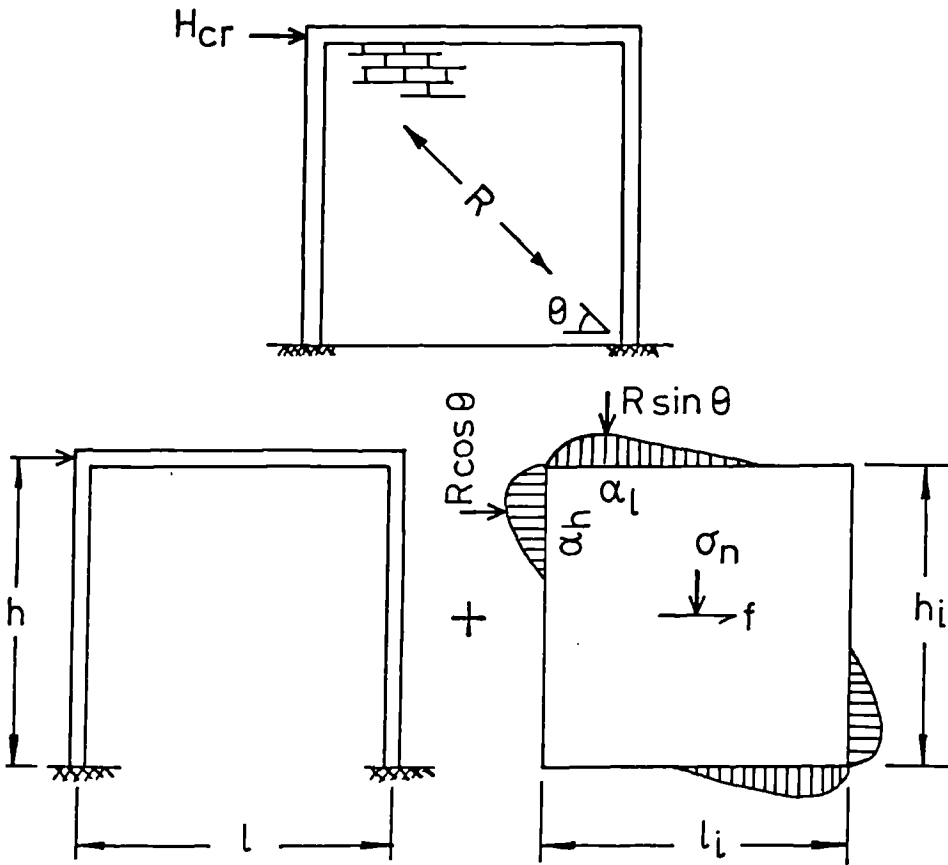


FIG.2.5 APPROXIMATION OF MASONRY INFILLED FRAME AT CRACKING LOAD AFTER KADIR [22]

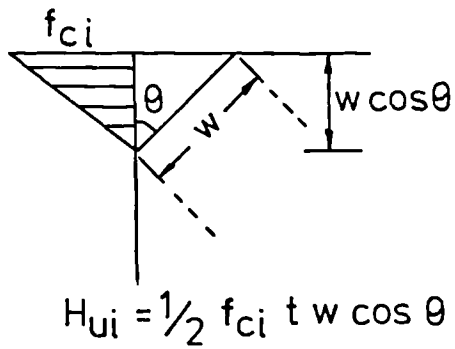


FIG.2.6 LOAD CARRIED BY THE INFILL AFTER KADIR [22]

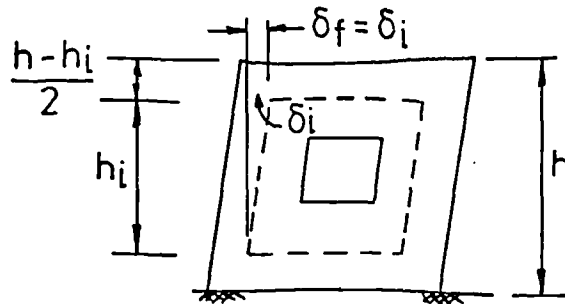


FIG.2.7 DIMENSIONS OF EQUIVALENT BRICKWORK FRAME AFTER KADIR [22]

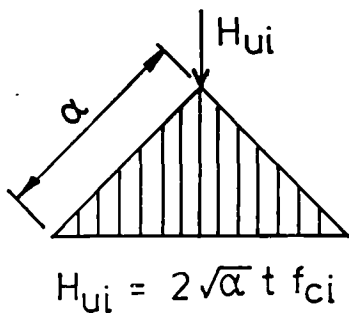


FIG.2.8 LOAD CARRIED BY THE INFILL AFTER S.SMITH [31]

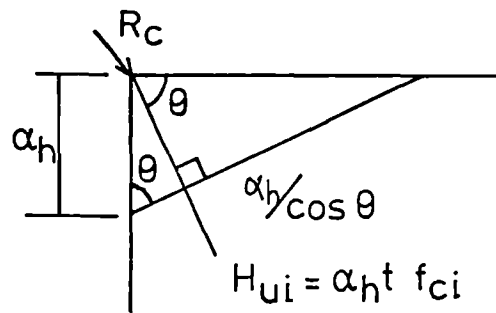


FIG.2.10 LOAD CARRIED BY THE INFILL AFTER S.SMITH [32]

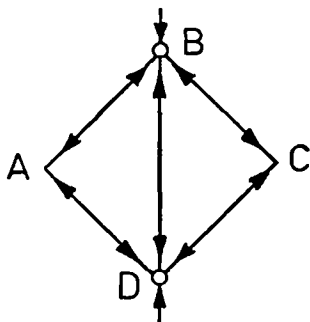


FIG.2.9 FORCE SYSTEMS FOR LATERALLY AND DIAGONALLY LOADED INFILLED FRAMES

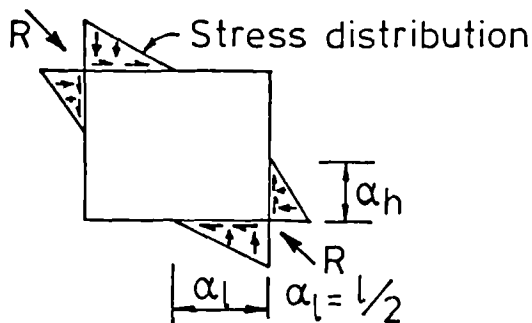
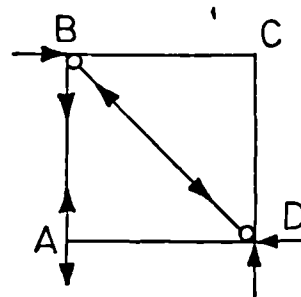


FIG.2.11 ASSUMED PANEL LOADING AFTER S.SMITH [33]

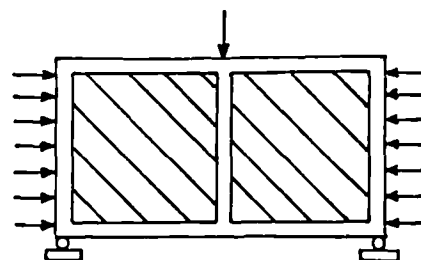


FIG.2.12 LOADING ARRANGEMENT IN REFERENCE [35]

ultimate compressive strength of the infill material, f_{ci} . Thus the ultimate load taken by the infill was $\frac{1}{2}f_{ci} tw \cos\theta$. Kadir has carried out an elastic analysis to obtain a relationship giving the percentage of the total lateral force applied to the frame-wall system carried by the wall, in terms of $\lambda_h h$. The frame was assumed to remain elastic.

For the post-cracking range, Kadir proposed to add to the ultimate capacity of the wall that of the frame at the deflection, δ_f , corresponding to the maximum load in the brickwork. This deflection was difficult to assess, but as an approximation based on experimental results, was calculated on the basis of an assumed brickwork strain at failure of 3,000 μ s. Design charts were derived in terms of $\lambda_h h$ to give the lateral stiffness of the composite system, the percentage of the total lateral force carried by the wall up to cracking, and the ultimate strength of the composite. An additional design chart for the cracking strength of the infill was derived in terms of $\lambda_\ell \ell$. These charts covered square and rectangular panels (ℓ_i/h_i up to 2). Comparison between Kadir's approximate theory and the results of tests covering a range of values of $\lambda_h h$ and $\lambda_\ell \ell$ between 2 and 10 showed that a good agreement existed between theoretical and experimental results. For the ultimate strength, for instance, the ratio of the two loads varied between approximately 0.8 and 1.1. The predicted ultimate loads using Holmes [15] and S. Smith [36] (see section 2.4.2) methods were found to be much higher. The ratio of theoretical to experimental loads varied from 1.1 to 3.6 for the first, and from 1.3 to 2.1 for the second. Comparison was also made between the predicted cracking strengths and those obtained from early full-scale tests carried out by L. G. Simms [26] and Benjamin and Williams [14]. The theoretical to experimental

load ratio varied from 0.8 to 1.3.

Kadir also carried out tests on models with various sized centrally placed openings in a square infilled panel. The load at first cracking was reduced by approximately 50 to 80%, and the ultimate load by 0 to 40%, as compared to a corresponding frame without openings. Kadir suggested an approximate method of analysing infilled panels with openings in which the panel is replaced by a diagonal member of equivalent stiffness. The stiffness of this diagonal was calculated by considering the brickwork as a frame as shown in figure 2.7. To this stiffness was added that of the frame.

2.3.6 S.K.Mallik and Barua

The experimental investigation whose first results were published in 1975 [9] and which was reported in section 2.2.2 was carried on a stage further by S.K.Mallik and Barua [2]. Six more specimens with $l_i/h_i = 1.125$ and 1.375 were tested and six out of the nine early ones were repeated. Thus, these experimental investigations covered a total of twenty-one third-scale reinforced concrete frames infilled with brickwork constructed and tested back to back. The major observations from tests were that neither separation, nor slip did occur at any stages of loading. Whereas these two phenomena were reported to have occurred for steel frames infilled either with concrete or brickwork by the different authors who tested these types of infilled frames. As in their previous investigation [9], the infill failed either by tension or bond shear depending on the strength of the mortar mix. The parameter found to have a major influence on the behaviour of such structures was the relative stiffness of the columns to the infill, $\lambda_h h$. Thus, the empirical equations derived for lateral stiffness, tensile and shear strengths were related to $\lambda_h h$. The use

of the empirical equations was suggested as being accurate enough for predicting the lateral stiffness and strength of the composite system. For the specimens tested, the predicted to experimental values ratio varied from 0.9 to 1.05 for lateral stiffness, from 0.82 to 1.15 for tensile strength and from 0.94 to 1.02 for bond shear strength. From the stress diagrams, the total shear force at the base of the infill was estimated to give the separate contribution of the infill in terms of $\lambda_h h$. The variation in strength for the six pairs of identical specimens ranged between 2 and 23%.

2.4 THEORETICAL INVESTIGATIONS

2.4.1 Sachanski and Barua and Mallick, S.K.

Sachanski [28] analysed the contact forces between the frame and the infill by assuming their mutual bond to be replaced by thirty redundant reactions. These were determined by forming and solving the equations for the compatibility of displacement of the frame and infill. A continuous bond at the interface between the frame and the infill was assumed. It was supposed that the continuous bond at the interface could be effected by transmission of normal and shear forces at a finite number of connecting points. The joints were cut and their action was substituted by the action of the redundant reactions. The plane-stress problem of the infill acted upon by a single concentrated unit load was then solved, by use of finite differences, with the unit load acting in turn at each joint in the separate directions of the normal and shear force at that joint. Corresponding 'unit' solutions were obtained for the frame. Using the condition of compatibility of displacement at the joints, a system of simultaneous equations, equal in number to the number of unknown forces, was obtained. Its solution produced the values of

the two forces at each joint, defining, thus, the character of the stress in the contact zone. From the stress analysis, the critical region was found to be the centre of the infill. The failure criterion was then to equate the principal tensile stress at the centre of the infill to the tensile strength of the infill material. This load was defined as the ultimate load. The derived equations for tensile strength included the effect of a possible opening in the infill. It was concluded that the load would be distributed between the frame and the infill according to their stiffness. This contribution was based on the equality of deformation of the frame and the infill.

In the same paper, Sachanski described tests on twenty-six half-scale reinforced concrete frames infilled with brickwork, made of mortars of different strengths, with and without openings. The experimental investigation also included large-scale reinforced concrete frames enclosing brickwork and concrete infills, and the destruction of a disused five-storey building. The specimens were subjected to a horizontal racking load and the windward column was restrained at the top. A good agreement was found for full-size tests. The observed to calculated tensile strength ratio varied from 0.7 to 1.1 with the majority around 1.1. The observed values, for the models, were 20 to 30% higher than the predicted. It was concluded that this discrepancy could be due to the scale modulus.

The approach suggested by Sachanski was later on taken up by S.K. Mallick and Barua [29]. The theoretical analysis, however, included the effects of separation and slip. The theory was checked against results of a large number of tests carried out on approximately $\frac{1}{20}$ scale steel frames infilled with mortar. The specimens were tested back to back. Two modes of infill failure were observed, diagonal cracking and corner crushing. The lengths of contact against beams,

α_ℓ , and columns, α_h , were found to vary with the loading. The theoretical analysis was found to provide good agreement with the test results. The ratio of experimental to theoretical values varied from 0.84 to 0.95 for stiffness and from 0.88 to 1.06 for the cracking strength of the infill. The agreement between the theory and the experimental results encouraged the authors to propose simple expressions, based on the test data, for lengths of contact at two stages of loading $\frac{H}{H_u} = \frac{1}{4}$ and 1, lateral stiffness, load causing first crack, ultimate load and share of load between the frame and the infill. These equations were derived in terms of $\lambda_\ell \ell$ for α_ℓ and in terms of $\lambda_h \ell$ for all the others.

2.4.2 Stafford Smith et al

S. Smith and his different collaborators have carried out extensive theoretical and experimental studies on single-storey and multi-storey steel frames infilled with mortar and model brickwork over a long period of years. The results were published at their respective time of development. In this section, it was thought useful that the different papers published should be reported chronologically and discussed as briefly as possible. The main changes occurring in the approach are also reported. The first paper was published in 1962 [30]. From preliminary tests on steel frames infilled with mortar and tested using the back to back method, it was concluded that the infill could be assumed to behave as a diagonal strut in compression as originally postulated by Polyakov [1, 2]. At first, efforts were made to determine the effective width of the diagonal strut theoretically and experimentally by diagonally testing isolated panels.

The attempt of predicting the diagonal stiffness of the panel

using a simple strength of materials approach (the diagonal load being resolved into components acting along the sides of the panel and resultant shear deflections combined to give the diagonal displacement) gave poor correspondence with the experimental results. Recourse was then made to the finite difference method to analyse the stress distribution over the infill. The stresses and diagonal deformations of the infill were derived to give values for the effective width of the diagonal strut for infills of different proportions. This width was found to vary from $d_i/4$ for a square infill to $d_i/11$ for an infill having a sides ratio of 5 : 1. It was then suggested that the lateral stiffness of the equivalent frame with infill replaced by diagonal strut could be calculated by conventional methods. It was concluded that calculations of deflections based on this approach might be erroneous because of the initial lack of fit between the frame and the infill.

In 1966 [31], the investigation of the behaviour of diagonally loaded square infilled frames was reported. The investigation was theoretical but it was checked against a large number of tests on $\frac{1}{20}$ th model steel frames infilled with mortar. The frames were made of mild steel rectangular sections of 13 mm width with varying thicknesses ranging from 4.8 mm to 19 mm. The theoretical investigation was conducted in the following manner. First of all, the relationship between the length of contact, α , and the relative stiffness of the frame and infill, λ_α , was considered. Three approaches were adopted. The first two assumed that a frame member was subjected to a triangular or parabolic distribution of the reaction from the infill acting over the length, α . The third was adopted from the equation for the length of contact of a free beam on an elastic foundation. Three curves relating α to λ_α were produced. Their closeness with the

experimental one led the author to adopt the third one which was expressed algebraically, $\frac{\alpha}{\ell} = \frac{\pi}{2\lambda\ell}$.

The second step was to relate the diagonal stiffness of the free infill to α . The finite difference approach was used assuming a triangular distribution of the reaction of the infill acting over different lengths of contact ($\frac{\alpha}{\ell}$ varying from $\frac{1}{8}$ to $\frac{5}{8}$). The analysis gave the strains along the compression diagonal. The average values of strains were used to determine the effective width, w , of the diagonal strut for each length of contact. The experimental and theoretical curves relating $\frac{w}{d}$ to $\frac{\alpha}{\ell}$ were not close. The latter being consistently higher, the difference ranging from 15.2 to 60%. The discrepancy was thought to be due to the assumption of the triangular distribution of reaction. The use of the experimental curve was suggested as being accurate enough for the rest of the analysis. The third step was to relate $\frac{w}{d}$ to $\lambda\ell$ ($\frac{\alpha}{\ell} = f(\lambda\ell)$ and $\frac{w}{d} = f(\frac{\alpha}{\ell}) \Rightarrow \frac{w}{d} = f(\lambda\ell)$) graphically. The last step was to find the correcting factor to allow for the frame contribution to the overall stiffness. Since the effective width was now determined, it remained to conduct an energy analysis of the redundant system assuming again a triangularly distributed reaction. The resulting graphical relationship between $\frac{P}{R}$ and $\lambda\ell$, where P is the total load and R the load on the strut, showed that unless $\lambda\ell$ was less than 5, the frame contribution was negligible.

Two modes of infill failure were observed in the model tests, cracking along the loaded diagonal and compressive failure near the loaded corners. The compressive failure, for the range and types of models tested, always took place, nevertheless, this was preceded by diagonal cracking for values of $\lambda\ell$ below 9.5. The criterion for tensile failure was to equate the maximum tensile stress found from the

stress analysis, and which occurred at the centre of the infill, to the tensile failing stress of the infill material. As for the compressive failure mode, assumption was made that the loaded corner, bounded by the lengths of contact as shown in figure 2.8, was in a plastic state at uniform stress equal to the compressive strength of the infill material. The method proposed to determine the effective width of the diagonal strut was for diagonally loaded infilled frames. Its use was, however, suggested as being applicable to laterally loaded infilled frames. This was checked experimentally with tests carried out on a pair of identical single panel infilled frames, in which one was diagonally loaded and the other laterally loaded. The test results were generally similar. In both cases the infill behaved as a diagonal strut however, the force systems were quite different as shown in figure 2.9. The same modes of infill failure were observed, diagonal cracking and crushing of concrete at the loaded corners.

A year later, in 1967, the analysis of laterally loaded multi-storey infilled frames was reported [32]. The parameters found to have the greatest influence were the relative stiffness of the columns and the infill, $\lambda_h h$, and the panel proportions. The beam-infill relative stiffness, $\lambda_\chi l$, was found to have little influence. Whatever the beam size, the length of contact against the beam, α_χ , was half the span. The stress analysis was conducted as previously. The width of the equivalent strut was predicted theoretically this time in relation to $\lambda_h h$ and the length - height proportions of the infill. As before, the theoretical values were found to be 15 to 60% higher than the experimental. These latter were adopted for the rest of the analysis. The modes of infill failure were similar to those under diagonal loading, and so were the criteria for determining the

different strengths. For the post-cracking stage, an assumed plastic region bounded by a line through the end of the length of contact against the column, α_h , and extending to the beam in a direction perpendicular to the loaded diagonal, as shown in figure 2.10, was used to predict the compressive failure mode. Design charts, expressing the cracking and crushing strengths in terms of $\lambda_h h$ and $l_i : h_i$, were derived. These charts showed that the possibility for rectangular infill to crack before crushing depended not only on $\lambda_h h$ but also on the ratio $l_i : h_i$. It was suggested that the lateral stiffness of the multi-storey infilled frame could be calculated by analysing the equivalent pin-jointed frame taking into account the axial forces in the frame members and replacing the infills by diagonal struts whose widths were determined from laterally loaded infilled panels.

In the same year, in a paper published in collaboration with Carter, S. Smith [33] reported the extension of the analysis to cover the behaviour of rectangular steel frames infilled with brickwork. An arbitrary diagonal load (100 units) was assumed to be triangularly distributed over each length of contact (figure 2.11), α_h against columns and $\alpha_l = \frac{l_i}{2}$ against beams. The stresses in the infill were analysed by a finite difference approach and the analysis was repeated for panels of different length - height proportions, each with a range of values for the length of column contact. The rest of the analysis was conducted as described previously. It was concluded that any prediction for stiffness was likely to be grossly in error, especially in the initial stages of loading. The reasons for that were the inaccuracy of determining the Young's modulus of brickwork and the lack of fit. The use of the method was suggested as being suitable only to indicate the order of horizontal stiffness. The infill

failed either by diagonal tension or by shear.

The tests had shown that behaviour of brickwork was approximately linear up to both tension and shear failure and it was therefore concluded that the elastic stress analysis was appropriate for predicting the panel stresses at failure. The results of the stress analysis were used next to determine the principal shear stresses and planes in the panel which, in conjunction with the internal friction caused by the compressive stresses and using the basic relationship for shear strength $f = f_{bs} + \mu\sigma_n$, provided the criterion for predicting the shear failure of the infill. The principal tensile stresses were also determined and used to predict the possibility of diagonal tension failure. Design charts were derived in terms of $\lambda_h h$ for infills of different proportions. The results of the proposed methods for predicting failure were compared with a number of published test results on masonry infilled frames reported by Simms [34], Polyakov [1] and Wood [16]. The theoretical to experimental load varied from 0.54 to 2.08 with the majority of results below 1.

Further tests, on small-scale ($\frac{1}{15}$ to $\frac{1}{8}$ approximately) steel frames infilled with mortar with properties similar to medium strength concrete, were carried out by S. Smith [35] to investigate the influence of vertical distributed loading on the horizontal stiffness and strength. The specimens were tested back to back with the loading arrangement as shown in figure 2.12. Initial tests were conducted to determine the horizontal strength and stiffness with a horizontal load only, and the vertical strength with a vertical load only. These were followed by tests to determine the horizontal stiffness and strength for different values of the vertical load between zero and the 'vertical load only' strength. Further series of similar tests were made on frames with different length - height ratios and

with varying beam and column sections.

It was concluded that the application of a uniformly distributed vertical load to a single-storey infilled frame, up to about one half its vertical strength, increased the horizontal strength and stiffness of the structure. For square panels, for instance, the strength increased by a factor ranging from 1.7 to 2.1 and the stiffness by approximately a factor ranging from 1.7 to 2.3. For vertical loads greater than approximately one half the vertical strength, the modes of failure were similar to those for a vertical load only (vertical tensile crackings and crushing along a line parallel to the application of vertical loads). For vertical loads less than half the vertical strength, the modes were similar to those for a horizontal load only (diagonal cracking and corner crushing). Interaction curves, defining the size of vertical load giving the maximum increase in the horizontal stiffness and strength, were derived.

In 1969, in a paper published with Carter, S. Smith [36] presented a compilation and condensation of the study with additional information to allow the prediction of the stiffness and strength of horizontally loaded infilled frames. The variation of the Young's modulus of the infill with increasing stress level was taken into account this time when determining the theoretical width of the diagonal strut. This width was found to vary throughout the whole range of loading whereas Holmes had suggested a constant width and Mainstone three specific widths at three stages of loading. Hence the equivalent strut width depended not only on the length of contact and panel proportions, but also upon the stress - strain characteristics of the infill material and on the value of the diagonal load on the panel, R , as a proportion of the diagonal compressive failing load, R_c . For determining the lateral stiffness, the limiting values

of $\frac{W}{d_i}$ were found to correspond to a value of $\frac{R}{R_c}$ between $\frac{1}{8}$ and $\frac{1}{4}$. Design charts were derived for this purpose. Once the effective width was determined, the infilled frame was then considered as a pin-jointed diagonally braced frame which could be analysed by conventional structural theory to estimate the lateral stiffness. This was justified since the presence of the infill was found to reduce the bending moments in frame members by about 90%.

The possible failure modes of the frame included the tensile failure of the windward column and the shear failure of the columns and beams and their connections. Three modes of failure were observed for brickwork infills, tensile, compressive and shear cracking along the mortar joints. The latter was found to be predominant. It was governed by $\lambda_h h$, $\lambda_i : h_i$ and the relative size of the bond shear strength, internal friction and diagonal tensile strength of the masonry. The greater the length : height ratio of the panel, the less the possibility of a tension failure. The lower the value of internal friction, the less likely is the panel to fail by the tensile mode. The compressive failure mode was found to be unlikely to occur for masonry infill. It was, however, suggested that the chart provided for concrete infilling could be used, assuming the compressive strength of the brickwork equal to the mortar strength.

The final development, reported by S. Smith and Riddington [37] was the use of a method of analysis of infilled frames using the finite element approach. The method developed took into consideration the possibility of separation between the frame and the infill and the loss of friction along the remaining lengths of contact. Two extreme cases were examined, where there was no friction and the infill was free to slide against the frame along the boundaries, and where there was a rigid connection between the infill and the frame

and no sliding was permitted. The programme used the basic four-node rectangular element with two degrees of freedom per node and linearly varying displacement functions along the boundaries. The use of adjacent nodes in the frame and the infill and the compatibility of displacements allowed separation to be taken into account.

Three types of infilled frame structures were analysed. The first type consisted of square and rectangular single panel frames subjected to a horizontal in-plane loading of 100 units. The second consisted of three-storey, single-bay, square infilled frames and the last consisted of single-storey, three-bay square infilled frames. Three values of $\lambda_h h$ were taken ($\lambda_h h = 3$ representing a very stiff frame, $\lambda_h h = 6.3$ a medium stiffness frame and $\lambda_h h = 15$ a flexible frame). The other variables investigated were the level of frictional contact along the infill-frame connections (two extreme cases examined), the variations in the flexural stiffness of the beam relative to the column and the variation of E_i/E_f where E_i is the Young's modulus of the infill and E_f that of the frame. The relative stiffness parameter, $\lambda_h h$, was found to control the stresses at the corner and therefore governed the compressive failure mode. The length to height ratio was found to control the shear and tension stresses at the centre, which was the critical region, and hence the shear and diagonal tension modes of failure. From the stress analyses, it was also found that the changing of the level of boundary friction affected most significantly the stresses in the compression corners of the infill and the lateral deflections. The stresses at the centre were found to be independent on the boundary friction level.

The analysis of square panels for example, showed a substantial increase in the corner compressive stresses (up to 400%) and an increase between 34 and 49% in lateral deflections when the infill

was allowed to slide into the corners of the frame. The variation in beam stiffness and its end connections did have a little effect, for example, in the no-friction single square analysis, a four-fold reduction in the beam stiffness produced a rise of only 15% in the corner compressive stresses, a reduction of 5% and less in the central stresses and a reduction in lateral stiffness of 9%. The effective width of the diagonal strut was calculated from the lateral deflection. This effective width was seen to reduce as the $h_i : l_i$ ratio reduced for the no-friction analyses, but increased as the $h_i : l_i$ ratio reduced for the friction analyses. This led the authors to conclude that the prediction of lateral deflection of an infilled frame could not be accurately estimated. It was suggested that only a conservative value for the width equal to one-tenth the diagonal length of the infill could reasonably be used to analyse the equivalent pin-jointed frame to estimate the lateral deflections and the axial forces in the frame members. It was also concluded that bending moments in frame members were not likely to exceed a value of $Hh/20$ (H: lateral load applied and h: the height of the frame).

A final compilation for design purposes was published in 1978 by the authors [38]. The method suggested was to consider all the possible modes of failure of the infill and then to check the strength of the frame by analysing the equivalent pin-jointed frame with infills replaced by diagonal struts of width equal to one-tenth the length of the diagonal. From the stress-analyses, equations were derived to predict the tension and shear failure loads for the infill. As for the compressive mode of failure, the authors suggested that Mainstone's equation [21] which took into account the stiffness of the column should be used. The equations were rewritten in limit state form by multiplying the stresses by the safety factors and including the partial safety factors for loads, stresses and materials

(γ_f , γ_{mv} and γ_m). It was suggested that the design method could be used for steel, concrete encased steel and concrete frames with brickwork or blockwork masonry infills, provided the appropriate modifications of $E_f : E_i$ are incorporated. The method was applicable for structures of $l_i : h_i$ varying from 0.3 to 3.

2.4.3 D.V. Mallick and Severn

The finite element approach was also used by D.V. Mallick and Severn [39] who pointed out the fact that the methods proposed for predicting the lateral stiffness of infilled frames up to 1967 did not take into consideration the slip that occurred between the frame and the infill. The main improvements in the computational procedure were to develop solutions for rectangular frames as well as for square frames, to take into consideration this slip, and that the length of contact, and the contact stresses, must be found as an integral part of the solution, and not assumed at the beginning. These improvements were incorporated in a method which made use of a finite element formulation based upon complementary energy so that the non-linear behaviour could be predicted. A series of tests was performed on steel frames infilled with KAFFIR-D plaster. The specimens were tested back to back. The agreement between theoretical and experimental stiffnesses was remarkably good for square frames, and less good, but still satisfactory for the rectangular frames. The theoretical to experimental stiffness ratio varied from 0.93 to 1.93.

It was concluded that the proposed method predicted more accurately the lateral stiffness than that proposed by S. Smith [31]. The theory was checked against five specimens tested by Smith. The theoretical predictions were found to be closer to the test results

than those using four other methods. The theoretical to experimental stiffness ratio varied from 1.03 to 1.16. A method based upon the concept of a 'shear structure' was proposed to predict the lateral stiffness of multi-storey frames. The horizontal sections were not supposed to rotate at the floor level and the relative displacement between floor was supposed to be horizontal. The stiffness of each storey depended only upon the relative displacement of the two floor levels of that storey. Each storey was considered as a beam element in shear only, and one shear displacement at each floor level was sufficient to define the deformed structure. The ultimate load was that which caused yielding of one of the corners. The lateral load to cause failure was predicted by multiplying the applied load used in the stress analysis by the ratio of compressive failing stress of the material to the calculated compressive stress at the point of separation between the frame and the infill. The theoretical to experimental failing load ratio varied from 0.93 to 1.14.

2.4.4 Liauw

A method of analysing infilled frames subjected to horizontal racking loads was presented by Liauw [40]. The materials were assumed to be isotropic and homogeneous. The infill was assumed to be bonded to the frame and the analysis made use of a general stress function, expressed in the form of a Fourier series, for the determination of the stress distribution in the infill, and subsequently for the determination of the deformation of the infilled frame. The solution was determined by use of the finite difference method. Three elastic models using the photoelasticity technique were used to check the theory. Good agreement was obtained between theoretical

and experimental values. From the stress analysis the critical regions were found to be the centre of the infill (maximum principal tension stresses) and the loaded corners (maximum principal compression stresses). At the interface, the stress distribution showed distinct non-linear characteristics, however, within the central portion it appeared to be approximately linear. Large proportions of the shearing load were found to be carried by the infill. Comparison of the theoretical values of the forces in the infilled frames with those of the open frames showed an important reduction of flexural moment in frame members (88 to 96%). This led to the conclusion that the frames might be regarded as non-flexural members, provided the bond between the infill and the frame was not broken. Finally, tests on a reinforced concrete closed frame, with and without infill, were carried out under a lateral load of 20 tons, to show the relative contribution of various infills to the stiffness of a frame. The infilled frame was found to be much stiffer than the open frame (from 76 times for a 114 mm brickwork infill to 187 times for 127 mm concrete infill).

Two years later, in 1972, the analysis was conducted using a different approach [41]. The method was approximate and was based on the equivalent frame method, in which parts of the infill were interpreted to act with adjacent frame members as composite sections in bending as shown in figure 2.13. The infilled frame was, thus, transformed into an equivalent frame whose members had the properties of the composite sections. The paper dealt with infilled frames with and without central openings. The central opening varying from 0 to 100% of the total area of the infill. The section properties, height and length of the equivalent structure were defined and expressions for the internal moments, shear forces, and the rotations of the

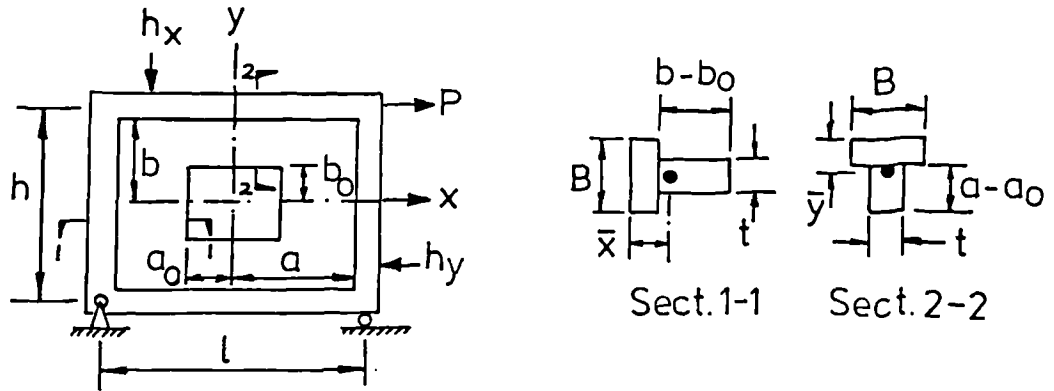


FIG. 2-13 EQUIVALENT FRAME AFTER LIAUW [41]

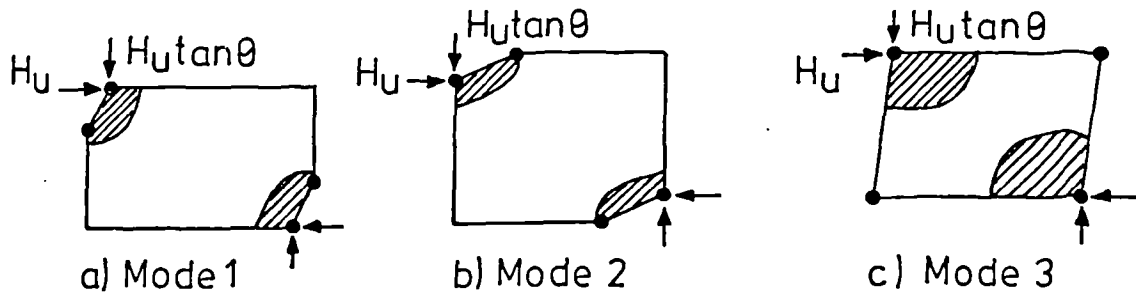
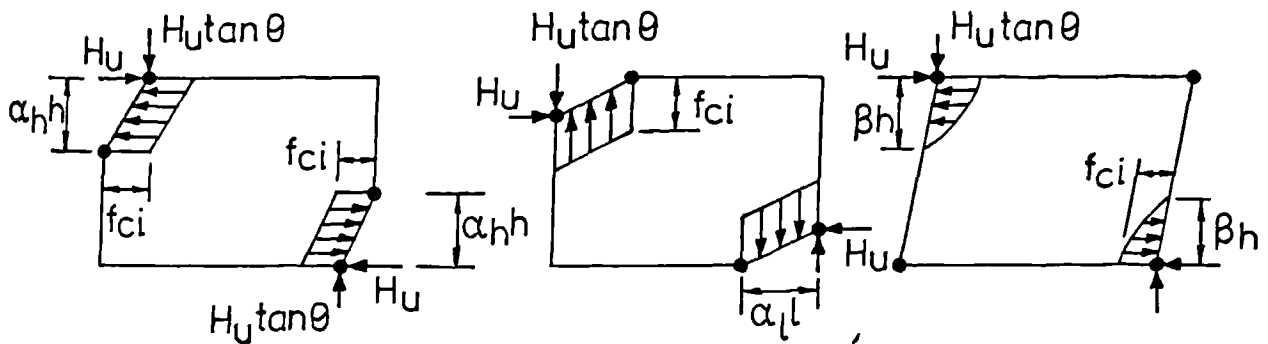


FIG. 2-14 COLLAPSE MODES IDENTIFIED BY LIAUW [43]



a) Mode 1 - corner crushing with failure in columns b) Mode 2 - corner crushing with failure in beams c) Mode 3 - Diagonal crushing

FIG. 2-15 ASSUMED STRESS DISTRIBUTION BY LIAUW [43]

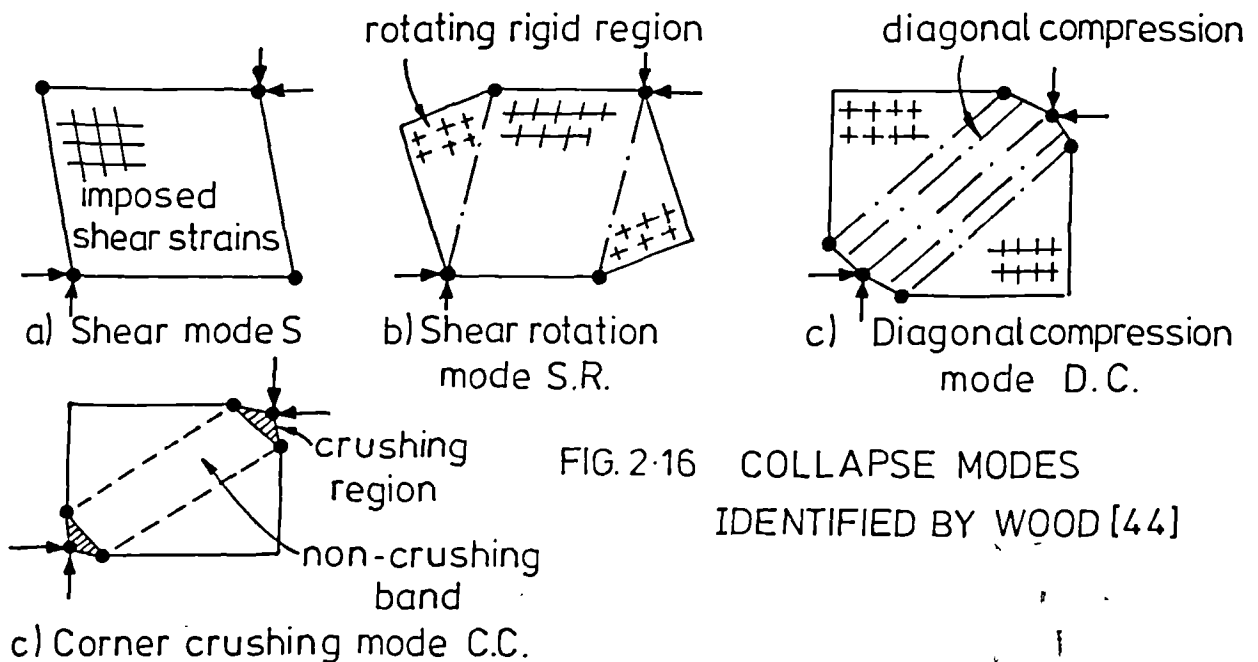


FIG. 2-16 COLLAPSE MODES IDENTIFIED BY WOOD [44]

members at the joints were derived. It was then proposed that the equivalent frame should be analysed by the various established methods. Two elastic models were made for the purposes of verification of the analysis. Both models were single closed frames constructed from perspex strips. The infills were made of rubber and gelatine. The specimens were tested under lateral loading. Good agreement was found between analytical and experimental results when the opening was more than 50% of the infill area. The method was, however, on a conservative side when the opening was less than 50%.

The method based on stress function in the form of Fourier series was again used to analyse infilled frames under diagonal loading by Liauw [42]. The stresses over the infill and the boundaries were analysed as previously described and with the same assumptions. Once the boundary stresses were determined, the infill panel was taken away and its effects on the bounding frame were represented by these boundary stresses. The problem was, then, that of a frame subjected to the external loads and the determined boundary stresses. A procedure of solving this problem was suggested by taking into account the compatibility conditions of displacement between the frame and the infill. The solution of the problem required the use of a computer. Three-dimensional and frozen-stress techniques of photoelasticity were used to give the necessary information about stresses in the infill for the three elastic models tested. Good agreement was found with the theoretical values. Two modes of infill failure were observed, tensile cracking along the compression diagonal and corner crushing at the compressive corners. From the stress analysis, the shear stresses were found to be predominant. It was concluded that the external shear load was largely taken up by the infill rather than the frame.

In 1983, in a paper published in collaboration with Kwan, Liauw [43] proposed a plastic theory for both single- and multi-storey infilled frames. Three collapse modes as shown in figure 2.14(a - c) were identified. These were respectively termed corner crushing with failure in columns, corner crushing with failure in beams and diagonal crushing. The first was associated with relatively weak columns and strong infill, the second with relatively weak beams and strong infill, and the third with relatively strong frame and weak infill. When analysing the different collapse mechanisms, assumption was made that the infill exerted a uniform pressure of intensity equal to the crushing stress of the infill material between the hinges in columns and the loaded corners for mode 1 and between the hinges in the beams and loaded corners for mode 2 (figure 2.15(a - b)). As for mode 3, a parabolic stress distribution was assumed against the lengths of contact of columns as shown in figure 2.15(c). The solution of the problem consisted then of resolving forces (horizontal for modes 1 and 3, and vertical for mode 2), neglecting axial forces in frame members for modes 1 and 2, and taking moments about loaded corners. Very good agreement was found between the proposed theory and experimental test results reported by Barua and Mallick [29], Mallick and Severn [39], Mainstone [20] and Kadir and Hendry [23].

2.4.5 Wood

From the observations of full-scale tests carried out at the B.R.E. (Building Research Establishment) by different investigators, a method based on the theory of plasticity was developed and presented by Wood [44] in 1978. Four collapse mechanisms as shown in figure 2.16 were identified. These were found to depend on the relative strength

of the frame to the infill defined by the parameter, m_n . Mode S (shear mode) was observed for strong frames with weak infills. Mode SR (shear rotation) observed for medium strength walls. Mode DC (diagonal compression) observed for weak frames with strong walls. Finally mode CC (corner crushing) was observed for strong walls with very weak frames. The theory was based on the work equation of the infilled frame when both the infill and the frame had reached the plastic limit. The dissipation of energy in the infilled frame was taken as the sum of the separate dissipations of energy in the infill and in the frame. Combining Nielsen's [45] idealized plastic yield criterion for membranes which are either crushed at constant yield stress or cracked at zero (constant) tensile stress, and using standard plastic theory for the framework, modes S, SR and DC were predicted in proper order of decreasing relative frame strength. The ultimate change to mode CC was predicted but Wood saw it rather as a particular case of mode DC. For each mode, an appropriate collapse mechanism was derived. The infill was supposed to exert a hydrostatic pressure on the frame.

Two non-dimensional parameters, f and m_n , were introduced. The first was used to determine the collapse load and the second was the nominal frame: infill strength ratio. The theoretical collapse loads were put in the form f controlled by m_n . The expression for f varies with the collapse mode identified. These parameters were capable of predicting changes of collapse modes and are discussed in more detail in 5.3.2 and 5.5.2. Initially the method was developed for the case where the beams and columns had an equal plastic moment. When the beams were different from the columns, f and m_n were redefined. Changes of f were studied for lower bounds only. Finally a simplification of the method for code of practice purposes was proposed.

Design charts were presented for single panels. It was concluded that the curves relating theoretical collapse loads and the nominal frame - wall strength, m_n , did not vary markedly with the shape of the panel. It was suggested that only the expression giving f for the case of square panels with equal plastic moments in beams and columns, f_s , should be taken as a basis, and that all the other curves should be plotted as an increment, Δf , to be added to f_s . Design charts were derived for this purpose. A penalty factor termed, γ_p , was, however, introduced to allow for idealization of plasticity. This factor was used to lower the effective crushing strength of the infill because of the limitation of yield strain. The effective relative strength parameter, m_e , was defined as m_n / γ_p . For steel frames, γ_p was found to vary between 0.23 and 0.45 for brickwork infills and from 0.2 to 0.65 for micro-concrete infills. γ_p was derived from tests on full-scale structures conducted at the B.R.E. [3, 7, 16] and from models carried out by Mainstone [20], Kadir and Handry [23] and by S. Smith [31].

The method was primarily developed for steel frames. It was, however, suggested that it could be used for reinforced concrete frames bearing in mind that these are more sensitive to the high hydrostatic pressure from the infill, which might induce shear failure in the frame, particularly if there is tension in the column on the windward side. From the tests conducted by Fiorato et al [18] on reinforced concrete frames infilled with brickwork, γ_p was found to be very low and varied from 0.05 to 0.12. Thus, a low value of γ_p was recommended to provide safeguards for combined tension, shear and bending. The design recommendations included the case of rectangular panels, multi-bay and multi-storey with or without wall panels.

The proposed method was highly disputed especially by Mainstone

[46]. The main criticisms concerned the limited ductility of the infill, the use of the penalty factor and the identification of the different collapse mechanisms. Mainstone pointed out the fact that all infills had limited ductility and, in nearly all cases of practical relevance, had passed their peak contributions to the composite strengths well before plastic hinges developed in the frames. The mode of failure of the infill was always essentially diagonal compression even when hinges developed in the frame. The empirical penalty factor, γ_p , was seen to reconcile calculated and measured strengths rather than to be a stress reduction factor. Mainstone claimed that the relationships between the different widths of the diagonal strut and the relative stiffness parameter, $\lambda_n h$, were more physically meaningful and more convincing than those between γ_p and m_n .

The use of γ_p was, however, defended by P. A. C. Sims. γ_p was found not only to affect the values of m_n and f , but also to ensure that an altered mode could be applicable to the panels. This was verified realistically by the tests giving considerable support to the theory. P.A.C. Sims concluded that γ_p was a little more complex than just being a penalty for the use of idealized plasticity theory. He suggested that γ_p must also contain effects from other parameters not considered in the basic theory, such as the effect of elastic deformations and the use of an idealized yield criterion. In his reply, Wood pointed out that rigid-plastic theory was only an approximation for real behaviour, that the penalty factor, γ_p , caused smaller wall resistance to be derived than was given by elastic theory. He also indicated that plastic theory enforced greater frame strength, so that less would be claimed for the wall.

2.4.6 P. A. C. Sims

The previous approach was used for analysing reinforced concrete infill panels by P. A. C. Sims [47]. It was assumed that the collapse modes identified by Wood [44] for unreinforced panels could also be applicable to reinforced panels. The analysis was conducted in the same way as by Wood in predicting these modes in their correct order of increasing relative frame/panel strength. Analytically, exact solutions for the pure shear mode, S, were obtained for single panels having equally strong beams and columns. Numerically, exact solutions for the shear rotation mode, SR, were obtained for rectangular panels and for square panels having isotropic reinforcement. A very restrictive set of conditions for which the diagonal compression mode was valid was determined. It was concluded that this latter point suggested that either there were better solutions for this mode or that a more suitable mode existed.

2.4.7 May

The rigid-plastic theory was also used by May [48] for analysing infilled frames. A different approach was, however, used for determining the dissipation of energy in the infill. First of all, the work done in tension, compression and shear yield lines was determined for a rigid plastic non-tension material satisfying a square yield criterion. These yield lines were then used to analyse shear panels with bounding frames. The external work done by the racking load was taken equal to the sum of the energy dissipation in the hinges and the energy dissipation in the infill. The determination of the work in the yield lines eased the problem of expressing the energy dissipation in the infill. The equations were found to be easier to formulate than those developed by Wood [44]. The technique was used to

reanalyse all the modes examined by Wood. The results were found to be identical to those obtained by Wood. It was claimed that the method had some advantages over the approach used by Wood, the major ones being that in many cases the modes matched the collapse mode noted in tests more closely, and also that it was easy to apply to more complex problems such as panels with openings. Thus, the method was then used to obtain upper bound solutions for square panels with centrally placed square holes.

The work done by Wood [44] was extended by May and Ma [49] to cover cases in which the ultimate moment capacity of the joint, $k M_p$, ($0 \leq k \leq 1$) was less than or equal to the ultimate moment capacity, M_p , of the beams and columns. This work was necessary because, as noted by Wood, premature failure of the joints occurred in a number of tests. The analysis was conducted in the same way as by Wood. Three collapse modes were identified, S, SR and RSR (Revised Shear Rotation). The RSR mode is similar to Wood's SR mode but permits areas of unstressed infill adjacent to the unloaded corners. It was noted that, at low values of m_n , this mode gives identical results to Wood's DC mode and this latter mode was therefore not required. For $k = 1$, many of the RSR mode analyses were exactly the same as Wood's SR mode. Numerical results were derived to determine the best upper and lower bounds on the collapse loads for panels with $l_i/h_i = 1$ and 3 and $k = 0, 0.25, 0.5, 0.75, \text{ and } 1$. For square panels, the numerical analysis produced identical upper and lower bound solutions. For rectangular panels ($l_i/h_i = 3$) the discrepancy between upper and lower bounds was small. The maximum discrepancy was observed for pin-joints frames ($k = 0$) and ranged from 0.4% to 11.0%.

2.5 SUMMARY OF PREVIOUS WORK

2.5.1 Test Methods

Most of the investigations have dealt primarily with single-storey free standing infilled frames. Four different test arrangements have been used as shown in figure 2.17:

- (i) Fixed base: The tests conducted by Fiorato et al [18] employed combined loading (vertical loads on columns plus horizontal racking load applied at the middle of the top beam) and horizontal racking loading only. The tests carried out by Ockleston [4], Read [6] and Benjamin and Williams [13, 14] employed horizontal racking loading only. As for Irwin and Afshar [11], the vertical load was applied only on the windward column, and the specimens were subjected to cyclic loading.
- (ii) Back to back (simulating a solid foundation): This arrangement has been used by Coull [8], Mallick et al [9, 27, 29], Kadir [22], S. Smith et al [30-33, 35-36] and D.V. Mallick and Severn [39].
- (iii) Diagonal loading: This arrangement has been used by Saneinejad [12] and S. Smith [31].
- (iv) Horizontal racking loading with the windward column restrained at the top. This arrangement has been adopted by Thomas [3], L. G. Simms [7], Holmes [15, 17], Sachanski [28], and Mainstone et al [19-21].

2.5.2 General Behaviour of Infilled Frames

The idealized load-deflection response of an infilled frame shows four distinct regions as shown in figure 2.18:

- (i) An initial non-linear response of an indefinite nature due to

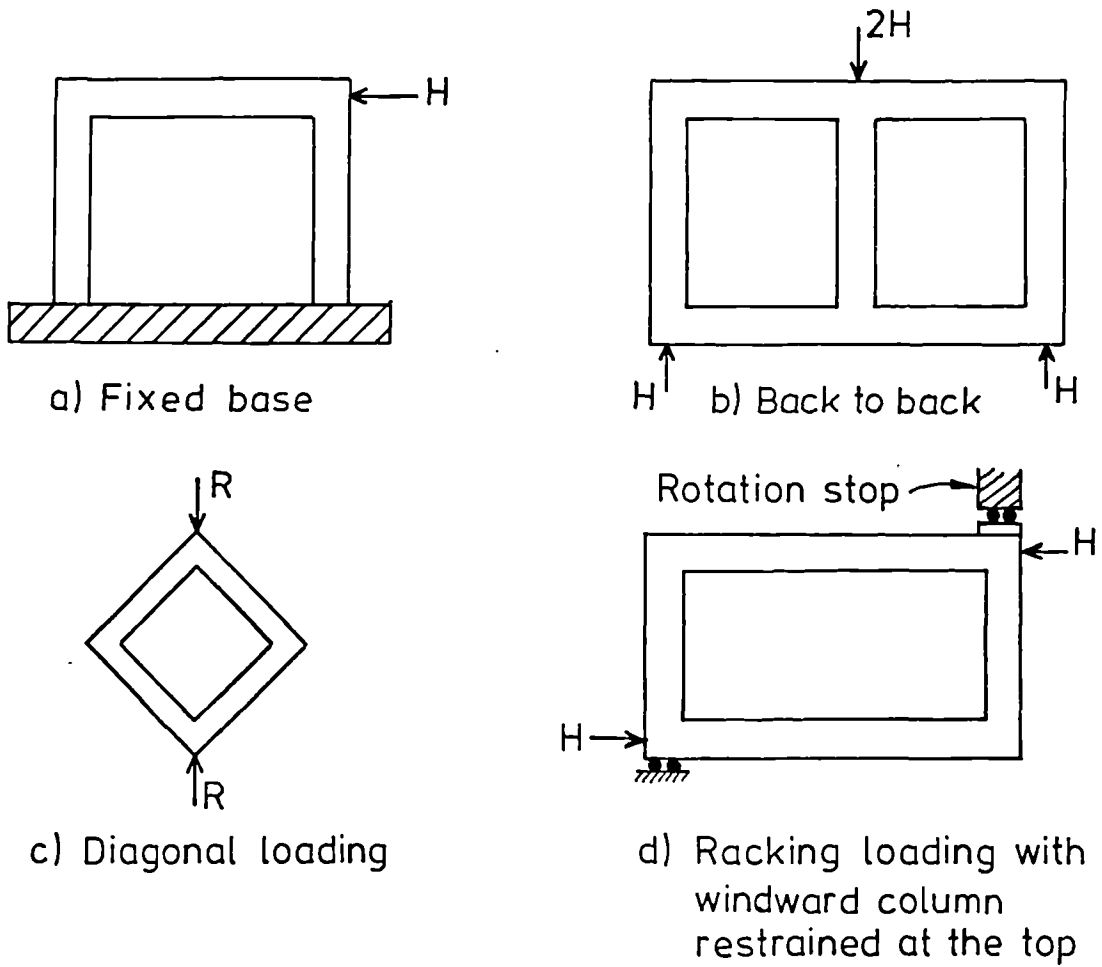


FIG. 2-17 DIFFERENT TEST ARRANGEMENTS FROM PREVIOUS WORK

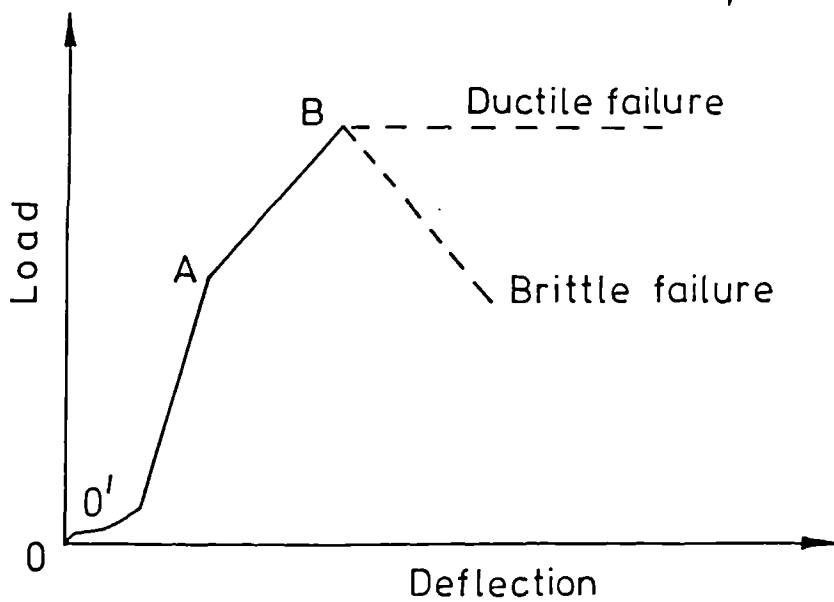


FIG. 2-18 IDEALIZED LOAD - DEFLECTION RESPONSE FOR STEEL INFILLED FRAMES

slip which occurs between the frame and the infill. This is the result of the lack of fit which is unavoidable in practical structures.

(ii) The second region is characterised by a straight line until the infill cracks or yields at one or both loaded corners whichever occurs first. In this region the composite structure behaves elastically and the experimental lateral stiffness is equal to the slope of the curve. During the loading, the infill and the frame separate and contact remains only in the vicinity of the loaded corners. The lengths of contact are referred to as α_λ against the beams and α_h against the columns.

(iii) Once the infill cracks or yields at one or both the loaded corners whichever occurs first, the response might still be idealized by a straight line with a smaller slope (after cracking occurs, the lateral stiffness drops). In this region the separation has already taken place.

(iv) Once the peak load is reached, the last part of the curve might be approximated either by a horizontal line defining, thus, a plastic plateau (ductile failure) or by a small horizontal line followed by a line with a negative slope, in the case of a brittle failure.

This type of response is basically for steel frames with infills of concrete or brickwork. The response for infilled reinforced concrete frames is slightly different because of the cracks occurring in the frame at an early stage of loading, the weakness of concrete in tension and the high sensitivity of reinforced concrete frames to shear pressures exerted by the infill which might lead to a premature failure. The difference in behaviour is discussed in more detail in

the light of test results in Chapter 4. The end of the initial elastic response shown in figure 2.8 might be seen as a serviceability limit state. The load causing the cracking of the infill was defined as an ultimate load by the investigators who concentrated on predicting only the initial elastic response of an infilled frame. This load may not in fact be the ultimate load carried by the composite structure. The composite may still be capable of carrying more load after the infill had cracked. The onset of stage (iv) constitutes the true ultimate limit state.

2.5.3 Stiffness Predictions

The initial lateral racking stiffness has been predicted empirically and theoretically. The methods used may be classified into the following:

(i) Methods based on strength of materials approach.

The infilled frame was treated as a vertical cantilever by Benjamin and Williams [13, 14] and by Fiorato et al [18]. Liauw [41] suggested a method based on the concept of an equivalent frame, wherein the parts of the infill were assumed to act compositely with the adjacent frame members, for infilled frames of centrally openings varying from 0 to 100% of the infill area. Kadir [22] used a similar approach for infilled frames with various sized centrally placed openings. The panel was replaced by a diagonal member of equivalent stiffness.

(ii) Methods based on the equivalent diagonal strut concept.

The infill was replaced by a diagonal strut whose thickness and Young's modulus were that of the infill and whose width has been defined differently by the various investigators. This width has

been predicted theoretically (S. Smith et al [30-33, 35-38]) by means of the finite difference or finite element approaches, or empirically (Holmes [15], Mainstone [19-21, 46] and Kadir [22]). S. Smith found that the theoretical values of w/d_1 were consistently higher than the experimental. These were adopted for calculating the lateral stiffness. Two widths of the diagonal strut were used in the calculations proposed by S. Smith and Carter [36]. But in the latest published papers, Smith [37, 38] suggested a conservative value of $w = 0.1d_1$.

For the infilled frames tested in the experimental investigation described in Chapter 3, w/d_1 was found to vary from 0.33 to 0.44 for $R/R_c = 0$ (R : diagonal load on infilled frame and R_c diagonal load to cause crushing of the infill) and from 0.12 to 0.13 for $R/R_c = 1$ for S. Smith and Carter's method [36]. It varied from 0.11 to 0.13 for Mainstone's [46] and from 0.27 to 0.48 for Kadir's method [22]. As for Holmes [15] and S. Smith and Riddington [37, 38] w/d_1 was respectively 0.33 and 0.1.

(iii) Methods based on direct applications of the finite difference and finite element analyses.

These two methods were used as a tool to predict the lateral deflections and therefore the lateral stiffness of an infilled frame. These methods were used by Sachanski [28], Mallick, S.K. and Barua [29], Mallick, D.V. and Severn [39] and Liaw [40, 42].

(iv) Methods based on the results of experimental investigations.

Empirical prediction equations for lateral stiffness were derived by S.K. Mallick and Barua for steel frames with concrete infill [29] and reinforced concrete frames with brickwork infill [27].

2.5.4 Strength Predictions

2.5.4.1 Tensile failure strength

This strength has been predicted empirically and theoretically. The empirical predictions were based either on the diagonal strut concept (Mainstone [19-21, 46]) or simply on test data (Mallick, S.K. and Barua [27, 29]). Mainstone proposed a specific width of strut based on test data for calculating this strength. The theoretical predictions were based either on the finite difference approach (S. Smith and Carter [36] and Sachanski [28]) or on the finite element approach (S. Smith and Riddington [37, 38]). From the stress analysis, the critical region was found to be the centre of the infill. The criterion was to equate the principal tensile stress in this region to the tensile strength of the infill material.

2.5.4.2 Shear failure strength

This mode was essentially observed for masonry infill panels. The basic relationship for shear strength, $f = f_{bs} + \mu \sigma_n$ was used by all investigators except Barua and Mallick, S.K. [27] who derived an equation for shear strength based on test results. The bond shear strength and the coefficient of friction were determined from tests. The shear and normal stresses were expressed at the centre of the panel in relation to the racking load. These stresses were, then, substituted in the basic relationship $f = f_{bs} + \mu \sigma_n$ to derive the cracking strength of the infill. In expressing these stresses, the approach differed from one investigator to another. For Benjamin and Williams [15] and Fiorato et al [18], the contribution of the frame was ignored and the horizontal and vertical reactions resulting from the loading were used to express the average shear and normal stresses. S. Smith and Carter [36] used the finite

difference approach, assuming a triangular distribution of interaction between the frame and infill over the lengths of contact, to express the stresses. S. Smith and Riddington [37] used the finite element method for the determination of these stresses. As for Kadir [22], he used early work by Seddon [25] on partially loaded concrete walls to express these stresses. Kadir [22] and S.K. Mallick and Barua [27] conducted an elastic analysis to add the frame contribution to this shear strength of the infill.

2.5.4.3 Ultimate strength

The ultimate strength of the composite structure has been predicted using three different approaches:

(i) Methods based on the diagonal strut concept.

The ultimate load carried by the structure was that which caused compressive failure of the infill. This failure was either localised to the compressive corners, corner crushing, (S. Smith and Carter [36], and Kadir [22]) or along the diagonal strut (Holmes [15], Mainstone et al [19-21, 46]). While S. Smith and Carter ignored the frame contribution, the others suggested that the frame strength could be added to that of the infill. Holmes and Mainstone proposed that the full plastic open frame strength should be added and Kadir suggested that the frame strength to be added is that calculated at a deflection, δ_f , corresponding to the maximum load in the infill. The criteria used for determining the ultimate load carried by the infill were different. Holmes and Mainstone assumed a uniform compressive stress distribution acting over an area $w \times t$ where w is the width of the diagonal strut and t , the thickness of the infill.

The criterion for failure was to equate the compressive stress

to the ultimate compressive strength of the infill material, f_{ci} . S. Smith and Carter [36] made the assumption that the compression corner was in a plastic state. This plastic region is shown in figure 2.10. The compressive stress distribution acted over an area $a_h t \sec \theta$. As for Kadir [22], the load carried by the infill was obtained by assuming a linear distribution of contact stresses over a length of the column equal to $w \cos \theta$ as shown in figure 2.6. The maximum stress occurring at the edge was taken equal to the ultimate compressive strength of the infill material. For the infilled frames described in Chapter 3, w/d_1 was found to vary from 0.16 to 0.23 for Mainstone's method [46], it varied from 0.30 to 0.57 for Kadir's method [22] and from 0.38 to 0.75 for S. Smith and Carter's method [36]. As for Holmes method w/d_1 was constant and equal to 0.33.

(ii) Empirical methods.

Based on test results, empirical equations were derived by S.K. Mallick and Barua [27, 29] and by Benjamin and Williams [13], to give the maximum load sustained by the structures.

(iii) Methods based on plasticity and collapse design approach.

The plastic analysis approach was used by Wood [44], Sims, P.A.C. [47] and May [48] to predict theoretically the different collapse loads corresponding to the different identified collapse mechanisms. Another mode of failure (knee-braced) was identified by Fiorato et al [18]. For this mode, the calculation of the ultimate load was, however, related just to the frame. The ultimate load was defined as the load necessary to develop the yield capacity of the braced columns.

2.5.5 Conclusions

There have been basically, three different approaches for investigating the behaviour of infilled frames: purely experimental work, experimental investigations leading to empirical prediction equations for stiffness and strength and theoretical investigations checked against experimental test results. Three types of frames, steel, concrete encased steel and reinforced concrete, have been used in combination with different types of infills made of brickwork, blockwork, concrete and reinforced concrete. The most widely used combinations of frame and infill have been those of steel frames infilled either with concrete or brickwork. The combination of reinforced concrete frames with lightweight blockwork appears to have been used only once, by Irwin [11]. The specimens were, however, subjected to cyclic loading.

The infill was found, not only, to increase considerably the strength and the stiffness of an infilled frame comparatively to a corresponding open frame, but also to reduce the flexural moments in the frame members (S. Smith [36] reported a reduction of 90%). The lateral stiffness and strength of the infilled frame were found to be greater than the sum of the two separate components acting alone. The parameters found to govern or influence the behaviour of infilled frames were the relative elastic stiffness of the frame to the infill, $\lambda_h h$, $\lambda_\ell \ell$ and $\lambda_n \ell$, and the relative plastic strength of the frame to the infill, m_n . Collapse of an infilled frame might occur through failure either of the frame or the infill. The possible failure modes of the frame included the tensile failure of the windward column and the shear failure of the columns and beams and their connections. The modes of infill failure when this latter was made of masonry were:

- (i) tension cracking along the mortar joints or through the masonry;
- (ii) local crushing near the loaded corners or along the compression diagonal;
- (iii) shear failure along the mortar joints.

This last mode did not occur for concrete infill. It was, however, found by most investigators to be the most critical for masonry infills.

There does not, as yet, appear to be any generally accepted method of design of infilled frames. Among the many possible reasons for this may be listed the following features of the various existing methods:

- (i) The wide range of different assumptions made.
- (ii) The wide range of approaches used.
- (iii) The large number of variables involved.
- (iv) The wide range of predicted stiffness and strength values (this is considered in more detail in Chapter 5).

The investigators who opted for empirical prediction equations for the lateral stiffness and strength of an infilled frame concluded that any sophisticated method would be superfluous because of the number of variables involved and the complexity of formulating them in exact mathematical form.

CHAPTER 3

CONSTRUCTION AND TESTING OF INFILLED AND OPEN FRAMES

3.1 CHOICE OF THE MODEL-SCALE

One of the major problems facing any experimental investigation on models is the choice of a suitable scale. The behaviour of the model should be representative of a practical full-scale structure and it must be ensured that the model size would neither alter the general behaviour nor the mode of failure. The scale effect is practically unavoidable for any model tested even if sometimes its effect is small and may be hidden in the general scatter of the test results. The choice of model scale is always to some extent a compromise. In order to minimize any possible scale effects the scale should be as large as possible but for reasons of economy and ease of building of specimens a small scale is desirable.

For the current experimental investigation a geometrical scale of 1 : 3 was chosen for the following reasons:

(i) It was shown from the test carried out by Benjamin and Williams [14] on third-scale reinforced concrete frames infilled with brickwork, by Hendry [50] on third-scale brickwork walls and by Rostampour [51] on third-scale blockwork walls, that the scale effect was not significant.

(ii) It was thought desirable that the block size should be large enough to enable the wall to be built in a vertical position using the normal block laying techniques used for full-scale walls. For a smaller model, the joint thickness would have to be reduced further and therefore it would be impractical to build the infill panel in the normal way. Investigators who used small-scale models ($\frac{1}{6}$ for Mainstone [19, 20] and $\frac{1}{8}$ for Fiorato et al [18]) had to build the

infill panels by laying the bricks horizontally with gaps for the horizontal and vertical joints and then injecting mortar to fill the gaps and form the 'bed' and 'perpendicular' joints.

(iii) The third-scale model was a convenient size to fit inside the available reaction frame.

3.2 TERMINOLOGY

Five different reinforced concrete frames referred to as frames 1 to 5 have been used in combination with three different infill panels. These infills have been labelled respectively S, M and W and were called conventionally, in relation to their thickness, strong wall ($t = 100$ mm), medium strength wall ($t = 57$ mm) and weak wall ($t = 35$ mm). Each individual specimen has been designated by three letters and one number.

- The first letter is either I or O, indicating whether it is an infilled frame or an open frame.
- The second letter characterises the type of loading to which the specimen was subjected: H, for horizontal racking loading only and C, for combined loading consisting of vertical loads on the columns together with the horizontal racking load.
- The third letter specifies the type of wall used, S, M or W.
- The number refers to the type of frame used, 1 to 5.

e.g., ICM4 indicates an infilled frame subjected to a combined loading system. The infill panel used is that of medium strength ($t = 57$ mm) bounded by frame type 4.

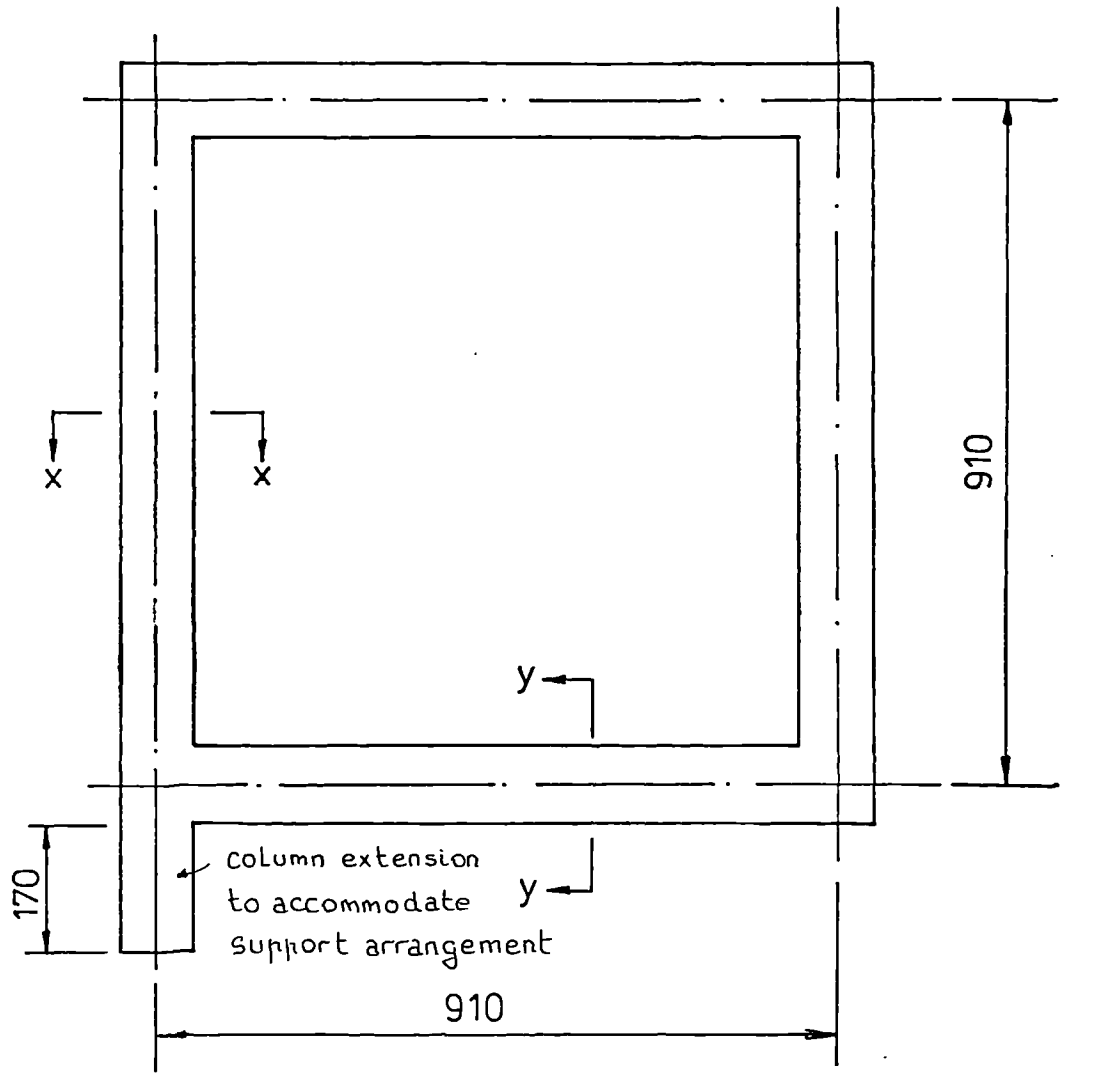
The duplicate specimens tested to check the repeatability have

been distinguished from their identical specimens by a star (IHM2 and IHM2*, ICM2 and ICM2*). One specimen, IHS1, which was subjected to horizontal loading only and for which failure occurred only in the windward column extension, was retested under combined loading and since it had the same dimensions and characteristics as ICS1, it was designated ICS1**. When the windward column extension failed, the response was still elastic. No noticeable changes occurred in the infill but the tension column had already cracked. The windward column extension was repaired by casting fresh concrete using rapid hardening cement around the steel tube which was rewelded to the reinforcing bars. (The details about frame description are given in section 3.3). The same type of failure occurred for IHM2. Its infill panel was damaged accidentally during removal from the rig. Its windward column extension was repaired in the same way and the specimen was retested as an open frame designated OH2⁰. The modes of failure are discussed in section 4.4.

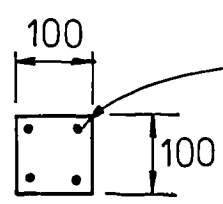
3.3 REINFORCED CONCRETE FRAMES

3.3.1 General Description

The frame sizes are shown in figure 3.1 and 3.2. The first three frames had the same geometrical characteristics and were symmetrically reinforced with four 6 mm, four 8 mm and four 10 mm high yield, deformed cold twisted bars. The schedule of reinforcement for all the frames is given in Appendix A . The extension of the windward column was of the same dimensions as the column and was 170 mm long. This extension was provided in order to accommodate the support arrangement (see section 3.6.1). It contained a 38 mm diameter core which was provided by casting a steel tube into the frame.



column extension
to accommodate
support arrangement



Four 6,8 or 10mm dia. bars
with 10mm cover

Section
x-x, y-y

Dimensions in mm

FIG. 3-1 GEOMETRICAL CHARACTERISTICS
OF FRAMES 1 TO 3

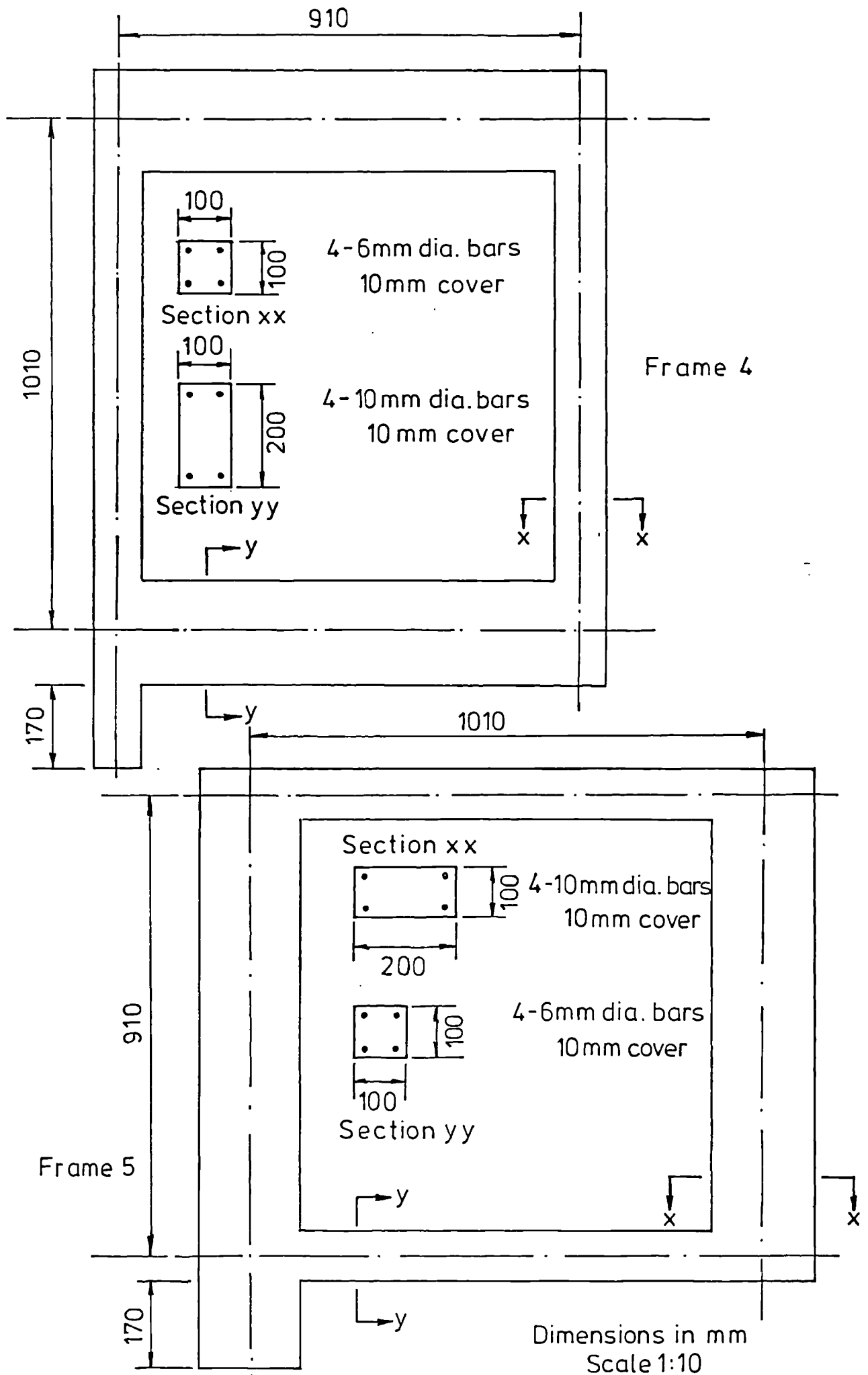


FIG. 3-2 GEOMETRICAL CHARACTERISTICS OF FRAMES 4 & 5

3.3.2 Concrete

Trial tests were conducted to find a suitable workable concrete mix with a target compressive strength of 40N/mm^2 . After a series of trial mixes, the concrete mix adopted and maintained for the whole programme was ordinary concrete made of ordinary Portland cement, locally available dry sand, and gravel of 10 mm nominal size. The mix proportions in parts by weight were 1 : 2.6 : 2.2 : 0.63 cement : sand : gravel : water. Details of the materials used are as follows:

Cement: ordinary Portland cement complying with BS 12 [52].

Fine Aggregates: sand of grading zone 2 complying with BS 882: Part 2: 1973 [53].

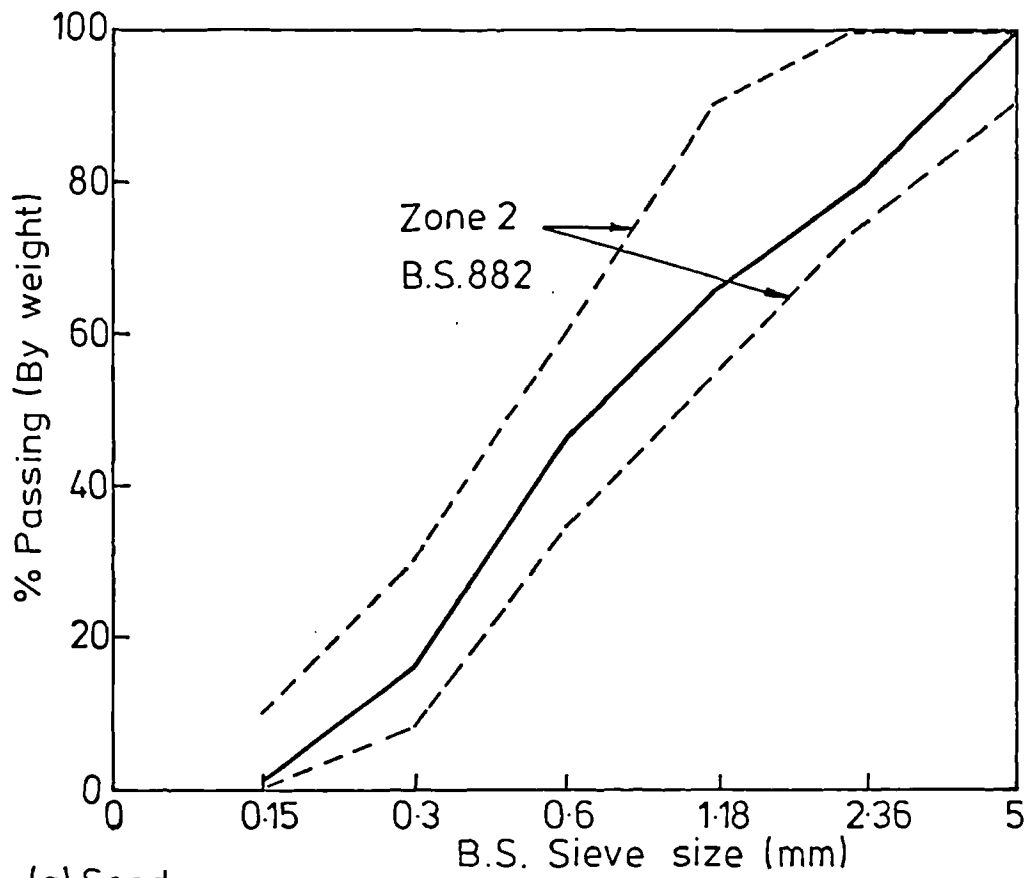
The grading curve is shown in figure 3.3(a).

Coarse Aggregates: gravel of 10 mm nominal size complying with BS 882: Part 2: 1973 [53].

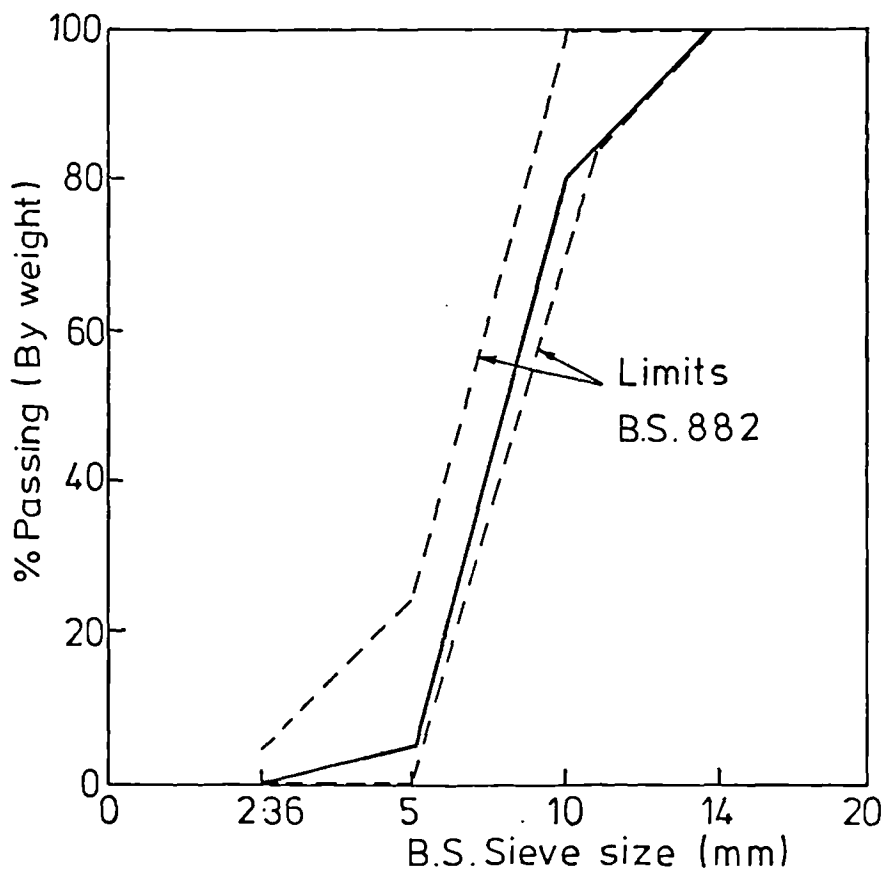
The grading curve is shown in figure 3.3(b).

Water: tap water free from any impurities.

Control test specimens in sets of three (prisms and cylinders) and in sets of six (100 mm cubes) were cast with each frame and cured with it (seven days under a sheet of polythene and then left uncovered in the laboratory atmosphere) were tested on the day the actual test on the infilled or open frame took place. In most cases this was at twenty-eight days after the casting of the frame. They were tested in accordance with BS 1881 [54] Parts 4 and 5. For the first two infilled frames tested, three beams 100 mm by 100 mm and 500 mm long were tested in flexure in accordance with BS 1881 Part 4 to give the flexural strength of the concrete. All the concrete control test results are given in Table 3.1.



(a) Sand



(b) Gravel of 10mm nominal size

FIG. 3.3 GRADING CURVES

FRAME DESIG- NATION	Cube com- pressive strength		tensile strength		flexural strength		static modulus of elasticity		age days
	f _{cu} N/mm ²		f _t N/mm ²		f _b N/mm ²		E _c KN/mm ²		
	M	SD	M	SD	M	SD	M	SD	
OHL	40.8	1.5	3.3	0.1	-	-	25.8	1.2	28
IHWL	43.4	1.1	3.5	0.1	-	-	24.9	2.9	28
IHML	43.4	0.3	3.5	0.2	-	-	27.0	0.6	28
IHSL	36.3	2.3	3.1	0.1	-	-	24.8	1.8	28
OCL	37.2	1.3	2.8	0.2	-	-	25.6	0.6	27
ICML	45.4	0.2	3.9	0.1	-	-	25.8	1.1	28
ICSL	41.3	0.7	3.7	0.3	-	-	28.0	0.6	28
ICSL**	36.3	2.3	3.1	0.1	-	-	24.8	1.8	43
OH2 ⁰	43.1	0.7	3.5	0.2	5.2	0.1	27.8	0.2	57
IHW2	36.3	0.9	2.8	0.2	-	-	25.7	1.7	28
IHM2	43.1	0.7	3.5	0.2	5.2	0.1	27.8	0.2	24
IHM2*	42.9	1.8	3.2	0.1	-	-	26.8	0.8	28
OC2	43.1	2.8	3.3	0.3	4.2	0.1	28.6	0.8	37
ICM2	46.8	1.0	3.4	0.3	3.9	0.1	27.0	0.2	115
ICM2*	45.2	2.0	3.1	0.2	-	-	27.7	0.2	27
IHW3	39.4	1.4	3.3	0.3	-	-	25.7	0.3	28
IHM3	44.6	0.5	3.5	0.2	-	-	25.6	0.6	29
ICM3	42.8	0.7	2.7	0.1	-	-	25.8	0.9	29
ICM4	39.9	1.4	3.2	0.2	-	-	26.8	0.6	28
ICM5	38.7	0.8	3.1	0.2	-	-	24.6	1.0	28

M: mean SD: standard deviation = $\sqrt{\text{VARIANCE}}$

$$\text{VAR} = \frac{\sum_{i=1}^N (X_i - \bar{X})^2}{N}$$

\bar{X} : mean -: no value available
 X_i : individual results

TABLE 3.1: CONCRETE CONTROL TEST RESULTS

3.3.3 Reinforcement Properties

The bars used as main reinforcement for the five different frames were high tensile cold twisted Tor bars of diameters 6 mm, 8 mm and 10 mm. These Tor bars complied in full with the requirements of BS 4461: 1978 [55]. The bars were of high bond strength, classified as type 2 deformed bars and readily weldable under normal conditions. The shear links were made from rolls of mild steel black annealed wire of diameter 3.25 mm. Results of the tensile test conducted on three specimens cut from each type of reinforcing bar and wire, in accordance with BS 18: Part 2, (1971): [56], are given in Table 3.2. Typical stress-strain curves for high tensile steel bars and black annealed wire are shown in figures 3.4 and 3.5.

3.3.4 Reinforcement Details

Beams and columns were reinforced with four bars yielding percentages of main reinforcement ranging from 1.1 to 3.1 and thus covering a realistic range for full-scale structures used in practice. Details of the arrangement of the reinforcement are given in Appendix A. One simplified 'typical' reinforcement arrangement is shown in figure 3.6. To ensure adequate anchorage, it was necessary to weld the bars at the corners. In the case of reinforced concrete frames subjected to horizontal racking loads, the reinforcement detailing in the two opening corners is very important to ensure a good efficiency; the efficiency of a corner being defined as the ratio of the corner strength from tests to the theoretical flexural strength of the members adjacent to it. The opening corner reinforcement detailing adopted for the five reinforced concrete frames was that which produced the highest efficiency in Taylor et al's tests [57-59]. It was found that all common details gave high efficiency

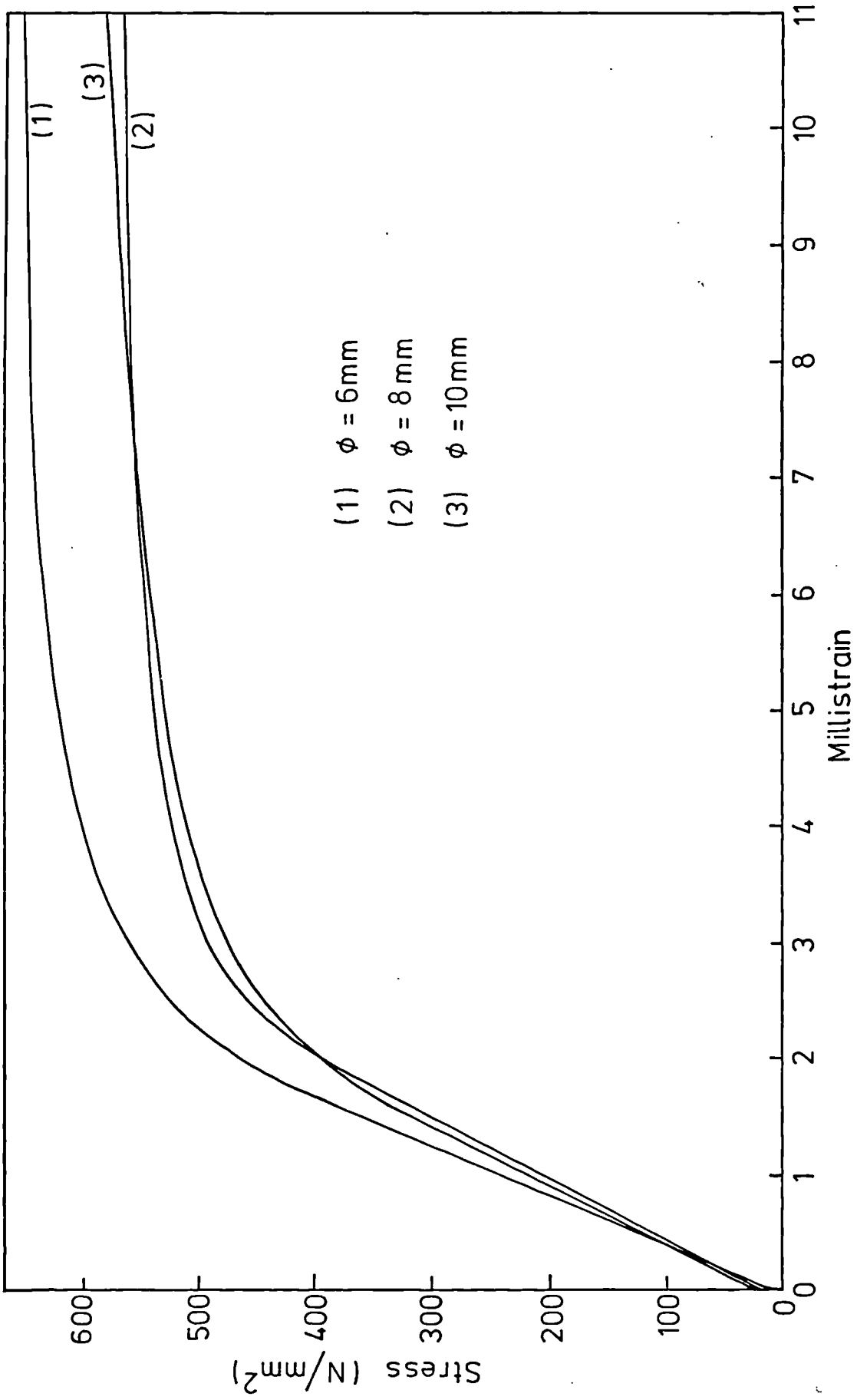


FIG.3-4 TYPICAL STRESS - STRAIN CURVES FOR HIGH TENSILE STEEL BARS

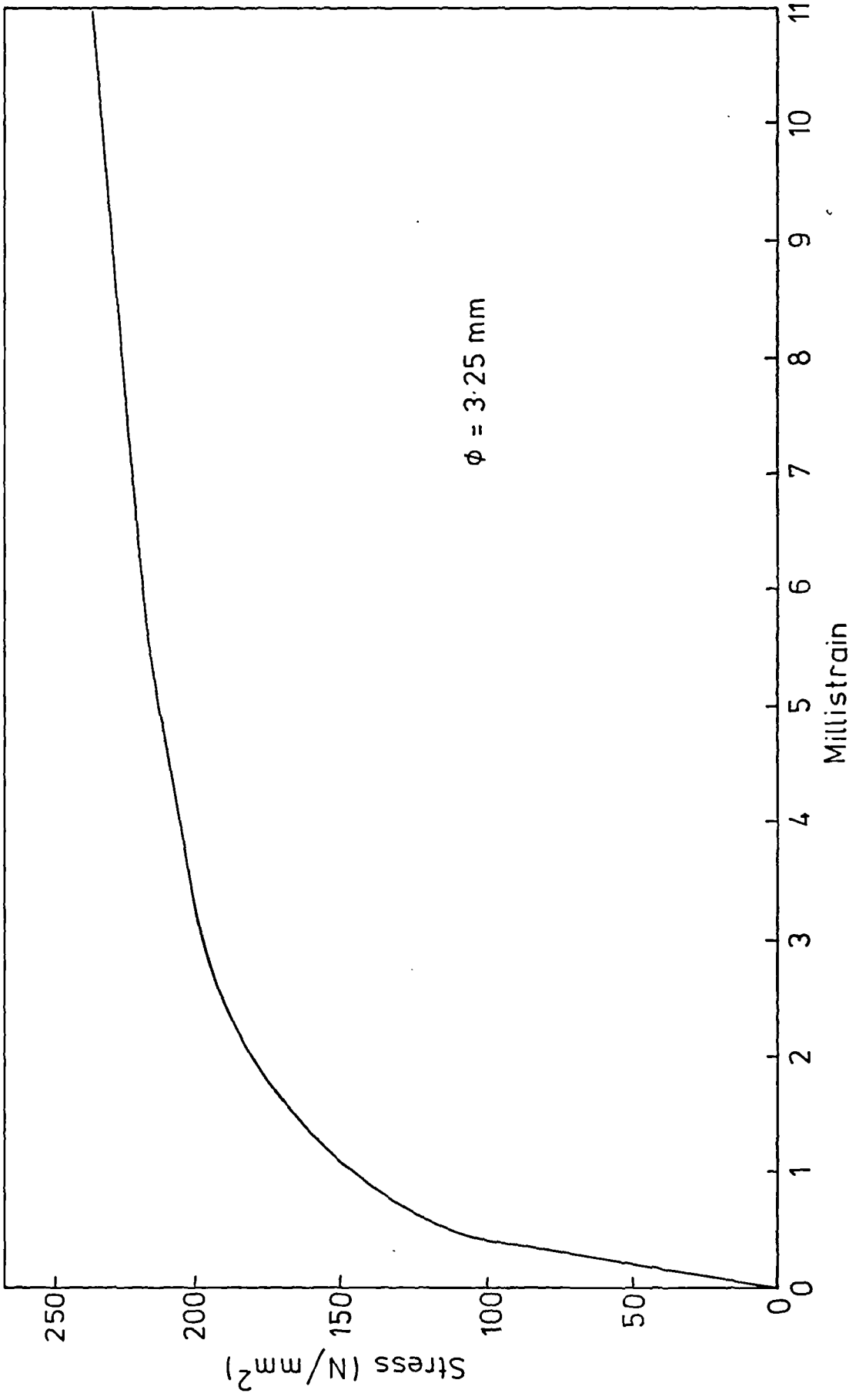


FIG.3.5 TYPICAL STRESS-STRAIN CURVE FOR WIRE

Scale 1:10 Dimensions in mm

•Welding

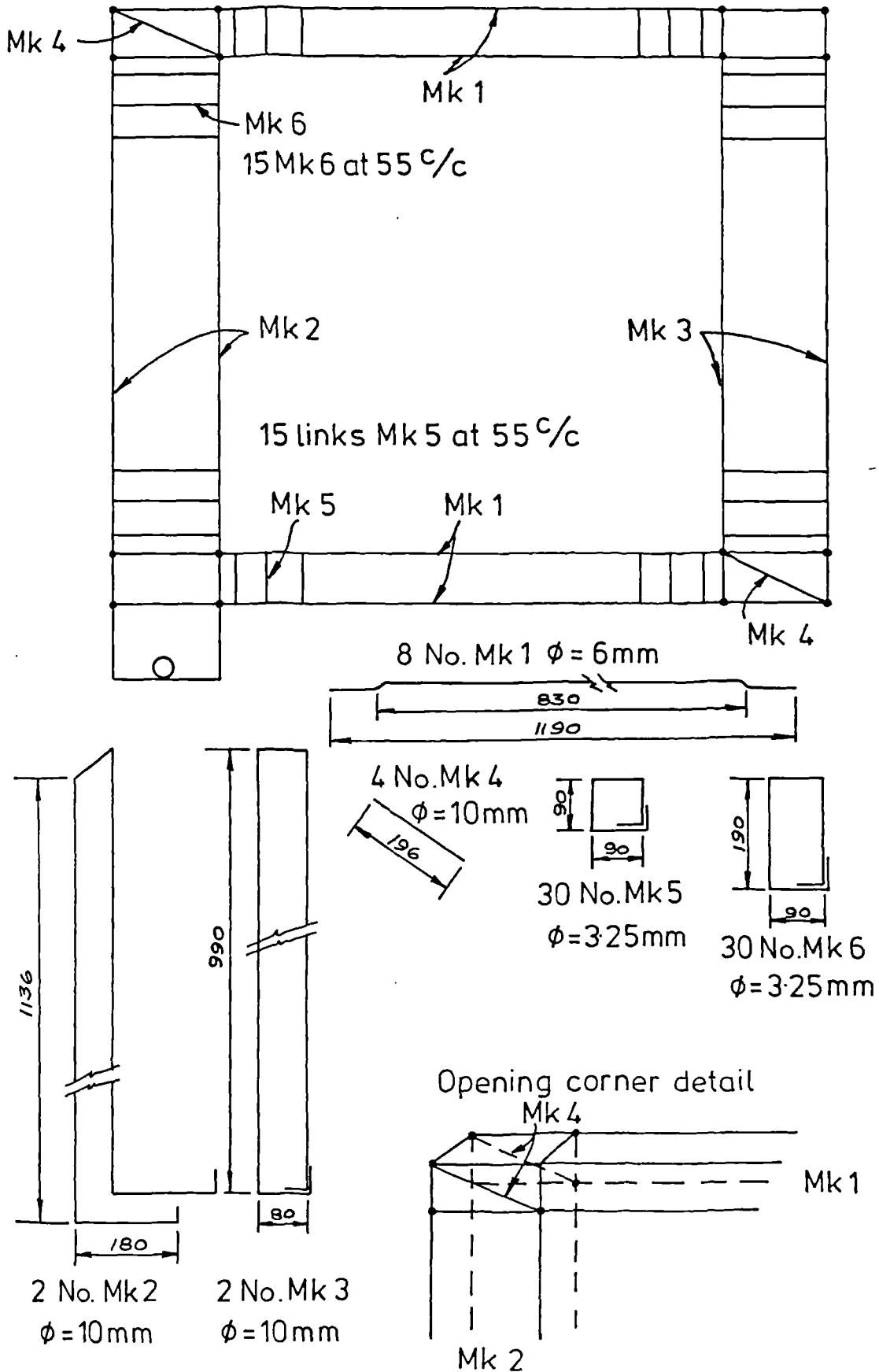


FIG.36 REINFORCEMENT DETAILS FOR FRAME 5

		ultimate strength f_u (N/mm ²)		yield strength				modulus of elasticity E_s (KN/mm ²)	
				f_{y1} (N/mm ²)		f_{y2} (N/mm ²)			
		M	SD	M	SD	M	SD	M	SD
HIGH YIELD COLD TWISTED BARS	$\phi = 6$ mm	724	18.8	628	16.1	633	15.6	232	6.2
	$\phi = 8$ mm	603	4.9	528	2.9	533	2.9	200	0.8
	$\phi = 10$ mm	621	4.0	540	2.4	542	3.3	196	1.9
BLACK ANNEALED WIRE ($\phi = 3.25$ mm)		305	4.6	189	8.5	199	11.5	171	8.8

M: mean of 3 test results

SD: standard deviation

f_{y1} : 0.2% proof stress

f_{y2} : yield stress determined from a 0.5% total elongation in accordance with BS 18 Part 2 [56]

E_s : static modulus of elasticity obtained by conducting a linear regression for all the points in the elastic region

TABLE 3.2: STEEL BAR AND WIRE TEST RESULTS

for closing corners but that the detail adopted here gave the highest efficiency (83%) for the opening corners. The main reinforcement of the beams and the columns were welded together at the four corners to form a stiff cage which itself was welded to the tube cast into the frame. All the main reinforcement bars had a cover of 10 mm.

3.4 INFILL PANELS

3.4.1 General Description

Three third-scale square infill panels 810 mm by 810 mm were used. The three infill thicknesses complied with the requirements of stability (a maximum slenderness ratio of 24 was recommended by Davies [60]). All infill panels consisted of twelve courses of lightweight aggregate concrete blocks laid with mortar of grade (iii) to BS 5628 [61]. The average thickness of the perpendicular and bed joints was 4.2 mm. All the blocks used in building the infill panels had the same face size 130 mm by 63 mm and were respectively 35, 57 and 100 mm thick.

3.4.2 Mortar

The mortar mix used was that recommended for laying blocks of specified characteristic strength varying from 2.8 to 10.5 N/mm² [62]. The mortar was made of ordinary Portland cement, hydrated lime and dry building sand. The nominal proportions in parts by volume were 1 : 1 : 5 (OPC : lime : sand). In order to ensure uniformity of the mix throughout the test programme it was decided to batch by weight. It was, therefore, necessary to measure the bulk densities of the three components. The measurements were conducted as follows: a quantity of material was poured without compaction into a gauge, the volume was recorded, then the quantity was weighed and the bulk

density determined as the ratio of weight to volume. The mean values of ten results for cement, lime and sand were respectively 1226, 491 and 1239 kg/m³. Thus, the mix proportions in parts by weight were 1 : 0.4 : 5.05 (OPC : lime : sand). The amount of water was found by conducting the dropping ball test in accordance with BS 4551 [63]. Finally the mix adopted was that which gave an average dropping number of 11 with a water cement ratio of 1 : 59 in parts by weight. This mortar mix was inspected by a qualified blocklayer who found it satisfactory for laying the blocks. The dropping ball test was conducted for the mortar before building commenced for all the infill panels. The dropping ball number results are given in Table 3.3.

Details of the materials used are as follows:

Cement: ordinary Portland cement complying with BS 12 [52].

Lime: calcium hydroxide (hydrated lime) complying with BS 890 [64] "Class A" code 190.

Sand: dry building sand complying with BS 1200: 1976 [65]. The grading curve is shown in figure 3.7. The sand was oven dried for twenty-four hours at a temperature of 100°C before it was used in the mortar mix.

Water: tap water free from any impurities.

Cubes in sets of three were prepared from each batch of mortar mixed and were tested in accordance with BS 4551 [63]. Due to non-availability of the required number of the same size cube moulds at the time of building the different infill panels, it was necessary to use three different sizes of cubes. The test results are given

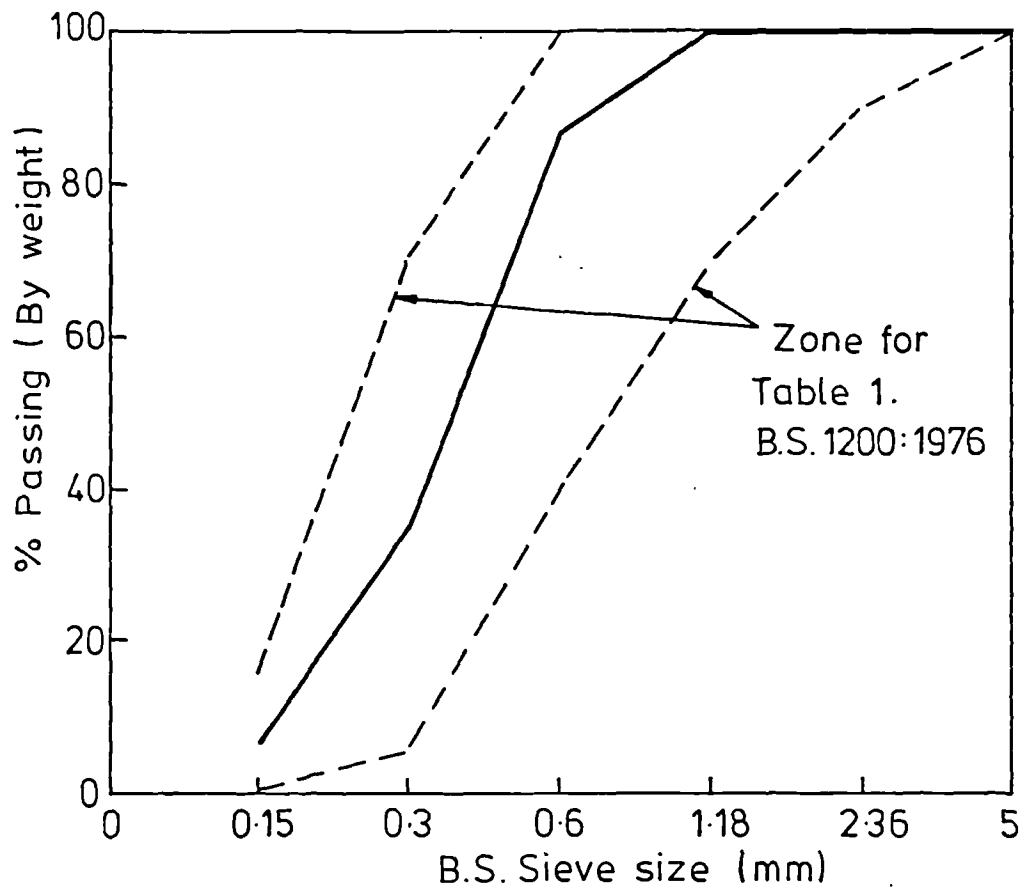


FIG. 3-7 GRADING CURVE FOR BUILDING SAND

Frame designation	compressive strength f_{cm} N/mm ²						splitting strength		dpn mm	age days
	(1)		(2)		(3)		f_{tm} N/mm ²			
	M	SD	M	SD	M	SD	M	SD		
IHW1	6.4	0.3	-	-	6.8	0.1	-	-	11.8	14
IHM1	7.0	0.9	-	-	6.5	0.2	-	-	10.8	15
IHS1	-	-	7.1	0.5	-	-	-	-	10.2	13
ICM1	8.1	0.2	-	-	6.0	1.0	-	-	10.0	13
ICS1	-	-	6.5	0.1	-	-	-	-	11.8	14
ICS1**	-	-	7.1	0.5	-	-	-	-	10.2	13
IHW2	7.1	0.2	-	-	-	-	-	-	10.6	15
IHM2	-	-	-	-	5.8	0.7	-	-	11.0	-
IHM2*	-	-	6.8	0.0	-	-	0.9	0.1	10.8	14
ICM2	-	-	-	-	6.4	0.4	-	-	11.0	100
ICM2*	-	-	6.0	0.4	-	-	0.3	0.0	11.0	14
IHW3	6.0	0.3	-	-	-	-	-	-	10.5	14
IHM3	-	-	7.2	0.4	-	-	-	-	11.8	17
ICM3	5.6	0.3	5.4	0.2	-	-	-	-	12.1	16
ICM4	-	-	5.8	0.3	-	-	0.6	0.1	11.8	14
ICM5	-	-	7.0	0.2	-	-	0.7	0.1	12.0	14

(1): mean of three 50 mm cubes

M: mean

(2): mean of three 75 mm cubes

SD: Standard Deviation

(3): mean of three 100 mm cubes

-: no values

dpn: dropping ball number in millimetres

f_{cm} : compressive strength of mortar

f_{tm} : tensile strength of mortar

TABLE 3.3: MORTAR CONTROL TEST RESULTS

in Table 3.3 and it can be seen that any influence of cube size is hidden in the general scatter of the test results. For some of the panels, cylinders of 50 mm diameter and 100 mm long were prepared in sets of three and tested to find the tensile strength of the mortar. The control specimens were cured in the same conditions as the infill panels and tested on the day the actual test took place (at fourteen days after construction of the wall panel). The rate of loading adopted for the compression and tension tests were respectively $4\text{N/mm}^2/\text{minute}$ and $0.4\text{N/mm}^2/\text{minute}$. These test results are also given in Table 3.3.

3.4.3 Blocks

The model blocks were obtained from full-scale solid 'Lytag' blocks with face size 440 mm by 215 mm and a thickness of 140 mm. The blocks had a specified characteristic strength of 7N/mm^2 [62]. The blocks were cut by a "Clipper" machine, using an abrasive blade and employing a wet cutting technique. The cutting, nevertheless, smoothed the surfaces. Thus the bedding and perpendicular surfaces of the model blocks were not similar to those of full size blocks. The method by which the three types of model blocks were obtained from full-scale blocks is shown in figure 3.8. Full-scale and model blocks were tested in accordance with BS 2028, appendices C and F [66]. They were either capped with two new pieces of 12 mm insulating board (fibre building board) complying with BS 1142 [67] or capped with mortar made of ferrocement and building sand. The mix proportions in parts by weight were 1 : 1.5 : 0.58 (ferrocement : building sand : water). The rate of loading adopted for testing the blocks or assemblies of blockwork was that for which failure would be expected after two minutes in accordance with BS 2028 [66]. This

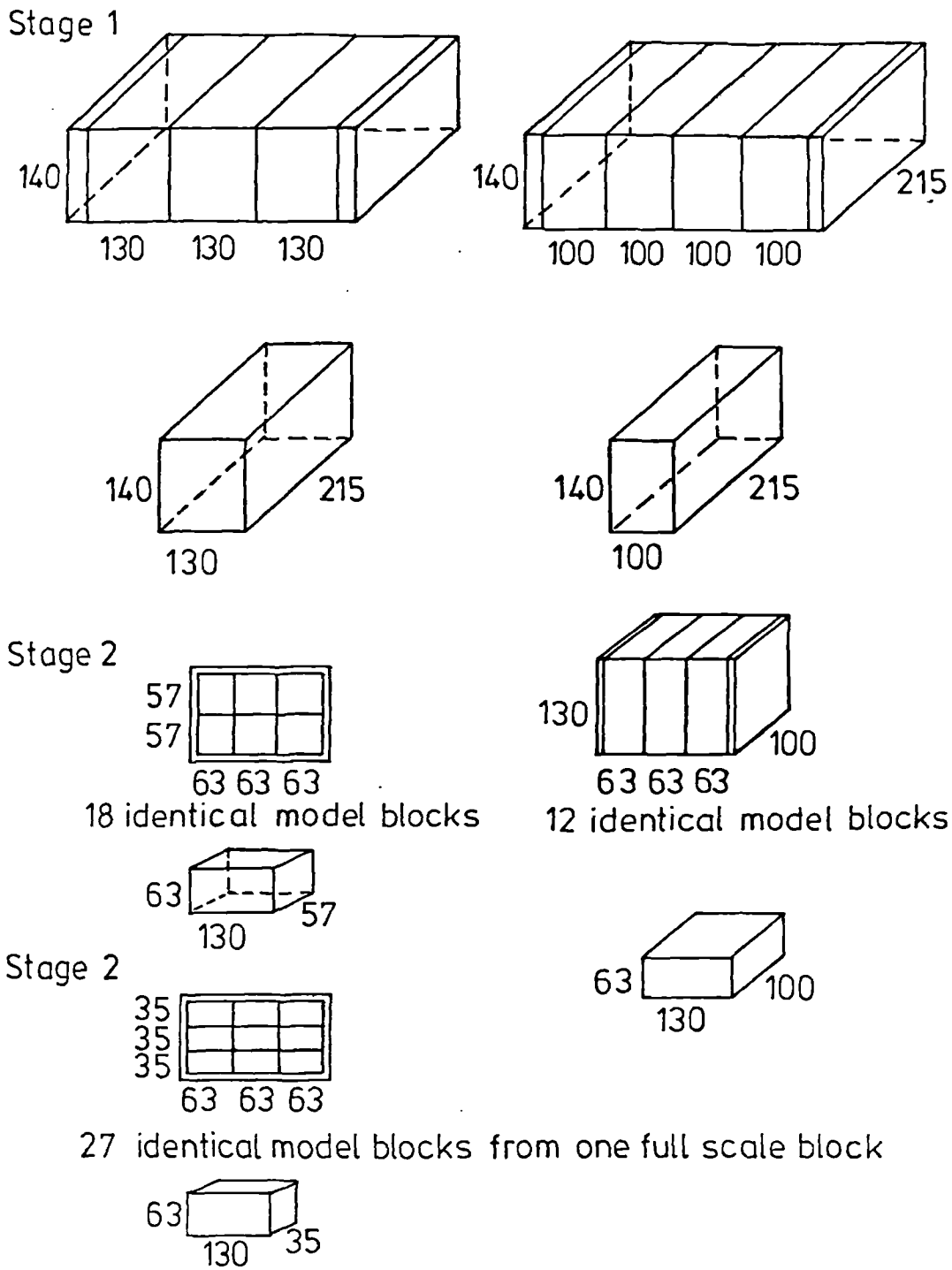


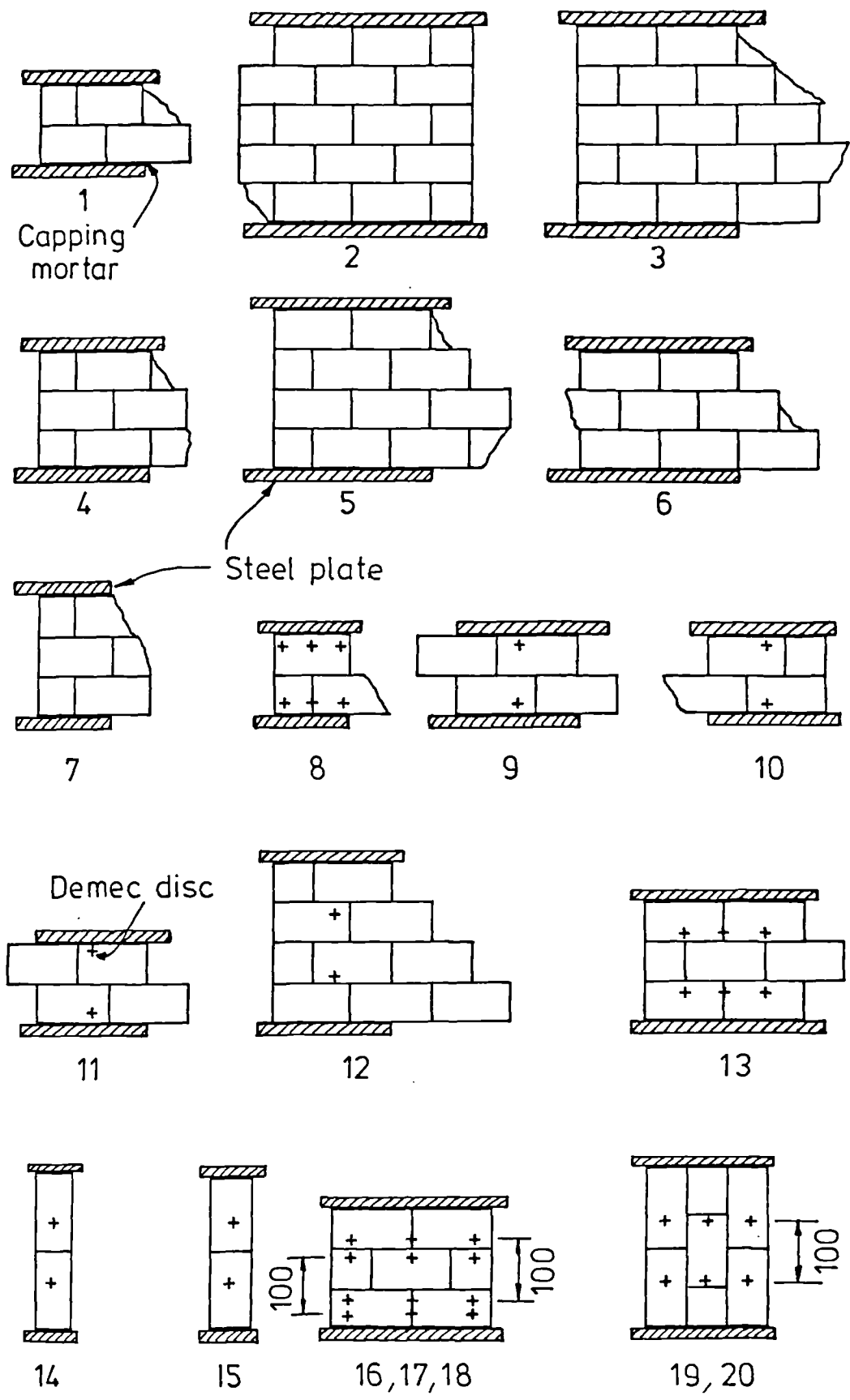
FIG. 3:8 METHODS OF CUTTING BLOCKS

rate was $4.5 \text{ N/mm}^2/\text{minute}$. The loading was applied perpendicularly to the bedding surfaces. Some model blocks were tested under a load normal to their perpendicular surfaces. All the results are given in Table 3.4.

3.4.4 Blockwork Compressive Strength

In order to determine the compressive strength of blockwork, five specimens as shown in figure 3.9 (specimens 16 to 20) were prepared and cured in the same conditions as the actual infill panels. The specimens were three course assemblies, as those adopted by Hamid and Drysdale [68], with two model blocks per course. A high prism with a slenderness of 3.6 was adopted in order to have the centre blocks free from any artificial confining effects. Three specimens were subjected to a compressive load perpendicular to the bed joints whereas the other two were subjected to a load parallel to the bed joints. The specimens were capped at each end, as for the blocks, with the same capping mortar whose five day compressive strength was 23.3 N/mm^2 . The specimens were tested at fourteen days. The thickness of all the specimens was 57 mm. The rate of loading was that adopted for testing the blocks ($4.5 \text{ N/mm}^2/\text{minute}$).

Compression tests were also conducted for some assemblies of blockwork recovered from the earlier infilled frames tested. These were also capped with mortar prior to testing. The configuration of the specimens tested is shown in figure 3.9. No attempt was made to cut the specimens (1 to 13 in figure 3.9) to a regular size, since it was felt that this might lead to damage to, or disintegration of, the specimens. The different results are grouped in Table 3.5. The compressive strengths given in the table are calculated on the basis of the bearing areas between the steel plates and the specimens.



Scale 1:10

FIG. 3-9 SPECIMENS USED FOR COMPRESSION TESTS

SERIES		compressive strength f_{cb} N/mm ²	
		MEAN	S. DEV
1	10 full-scale blocks capped with insulating boards. The blocks were immersed in water for 138 hours prior to testing.	9.0	0.6
2	10 model blocks capped with insulating boards. The specimens were stored in a mist room for 96 hours prior to testing.	10.1	1.0
3	44 model blocks recovered from IHM1, IHM2, ICM1, ICM2, IHM3 and ICM3. The blocks were capped with mortar.	10.4	1.6
4	3 model blocks with load applied normal to the perpendicular surfaces. Both blocks capped at both ends with mortar.	5.7	1.0

Note: the model blocks tested had a face size of 130 mm by 63 mm and a thickness of 57 mm.

TABLE 3.4: BLOCK COMPRESSIVE STRENGTH

SERIES	SPECIMEN TYPE (FIG 3.9)		$\frac{h}{t}$	θ	age (days)	f_{cbw} (N/mm ²)			E_{bw} (KN/mm ²)		
							M	SD		M	SD
1	1	recovered	2.5	90	421	5.8			-	-	-
	5	from ICM2	4.8	90	421	5.0			-	-	-
2	2	recovered from ICML	6.1	90	158	6.3			-	-	-
	3		6.1	90	158	4.6	5.4	0.4	-	-	-
	4		3.6	90	158	5.2			-	-	-
3	6	recovered	3.6	90	224	5.9	5.6	0.3	-	-	-
	7	from IHM3	3.6	90	224	5.3			-	-	-
4	8	recovered from IHM2	2.5	90	125	10.3	8.6	1.4	9.5	1.6	
	9		2.5	90	125	8.8			4.6		
	10		2.5	90	125	10.0			6.9		
	11		2.5	90	125	7.1			8.0		
	12		4.8	90	125	6.6			6.1		
	13		3.6	90	125	8.9			5.6		
5	14	recovered	4.8	0	125	7.6	7.3	0.3	7.6		
	15	from IHM2	4.8	0	125	7.0			-	-	-
6	16	constructed in same conditions as the infill panels	3.6	90	14	8.1			4.3		
	17		3.6	90	14	7.1	7.8	0.5	6.7	5.2	1.1
	18		3.6	90	14	8.3			4.6		
7	19	same conditions as the infill panels	4.8	0	14	5.7	5.8	0.1	6.9	5.9	1.0
	20		4.8	0	14	5.9			4.9		

θ : angle between bed joint and line of application of load

$\frac{h}{t}$: slenderness ratio of the specimens

f_{cbw} : blockwork compressive strength

E_{bw} : static modulus of elasticity for blockwork

N.B. The mortar compressive strength for series 6 and 8 was 6.7N/mm² with a standard deviation of 0.2N/mm²

TABLE 3.5: COMPRESSIVE STRENGTH AND STATIC MODULUS OF BLOCKWORK

Compression tests on concrete blockwork, using four types of $\frac{1}{3}$ scale lightweight aggregate blocks commercially known as thermalite, leca, lytag and aglite, were carried out by Rostampour [51]. The test results were found to be closely predicted by the empirical formula proposed by Herrmann [69]. This formula was derived from numerous test results for a variety of blocks, both hollow and solid, and was expressed as $w = k \sqrt[3]{m \cdot s^2}$ where

w: blockwork compressive strength

m: mortar strength

s: block strength

k: block characteristic constant.

Rostampour [51] suggested that a value of $k = 0.9$ should be used. Herrmann's formula is also found to predict satisfactorily the ultimate compressive strength of the assemblies of blockwork, constructed in the same conditions as the infill panels and tested at the same age (fourteen days) (series 6 of Table 3.5). The block strength being 10.4N/mm^2 (Table 3.4) and the mortar strength 6.7N/mm^2 (Table 3.5), the predicted compressive strength is therefore equal to 8.1N/mm^2 . The difference between the mean compressive strength from tests and the predicted is, thus, less than 4%. The agreement is, however, less good for series 1, 2 and 3 and conservative for series 4. For this last series, the specimens were recovered from an uncracked infill (IHM2) whereas for the first three series, the specimens were recovered from cracked infills. The specimens were, nevertheless, inspected prior to testing and did not seem to contain any visible cracks. The fact that they were recovered from infills which were highly stressed could explain the relatively low compressive strength they produced.

3.4.5 Static Modulus of Blockwork

The initial tangent modulus of blockwork was calculated for the five specimens prepared and cured in the same conditions as the actual infill panels. Three pairs of Demec discs were stuck symmetrically about the centre line (specimens 16 to 20 in figure 3.9) in order to obtain a better estimation of the strain at the middle section. Strains were measured with a hundred millimeter mechanical Demec gauge. A typical stress-strain curve for this blockwork is shown in figure 3.10. The initial tangent modulus was also calculated for the assemblies of blockwork recovered from IHM2 (specimens 8 to 14 in figure 3.9). The static modulus was obtained by conducting a linear regression for all the points in the linear part of the curve. These results have also been given in Table 3.5.

3.4.6 Shear Strength of Blockwork Assemblies

It is generally accepted that the shear strength of masonry follows Coulomb's law. Thus the shear strength is expressed as the sum of the initial shear strength between the mortar and the masonry units (bond shear strength) and an additional strength due to friction $f = f_{bs} + \mu \sigma_n$. μ being the coefficient of friction and σ_n the pre-compression applied. In order to determine f_{bs} and μ , twenty-two specimens were fabricated using model blocks as shown in figure 3.11. The specimens were cured for three days under polythene sheeting and then left uncovered in the laboratory until they were due for testing (fourteen days). They were tested under different levels of pre-compression. The specimens were capped prior to testing with the same mortar used for testing the blocks and assemblies of blockwork. The shear test equipment is also shown in figure 3.11. The pre-compression was applied by tightening the nuts on the two threaded rods.

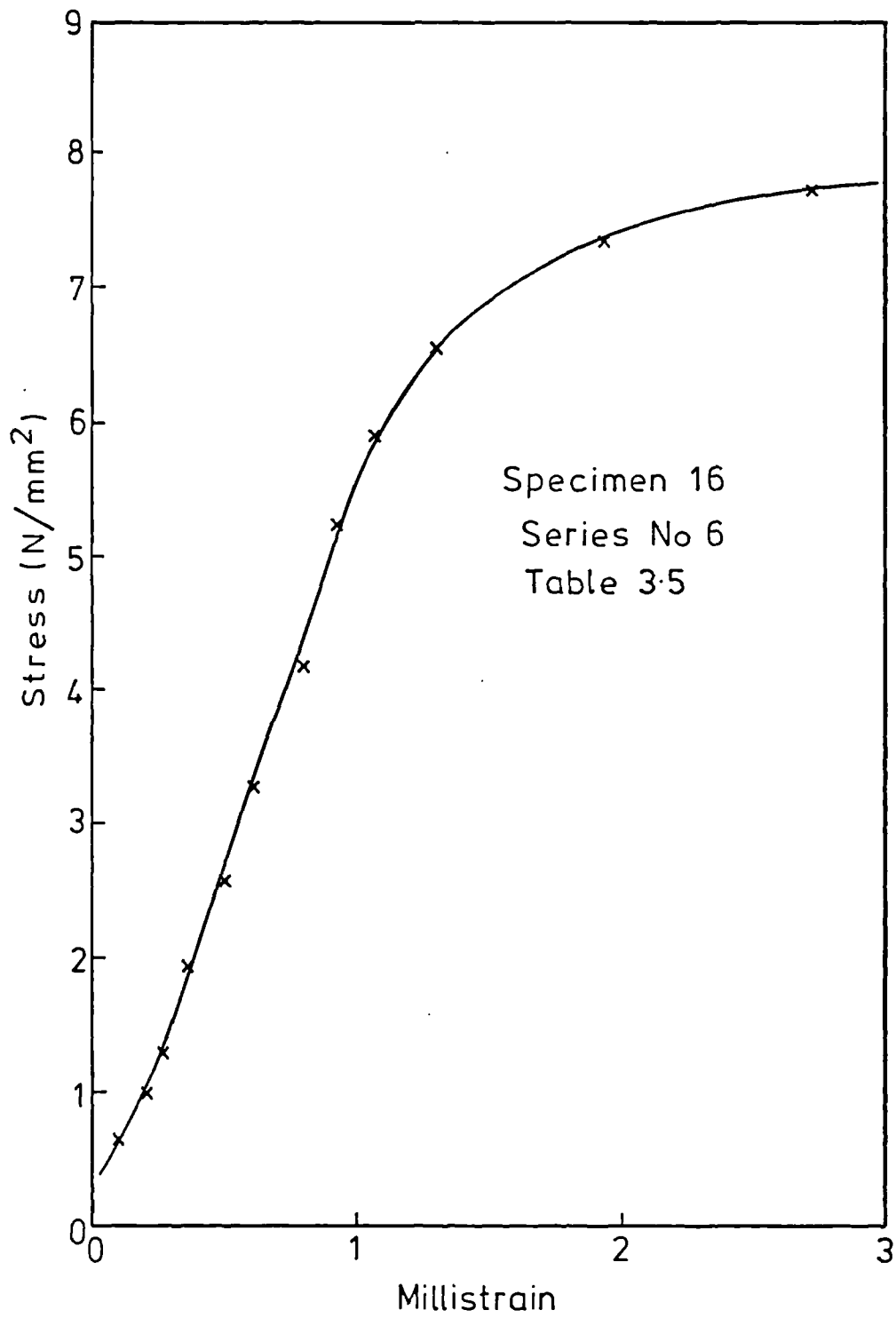


FIG. 3-10 TYPICAL STRESS-STRAIN CURVE FOR BLOCKWORK

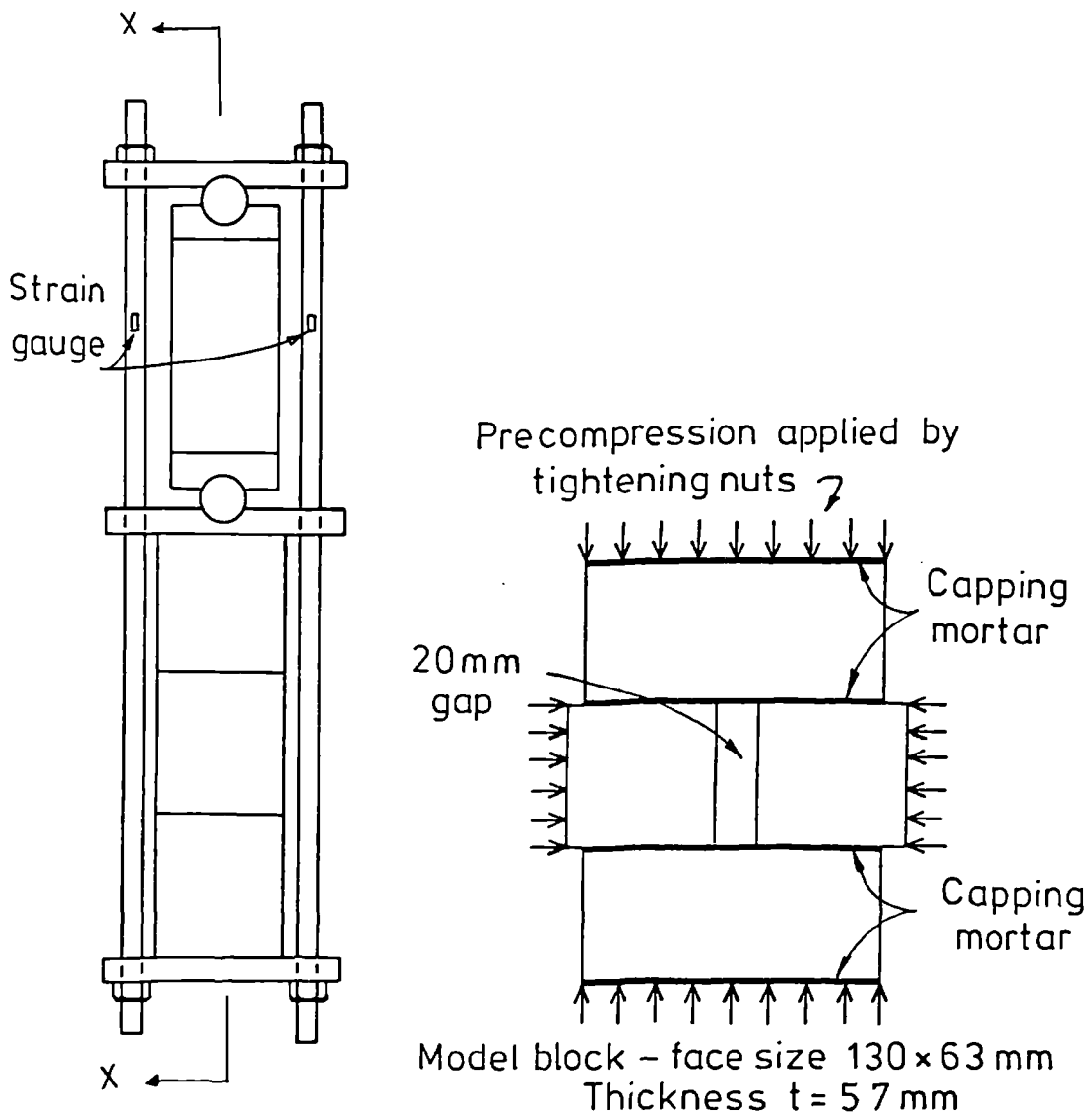
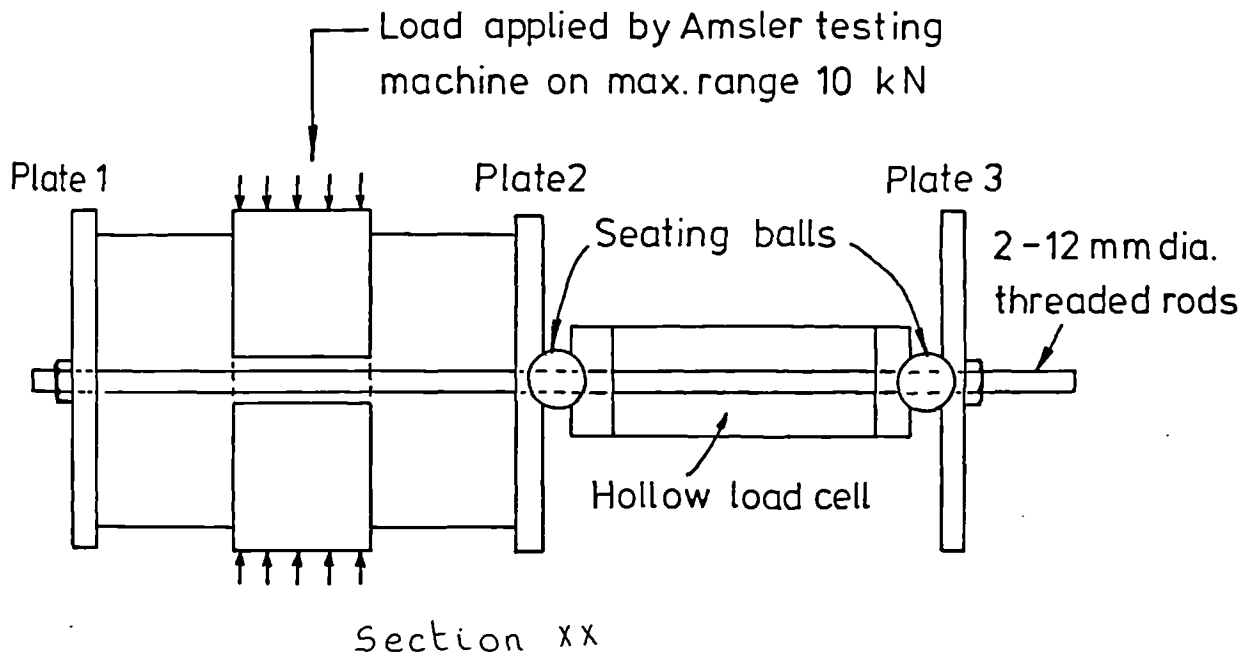


FIG. 3-11 SPECIMEN AND SHEAR TEST EQUIPMENT

The distribution of the loads was monitored by means of two electrical strain gauges fixed to the two rods. The readings from the gauges were monitored and used to control the tightening of the nuts so that equal loads were applied to each rod. The load-cell was used to monitor the total precompression load since it was 2.6 times more sensitive than the strain gauged rods. This load was given to an accuracy of $\pm 9\text{N}$. The calibration factor and the degree of accuracy are given in Table 3.7.

Table 3.6 summarizes the tests carried out and the results obtained. Some of the specimens were retested under a higher level of precompression after some or all of the joints had failed. In effect, once the joints had failed, the pieces were re-assembled and were subjected to a higher level of precompression and then retested again in shear. The failing load would, then, give the additional strength due to friction $\mu\sigma_n$ and therefore the coefficient of friction μ . But, as can be seen from Table 3.6, the value of μ seems to increase with the level of precompression applied. The mean value of μ varying from 0.27 for $\sigma_n = 0.5\text{N/mm}^2$ to 0.77 for $\sigma_n = 2.4\text{N/mm}^2$ (figure 3.12). One reason for this might, be attributed to the testing procedure and the difficulty of reassembling the pieces in their exact original places after the joints had failed.

For Hamid et al' [70] test results, the opposite effect was observed, μ decreased with increasing level of precompression for the retested specimens. Adopting the same testing procedure and the same type of blocks as those used in the current experimental investigation with a mortar mix 1 : 1 : 6 in parts by volume, Rostampour [51], however, found that the shear strength of blockwork masonry triplet due to friction was proportional to the applied precompression, $f = 0.73 \sigma_n$. The initial bond shear strength was found experimentally

f , f_{bs} and $\mu\sigma_n$ in N/mm^2

SPECIMEN NO.	σ_n (N/mm^2)												
	0	0.5		1.0		1.2		1.5		2.0		2.4	
	f_{bs}	$\mu\sigma_n$	f										
1	0.33					0.46	-					1.76	-
2	0.46					0.57	-					1.95	-
3	0.28	0.15	-	0.31	-			0.81	-	1.14	-		
4	0.28	0.12	-	0.42	-			0.75	-				
5			0.86					0.87	-				
6			0.68					0.90	-				
7			0.62			0.51	-			1.30	-		
8					1.00					1.27			
9					1.20			0.93	-				
10					1.10							1.81	-
11							1.10			1.70	-		
12							1.30			1.55	-		
13							1.35					1.92	-
14									1.52				
15									1.34				
16									1.58				
17										1.99	1.84		-
18										1.70			
19										1.89			
20													2.00
21													2.30
22													2.18

N.B. Mean compressive strength of three 100 mm cubes of mortar was $6.8 N/mm^2$
SD: $0.2 N/mm^2$

TABLE 3.6: SHEAR TEST RESULTS

to be equal to $0.5N/mm^2$. Since testing triplets with failed joints produced three different answers, μ increasing with increasing σ_n , μ decreasing with increasing σ_n and μ and σ_n proportional, the logical conclusion would be to reject this testing procedure and to rely only on results obtained for triplets with unfailed joints and under different level of precompression. The relationship obtained by conducting a linear regression for the test results of the twenty-two specimens (omitting those of the retested specimens) was $f = 0.34 + 0.76\sigma_n$ as shown in figure 3.12.

3.5 CONSTRUCTION OF THE INFILLED FRAME

3.5.1 Reinforced Concrete Frame

The mixing was conducted in accordance with BS 1881 [54]. Only one mix batch was necessary to cast the frame, six 100 mm cubes, three cylinders and three prisms. The aggregate and the cement were placed in the $0.2m^3$ mixing bowl and mixed for about two to three minutes to ensure adequate dispersion. Then, while mixing, the water was poured at a uniform rate into the bowl, mixing continued for two minutes after the water had been poured. The mixer was then stopped and the paddle and sides of the bowl were cleared down. The mould for the frame, whose detail is given in figure 3.13, and those for the control specimens were put on a vibrating table. The frame was cast horizontally. The reinforcing cage was welded to the tube which was bolted down to the bottom of the mould. The different moulds were, then, filled to about half their height and vibrated for about two minutes to achieve compaction.

The moulds were then over filled and vibrated until all bubbles of air disappeared to ensure a good compaction. The surfaces were then struck off plane and levelled with the tops of the moulds using

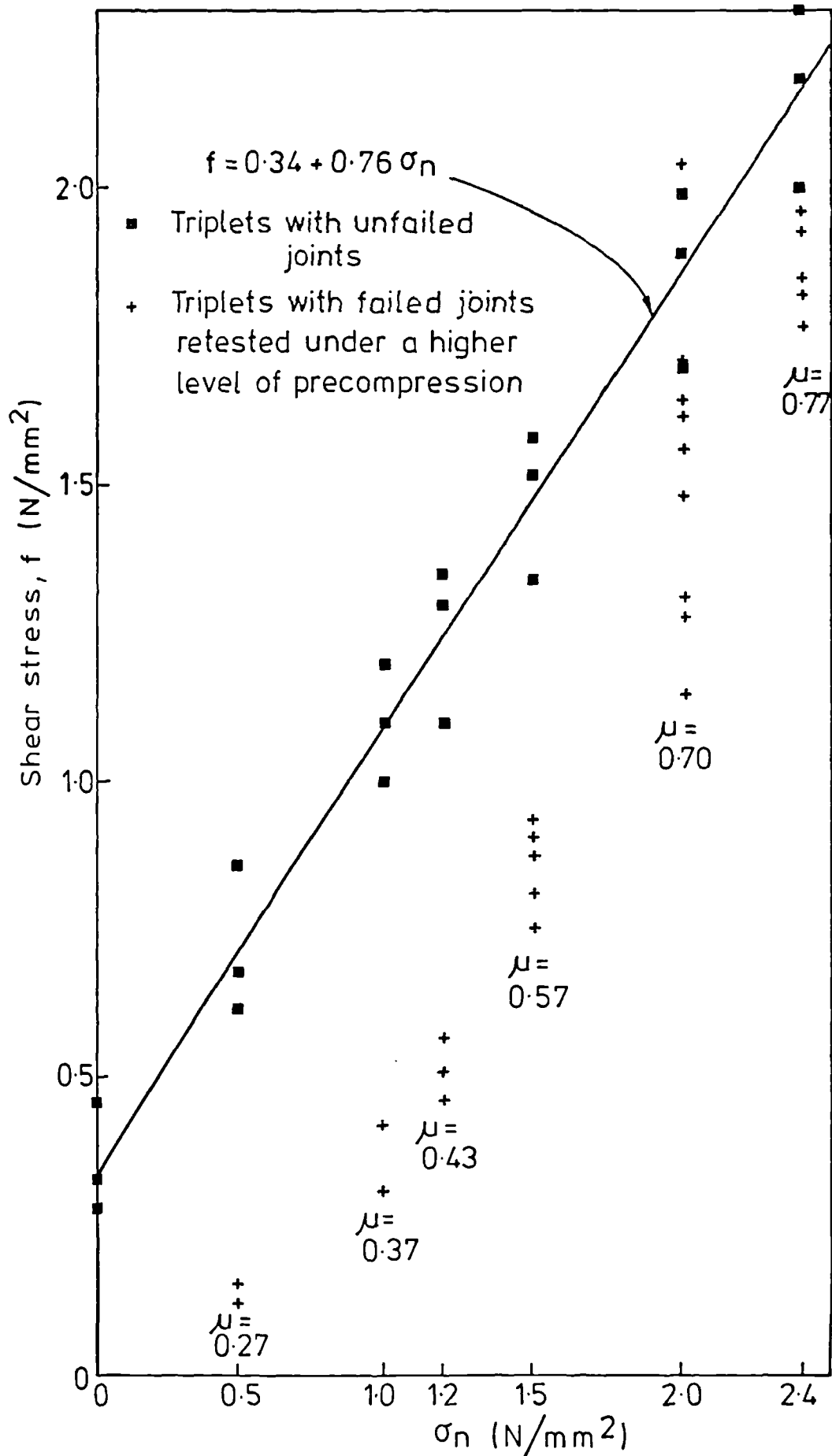
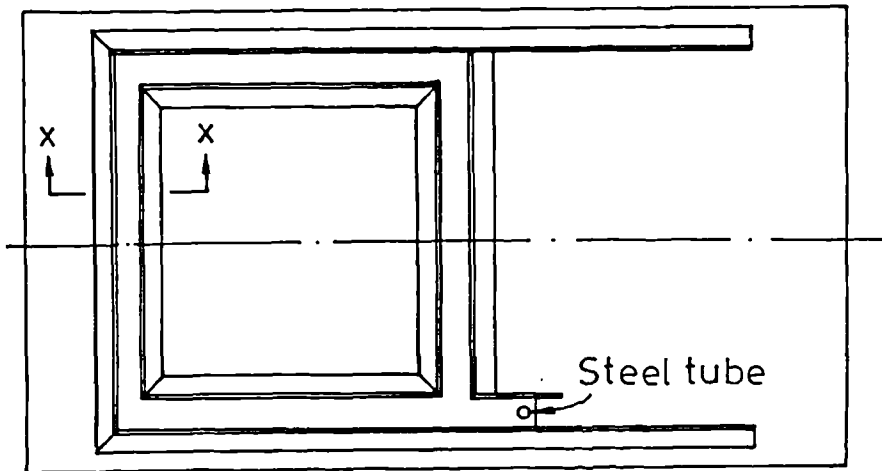
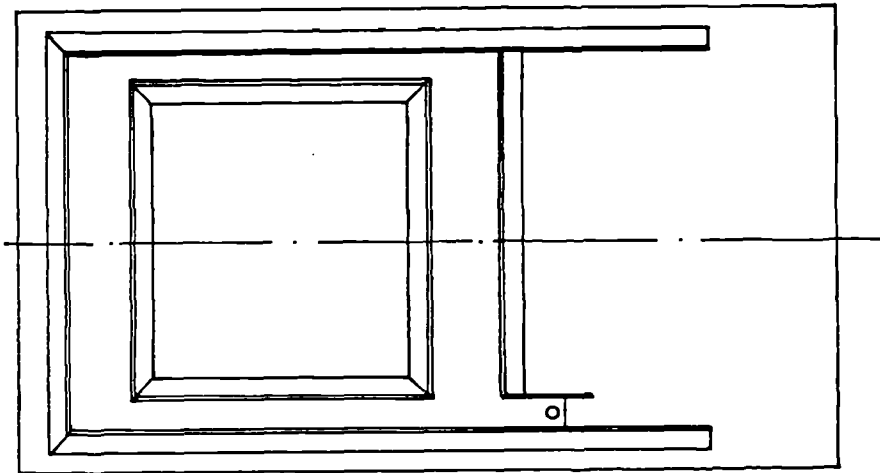


FIG. 3-12 SHEAR TEST RELATIONSHIP

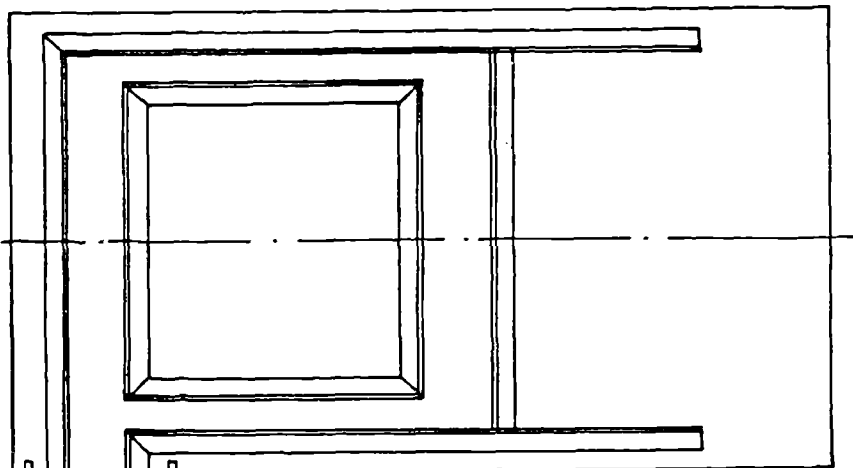
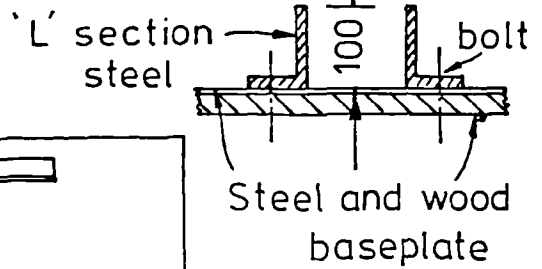


Frames 1, 2 and 3



Frame 4

Section x-x



Frame 5

Scale 1:20

Extension piece (wood)

FIG. 3-13 MOULDS FOR THE FRAMES

a palette knife. About three hours after casting, all the moulds were covered by a sheet of polythene. The inner part of the mould of the frame was removed less than twenty-four hours after the casting to avoid any cracks in the corners due to shrinkage. The complete demoulding took place twenty-four hours later. The frame and control specimens were kept under polythene sheeting for seven days. The test specimens and the frame were then uncovered and the frame was put into a vertical standing position and cured for a further seven days in the laboratory atmosphere before the infill panel was constructed.

3.5.2 Infill Panel

The infill panel was built two weeks after the reinforced concrete had been cast. Before building took place, the dimensions and squareness of the frame were checked. Since the whole building operation lasted between six and eight hours, only half the quantity of mortar needed was mixed, at a time, in accordance with BS 4551 [63]. Three cubes were prepared from each batch of mortar. Each block was damped in water for five seconds before it was laid. When the first course was completed, approximately fifteen minutes were allowed for it to set before starting the second. The process was repeated for each course until the panel was completed. The main difficulty arising was that of filling the gap between the top course of blocks and the underside of the top beam. This joint was filled as completely as possible by ramming in mortar from each side. As the building operation lasted several hours and the mortar mix tended to dry out, it was necessary to continually add water and remix the mortar by hand in order to maintain a uniform consistency of mortar for the whole operation. This involved a maximum total addition of approximately

15% of the initial quantity of water in the mix. When completed the infilled frame was covered by a sheet of polythene for three days in accordance with BS 5628 (A.2.6) [61]. After this, curing continued in the open laboratory. The test took place two weeks after the wall had been built.

3.6 TESTING OF INFILLED AND OPEN FRAMES

3.6.1 Test Arrangement

The tests took place inside an outer reaction frame made of bolted steel blocks, identical to those shown in figure 3.14, the width of which was 305 mm. The inside dimensions of the test-rig were 3654 mm (width) by 3148 mm (height). When designing the test-rig components, the arrangement, initially thought of, was to apply the horizontal racking load at the top left-hand corner and to have the vertical jack hinged at both ends with the specimen resting on two simple supports. Difficulties were experienced in maintaining all of the components of this set up in a vertical plane and the test arrangement was revised to that shown in figure 3.14. The racking load was applied at the bottom right-hand corner and the vertical jack was fixed at its top end. Since half of the specimens were to be subjected to a horizontal racking load only, it was necessary to design the left-hand support to be capable of allowing horizontal and rotational displacements whilst supplying either a downwards or upwards reaction. In order to achieve this, the left-hand column was extended. A tube was cast with the frame to provide a 38 mm diameter core. This latter was an integral part of the support.

A steel axle was inserted into the core and had one ball race bearing bolted to it at each end. The bearings were tightened by self locking nuts. Two 200 mm tracks were designed for these bearings

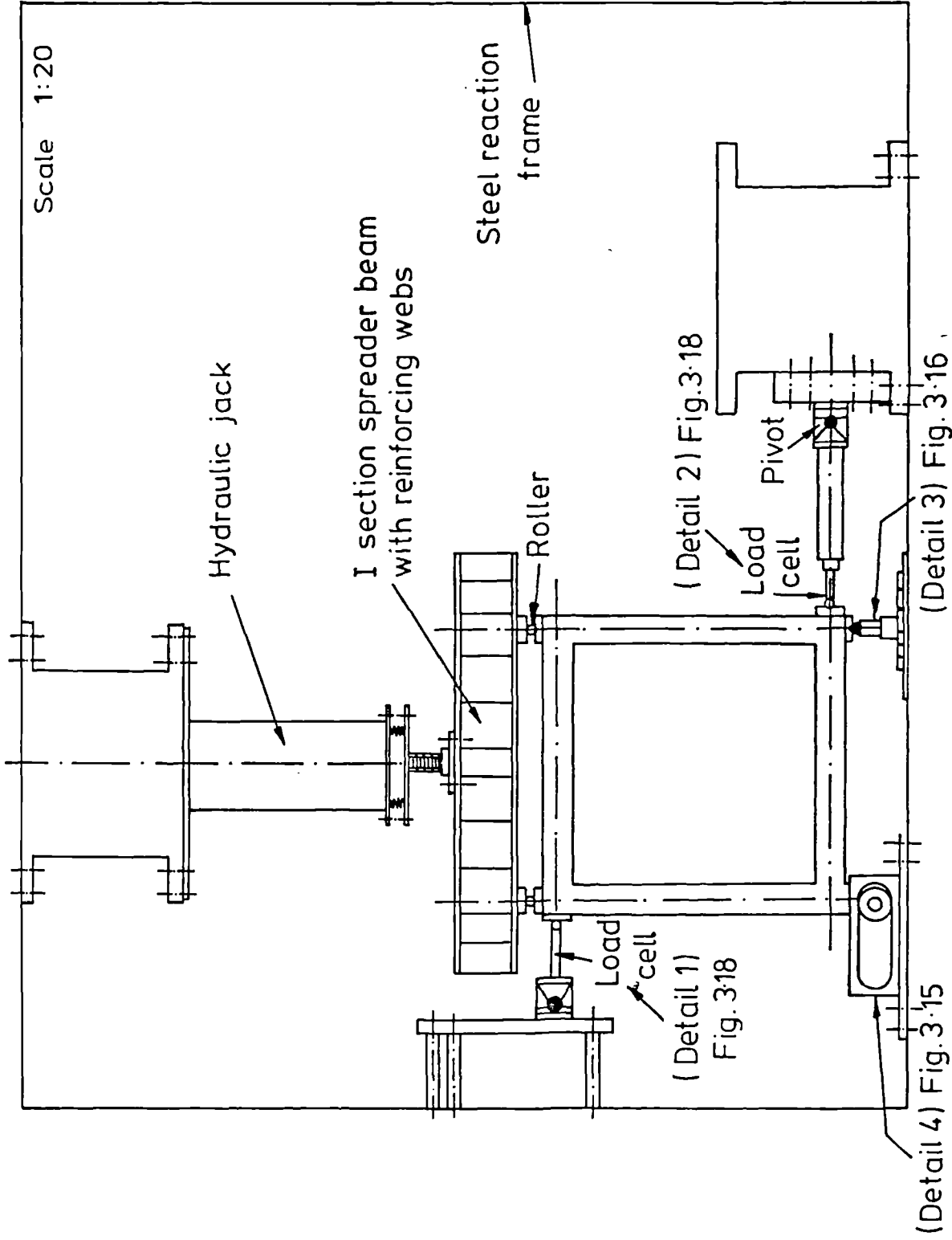


FIG. 3.14 TEST RIG

to keep them in parallel planes to the specimen and to prevent them from lifting (figure 3.15). Thus, the corner was free to rotate and to translate. The whole support was bolted down to the outer frame. Two pairs of bolts passing through the base of the support and resting on the outer frame were necessary for the final adjustment of the specimen. The right-hand support whose detail is shown in figure 3.16 was also designed to allow the free translation and rotation of the bottom right-hand corner. The semi-circular seating was used to facilitate the final adjustment of the specimen, to ensure it was truly vertical. The vertical load was applied by means of a hydraulic jack connected to a pump unit console. The load was distributed equally between the two columns by means of an I section spreader beam. This consisted of a 203 x 152 mm universal beam section with ten web stiffeners. The spreader beam was bolted to the lowest plate of the vertical jack for safety reasons.

Two stabilizers as shown in figure 3.17, hinged at both ends, were used to resist any tendency for the test panel to move out of the vertical plane. For the specimens tested under combined loading, these were bolted to two of the stiffening webs of the spreader beam at one end and fixed to an adjacent steel testing frame at the other. For the specimens tested without vertical loads, the stabilizers were bolted to two steel chairs placed on the top beam of the reinforced concrete frame at one end and fixed to the adjacent steel frame at the other. The horizontal reaction was measured by a load-cell made of high tensile steel of a diameter of 25 mm and 140 mm long. This load-cell was hinged at both ends. It was bolted at one end to the pivot and had a seating ball at the other (detail 1, figure 3.18). The horizontal racking load was applied by means of a 23t hydraulic jack, CRC 2510, with a 260 mm stroke. The jack was connected to a

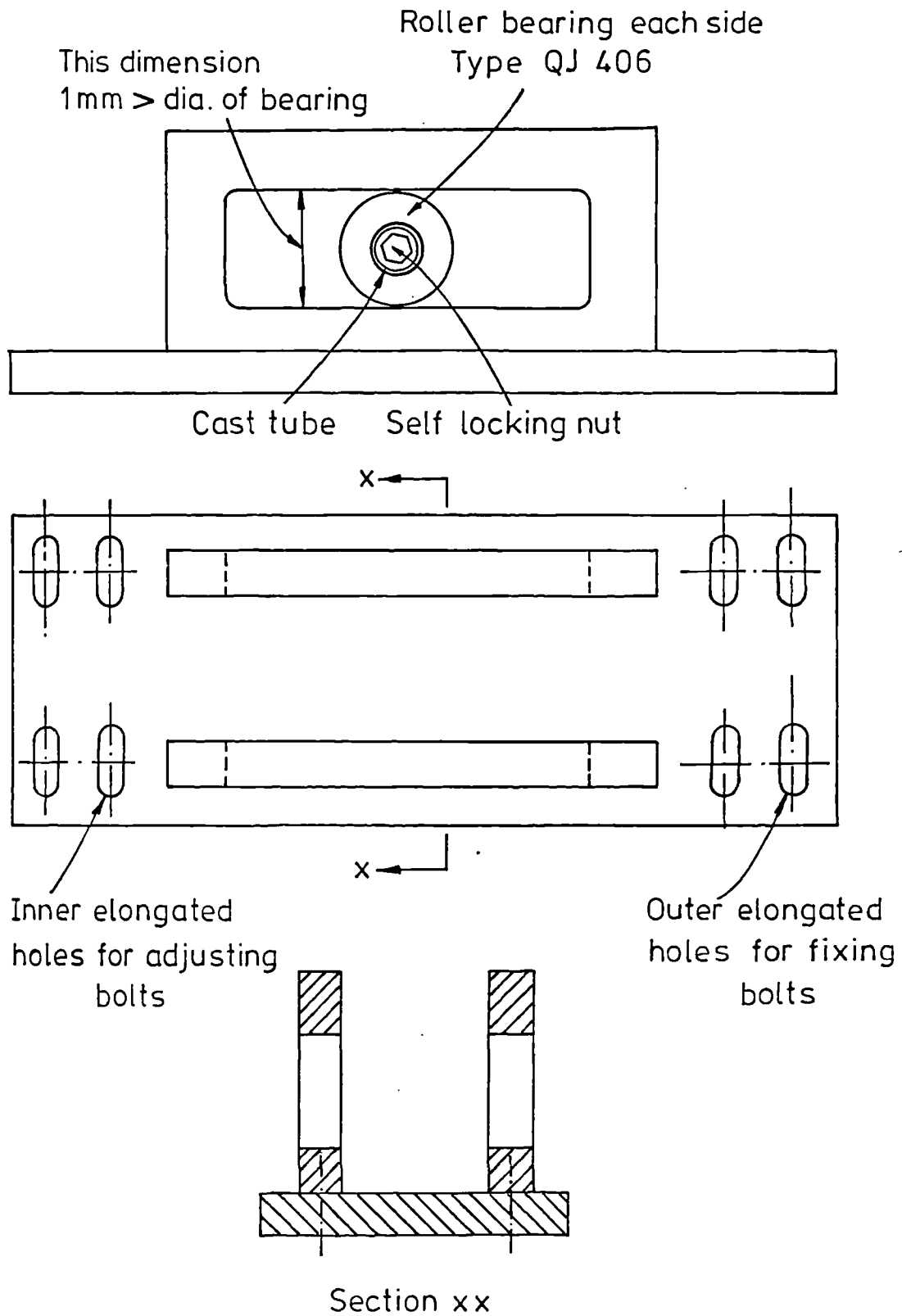


FIG. 3-15 LEFT HAND SUPPORT

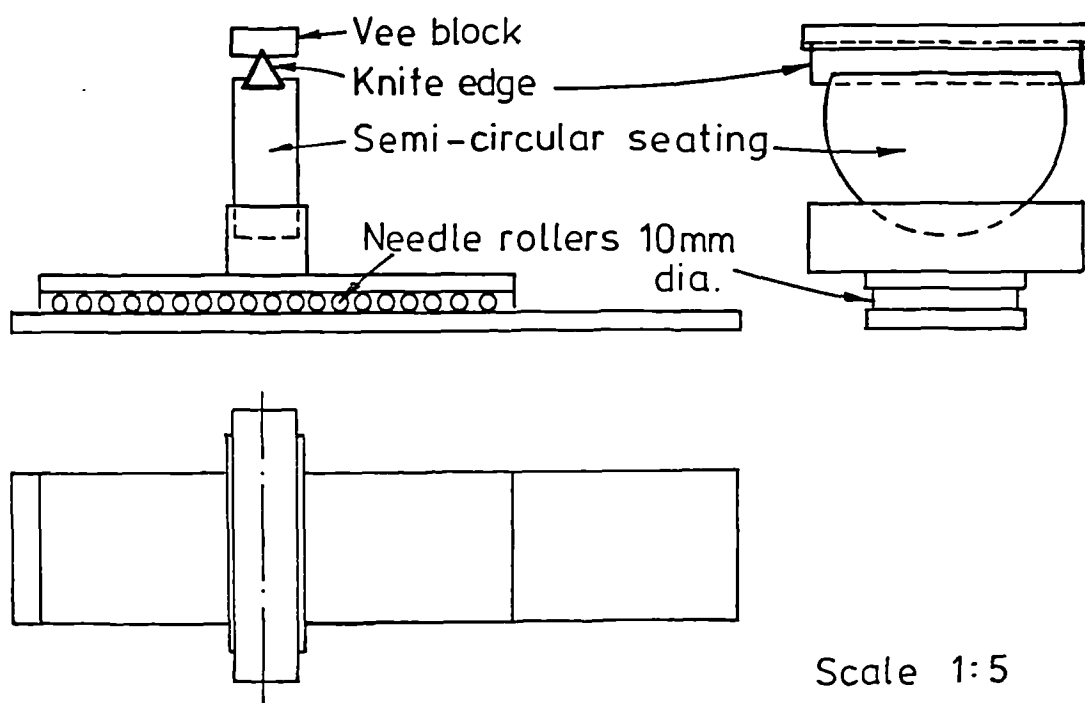


FIG. 3-16 RIGHT HAND SUPPORT

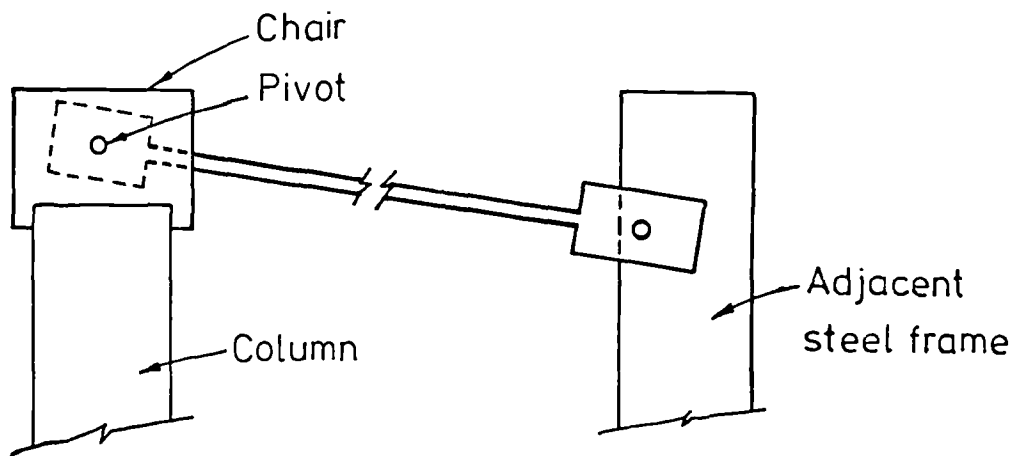
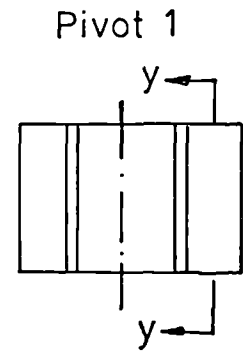
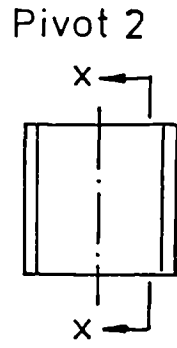
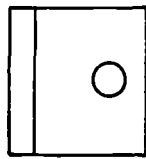


FIG. 3-17 STABILIZER DETAILS

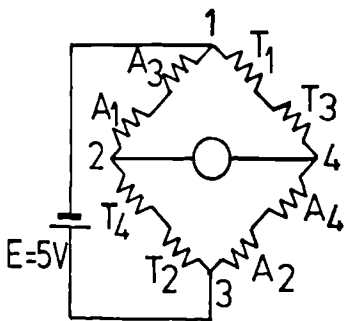
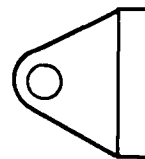
Scale 1:5



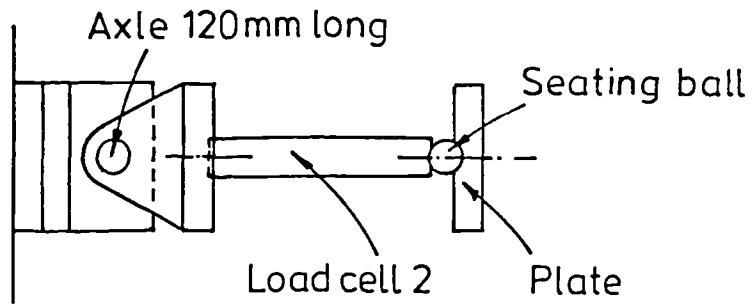
Pivot 1
Section yy



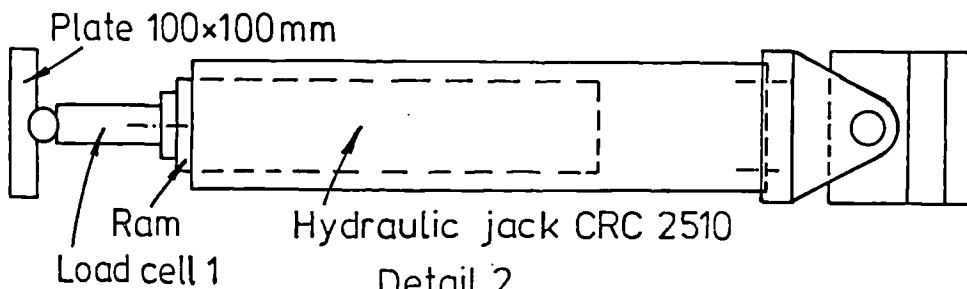
Pivot 2
Section xx



Measuring circuit
for load cell 2

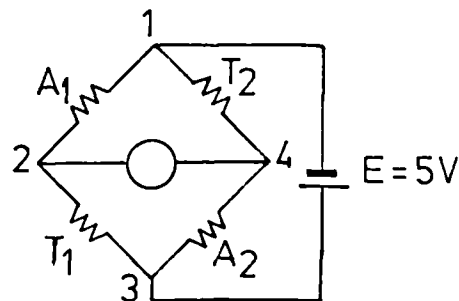


Detail 1



Detail 2

A - Axial
T - Tangential



Measuring circuit
for load cell 1

FIG. 3-18 PIVOT DETAILS

pressure gauge and was hinged at both ends. Another similar load-cell was inserted between the jack and the seating ball (detail 2, figure 3.18). This load-cell was bolted at the end of the ram of the jack which itself was bolted to the pivot. Details of both load-cells are given in the following section.

3.6.2 Instrumentation

3.6.2.1 Loads

The vertical load applied was directly given by the machine to which the vertical jack was connected. This equipment is regularly calibrated to class B, BS 1610: 1964 [71], and no special calibration was therefore carried out for these tests. The horizontal racking load applied was obtained by two means, pressure gauge connected to the jack and load-cell fixed at the end of the ram of the jack. Recording the readings from the pressure gauge was found to be impractical and inaccurate. So recourse was made to a more precise instrument (load-cell) to measure the actual horizontal load applied. The load-cell calibration factor and its degree of accuracy are given in Table 3.7. The details for the accuracy calculations are in Appendix B1. Four electrical strain gauges of a self temperature compensating type were fixed to the load-cell at its middle section. These constituted a full Wheatstone bridge (figure 3.18) whose sensitivity was 2.6 times that of a quarter bridge (one electrical strain gauge only). Their gauge factor and gauge resistance were respectively 1.78 and 120 Ω . The input voltage was provided by a power supply and was of five volts. The output in millivolts was recorded by an IMP data-logger printer. The horizontal reaction was also obtained by converting the second load-cell readings into KN in a similar way. The calibration factor and the accuracy of the

	CALIBRATION FACTOR		ACCURACY OF READINGS			
	*MEAN	S. DEV	(1)	(2)	(3)	(4)
horizontal jack pressure gauge	9.8 KN/div	0.058 KN/div	±200N	-	-	-
load-cell 1	15.603 KN/mv	0.025 KN/mv	±25N	±30N	±9N	±34N
load-cell 2	15.524 KN/mv	0.012 KN/μs	±12N	±19N	±9N	±20N
load-cell 3 used for shear tests	0.119 KN/μs	9x10 ⁻³ KN/μs	±9N	±15N	-	-
L.V.D.T. 1 50 mm stroke	5.563x10 ⁻³ mm/mv	5x10 ⁻⁴ mm/mv	±0.5x10 ⁻³ mm	±2x10 ⁻³ mm	-	-
L.V.D.T. 2 100 mm stroke	10.2x10 ⁻³ mm/mv	2x10 ⁻⁴ mm/mv	±0.2x10 ⁻³ mm	±1x10 ⁻³ mm	-	-
ELECTRICAL DEMEC GAUGE	16.2 μs/mv	24.3x10 ⁻³ μs/nv	±24.3x10 ⁻³ μs	±7μs	-	-

* MEAN of 6 calibrations

The details of calculations are given in Appendix B1.

TABLE 3.7: CALIBRATION FACTORS AND ACCURACY OF READINGS

readings are also given in Table 3.7.

3.6.2.2 Deflections

Two L.V.D.T.'s (Linear Variable Differential Transducers) were used to measure the lateral displacement of the lower beam and therefore of the whole structure. These L.V.D.T.'s were set at the bottom right and bottom left corners and had respective strokes of fifty and a hundred mm. The L.V.D.T.'s were connected to the data-logger with the same power input of five volts. They were calibrated against a mechanical dial gauge. Their calibration factors and the sensitivity of the readings are also given in Table 3.7.

3.6.2.3 Photography

A precision camera (WILD C40 stereometric using one component) was used to take photographs at different stages of loading. The good quality, large format photographs obtained were used to record the qualitative aspects of the behaviour such as the development of cracking, the bending and rotation of frame members and the locations of plastic hinges. At the same time, it was hoped that using photogrammetry techniques, it would be possible to measure strains for the whole infill panel and the frame. Unfortunately the technique was found not to be a viable means for recording strains in the elastic range. The strains were given to $\pm 4900\mu$ strain. The detail of this is given in Appendix B2.

3.6.2.4 Strain measurements

Initially, the means used for the strain measurements was a 100 mm Cambridge electrical extensometer. Though it was satisfactory when calibrated, when the actual test took place the readings

were found to be rather variable. The reason for that might be attributed to the type of Demec discs used. In effect the extensometer ball points did not fit perfectly into the holes of the Demec discs. The extensometer also failed to record large strains (failure of strain gauges). It was therefore decided to use a 100 mm mechanical Demec gauge. This proved to be very satisfactory with nonetheless two disadvantages:

(i) Possibility of making errors when recording the readings or when writing them down.

(ii) Long time to take one set of readings (forty to fifty minutes).

In order to overcome these difficulties, later tests employed a newly developed 100 mm electrical Demec gauge adapted from a standard mechanical Demec gauge.

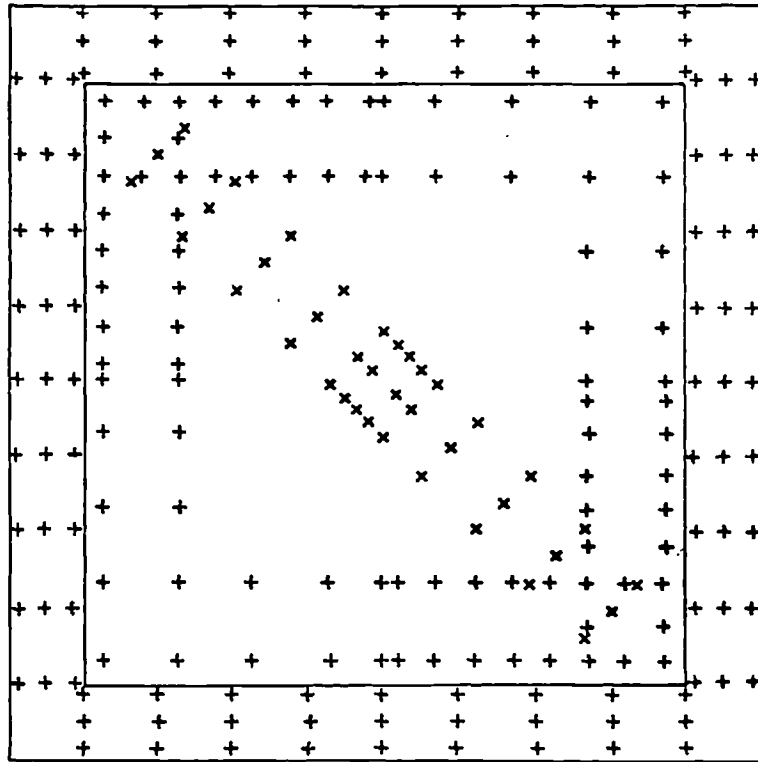
The dial gauge indicator was removed and replaced by a L.V.D.T. This latter was set up with a stabilized power supply which was set to five volts $\pm 2\mu\text{v}$. The gain factor for the output of the L.V.D.T. was altered so that one mv output was equivalent to one division in the mechanical Demec gauge. The L.V.D.T. spindle was at the same height as the original one. This electrical Demec gauge was connected to the data-logger and was provided with a switch to trigger the logger in order to increase the speed with which the readings are taken and also to give the possibility to retake some doubtful readings. The data-logger was programmed accordingly. The electrical Demec gauge proved to be very efficient (time of taking a set of readings was reduced by 50%) and was as accurate as the mechanical Demec gauge against which it was calibrated. The calibration factor and the accuracy of readings are given in Table 3.7. The strains

were measured along the two diagonals and the periphery of the wall and for thirty-six sections of the frame. The Demec disc dispositions are given in figure 3.19.

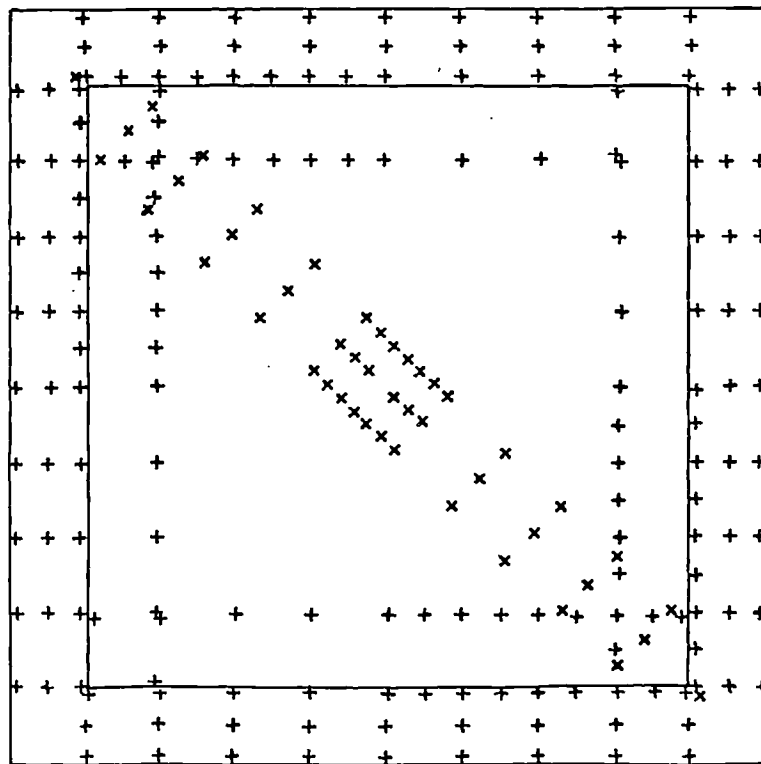
3.6.3 Setting Up and Test Procedure

When due for testing, each specimen was painted with white emulsion in order to facilitate the detection of cracks. The specimen was lifted into the test-rig with a fork lift and supported in an upright position. The left-hand support was bolted down to the outer reaction frame. The specimen was then brought to the middle and the axle was inserted into the core of the left-hand column extension. Then the two ball race bearings were tightened to it. This by itself stabilized the specimen. The right-hand support was then arranged under the specimen. The two pairs of bolts of the left-hand support were then adjusted to bring the specimen into a truly vertical position. Once the specimen was set square in the test-rig, a small horizontal pressure was exerted in order to hold the two vertical plates against the specimen. It was ensured that the horizontal jack and the two load-cells were parallel. In tests involving the application of vertical loads on the columns, the horizontal plates and the rollers were set and the spreader beam was brought down until contact took place. The stabilizers were then bolted to it. This constituted the initial stage. The first photograph and the first set of Demec readings were taken.

The vertical load was then applied in increments of 50 KN up to 250 KN. For each stage, readings of the two load-cells and the deflections were recorded. At the end of the application of the vertical load, a second set of Demec readings was taken. The application of vertical loads on columns resulted in a very small lateral movement



(a) Infill panels W and M



(b) Infill panels S

Scale 1:20

FIG. 3-19 DEMEC DISC DISPOSITION FOR INFILLED FRAMES

and therefore in a very small horizontal reaction. This movement was either negative (opposite sense to the application of the horizontal load) or positive. It varied from -0.2 mm to 0.9 mm and the resulting horizontal reaction was of the order of 1 KN.

Then the horizontal load was applied in small increments. In the initial part of the load-deflection response, readings were recorded almost every ten seconds. The loading was halted when taking Demec readings or at each significant change in behaviour in order to mark the cracks in frame and infill and to take photographs. These photographs were taken only when major changes occurred. The cracks were marked and given a number indicating the stage in order to follow the sequence of their development and also to record them in the load-deflection diagrams. This would facilitate the analysis of the photographs and the identification of collapse mechanisms. This is discussed in Chapter 4.

During the period in which each set of Demec readings was taken, the horizontal deflection was kept constant and this resulted in a dropping off of the load in the jack and necessitated small adjustments of jack pressure. The load also dropped at each major crack in infill or frame. This drop was more significant when the cracks occurred in the infill. This effect is shown in the respective load-deflection diagrams in the following chapter. It was very difficult to monitor precisely the loads at which the first cracks occurred in the frame and in the infill and the peak load reached in the tests. The load-deflection readings were taken well beyond the peak load in order to follow the descending branch until collapse eventually occurred.

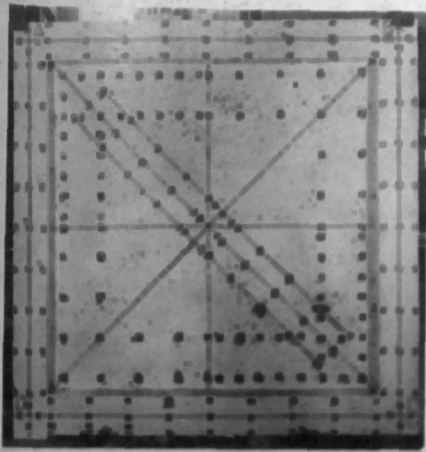
CHAPTER 4

PRESENTATION AND DISCUSSION OF TEST RESULTS

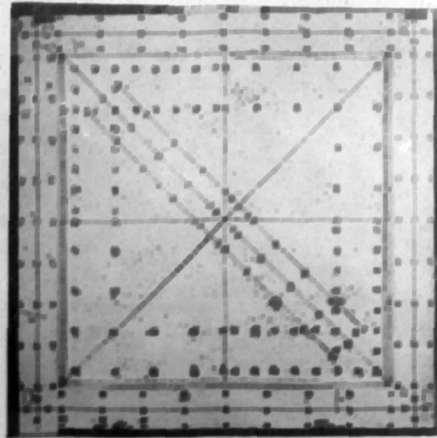
4.1 GENERAL OBSERVATIONS

When subjected to an in plane racking load, the response of an infilled frame passes through several phases. These phases are best illustrated by two sets of photographs (figures 4.1 and 4.2) taken at different stages of loading for respectively a typical 'IH' specimen (infilled frame under horizontal loading only) and a typical 'IC' specimen (infilled frame under combined loading). During the early stages of loading, the distortion seemed to be symmetrical with a very small sidesway movement and both columns remaining sensibly straight. The first visible cracks detected were those which formed adjacent to the unloaded corners. These boundary or peripheral cracks occurred at the mortar-concrete or mortar-blocks interfaces and were very fine. They, sometimes, ran down some perpendicular joints particularly for the 'IC' specimens. It was only at later stages of loading, when the flexural deformations of the frame members increased, that they opened up. These boundary cracks preceded or occurred at the same time as those which developed in the frame. These latter occurred at one or both loaded corners and/or in the windward column for the 'IH' specimens.

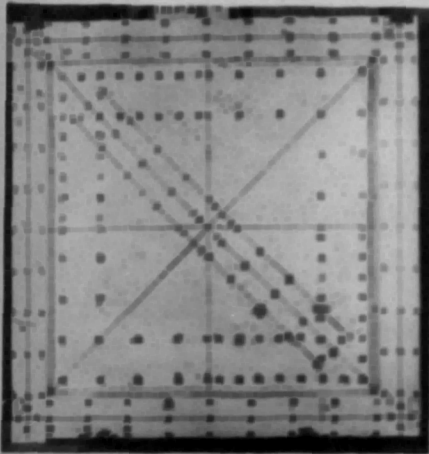
At this stage, the distortion of the 'IH' frames was clearly non-symmetrical. For the 'IC' specimens both columns remained uncracked. Following the initial cracks, more cracks developed in the frame until the infill cracked. For some infilled frames, the infill and the frame cracked simultaneously. The first visible cracks in the infill occurred along the compression diagonal and once initiated they usually ran through both mortar and blocks. Following this initial diagonal crack, more cracks developed and



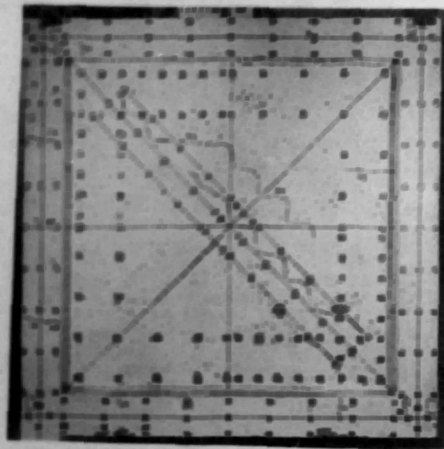
(a) initial



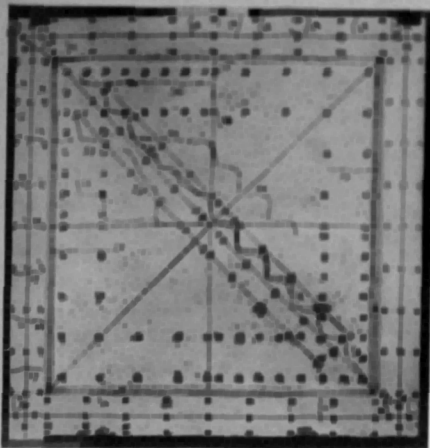
(b) peripheral cracks; first cracks in frame



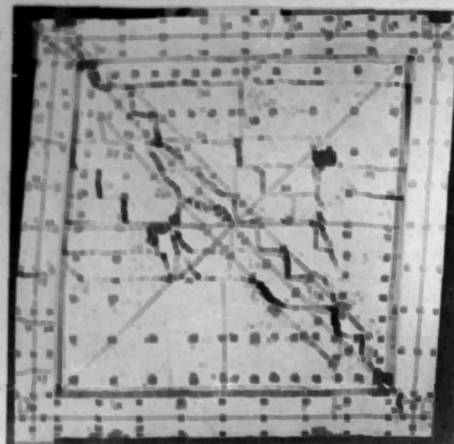
(c) first crack in infill



(d) propagation of cracks in frame and infill

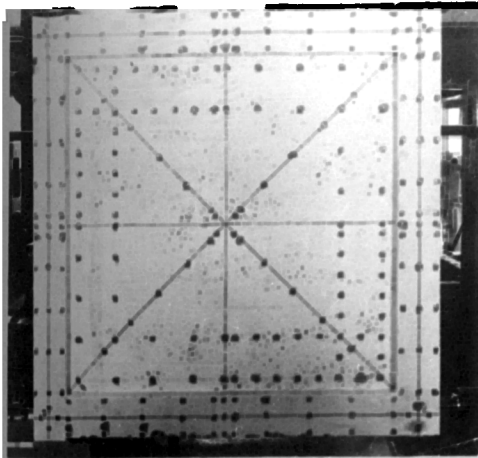


(e) concentration of cracks in the windward end (peak load)

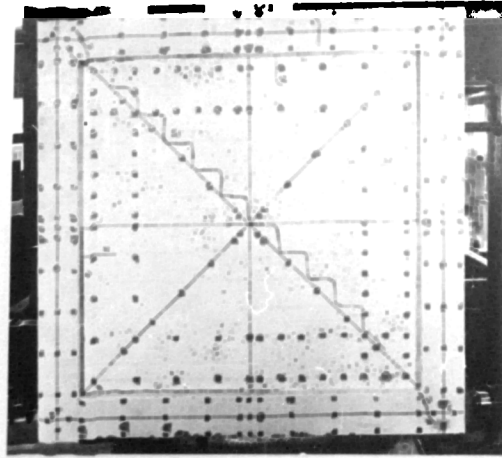


(f) specimen at large deflection

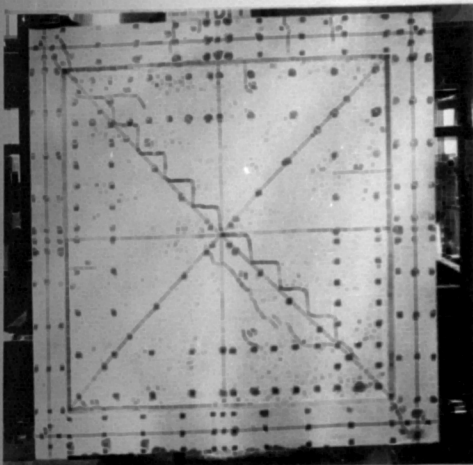
FIGURE 4.1: FAILURE SEQUENCE FOR A TYPICAL 'IH' SPECIMEN



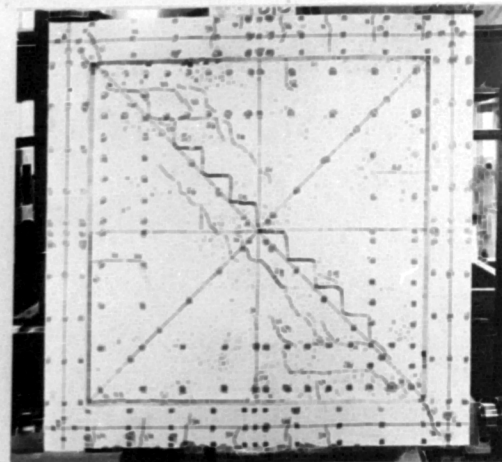
(a) initial



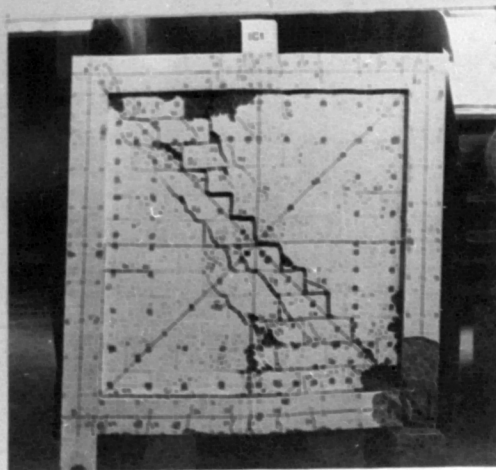
(b) peripheral cracks; cracks in frame and infill



(c) propagation of cracks



(d) specimen at peak load



(e) specimen after failure

FIGURE 4.2: SEQUENCE OF FAILURE FOR A TYPICAL 'IC' SPECIMEN

seemed to converge towards the bottom right corner. The other phenomenon observed was the relative weakness of the infill top course. In effect, for most of the infilled frames tested, a horizontal crack formed along a part of, or the whole bed joint of the top course. Cracking of the infill did not constitute the end of the test. The structures were capable of carrying more load until collapse occurred in the frame. The different modes of failure are discussed in section 4.4. For most of the infilled frames tested, the leeward column remained sensibly straight and uncracked when collapse occurred.

4.2 LOAD-DEFLECTION GRAPHS

Three sets of load-deflection diagrams have been plotted. The first set gives the actual load-deflection diagrams. The second gives the simplified or idealized ones and the third gives the initial elastic response for all the specimens at an enlarged scale. The first set gives a full picture of the whole response. The second set has been necessary for fixing the limits for the different zones of the load-deflection diagrams and also for defining the plastic collapse load and therefore might be exploited for design purposes. The third set has been used to calculate the racking stiffness values. Plotting the load-deflection graphs at an enlarged scale has eased the problem of fixing the limits for each zone of the load-deflection diagrams. From these graphs, it has also been possible to estimate the loads causing the first cracks in the frame and in the infill. These are reported and compared to the observed values in Table 4.1. The enlarged diagrams have also been used for the calculations of the lateral racking stiffness prior to cracking of the frame, after cracking of the frame and after cracking of both the infill and the frame. The actual load-deflection graphs

are given in figures 4.3 to 4.7, the idealized graphs in figures 4.8 to 4.10 and the enlarged scale plots are given in Appendix C.

4.3 GENERAL RESPONSE OF INFILLED FRAMES

4.3.1 Response Prior to Cracking of Infill

Prior to cracking of the infill, the response might be considered linear. Five distinct types of load-deflection responses have been obtained depending upon the order of cracking of the frame and the infill. These have been illustrated in figure 4.11. The general load-deflection response, prior to cracking of the infill, may be subdivided into three stages.

Stage 0: Initial "bedding in"

During the early stages of loading, the response is non-linear and of an indefinite type. This initial non-linear portion varies for each specimen tested. It has been represented in the idealized load-deflection diagrams as O_0' and represents a small proportion (2 to 15%) of the peak load (column 12, Table 4.1). It is possible that this might be due to slip between the frame and the infill, lack of fit (especially for the top course as discussed in section 3.5), or setting up imperfections. From the tests, there was no visible evidence of a slip occurring between the frame and the infill. The lack of fit, if present concerns only the top course. It seems likely, therefore, that setting up imperfections, are mainly responsible for this initial non-linearity.

Stage 1: Linear uncracked response

After O_0' , the response is linear until the frame cracks. In the meantime, the peripheral cracks will have occurred. For some infilled

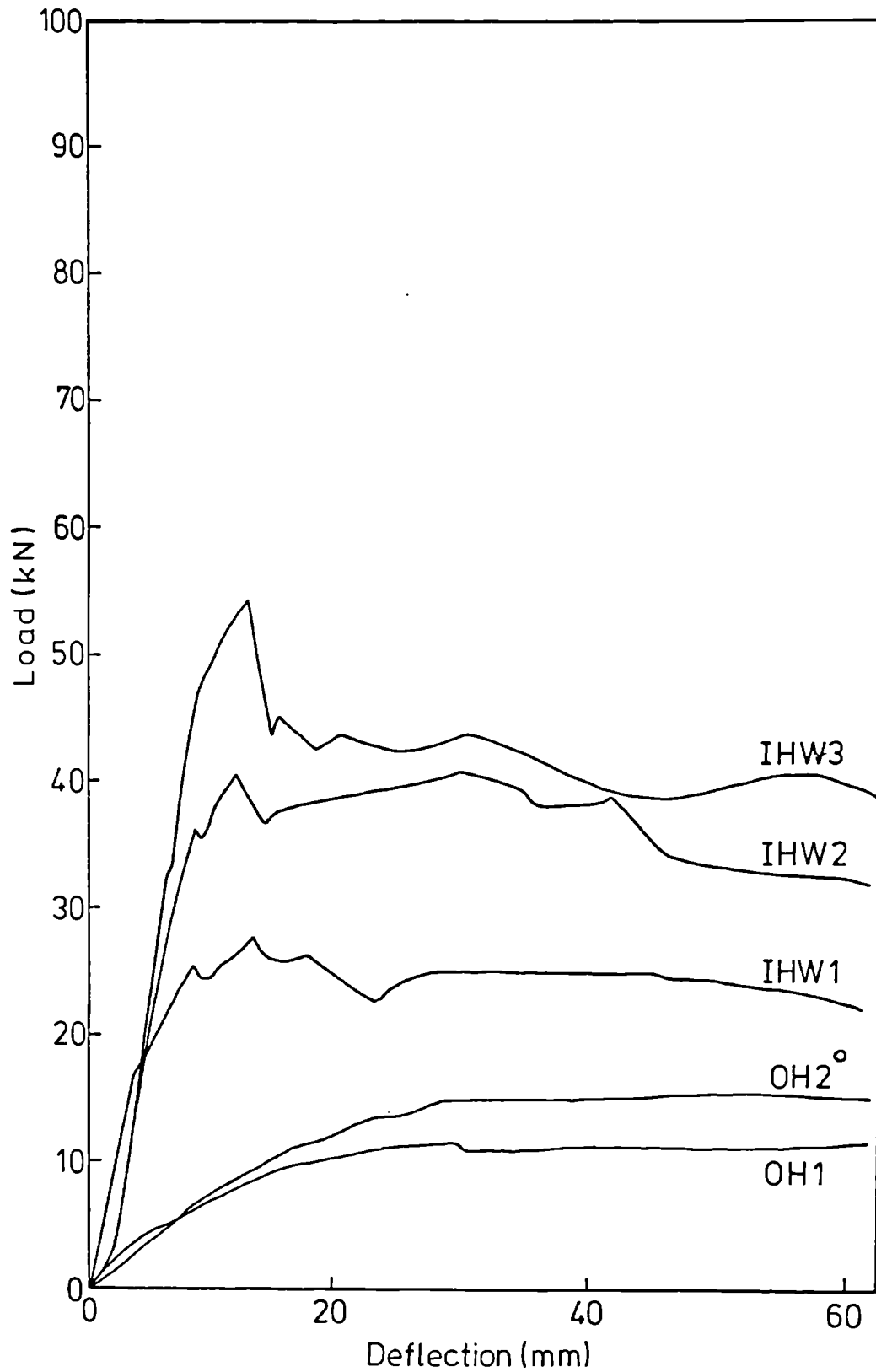


FIG.4.3 LOAD-DEFLECTION DIAGRAMS FOR WEAK INFILL AND HORIZONTAL LOADING

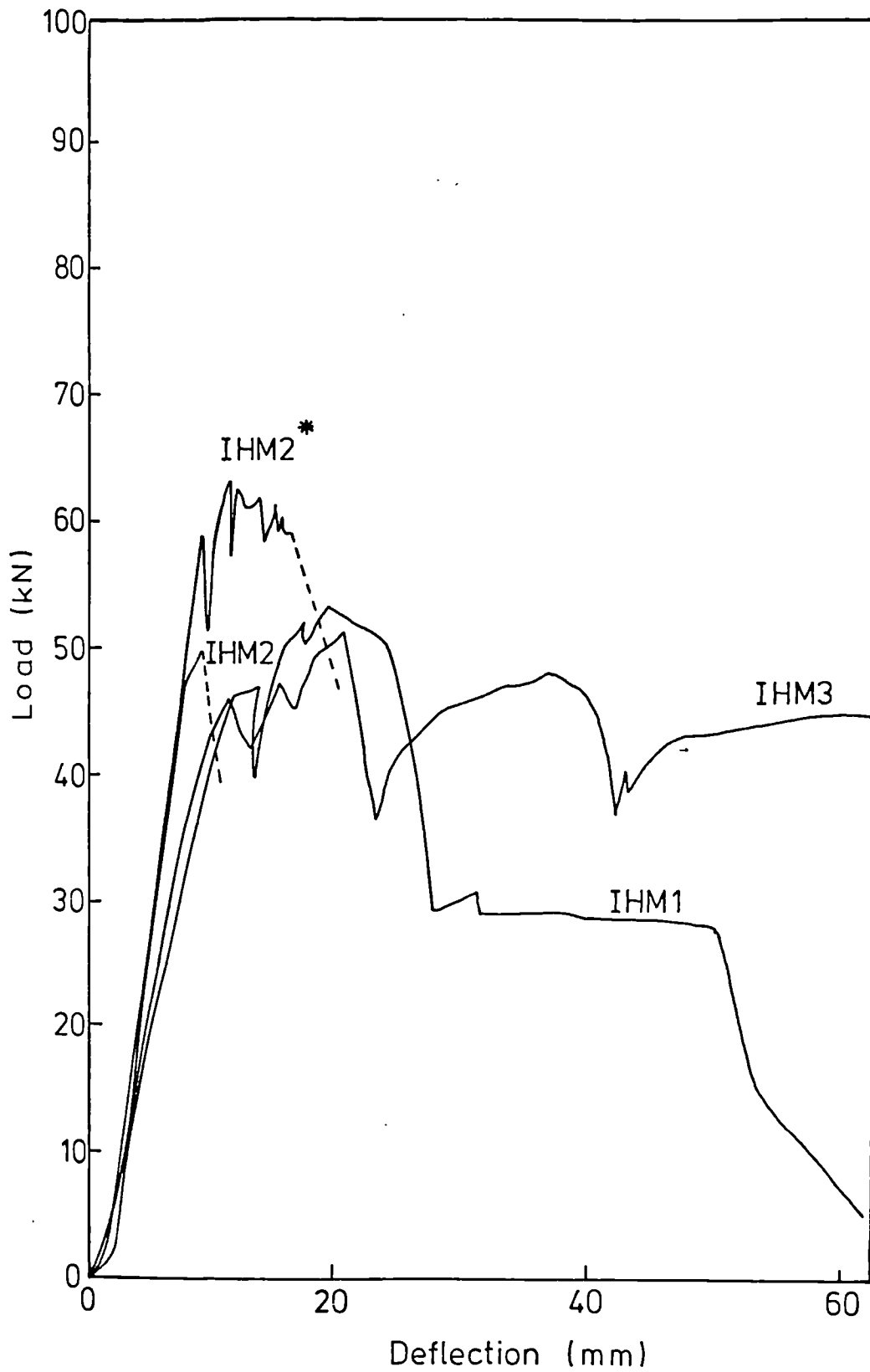


FIG. 4-4 LOAD-DEFLECTION DIAGRAMS FOR MEDIUM STRENGTH INFILL AND HORIZONTAL LOADING

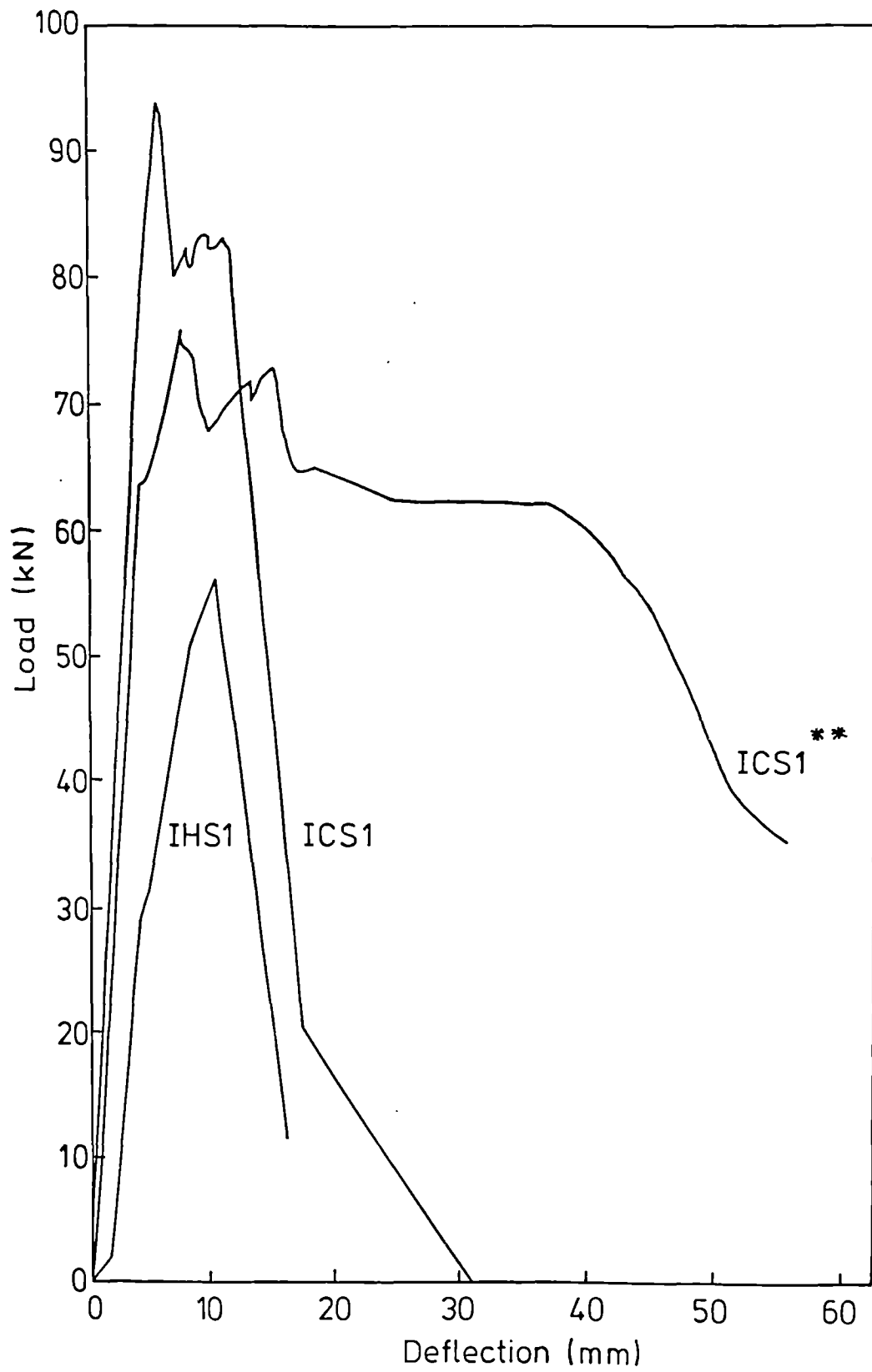


FIG.4.5 LOAD -DEFLECTION DIAGRAMS FOR STRONG INFILL

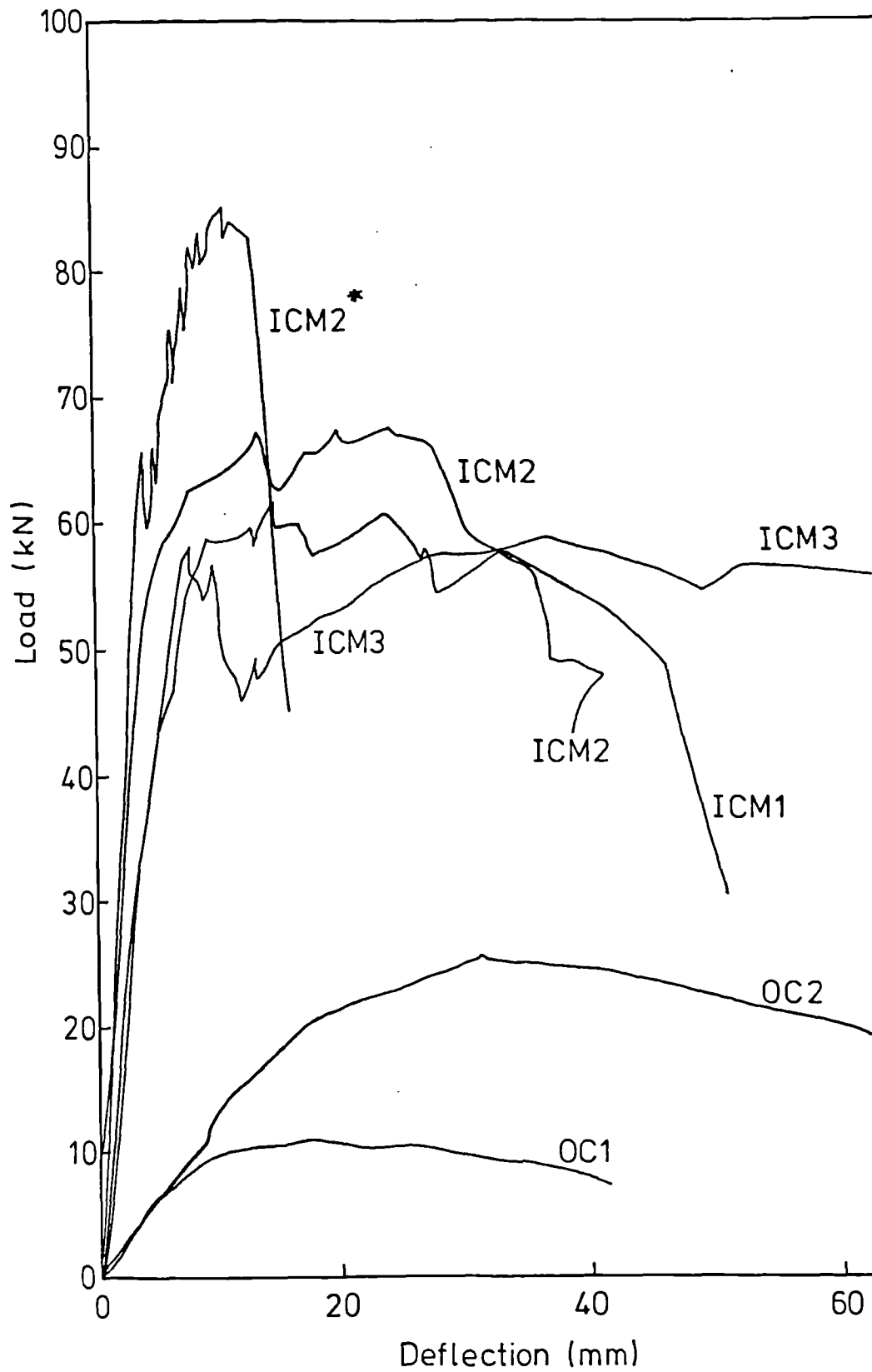


FIG.4.6 LOAD -DEFLECTION DIAGRAMS FOR MEDIUM STRENGTH INFILL AND COMBINED LOADING

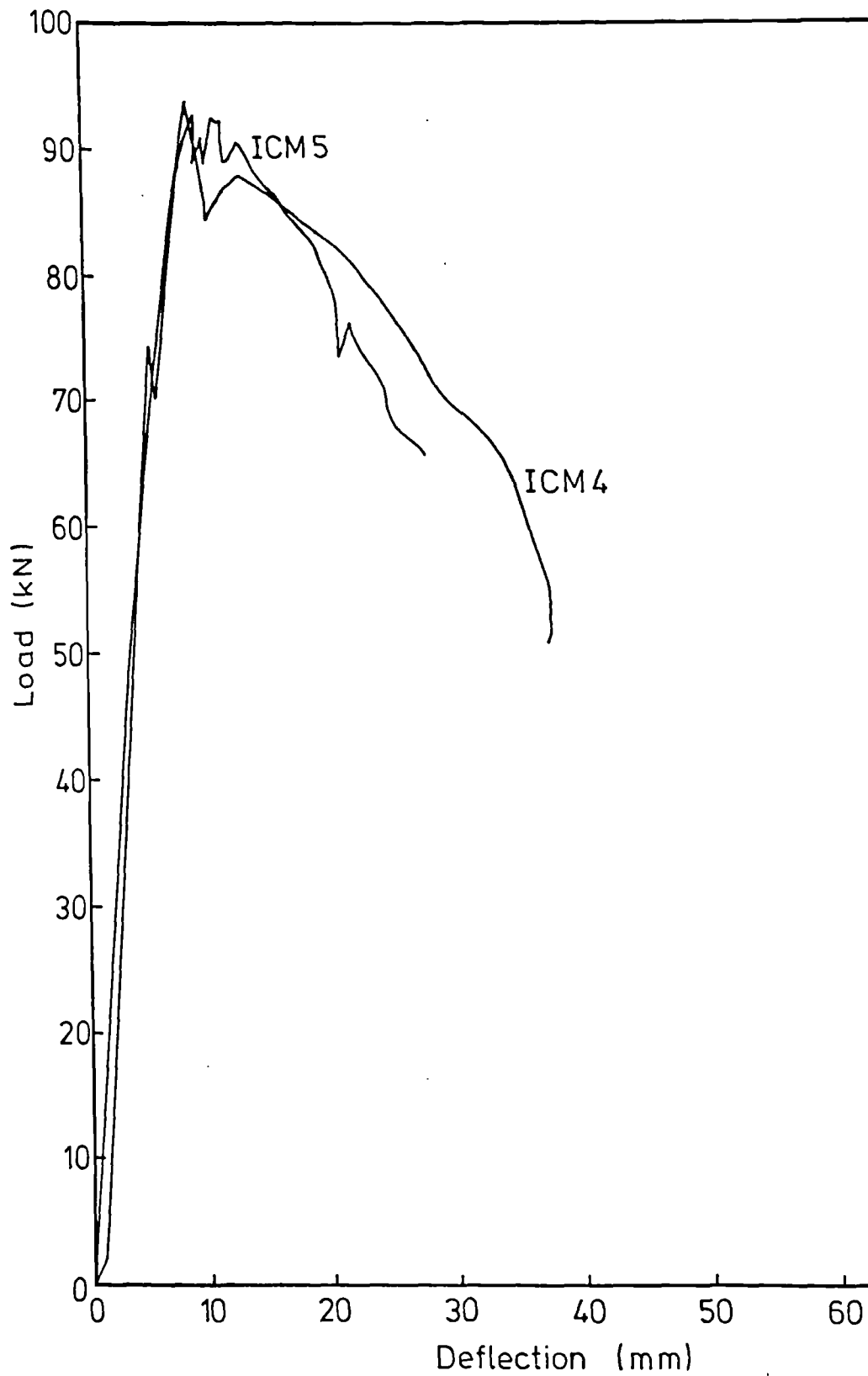


FIG.4.7 LOAD -DEFLECTION DIAGRAMS FOR FRAMES WITH DEEP BEAMS OR DEEP COLUMNS

CF - First visible cracks in the frame
 CI " " " in the infill

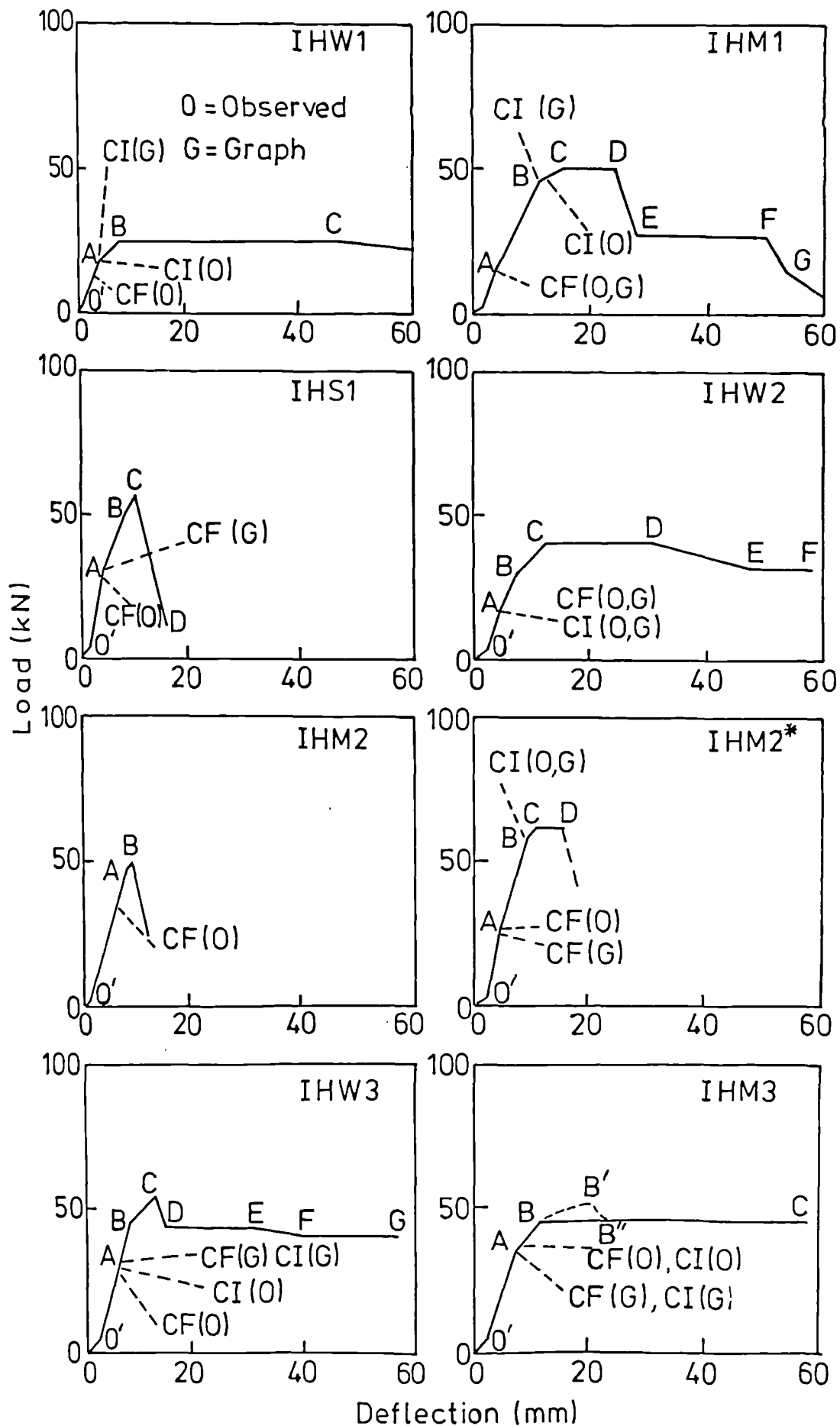


FIG.48 IDEALIZED LOAD-DEFLECTION DIAGRAMS FOR 'IH' SPECIMENS

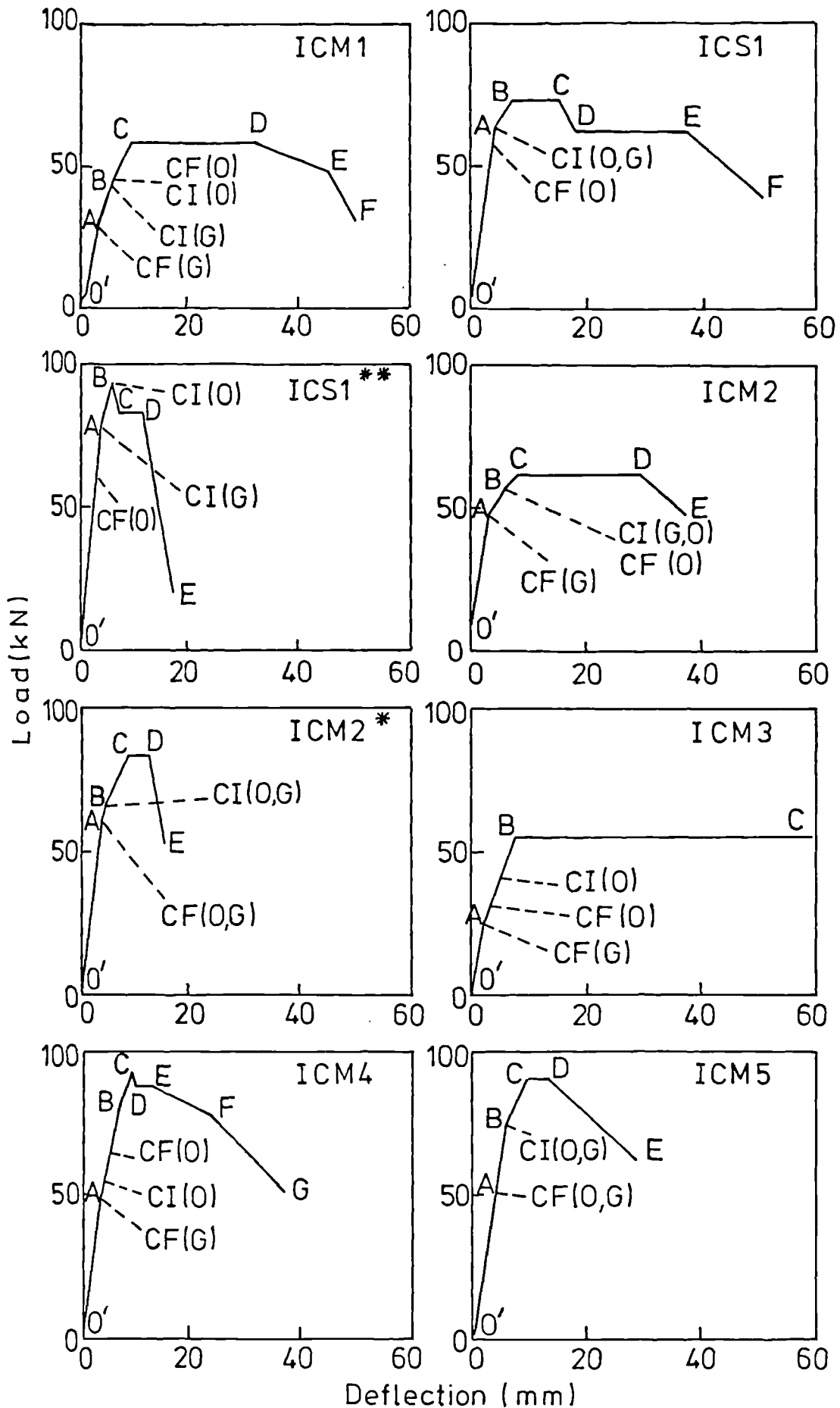


FIG. 4.9 IDEALIZED LOAD-DEFLECTION DIAGRAMS FOR 'IC' SPECIMENS

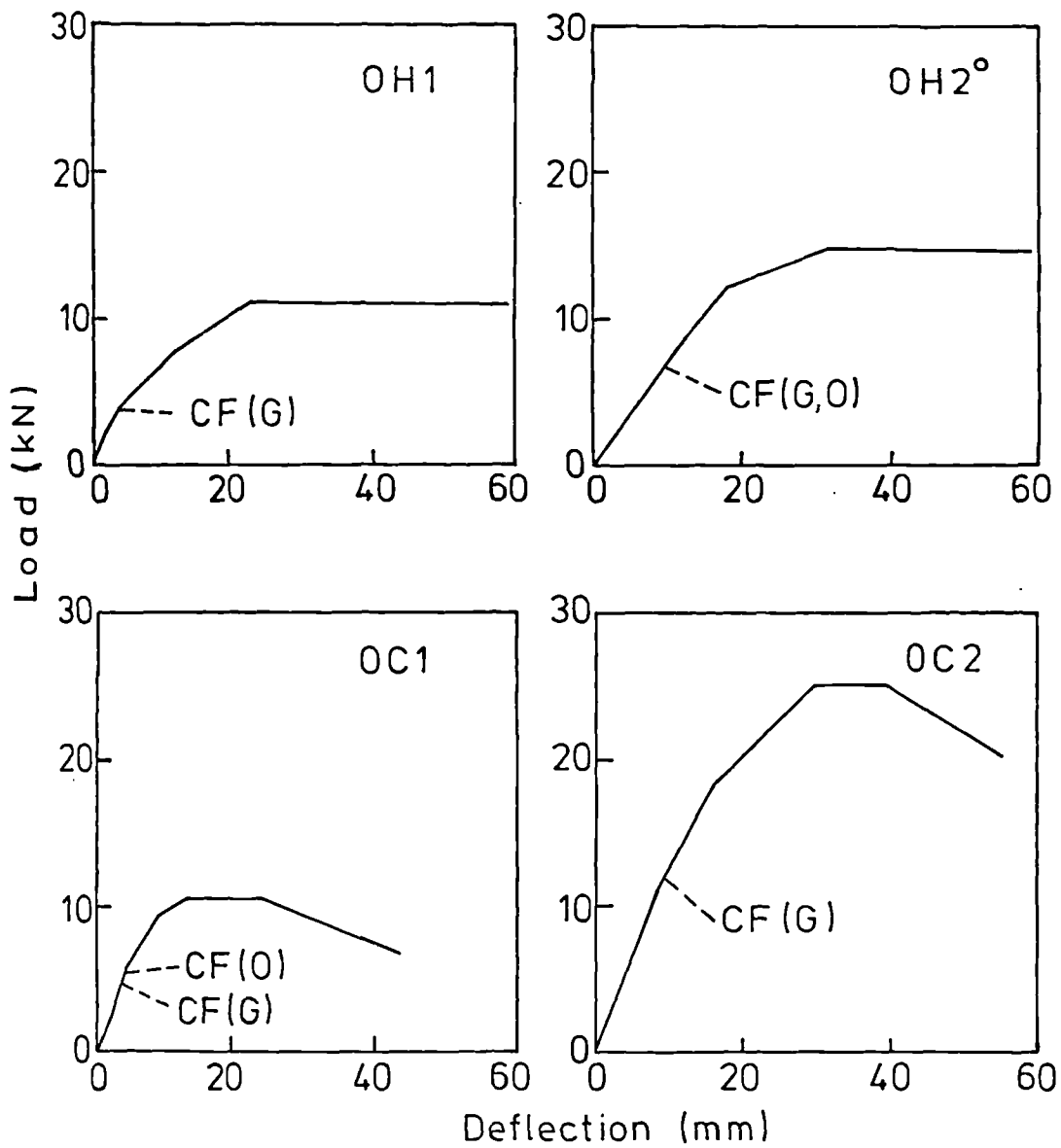
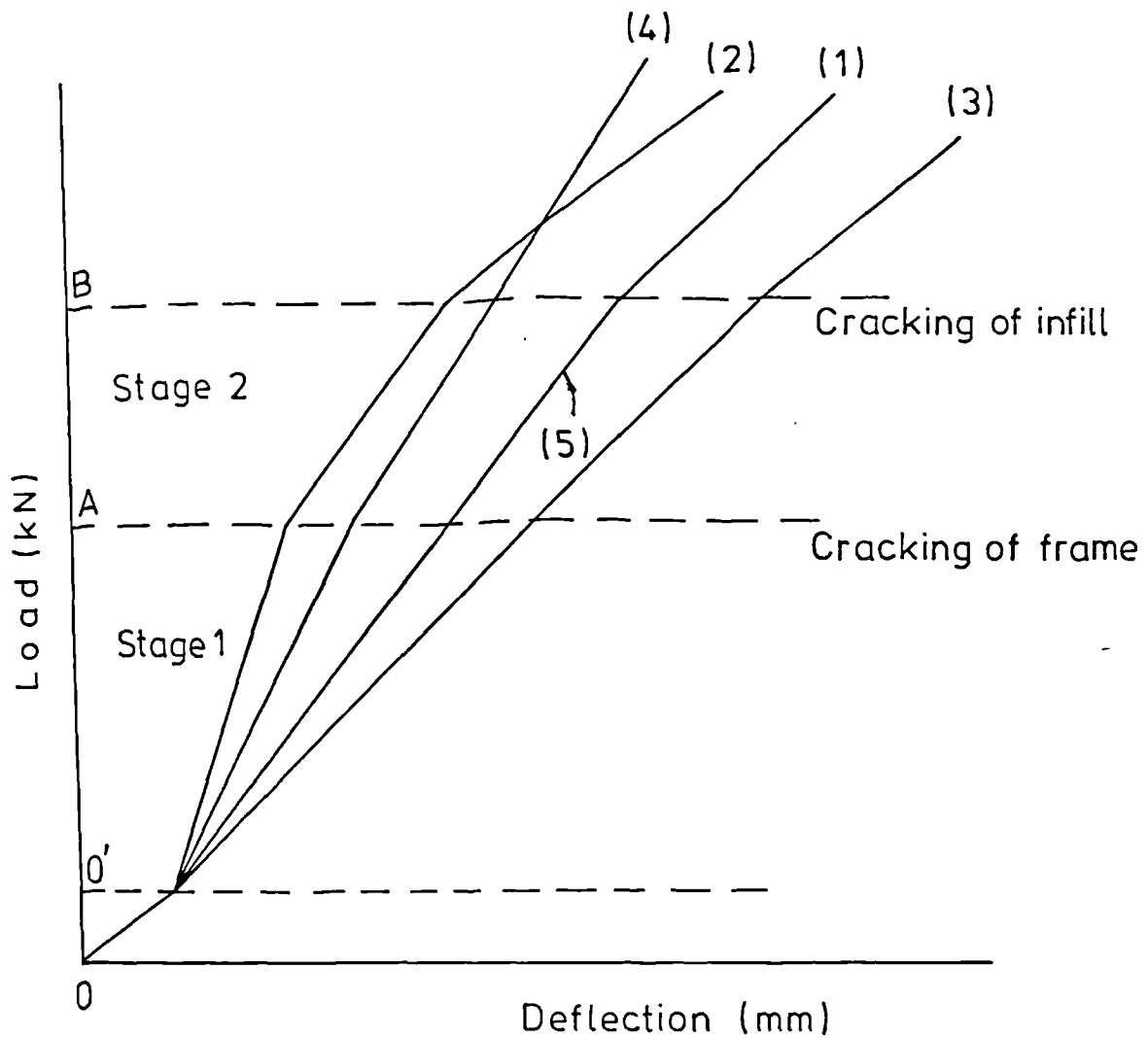


FIG. 4.10 IDEALIZED LOAD-DEFLECTION DIAGRAMS
FOR OPEN FRAMES



- (1) No change in slope after frame cracks
IHW1, ICS1 and ICS1**
- (2) Change in slope after both infill and frame cracking
IHM1, ICM1, IHM2*, ICM2, ICM2* and ICM5
- (3) Infill and frame crack simultaneously
IHW2 IHW3 and IHM3
- (4) No change in slope after infill cracks
ICM3 and ICM4
- (5) Failure of frame without failure of infill
IHM2 and IHS1

FIG. 4-11 DIFFERENT LOAD-DEFLECTION RESPONSES PRIOR TO CRACKING OF THE INFILL

frames, the peripheral cracks occurred at the same time as those which developed in the frame. These peripheral cracks were observed, instead of the neat separation described by investigators testing infilled steel frames, because of the existence of a better bond between the frame and the infill. Their occurrence, however, did not significantly affect the response which remained linear elastic with no changes in lateral stiffness (observations from the actual load-deflection graph). The slope of the load-deflection relationship in this region may be termed the initial racking stiffness. This has been represented as O'A in the idealized load-deflection diagrams or O'B when the infill and the frame crack simultaneously.

Stage 2: Linear reponse after frame cracking

The cracking of the frame, especially in the windward column, was accompanied by a change in stiffness except for three infilled frames (Graph 1, figure 4.11). The response remained, however, linear at this reduced stiffness until the infill cracked. The dropping in stiffness varied from 0 to 63% (column 6, Table 4.1). This zone has been represented as AB in the idealized load-deflection diagrams. During this stage, more cracks developed in the frame and some of the initial cracks propagated or opened up.

4.3.2 Post-Cracking Response

For the type of infilled frames tested, cracking of the infill, in general, constituted a critical stage because the load-deflection response changed from a linear state to a non-linear one. The cracking of the infill was, in general, followed by a substantial drop in stiffness (column 7, Table 4.1). In one case (ICSl**) the load causing the cracking of the infill was the actual peak load reached in the test. The dropping in stiffness varied from 0 to 169%.

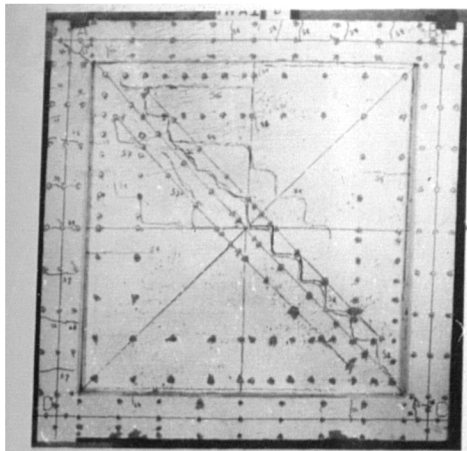
The post cracking response may be subdivided into two phases forming Stage 3 and 4 of the overall load-deflection diagrams: stage 3 covering parts of the load-deflection diagrams until the peak load is reached and Stage 4 covering the post peak load response.

Stage 3: Pre-peak load response

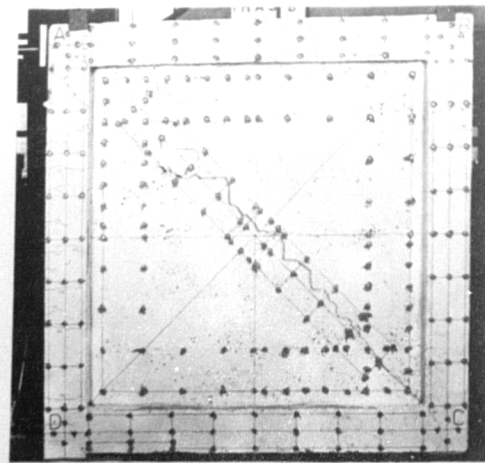
Once the frame and the infill had cracked, the response became slightly non-linear due to increasing amounts of cracking both in frame and infill. This part has, nevertheless, been approximated by one or two straight lines in the idealized load-deflection diagrams (figures 4.8 and 4.9). After the initial diagonal crack had occurred in the infill, more cracks formed and seemed to concentrate in the top left quarter of the infill. The condition of the infilled frames at peak load is shown in figures 4.12 to 4.14. It can be seen that in most cases the extent of cracking and crushing in the infills is relatively minor. The exceptions are the two weaker frames with the weak infill (IHW1 and IHW2), in which there is quite extensive cracking but still no significant crushing.

Stage 4: Post-peak load response

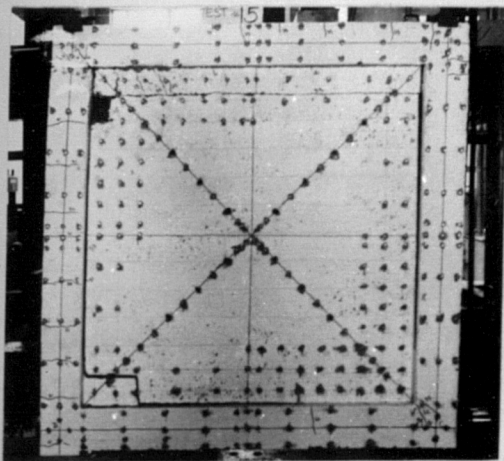
Once the peak load had been reached, the responses may be classified as either plastic (presence of one or two long plastic plateaux) or brittle (presence of a very short plastic plateau followed by a rapid drop in load). The individual idealized load-deflection diagrams have been given in figures 4.8 and 4.9. When the peak load had been reached and passed, the cracks, both in infill and frame, opened up, and new cracks developed. Eventually crushing occurred in the infill at one or both loaded corners. At this stage, there was considerable disintegration of the infill and in some cases even blocks in the centre of the infill were crushed. In most cases, the failure of the bounding frame was due to the development of a sufficient



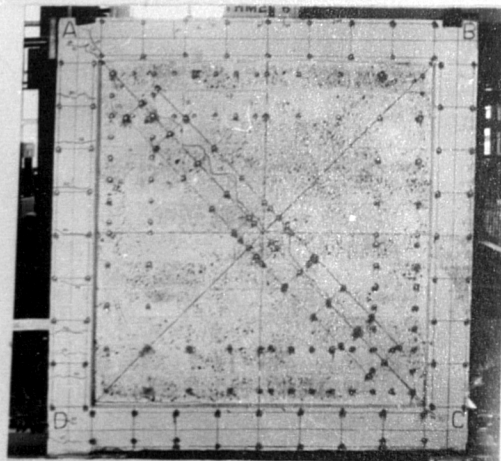
(a) IHW1



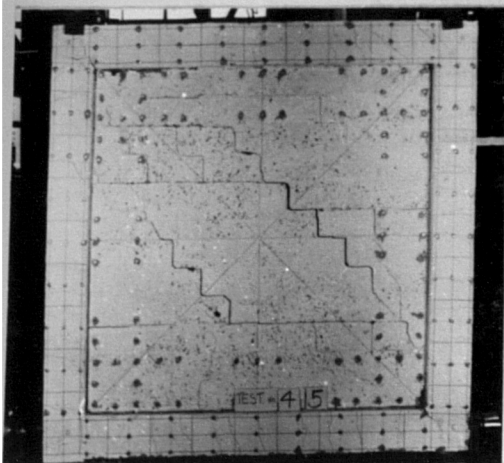
(b) IHW3



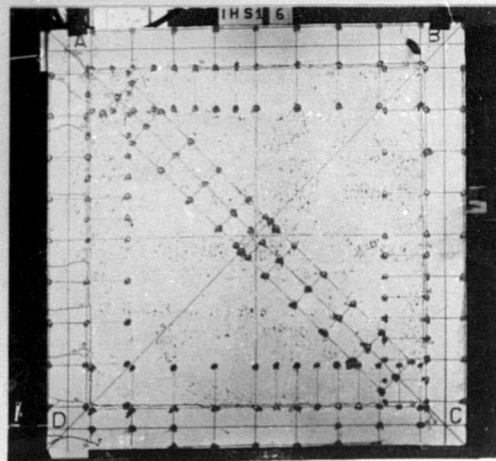
(c) IHM1



(d) IHM2*

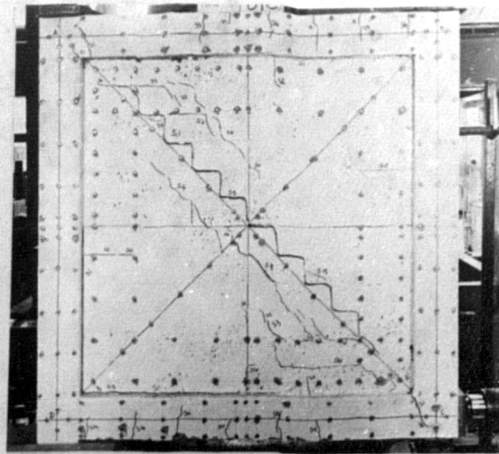


(e) IHM3

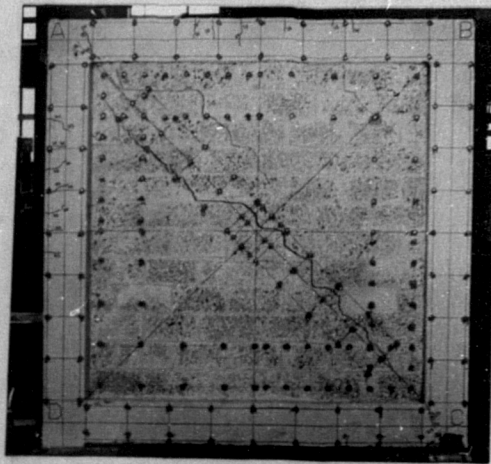


(f) IHS1

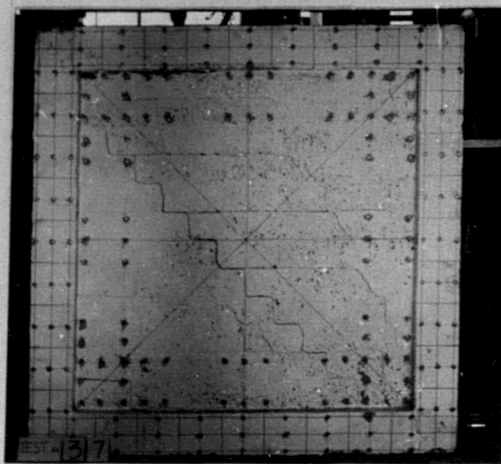
FIGURE 4.12: 'IH' SPECIMENS AT PEAK LOAD



(a) ICM1

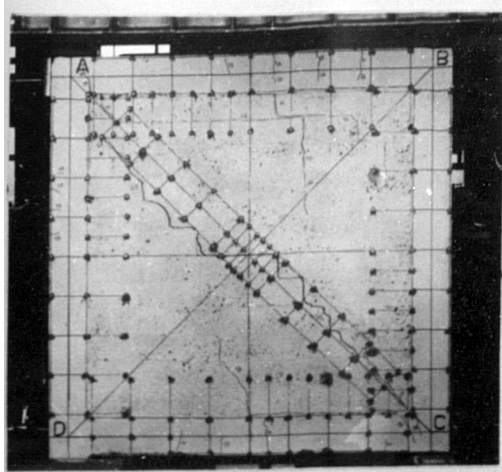


(b) ICM2*

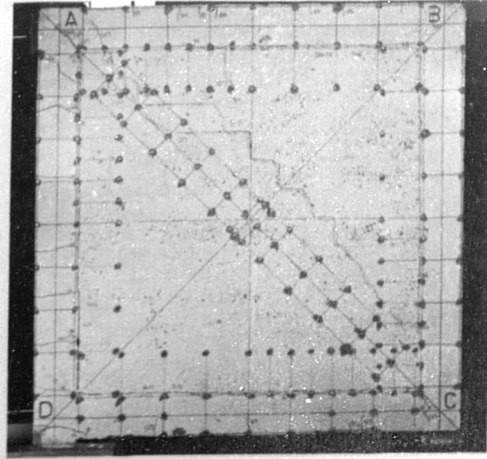


(c) ICM3

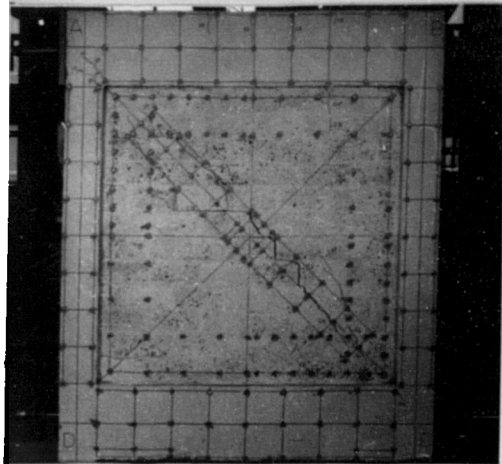
FIGURE 4.13: 'ICM'SPECIMENS AT PEAK LOAD



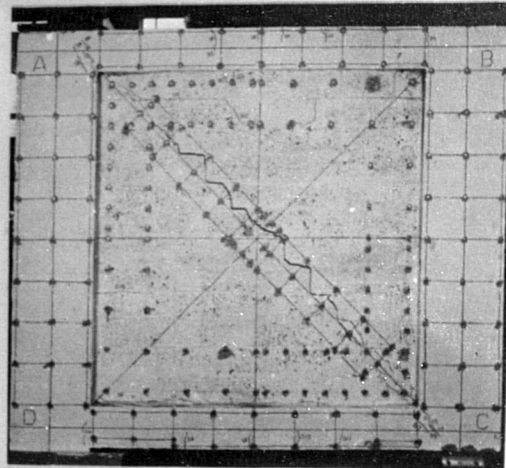
(a) ICS1



(b) ICS1**



(c) ICM4



(d) ICM5

FIGURE 4.14: 'IC' SPECIMENS AT PEAK LOAD

number of plastic hinges to give rise to a plastic collapse mechanism. In some cases, however, shear failure or tensile failure occurred before the plastic collapse mechanism had fully developed. Figures 4.15 to 4.17 show the infilled frames at large deflection or after complete failure. Two plastic collapse mechanisms have been identified. A detailed description of the different modes of failure and their classification is given in section 4.4.

From the idealized load-deflection diagrams, the post-peak load responses may be categorised as follows:

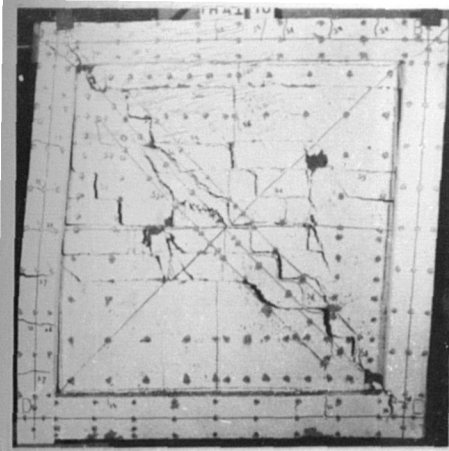
(i) Presence of a long plastic plateau

This type of response was observed in some of the infilled frames which developed a plastic collapse mechanism (IHW1, IHM3, ICM1 and ICM3) and also in ICM2 in which collapse was due to shear failure of the lower beam (figure 4.16(b)).

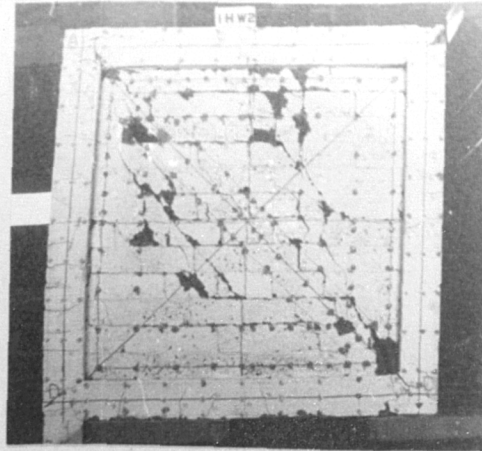
(ii) Presence of two plastic plateaux

At the end of the first plastic plateau, there was a sudden drop in load. This might be attributed to the increasing amount of cracking, especially in the infill. This drop was particularly important for IHM1, because at that stage, the top course separated from the rest of the infill and extensive crushing occurred in the top left-hand corner of the infill. Afterwards, the load stabilized for a while. This resulted in a development of a second plastic plateau until collapse occurred. This type of response was also observed in some specimens which developed a plastic collapse mechanism (IHW2, IHW3 and ICS1) and in IHM1 which would have developed one if a premature failure of the infill did not occur (this is discussed in section 4.4.3).

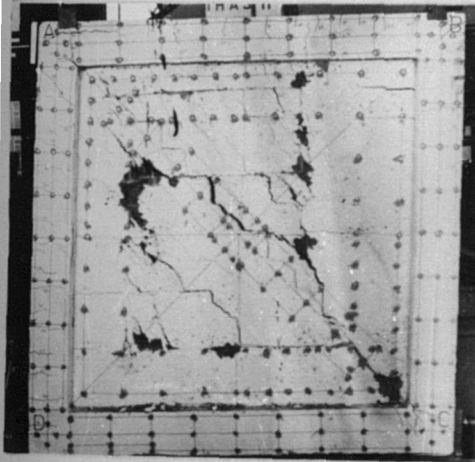
(iii) Presence of a very short plastic plateau



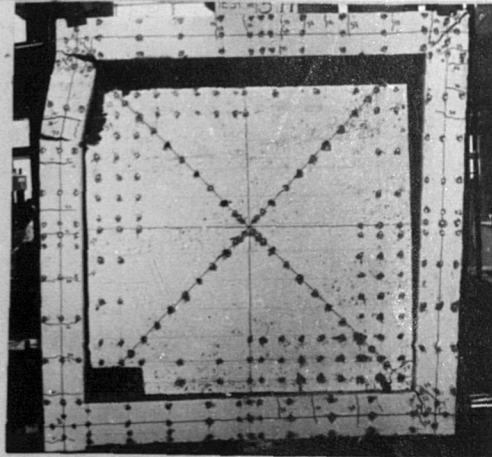
(a) IHW1



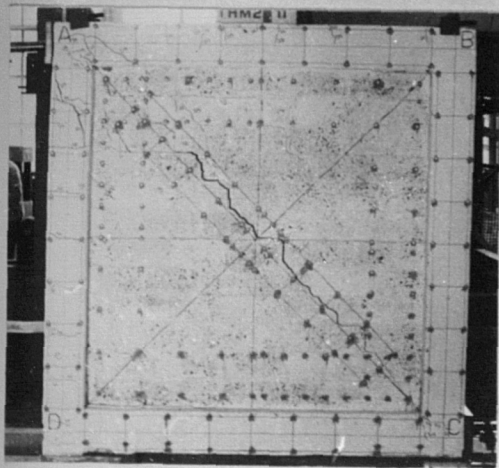
(b) IHW2



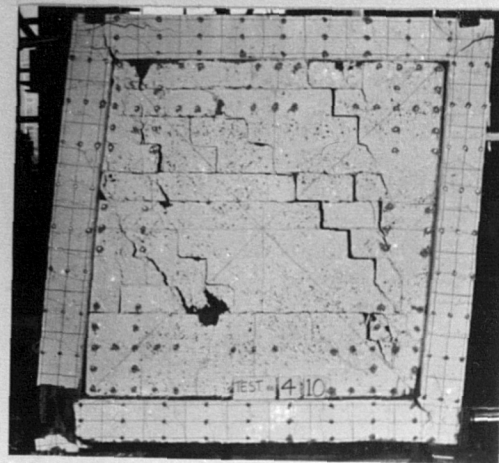
(c) IHW3



(d) IHM1

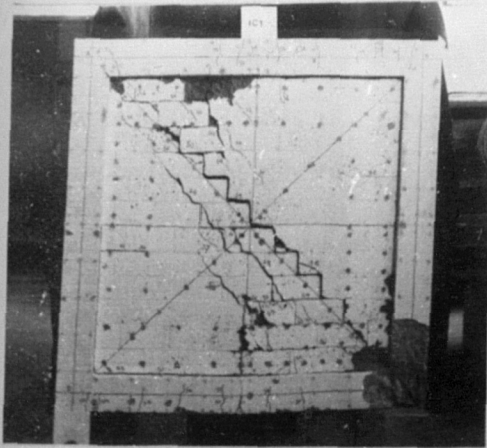


(e) IHM2*

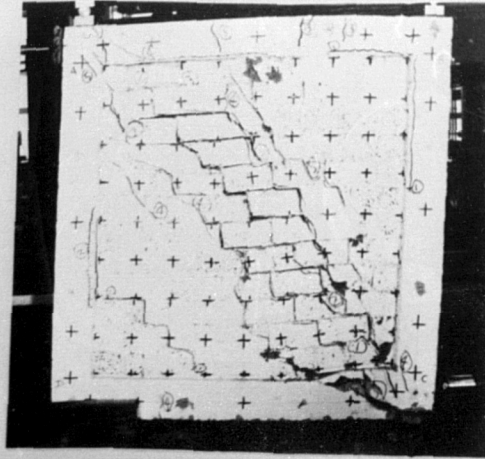


(f) IHM3

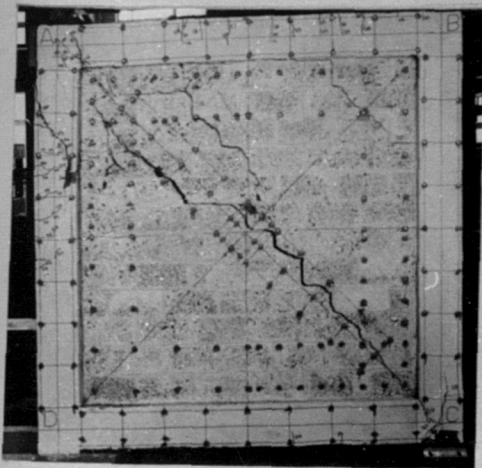
FIGURE 4.15: 'IH' SPECIMENS AT LARGE DEFLECTION OR AFTER FAILURE



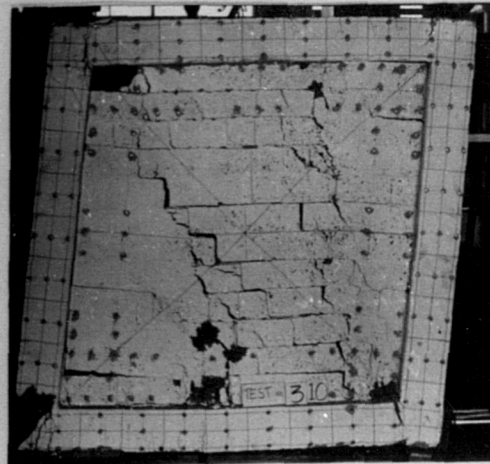
(a) ICM1



(b) ICM2

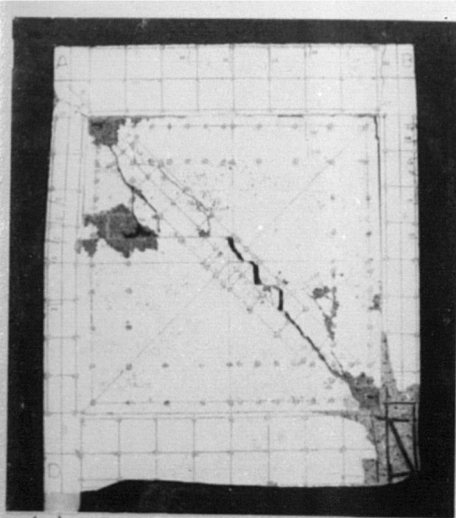


(c) ICM2*

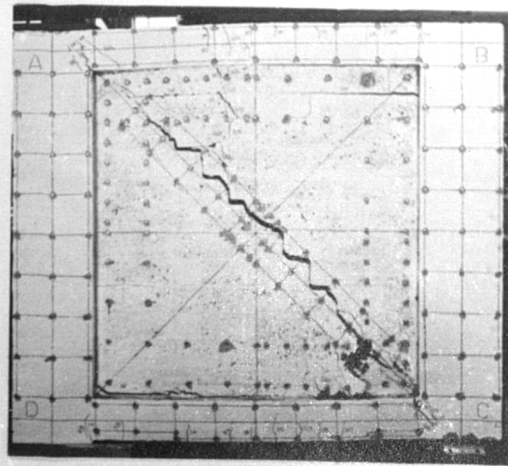


(d) ICM3

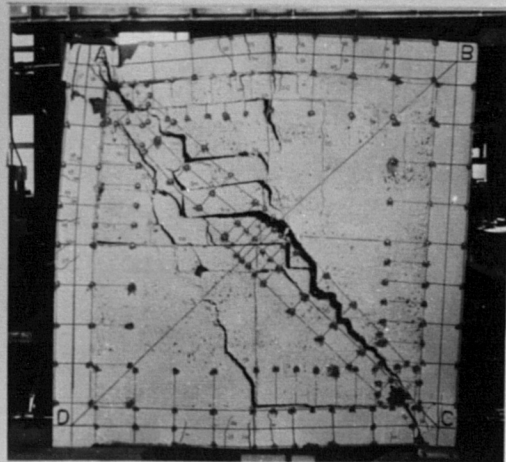
FIGURE 4.16: 'ICM'SPECIMENS AT LARGE DEFLECTION OR AFTER FAILURE



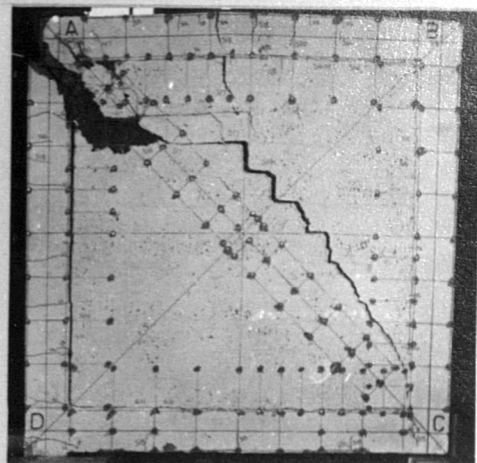
(a) ICM4



(b) ICM5



(c) ICS1



(d) ICS1**

FIGURE 4.17: 'IC' SPECIMENS AT LARGE DEFLECTION OR AFTER FAILURE

For this category, there have been three possible responses:

- a) The load causing the infill to crack was the peak-load. Following the cracking of the infill, the load dropped and then stabilized for a while to allow the development of a short plastic plateau. This was followed by a drastic drop in load (case of ICS1**).
- b) A short plastic plateau was reached after peak-load. It was followed by a drastic drop in load, as in a). This type of response was observed for IHM2* and ICM2*. For cases a) and b), the bounding frame eventually failed in shear (the failure occurred in the windward column near the junction with the top beam) as shown in figures 4.15(e) and 4.16(c).
- c) The response was similar to b) but with a relatively smooth descending branch. This type of response was observed for ICM4 and ICM5. For these two infilled frames, at peak-load, frame deformations were concentrated in the opening corners (figure 4.14(c) and (d)).

4.4 MODES OF FAILURE OF INFILLED FRAMES

4.4.1 General

From the observations made during the test and from a careful study of the photographs taken as each test progressed, a number of different modes of failure have been identified on the basis of the behaviour of the bounding frame. Most of the infilled frame failures involved the formation of a mechanism in which flexural failure only of the reinforced concrete frame occurred at various locations. In addition to these modes of failure, some frames failed either in shear or due to tension in the windward column.

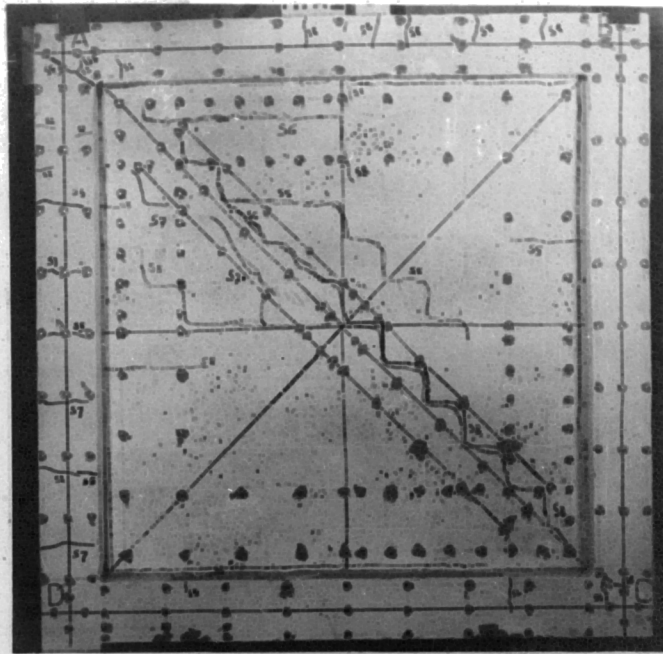
4.4.2 Normal Collapse Mechanisms, Involving Flexural Failure of Frames

Two collapse mechanisms have been identified (figures 4.18 and 4.21

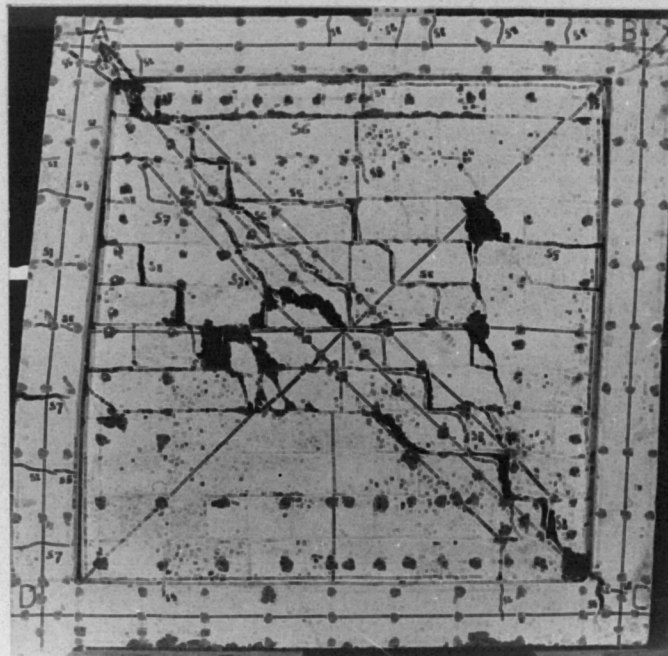
as representing the normal behaviour of the majority of the frames. The first one was associated with the 'IH' specimens and the second with the 'IC' specimens. One specimen, ICS1, did however develop a mechanism which was a combination of the two. The detailed discussion for these mechanisms is given below.

a) Mechanism 1

This mechanism was observed for half of the 'IH' specimens (IHW1, IHW2, IHW3 and IHM3). The description of failure modes for the other half is discussed in section 4.4.3. The idealized representation for this mechanism is shown in figure 4.19. Figure 4.18 illustrates this mode at peak load and at large deflection. The first hinges in the bounding frame occurred in the loaded corners. The windward (tension) column showed many horizontal cracks but only one of them was critical and it was at this position that the plastic hinge formed. The cracking in the top beam formed in the right half to yield a long zone of curvature which may be represented by an idealized plastic hinge occurring in the vicinity of the middle of the top beam. Following the first diagonal crack in the infill, more cracks developed in the top left quarter of the infill and seemed to converge towards the bottom right loaded corner. The infill was more strained towards the top of the diagonal than the bottom. This phenomenon has been confirmed by the strain readings taken along a hundred mm wide band of the compression diagonal while the response was still linear (Appendix D). The reason for this might be attributed to the non-symmetrical distortion of the infilled frame. This is probably due to the difference in behaviour of the two columns. The leeward (compression) column remained straight and uncracked even after failure, whereas a hinge formed in the windward (tension) column, which was subjected to a combination of tension, flexure and shear

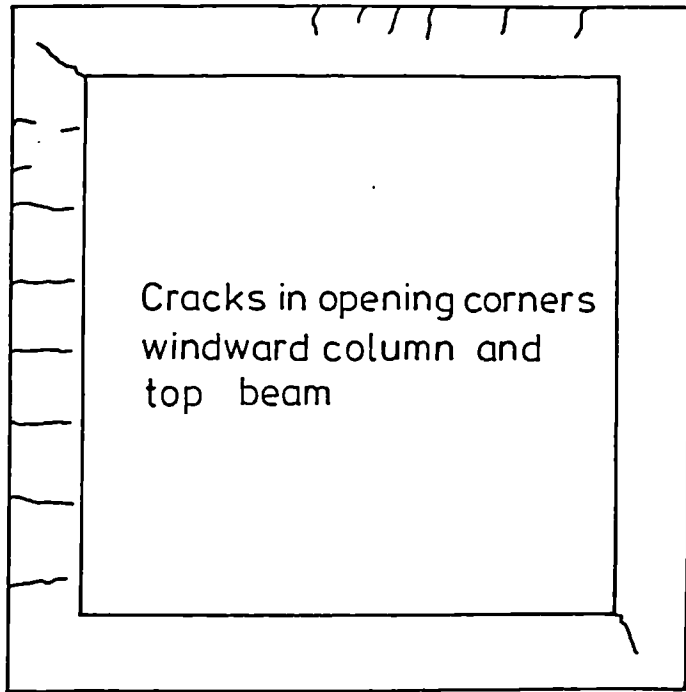


(a) at peak load

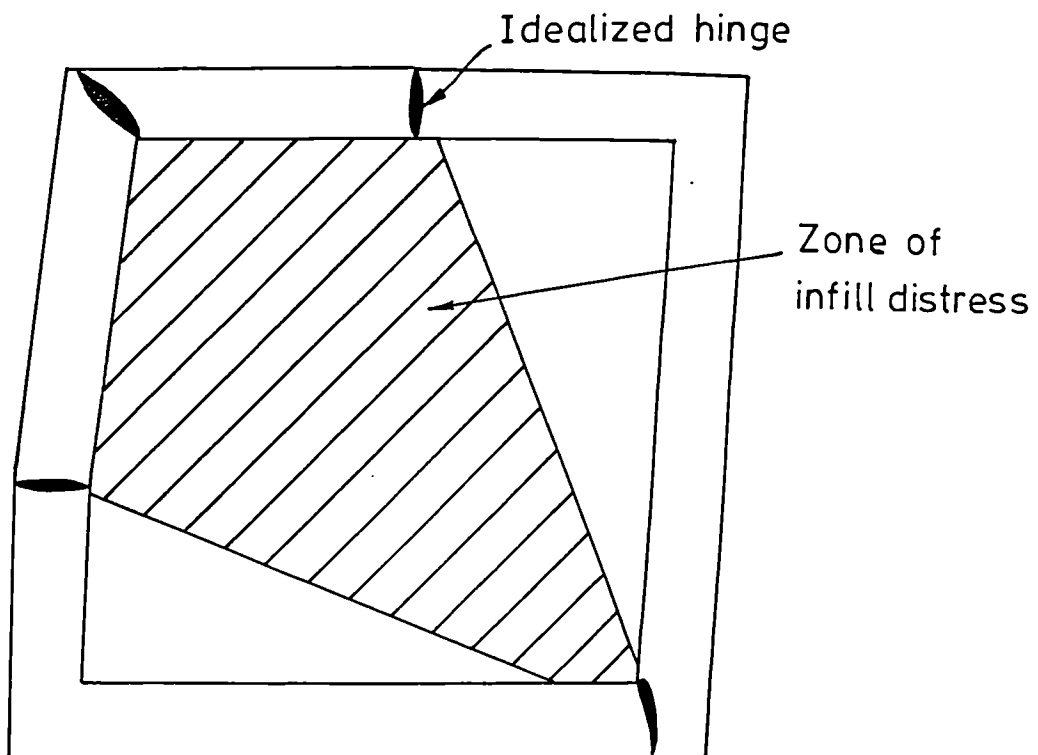


(b) after failure

FIGURE 4.18: TYPICAL ILLUSTRATION OF MECHANISM 1

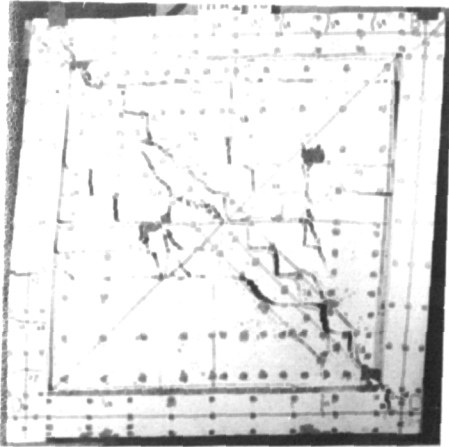


(a) Frame distortion at peak load

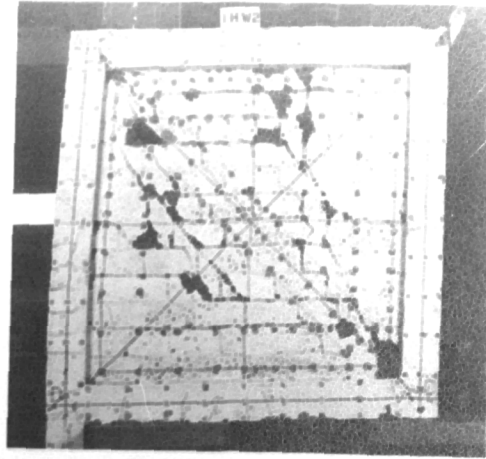


(b) Specimen at large deflection

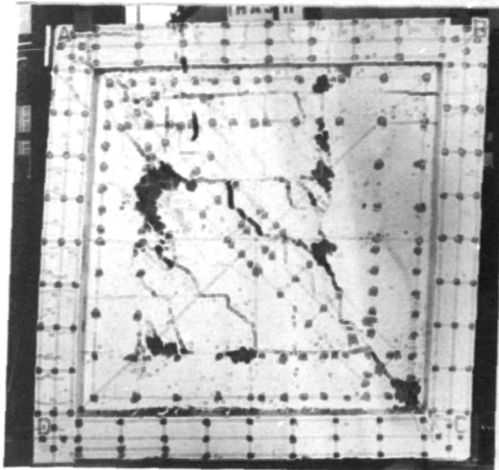
FIG.4.19 IDEALIZED REPRESENTATION OF MECHANISM 1



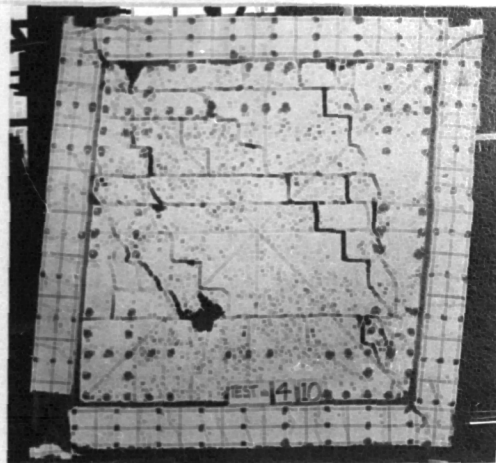
(a) IHW1



(b) IHW2



(c) IHW3



(d) IHM3

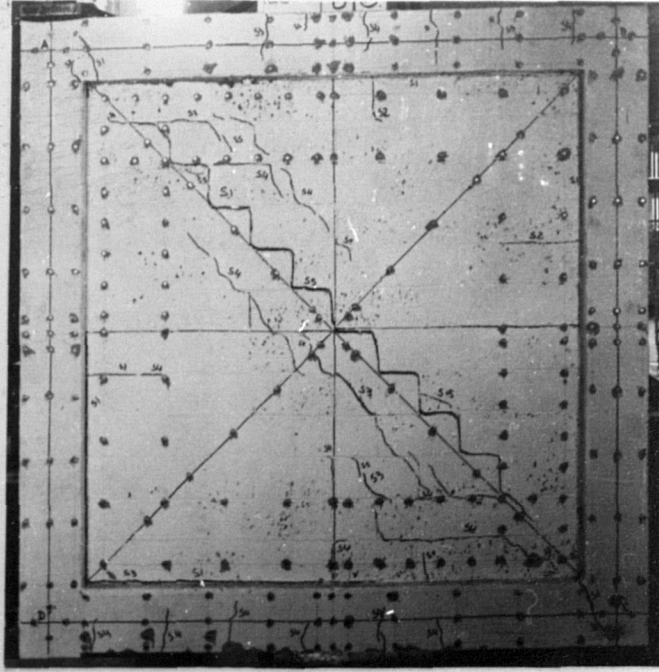
FIGURE 4.20: SPECIMENS DEVELOPING MECHANISM 1

b) Mechanism 2

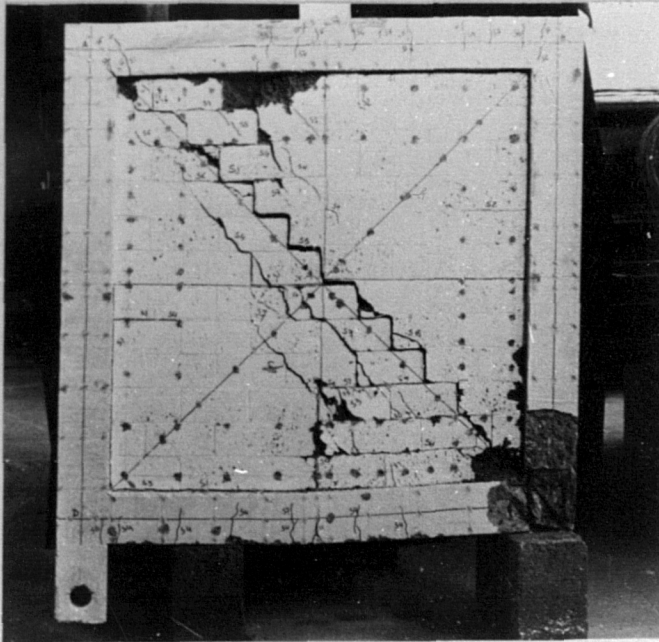
Three 'IC' specimens, ICM1, ICM3 and ICM5, developed mechanism 2. This was characterised by the relative symmetrical distortion especially at peak load as shown in figures 4.21 and 4.22. In effect both columns seemed to have remained straight while hinges were enforced approximately in the middle of both beams and in the loaded corners. Even after peak load, the two columns remained almost uncracked. For ICM5, however, the hinges in both beams developed well after the peak load had been reached and its infill showed one major diagonal crack which continued to open up until failure. At failure the whole bed joint of the top course was cracked. Eventually, the infill crushed in the vicinity of the bottom right-hand corner and in the top left quarter of the infill as shown in figure 4.23(d). For ICM1, after the infill had crushed at both ends, the concrete of the right support disintegrated after failure (figure 4.23(a)). For ICM3, at later stages of loading, a diagonal crack at the top of the windward column developed but failure of the frame eventually occurred by disintegration of the left support concrete. A lot of movements of parts of the infill were observed as for IHM3. There was also a bond failure of the top course as shown in figure 4.23(b).

c) Combination of the two mechanisms

The difference from the previous mechanism was that a hinge developed also in the windward column as shown in figure 4.24. This was observed only for one infilled frame, ICS1. When the peak load was reached, only one major diagonal crack was observed together with a horizontal crack along almost the whole bed joint of the top course. Flexural cracks were also observed in the windward column. Eventually, towards failure, the diagonal crack in the infill opened up and more minor cracks developed mainly in the top left quarter of the infill.

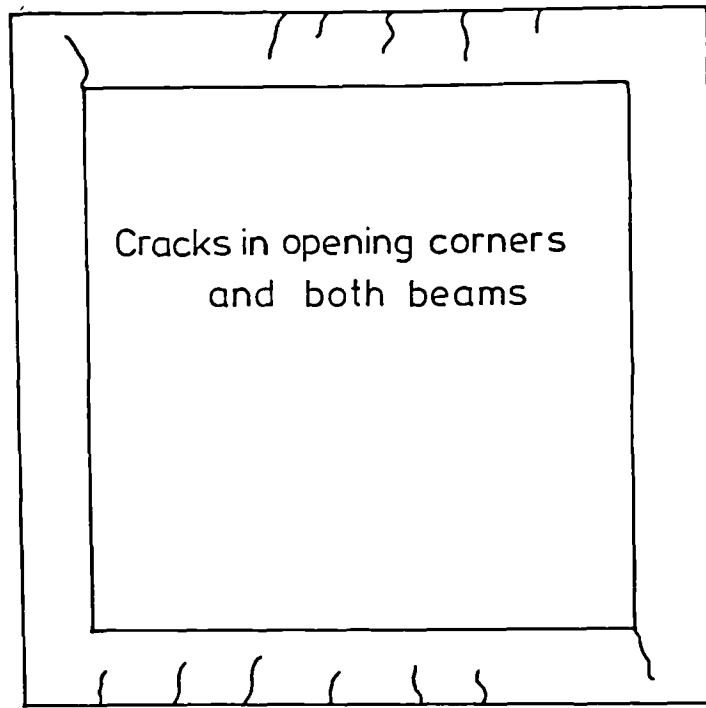


(a) at peak load

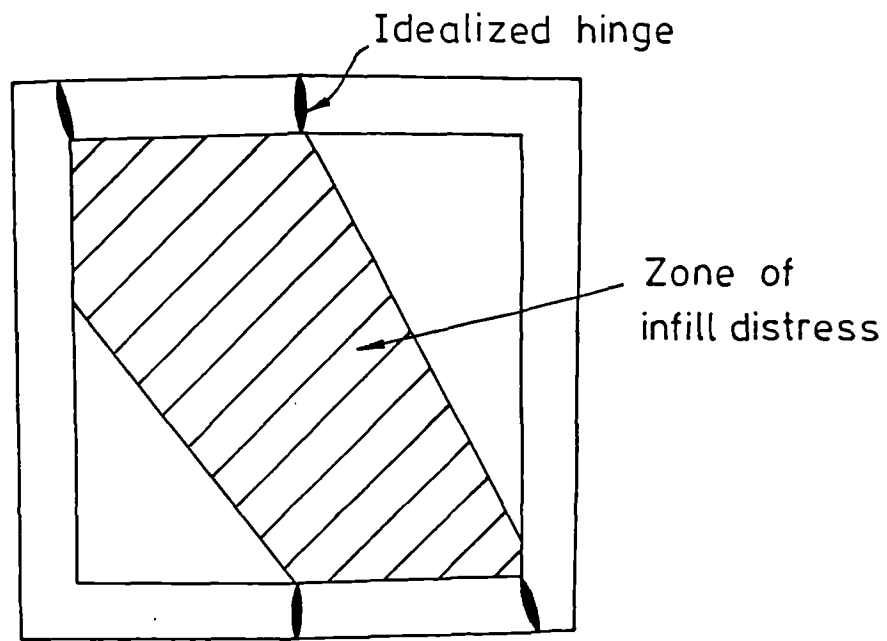


(b) after failure

F GURF 4.21: TYPICAL ILLUSTRATION OF MECHANISM 2

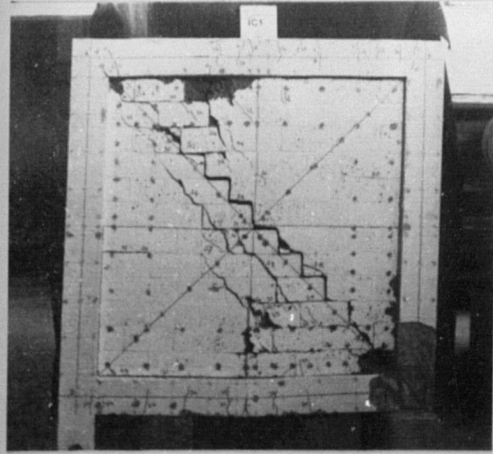


(a) Frame distortion at peak load

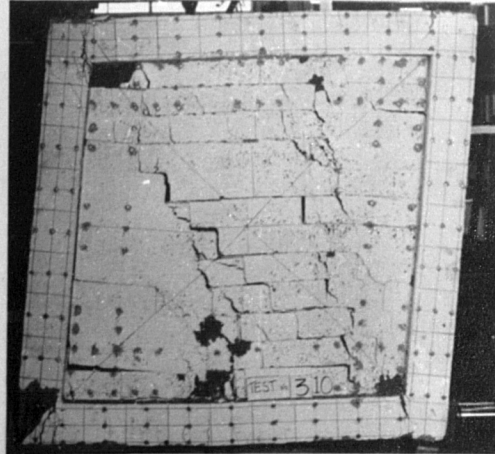


(b) Specimen after failure

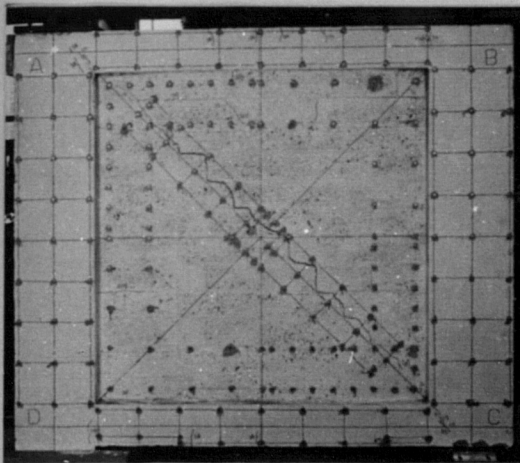
FIG.4.22 IDEALIZED REPRESENTATION OF MECHANISM 2



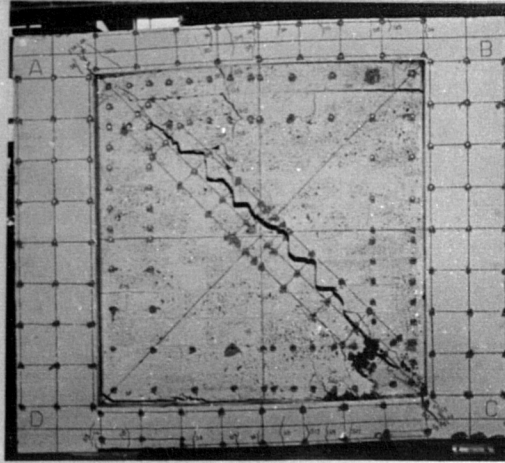
(a) ICM1



(b) ICM3

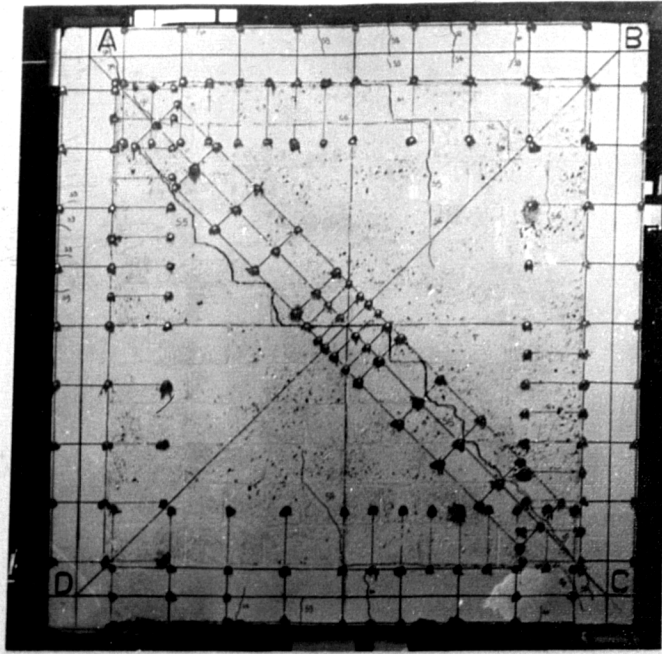


(c) ICM5 at peak load

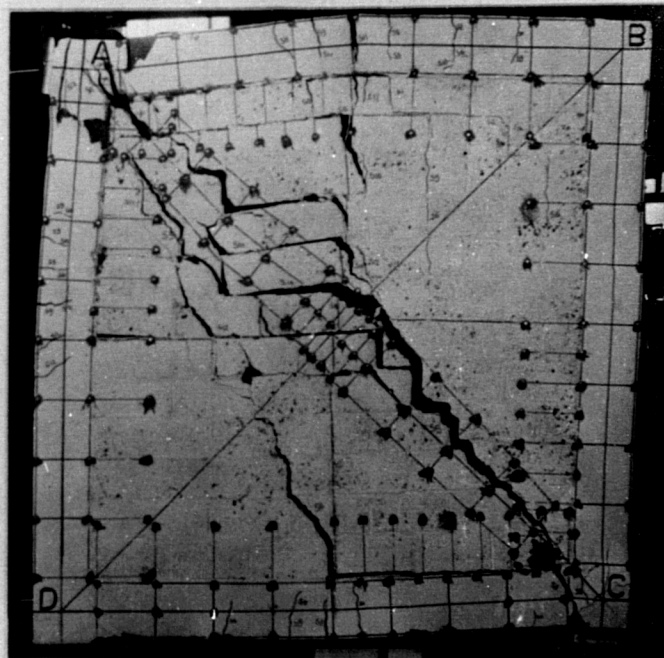


(d) ICM5 after failure

FIGURE 4.23: SPECIMENS DEVELOPING MECHANISM 2



(a) at peak load



(b) after failure

FIGURE 4.24: SPECIMEN DEVELOPING A COMBINATION OF MECHANISMS 1 AND 2

At the same time, the hinges in the bounding frame definitely opened up and collapse followed. The leeward column remained straight.

4.4.3 Special Cases

The infilled frames which developed mechanisms different from those described in the previous section may be classified into five groups.

a) Premature failure of frame (case of IHM2)

Only the windward column extension failed. The concrete around the cast tube which is part of the support crushed and the steel welded to the main cage yielded without breaking. This additional steel was not welded to the tube and that might have been the reason for this type of failure. The infill remained uncracked and absolutely intact (figure 4.25(a)). When failure occurred, the load-deflection response was still linear elastic. The only cracks observed in the frame developed in the loaded corners and the windward (tension) column.

b) Premature failure of infill (case of IHM1)

For most of the infilled frames tested, there had been a bond failure of a part of, or the whole bed joint of the top course after the occurrence of the initial diagonal crack in the infill. For IHM1, this bond failure of the top course occurred prematurely and no diagonal crack developed. The rest of the infill remained intact as shown in figure 4.25(b). The frame, however, developed hinges in the tension column (approximately 180 mm from bottom face of top beam as also shown in figure 4.25(b)) and in the loaded corners. Flexural cracks formed in the top beam. One of these cracks would have probably developed into a hinge if the top course had not failed. This resulted in a release of the pressure exerted by the infill against the top beam. The frame distortion was fairly similar to those

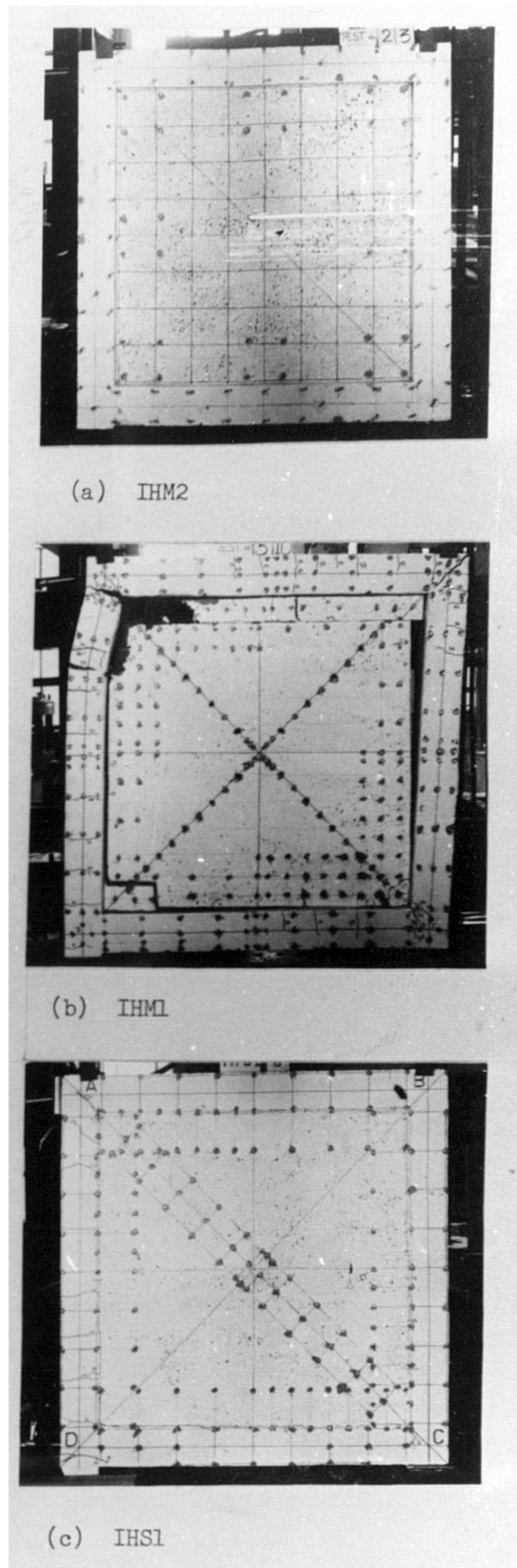


FIGURE 4.25: ILLUSTRATION OF FAILURE INVOLVING OTHER FRAME FAILURE MODES (special cases (a-c))

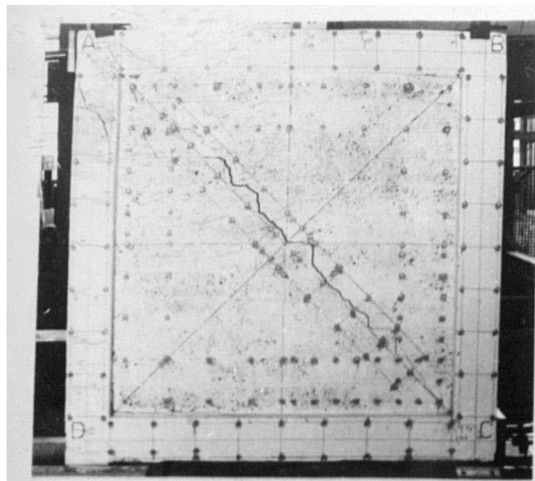
developing mechanism 1. Thus, IHM1 would have probably developed mechanism 1 if the diagonal crack in the infill had occurred. The load-deflection response showed two plastic plateaux (section 4.2).

c) Failure of the frame without failure of the infill (case of IHS1)

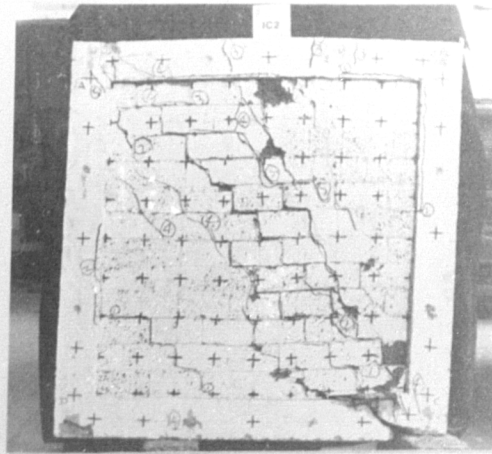
For this combination of the weakest frame and the strongest infill, S, the windward column reached its ultimate strength and the reinforcement yielded at the column extension. No cracks were produced in the infill, as shown in figure 4.25(c). When failure occurred, the load-deflection response was still linear elastic. After failure only peripheral cracks in the unloaded corners and horizontal cracks in the tension column were observed. A diagonal crack had developed in the tension column near the junction with the top beam. The ultimate load reached was less than the ultimate tension load based on yielding of the four main reinforcing bars in tension. It is thought this was probably because the windward column was subjected to a combination of tension and flexure.

d) Frames in which shear failure limited the development of hinges

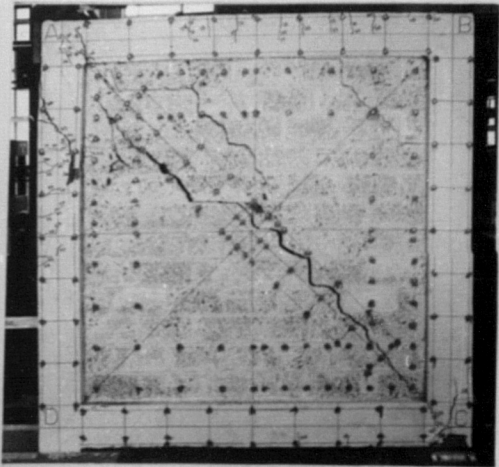
The shear failure occurred either in the windward column, near the junction with the top beam (IHM2*, ICM2* and ICS1**) as shown in figure 4.26(a, c and d) or the lower beam (ICM2) (figure 4.26(b)). In the first case, only one major diagonal crack in the infill was observed at peak load. It continued to open up accompanied by increased flexural frame deformation until shear failure occurred. The three load-deflection responses were similar (short plastic plateau followed by a drastic drop in load when the shear failure occurs). As for ICM2, though it failed in shear of the lower beam, the load-deflection response showed a long plastic plateau. The pattern of cracking in the infill was similar to that observed in specimens which developed either mechanism 1 or 2. Because of the



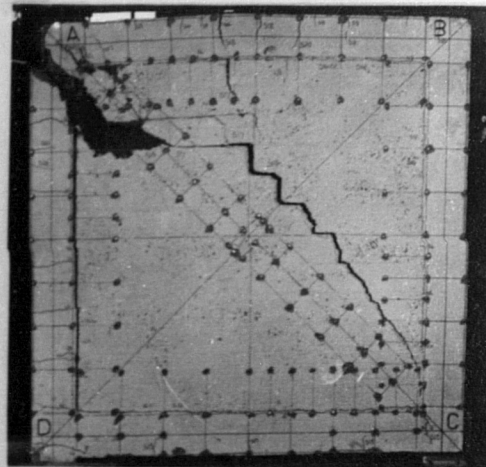
(a) IHM2*



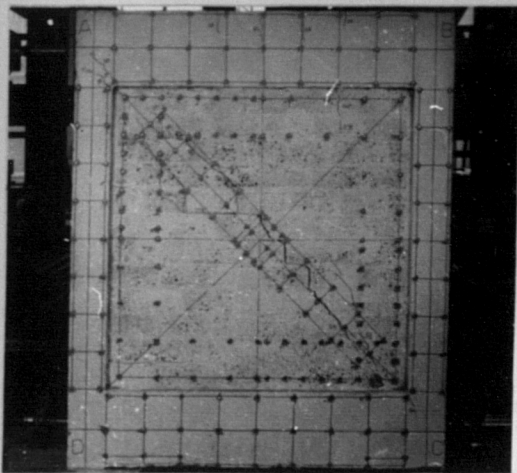
(b) ICM2



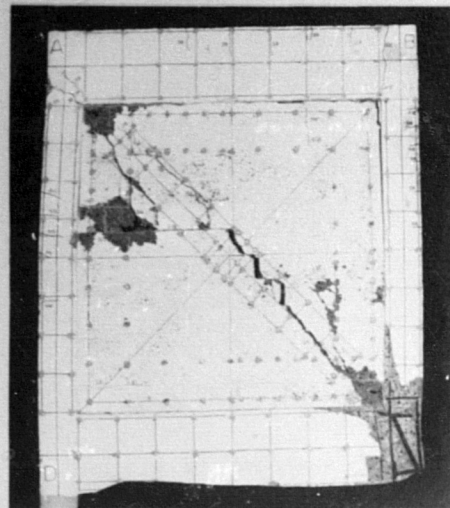
(c) ICM2*



(d) ICS1**



(e) ICM4 at peak load



(f) ICM4 after failure

FIGURE 4.26: ILLUSTRATION OF FAILURE INVOLVING OTHER FRAME FAILURE MODES (special cases (d and e))

similarity of the infilled frame distortion with those of ICM1, ICM3 and ICM5, ICM2 would have probably developed into mechanism 2 if shear failure of the lower beam had not occurred. Similar comments may be made about IHM2*, ICM2* and ICS1**. The first would have developed into mechanism 1 and the last two would have developed either mechanism 1 or a combination of mechanisms 1 and 2 as ICS1 if shear failure of the windward column had not occurred.

e) Frame in which only three hinges developed (case of ICM4)

At peak load, frame deformations were concentrated only in the opening corners (figure 4.26(e)) and the infill showed only one major diagonal crack. This crack continued to open until failure occurred (figure 4.26(f)). After the peak load had been passed, a hinge developed in the windward column. No hinge developed in the top beam but flexural cracks formed, and at a later stage cracks also formed at the top of the leeward column (see figure 4.26(f)). Thus, although this specimen failed to fully develop mechanism 1, the mode of deformation is similar with the concentrated beam hinge being replaced by distributed deformation in the beam and the top of the leeward column.

4.5 PRINCIPAL PARAMETERS FROM TESTS

4.5.1 Load Causing the First Cracks in the Frame

This load has been estimated in two ways:

- (i) From the recorded load when the first visible cracks were detected with the aid of a magnifying glass. This load is referred to as $H_{CF(0)}$.
- (ii) From the change in slope of the load-deflection graph. This load is referred to as $H_{CF(G)}$.

The agreement between the two estimates was found to be poor. The

difference ranged from 9% to -20%. Both estimates are recorded in Table 4.1. The reason for this discrepancy might be attributed to the difficulty of monitoring the precise load at which the first crack in the frame occurred. In effect, the recorded load was in general taken after the cracks had already formed.

4.5.2 Load Causing the First Cracks in the Infill

It was difficult to record the precise load at which the first cracks in the infill were observed because of their sudden occurrence and the subsequent drop in load which followed. This load, $H_{CI(0)}$, has been checked against the one obtained from the graph $H_{CI(G)}$ (major change in stiffness). The agreement between the two estimates was good with the difference ranging from -5% to 9%. The load obtained from the graph $H_{CI(G)}$ is adopted and defined as the one to cause the infill to crack. This is used in Chapter 5 where the test results are compared to those obtained from the theoretical and the empirical methods available. $H_{CI(G)}$ and $H_{CI(0)}$ are also recorded in Table 4.1.

4.5.3 Ultimate Carrying Capacity

Like the previous one, the precise value of this load was difficult to monitor. But unlike the previous load, this value could not be checked. The values recorded in Table 4.1 are the highest loads recorded by the data-logger. This load is referred to as H_{ue} .

4.5.4 Plastic Load

This value has been obtained from the simplified load-deflection diagrams and is referred to as H_{pe} . This is thought to be more reliable than H_{ue} as a measure of the ultimate load of the structure. The recorded values of H_{pe} are also given in Table 4.1.

4.5.5 Racking Stiffness Values

The initial racking stiffness, S_{He} , has been obtained from the slope of the 'best fit' line drawn in graphically, O'A, and from the best fit by linear regression ignoring the O point to eliminate any initial zero errors. The agreement between the two estimates was found to be remarkably good. The latter estimates are thought to be more accurate and are therefore adopted and reported in Table 4.1. The lateral stiffness has also been estimated in a similar way after cracking of the frame (section AB on the graph) and cracking of both the infill and the frame (section BC on the graph). The results are reported in Table 4.1 which also contains the various loads obtained from the tests. The secant 'stiffness' values (from O' to point of first infill cracking) are also reported in the same table.

4.6 EFFECT OF THE DIFFERENT VARIABLES

4.6.1 Effect of the Infill

The presence of the infill inside the frame not only increased the initial lateral racking stiffness and the ultimate strength of the open frame, but also changed the mode of frame distortion and greatly reduced the sidesway at maximum load and at the onset of plastic collapse. The occurrence of the cracks in the frame was also delayed. Table 4.2 clearly illustrates the effect of the infill by comparison between the principal parameters obtained for the infilled frames and their corresponding open frames. From Table 4.2, it can be seen that the initial racking stiffness increased by a factor ranging from 5.9 to 14.0. The increase in strength by a factor ranging from 2.4 to 8.6 and the increase in the frame cracking load by a factor ranging from 2.5 and 12.3. The reduction in sidesway deflection when the plastic stage was reached ranged from 25 to 73%.

Specimen Designation	H_{CF} (KN)		H_{CI} (KN)		Stiffness (KN/mm)				H_{pe} (KN)	H_{ue} (KN)	$\frac{H_{pe}}{H_{CI}}$	$\frac{H_{O'}}{H_{ue}}$ %
	0	G	0	G	1	2	3	4				
OHL	4.4	4.0	-	-	0.9	0.4	-	-	11.2	11.5	-	20.9
IHW1	12.8	-	18.0	17.0	5.3	5.3	2.0	5.4	25.0	27.6	1.47	4.7
IHM1	15.5	15.5	47.6	46.0	6.3	4.6	1.1	4.6	50.5	53.6	1.10	4.7
IHS1	28.1	30.6	-	-	10.4	5.6	-	-	-	56.3	-	8.5
OC1	5.6	4.9	-	-	1.5	0.9	-	-	10.6	10.9	-	20.2
ICM1	44.9	29.0	45.1	44.6	12.1	6.5	3.8	9.0	58.6	61.9	1.31	8.1
ICSI	57.6	-	63.7	63.7	15.5	15.5	3.9	15.5	73.0	76.0	1.15	8.8
ICSI**	60.3	-	93.9	-	16.0	16.0	11.0	16.0	82.9	93.9	1.00	7.1
OH2 ⁰	7.0	7.0	-	-	0.8	0.6	-	-	15.0	15.6	-	2.6
IHW2	17.4	17.4	17.4	17.4	7.4	4.6	4.6	7.4	40.8	41.0	2.34	13.4
IHM2	35.2	-	-	-	6.7	6.7	-	-	-	50.0	-	9.2
IHM2*	27.4	25.9	59.3	59.3	9.1	7.3	0.9	7.9	61.5	63.4	1.04	5.5
OC2	-	12.4	-	-	1.2	0.9	-	-	25.0	25.6	-	0.0
ICM2	57.9	48.1	57.9	57.9	11.4	4.2	2.1	8.4	62.5	67.3	1.08	14.9
ICM2*	60.3	-	65.8	65.8	16.9	13.2	4.2	15.6	81.9	85.1	1.24	2.2
IHW3	28.3	32.5	29.7	32.5	7.8	5.9	5.9	7.8	44.0	54.3	1.35	7.9
IHM3	36.8	35.8	36.8	35.8	5.5	2.6	2.6	5.5	45.0	51.4	1.26	11.9
ICM3	31.6	25.0	41.0	-	12.0	6.3	6.3	7.5	55.0	58.9	1.34	8.3
ICM4	65.2	48.5	55.0	-	14.4	9.4	9.4	14.3	88.0	93.7	1.60	6.0
ICM5	51.7	51.7	74.1	74.1	16.2	12.3	6.2	14.6	90.9	92.7	1.23	3.0

Notes 1: Initial lateral racking stiffness

2: After cracking of frame

3: After cracking of frame and infill

4: Secant stiffness

0: Observed: G; Graph; $H_{O'}$; Load at 0'

TABLE 4.1: PRINCIPAL PARAMETERS FROM TESTS

specimen designation	increase in stiffness %	increase in strength H_{ue} %	increase in strength H_{pe} %	increase in H_{CF} %	reduction in δ_{ue} %	reduction in δ_{pe} %
OH1	-	-	-	-	-	-
IHW1	489	140	123	220	78	65
IHML	600	366	351	288	69	30
IHS1	1056	390	-	665	83	-
OH2 ^o	-	-	-	-	-	-
IHW2	825	163	172	149	42	60
IHM2	738	221 [▲]	-	403	82	-
IHM2*	1038	306	310	270	78	63
OC1	-	-	-	-	-	-
ICML	707	468	453	492	11	25
IGS1	933	597	589	1076	52	44
IGS1**	967	762	682	1131	63	46
OC2	-	-	-	-	-	-
ICM2	850	163	150	282	35	73
ICM2*	1308	232	228	386	63	71

▲: specimen failed prematurely

H_{CF} : load causing the first cracks in the frame

δ_{ue} : deflection at peak load from experiment

δ_{pe} : deflection when plastic plateau is reached

TABLE 4.2: EFFECT OF THE INFILL

4.6.2 Effect of the Infill Thickness

Table 4.3 illustrates the effect of the infill thickness by comparing the same frames used in combination with infills of different thicknesses for both 'IH' and 'IC' specimens. From Table 4.3, it can be seen that the thicker the infill, the stiffer and the stronger is the infilled frame. The use of a thicker infill also delayed the occurrence of cracks both in infill and frame.

There was, however, one case where a theoretically stiffer and stronger specimen, IHM3, was less stiff and of approximately the same strength as IHW3. The possible explanations for this unexpected result might be attributed to the following factors:

- a) The frame of IHM3 was dropped accidentally prior to building of the infill and this caused some slight cracking in all elements of frame. This could be expected to have a direct influence on stiffness only.
- b) The disposition of reinforcement for the frame of IHM3 was slightly different from that of IHW3 (see Appendix A), especially in the opening corners. This could be expected to have a direct influence on the strength of the frame and therefore on that of the infilled frame.
- c) Since IHW3 was constructed and tested well after IHM3, the improvement in workmanship could be expected to have a direct influence on the strength of the infill. The sort of movements observed in the infill of IHM3 during the test as described in section 4.4.2 suggest that the bed and perpendicular joints were badly filled since most of the cracks occurred in the joints rather than in the blocks.

specimen designation	increase in stiffness %	increase in strength H _{ue} %	increase in strength H _{pe} %	increase in H _{CF} %	increase in H _{CI} %
IHW1	-	-	-	-	-
IHM1	19	94	102	21	171
IHS1	96	104	-	139	-
IHW2	-	-	-	-	-
IHM2*	23	55	51	49	241
IHW3	-	-	-	-	-
IHM3	-30	-5	2	10	10
ICM1	-	-	-	-	-
ICS1	28	23	25	99	43
ICS1**	32	52	42	108	111

Note: Minus sign indicates a reduction

TABLE 4.3: EFFECT OF THE INFILL THICKNESS

4.6.3 Effect of the Vertical Loads

The application of vertical loads on columns resulted in a substantial increase in stiffness. The 'IC' specimens were also stonger than the corresponding 'IH' ones. An increase in the cracking load of the frame, H_{CF} , and a reduction in the sidesway deflection were also observed. This increase in stiffness was also observed for the open frames. As far as the ultimate strength of open frames is concerned, this is discussed in section 5.1.4. The 'IC' specimens which did not fail in shear developed either mechanism 2 or a combination of mechanism 1 and 2 (4.4.2 and 4.4.3) whereas the 'IH' specimens developed mechanism 1. The application of vertical loads enforced two plastic hinges approximately in the middle of both beams. Table 4.4 illustrates the effect of the vertical loads by comparing the 'IC' specimens with the corresponding 'IH' ones. From Table 4.4 it can be seen that the major effect of the vertical loads is the substantial increase in stiffness and the increase in strength.

4.6.4 Effect of the Amount of Reinforcement

Three series of infilled frames are available for studying the effect of changes in the amount of reinforcement used in the frames ($\rho_t = A_s + A'_s/100 = 1.1\%$, 2% and 3.1%). From Table 4.5 it can be seen that this effect was pronounced for the first series (frames used in combination with the weak infill, W). Figure 4.3, also, illustrates this effect. For the other two series, this effect might be seen as hidden in the general scatter of the test results.

4.6.5 Effect of the Beam Stiffness and Strength

The effect of the variation in beam stiffness and strength is studied by comparing IC1 and IC4. Doubling the beam depth and reinforcing it with four 10 mm bars resulted in an increase in

specimen designation	increase in stiffness %	increase in strength H_{ue} %	increase in strength H_{pe} %	change in H_{CF} %	change in H_{CI} %	reduction in δ_{ue} %	reduction in δ_{pe} %
IHM1	-	-	-	-	-	-	-
ICM1	92	16	16	87	-3	24	37
IHS1	-	-	-	-	-	-	-
ICS1	49	35	-	88	-	25	-
ICS1**	54	67	-	97	-	41	-
IHM2*	-	-	-	-	-	-	-
ICM2	25	6	2	86	-2	73	26
ICM2*	86	34	33	133	11	3	21
IHM3	-	-	-	-	-	-	-
ICM3	118	15	22	-30	34	75	66

Notes (i) a minus sign indicates a reduction.

(ii) the compared values of H_{CI} and H_{CF} are those obtained from the graph. If a value is not available then, the observed one is used for the comparison.

TABLE 4.4: EFFECT OF THE VERTICAL LOADS

specimen designation	change in stiffness %	change in strength H_{ue} %	change in strength H_{pe} %	change in H_{CF} %	change in H_{CI} %
IHW1	-	-	-	-	-
IHW2	40	49	63	36	2
IHW3	47	97	76	154	91
IHM1	-	-	-	-	-
IHM2	6	-7▲	-	127	-▲
IHM2*	44	18	22	67	29
IHM3	-13	-4	-11	131	-22
ICM1	-	-	-	-	-
ICM2	-6	9	7	66	30
ICM2*	40	38	40	108	48
ICM3	-1	-5	9	-14	-8

Notes (i) ▲: IHM2 failed prematurely; infill remained uncracked

(ii) minus sign indicates a reduction

TABLE 4.5: EFFECT OF THE AMOUNT OF REINFORCEMENT

stiffness (19%), strength (51%), infill cracking load (23%) and frame cracking load (67%).

4.6.6 Effect of the Column Stiffness and Strength

The effect of the variation in column stiffness and strength is studied by comparing IC1 and IC5. The latter was 34% stiffer and 50% stronger. The infill cracking load increased by 66% and the frame cracking load by 78%.

4.7 DISCUSSION OF TEST RESULTS

4.7.1 General

The comparative study of the test results primarily concerns the two most important parameters obtained from the quantitative analysis: the initial racking stiffness and the ultimate strength. As for the development of cracks in frame and infill, it is a statistical phenomenon and depends to a large extent on the materials. The plastic load, H_{pe} , is thought to be more reliable than the peak load, H_{ue} , as a measure of the ultimate load because the peak load frequently represented an unstable condition and was to a large extent governed by the cracking strength of the infill. The peak load was also usually followed by a sudden drop in load.

4.7.2 Stiffness Comparison

From Tables 4.1 and 4.5, it can be seen that the stiffness of the infilled frame increases with the thickness of the infill and with the strength of the frame. It can also be seen from Table 4.4 that the stiffness of the infilled frame is directly influenced by the application of vertical loads on columns. All the 'IC' specimens were stiffer than the corresponding 'IH' ones. There are, however, cases of theoretically less stiff specimens being stiffer than theoretically stiffer ones. This was the case for IHW2 and IHM2, IHW3 and IHM3,

and the 'ICM' specimens. For the first two pairs of infilled frames, the most likely reason is workmanship. In effect IHW2 and IHW3 were respectively constructed well after IHM2 and IHM3. Nine months for the first and six for the second. Thus an important improvement in workmanship must have been accomplished.

As for the 'ICM' series, it can be seen from Table 4.5 that compared with ICML the stiffness increased with increasing reinforcement for ICM2* but decreased for ICM2. For ICM3, there was a small increase over ICM2 and the stiffness was still less than that of ICML. This result suggests that the amount of frame reinforcement has little effect on the stiffness of infilled frames and that the variations observed might be due to workmanship or can simply be seen as part of the general scatter of the test results.

The small effect the variation in frame strength seems to have on the stiffness of infilled frames is confirmed by the comparison of ICM2* and ICM5. Doubling the column depths and reinforcing them with four 10 mm bars, whereas frame type 2 was reinforced with four 8 mm bars yielded a stiffness for the infilled frame ICM5 of the same order as that of ICM2*. In fact ICM5 was 4% less stiff. This result suggests that the stiffness of an infilled frame may be governed by the stiffness of the infill only.

4.7.3 Ultimate Strength Comparison

From Tables 4.1 to 4.5, it can be seen that the strength of the infilled frame increases with the thickness of the infill and with the strength of the frame. As for the stiffness, the strength was also directly affected by the application of vertical loads on columns. All the 'IC' specimens were stronger than the corresponding 'IH' ones. From sections 4.6.5 and 4.6.6, it can be seen that doubling either the

beam depths or the column depths resulted in an increase of 50% for the strength. This result concerning the effect of the stiffness and strength of the beams shows that they are as important as the columns in determining the resistance to lateral racking load. Other investigators, such as S. Smith, Mainstone, etc., reported that the beams for steel infilled frames had little effect. This, however, needs to be investigated further because only one infilled frame with deep beams was tested.

As for the stiffness comparison, there are cases of theoretically less strong specimens being stronger than theoretically stronger ones. The major problems arose for IHM3 and ICM3. The first is 11% weaker than IHM1 and of approximately the same strength as IHW3 (same type frame in combination with a weaker infill). The second, ICM3, was of approximately the same strength as ICM2 but 33% weaker than ICM2*. The reasons for this might be attributed to the following factors:

(i) The disposition of reinforcement for the frames of IHM3 and ICM3 was slightly different from that of the other frames. No diagonal links were put in the opening corners (figure A.3). In Taylor's tests [57], the efficiency of the opening corners for this disposition of reinforcement was of 20%. Thus for these two specimens the frames might have contributed less to the overall strength.

(ii) Poorer workmanship for IHM3 and ICM3. The sort of movements observed in their infills during the tests as discussed in section 4.4.2 suggest that bond at the bed and perpendicular joints may have been poorer since most of the cracks occurred in the joints rather than in the blocks. The effect of workmanship is confirmed by the comparison of the duplicate specimens.

4.7.4 Duplicate Specimens

Three pairs of nominally identical specimens were tested to check the repeatability of the test results.

(a) Case of IHM2 and IHM2* .

Since IHM2 failed prematurely (failure occurred in the windward column extension and the infill remained intact), the only comparison which could be made is about the initial racking stiffness. IHM2* was 36% stiffer than IHM2. This might be attributed to two factors:

(i) effect of importance of disposition of reinforcement for IHM2 as discussed in section 4.7.2;

(ii) improvement in workmanship, since IHM2* was the last specimen to be constructed and tested.

(b) Case of ICM2 and ICM2*

ICM2* is stiffer (48%) and stronger (31% when the plastic loads are compared and 26% when the peak loads are compared) than ICM2. These two infilled frames developed two different modes of failure. Both failed in shear. For the first the shear failure occurred in the windward column near the junction with the top beam and for the second it occurred in the lower beam near the junction with the leeward column. The two load-deflection diagrams were different (long plastic plateau for ICM2 and short plastic plateau for ICM2*). The shear failure, however, occurred at the end of both plastic plateaux. This indicates that the ultimate load was not governed by the shear failure. The possible reasons for this difference in the test results and in behaviour might be attributed to the following factors:

(i) conditions of supports were different. ICM2 did not have an

extension in the windward column and it rested on a 50 mm wide plate on the right hand side, so a concentration of stresses was localized at the bottom of the leeward column which might have encouraged the development of a diagonal crack in the lower beam near the junction with the leeward column, that is where the shear failure occurred;

(ii) improvement in workmanship for ICM2*. ICM2 was the first specimen tested.

(c) Case of ICS1 and ICS1**

It must be pointed out that ICS1** was first tested under horizontal racking loading only as IHS1. Failure in this case was a tensile failure of the windward column extension. Its infill, however, remained intact. Only peripheral cracks in the unloaded corners were observed. When it was retested under combined loading, the application of vertical loads on columns closed up the peripheral cracks and released somehow the pressure on both beams, whereas for ICS1 flexural cracks in both beams formed just after the application of vertical loads on columns. This might explain why ICS1 developed five hinges, two of which formed in the middle of both beams. The two specimens were approximately of the same stiffness (ICS1** was 3% stiffer than ICS1). The difference in strength is, however, more important, 24% when the peak loads are compared and 14% when the plastic loads are compared. As it was explained previously, comparing the peak loads may not be a good indicator because these depended to a large extent on the cracking strength of the infill. The difference in strength may be seen as part of the scatter of test results or due to the age of the specimens when tested. ICS1 was tested at twenty-eight days and ICS1** was first tested as IHS1 at twenty-eight days and retested as ICS1** at forty-three days. For these two specimens, the load-deflection responses were different (two plastic plateaux for ICS1 and

one short plastic plateau for ICS1**). The modes of failure were also different. ICS1 developed a combination of mechanism 1 and 2 (section 4.4.2) whereas ICS1** failed due to shear at the position of the diagonal crack that had resulted from the testing of IHS1. This might have been a plane of weakness when ICS1** was tested.

CHAPTER 5

COMPARISON OF TEST RESULTS WITH THEORETICAL AND EMPIRICAL PREDICTIONS FROM EARLIER WORK

5.1 PHYSICAL PROPERTIES OF REINFORCED CONCRETE FRAMES

5.1.1 Estimated Ultimate Resistance Moments of Frame Members

The ultimate moments of resistance of frame members were estimated by three methods:

- (i) HOGNESTAD
- (ii) CP 110 stress-block with $\gamma_m = 1.0$
- (iii) Simplified stress-block or rectangular stress-block with $\gamma_m = 1.0$

The values of ultimate moments were computed using the actual stress-strain curve of reinforcing bars (Figure 3.4) and the actual concrete cube compressive strength obtained from tests (Table 3.1) together with the appropriate stress-block factors taken from Kong and Evans [72]. For combined loading cases, the calculations for column sections took into account the vertical load (125 KN per column) applied prior to the application of the racking load. The ultimate moments of resistance were also calculated for the beams at the corner section because the reinforcing bars were cranked at this level (see Appendix A). The geometrical characteristics of the frames are given in Table 5.1, and the estimated moments of resistance of frame members by the three methods are given in Table 5.2 together with the concrete cube strength.

5.1.2 Shear Resistance of Frame Members

The shear resistance of frame members was calculated using the CP 110

Specimen designation	$l \times h$ (mm x mm)	Beam				Column		
		$b \times d_t$ (mm x mm)	$A_s = A'_s$ (mm ²)	d' (mm)	d'_1 (mm)	$b \times d_t$ (mm x mm)	$A_s = A'_s$ (mm ²)	$d' = d'_1$ (mm)
OH1	910 x 910	100 x 100	56.6	13.0	20.5	100 x 100	56.6	13.0
IHW1	"	"	"	"	28.0	"	"	"
IHM1	"	"	"	"	19.5	"	"	"
IHS1	"	"	"	"	26.0	"	"	"
OC1	"	"	"	"	21.5	"	"	"
ICM1	"	"	"	"	21.5	"	"	"
ICS1	"	"	"	"	25.0	"	"	"
ICS1**	"	"	"	"	26.0	"	"	"
OH2 ⁰	"	"	100.5	14.0	14.0	"	100.5	22.0
IHW2	"	"	"	"	21.5	"	"	14.0
IHM2	"	"	"	"	14.0	"	"	22.0
IHM2*	"	"	"	"	23.0	"	"	14.0
OC2	"	"	"	"	14.0	"	"	14.0
ICM2	"	"	"	"	14.0	"	"	22.0
ICM2*	"	"	"	"	21.5	"	"	14.0
IHW3	"	"	157.1	15.0	24.0	"	157.1	15.0
IHM3	"	"	"	"	25.0	"	"	"
ICM3	"	"	"	"	25.0	"	"	"
ICM4	910 x 1010	100 x 200	"	"	22.5	"	55.6	13.0
ICM5	1010 x 910	100 x 100	56.6	13.0	21.0	100 x 200	157.1	15.0

- Notes
- (i) d'_1 : depth to compression reinforcement at the corner level
 - (ii) " : idem result
 - (iii) l, h, b, d_t, A_s, A'_s and d' see notations

TABLE 5.1: GEOMETRICAL CHARACTERISTICS OF FRAME MEMBERS

Specimen designation	f_{cu} (N/mm ²)	M_{ub} (KN.m)			M_{ubc} (KN.m)			$M_{uc} = M_{ucc}$ (KN.m)		
		a	b	c	a	b	c	a	b	c
OHL	40.8	3.0	3.0	3.0	2.8	2.8	2.8	3.0	3.0	3.0
IHWL	43.4	3.1	3.1	3.1	2.6	2.7	2.7	3.1	3.1	3.1
IHML	43.4	3.1	3.1	3.1	2.8	2.8	2.9	3.1	3.1	3.1
IHSL	36.3	3.0	3.1	3.1	2.6	2.6	2.6	3.0	3.1	3.1
OCL	37.2	3.0	3.0	3.0	2.7	2.8	2.8	5.0	5.1	5.0
ICML	45.4	3.0	3.1	3.1	2.8	2.9	2.9	5.6	5.8	5.7
ICSL	41.3	3.0	3.0	3.1	2.6	2.7	2.7	5.4	5.6	5.4
ICSL**	36.3	3.0	3.1	3.1	2.6	2.6	2.6	5.4	5.6	5.4
OH2 ⁰	43.1	4.3	4.3	4.4	4.3	4.3	4.4	3.8	3.8	3.9
IHW2	36.3	4.3	4.3	4.4	3.7	3.8	3.9	4.3	4.3	4.4
IHM2	43.1	4.3	4.3	4.4	4.3	4.3	4.4	3.8	3.8	3.9
IHM2*	42.9	4.3	4.3	4.4	3.8	3.8	3.9	4.3	4.3	4.4
OC2	43.1	4.3	4.3	4.4	4.3	4.3	4.4	5.9	6.0	5.9
ICM2	46.8	4.4	4.4	4.4	4.4	4.4	4.4	5.6	6.1	5.8
ICM2*	45.2	4.3	4.4	4.4	3.8	3.9	3.9	6.6	7.0	6.8
IHW3	39.4	6.5	6.5	6.6	5.2	5.2	5.3	6.5	6.5	6.6
IHM3	44.6	6.5	6.6	6.7	5.1	5.2	5.3	6.5	6.6	6.7
ICM3	42.8	6.5	6.6	6.7	5.1	5.2	5.3	8.0	8.5	8.2
ICM4	39.9	15.6	15.5	15.6	14.7	14.6	14.7	5.2	5.6	5.3
ICM5	38.7	3.1	3.0	3.1	2.7	2.8	2.7	23.5	23.8	23.5

Notes 1) Estimation of ultimate moments of resistance

- a) Hognestad's method
- b) CP 110 stress-block with $\gamma_m = 1.0$
- c) simplified stress block or rectangular stress block with $\gamma_m = 1.0$

2) f_{cu} , M_{ub} , M_{ubc} , M_{uc} and M_{ucc} see notations

TABLE 5.2: ESTIMATED ULTIMATE MOMENTS OF RESISTANCE BY THREE METHODS

method [73]. The partial safety factors suggested by CP 110 were however omitted. The results are given in Table 5.3

$$b(v - 1.5v_c) \leq f_{yv} A_{sv} / S_v \quad (1)$$

where b : is the width of the section

v : shear stress in frame members

v_c : ultimate shear stress in concrete

A_{sv} : cross-sectional area of the two legs of a link

S_v : spacing of links along the member

f_{yv} : yield strength of link reinforcement

v_c is taken from Table 5 of CP 110 and f_{yv} from Table 3.2 in section 3.3.

from (1) $v \leq \frac{f_{yv} A_{sv}}{b S_v} + 1.5v_c$

The shear strength is therefore $V = v \times b \times d$

	$1.5v_c$ N/mm ²	f_{yv} N/mm ²	S_v mm	b mm	A_{sv} mm ²	v N/mm ²	$V = v \times b \times d$ (KN)
Frame 1	0.83	199	55	100	17	1.45	14.5
Frame 2	1.13	"	"	"	"	1.75	17.5
Frame 3	1.30	"	"	"	"	1.92	19.2
Frame 4 beam	0.98	"	"	"	"	1.60	32.0
column	0.83	"	"	"	"	1.45	14.5
Frame 5 beam	0.83	"	"	"	"	1.45	14.5
column	0.98	"	"	"	"	1.60	32.0

Note " idem

TABLE 5.3: SHEAR STRENGTH OF FRAME MEMBERS

5.1.3 Ultimate Resistance Moments from Tests

After the first infilled frames had been tested, some of the uncracked blocks and assemblies of blockwork were recovered and tested in compression (sections 3.4.3 and 3.4.4). Then, the remaining parts of the infill panels were removed and the frames were cut at the four corners. The frame members were tested in flexure in an Amsler machine. Because it was not always possible to save the total length of the frame members and since the stronger frame members failed in shear, four arrangements for the supports and for the application of point loads were made (figure 5.1(a)) in order that the specimens should fail in flexure. Figure 5.1(b) shows a typical load deflection graph for flexure failure. The test results are given in Table 5.4. The calculation for the plastic moment of resistance was based on the plastic load.

5.1.4 Ultimate Resistance Moments from the Analysis of Open Frame Test Results

The load-deflection diagrams for the four open frames tested are shown in figure 5.2. The principal parameters obtained from tests such as the racking stiffness, the cracking load etc., have been given in Table 4.1. Table 5.5, however, gives the peak load reached in the test, H_{ue} , and the plastic load obtained from the idealized diagrams (figure 4.10). The estimated moments of resistance of frame members are also given in Table 5.5 (columns 4 to 15). These moments are also estimated by taking into account the axial loads induced in frame members by respectively H_{ue} and H_{pe} , and the initial vertical loads applied on each column (125KN for OC1 and 50KN for OC2) prior to the application of the racking load.

Since the plastic hinges occurred in the beam near the junction with the columns and if an efficiency of 100% for the opening corners were assumed, then, the ultimate moments of resistance of the beams at

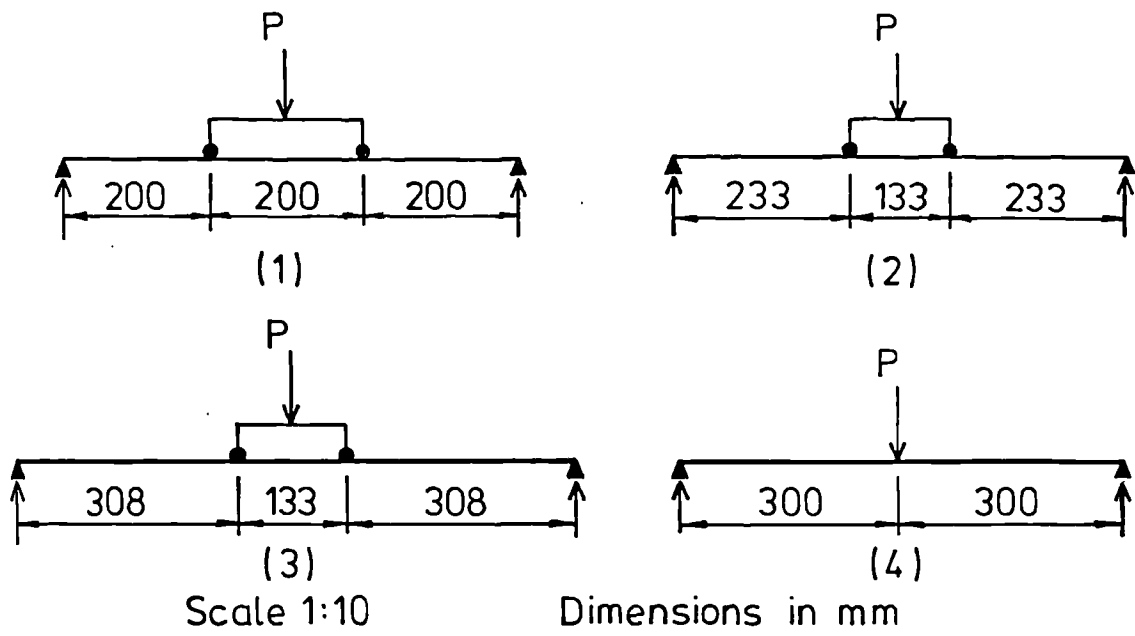


FIG. 5.1a ARRANGEMENTS OF SUPPORTS FOR TESTING FRAME ELEMENTS

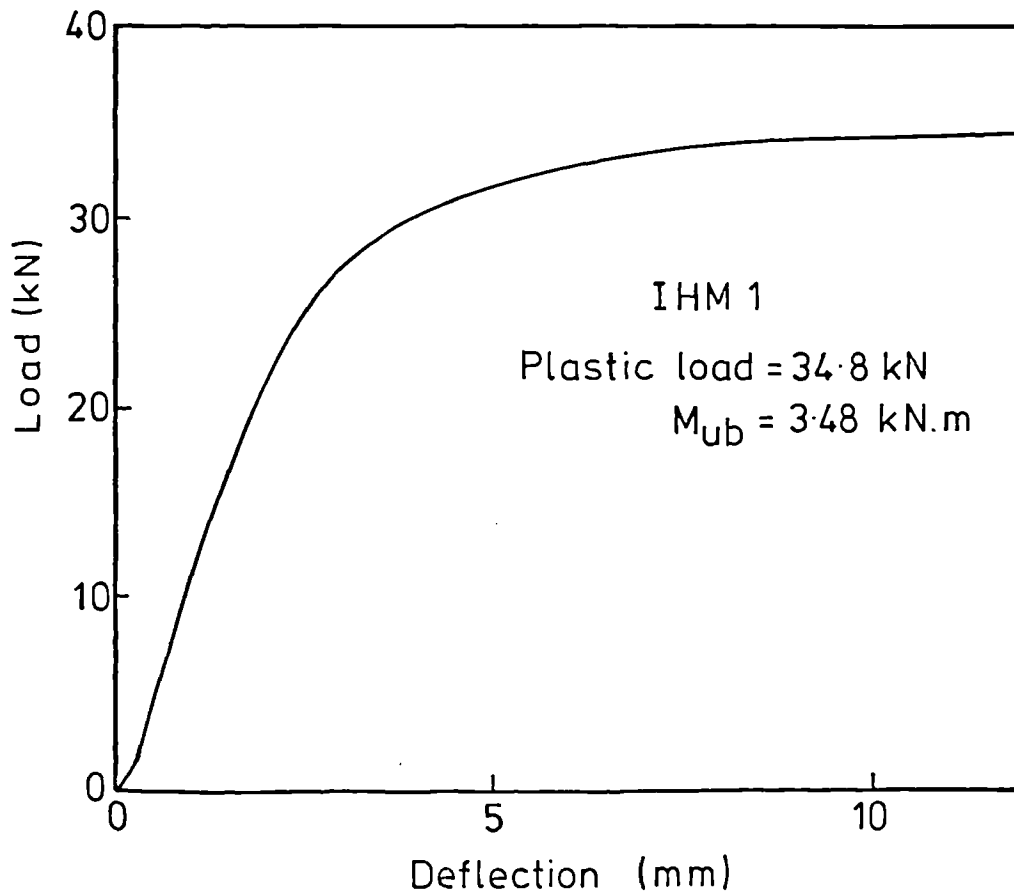


FIG. 5.1b TYPICAL LOAD-DEFLECTION GRAPH FOR FRAME MEMBER TESTED IN FLEXURE

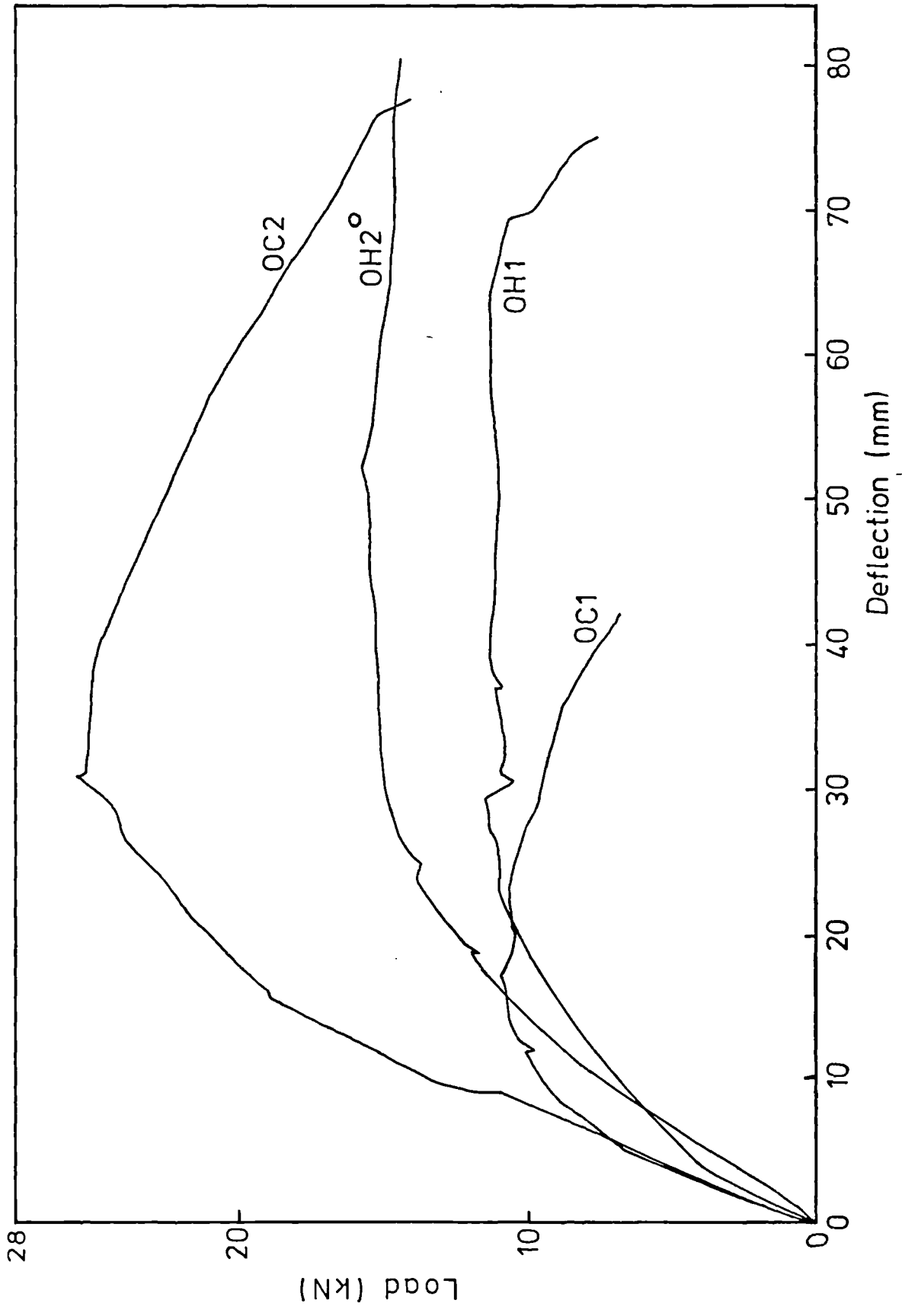


FIG.5.2 LOAD - DEFLECTION DIAGRAMS FOR OPEN FRAMES

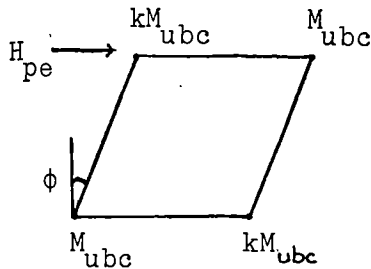
specimen designation		age (days)	test arrangement	failure Load (KN)	type of failure	M_{ut} (KN.m)	M_{ues} (KN.m)	V_t (KN)	V_{es} (KN)	M_{ues}/M_{ut} (%)	V_{es}/V_t (%)
IHM1	b	96	1	34.8	F	3.5	3.1			88.6	
	b	96	1	34.1	F	3.4	3.1			91.2	
	c	97	2	31.0	F	3.6	3.1			86.1	
IHM2	b	238	1	40.5	S	-		20.3	17.5		86.2
	b	239	3	30.6	F	4.7	4.3			91.5	
	c	238	1	41.7	S	-		20.9	17.5		83.7
	c	238	1	44.7	S	-		20.9	17.5		83.7
OC2	b	217	4	32.8	F	4.9	4.3			87.8	
	b	217	4	32.5	F	4.9	4.3			87.8	
	c	217	4	32.3	F	4.9	4.3			87.8	
	c	217	4	32.7	F	4.9	4.3			87.8	
IHM3	b	147	1	44.1	S	-		22.1	19.2		86.9
	b	147	4	45.8	F	6.9	6.5			94.2	
	c	147	3	36.3	S	-		18.2	19.2		105.5
ICM3	b	148	2	52.5	S	-		26.3	19.2		73.0
	b	149	4	38.5	F	5.8	6.5			112.1	
	c	148	1	58.6	S	-		29.3	19.2		65.5
	c	149	4	47.3	F	7.1	6.5			91.5	

- Notes
- (i) b and c indicate beam and column
 - (ii) test arrangement as shown in figure 5.1(a)
 - (iii) F: flexural failure; S: shear failure
 - (iv) M_{ut} : moment from tests
 M_{ues} : moment estimated by Hognestad's method (Table 5.2)
 V_t : shear strength from tests
 V_{es} : shear strength estimated (Table 5.3)
 - (v) -: no value

TABLE 5.4: ULTIMATE RESISTANCE MOMENTS AND SHEAR STRENGTHS FROM TESTS

the junction with the columns for the four open frames would be those reported in column 17 of Table 5.5. Comparing columns 5, 9, 13 and column 17 of Table 5.5 would lead to the following conclusion: Hognestad's proposed method overestimated M_{ubc} for the first three open frames and underestimated it for the last one. Consequently, the theoretical collapse loads ($H = 4(\text{smaller } M_u)/h$) would be less than the respective H_{pe} (plastic load from test) for the first three open frames, OH1, OH2^o and OC1. But the test carried out by Taylor et al [57 - 59] on opening and closing corners of reinforced concrete frames showed that the first were weaker than the adjacent members and the second were as strong as or even stronger than the adjacent members.

A way of finding the efficiency of the opening corners is to analyse the frames assuming that the closing corners are 100% efficient.



where k is the ratio of ultimate moment of joint to ultimate moment of beam or column.

$$2kM_{abc}\phi + 2M_{abc}\phi = H_{pe}h\phi$$

$$\implies k = \frac{H_{pe}h}{2M_{abc}} - 1$$

Thus the values of k for the four open frames OH1, OC1, OH2^o and OC2 are 0.82, 0.79, 0.59 and 1.65 respectively when the values of M_{abc} used are those of column 5 of Table 5.5. If a better result is desired then it would be appropriate to use the values taking into account the effect of axial loads. The values of k for OH1, OC1, OH2^o and OC2 are 0.76, 0.82, 0.45 and 1.37 respectively.

There must be some doubt about the accuracy of the efficiency

Frame designation	age of test (days)	H_{pe}^d (KN)	H_{ue}^e (KN)	(a) (KN.m)			(b) (KN.m)			(c) (KN.m)			Location of hinges	H_{pe}^d (KN.m)	H_{ue}^e (KN.m)				
				M_{ub}	M_{ubc}	M_{ucw}	M_{ucL}	M_{ub}	M_{ubc}	M_{ucw}	M_{ucL}	M_{ub}				M_{ubc}	M_{ucw}	M_{ucL}	
OHL	28	11.2	11.5	3.0	2.8	3.0	3.0	3.0	3.3	2.9	2.8	2.8	3.3	3.2	2.9	2.8	3.2	2.6	2.6
OCL	27	10.6	10.9	3.0	2.7	5.0	5.0	3.2	3.2	2.8	5.1	5.0	3.3	3.3	2.8	5.1	5.0	2.4	2.5
OH2 ⁰	57	15.0	15.6	4.3	4.3	3.8	3.8	4.7	4.7	4.7	3.6	4.0	4.6	4.6	4.6	3.6	3.9	3.4	3.6
OC2	37	25.0	25.6	4.3	4.3	5.9	5.9	4.8	4.8	4.8	5.6	6.1	4.8	4.8	4.8	5.7	6.1	5.7	5.8

Notes 1) estimation of ultimate moments of resistance:

(a) ignoring axial loads in frame members

(b) taking into account axial loads induced in frame members by H_{ue}

(c) taking into account axial loads induced in frame members by H_{pe}

2) M_{ub} , M_{ubc} , H_{pe} , H_{ue} and h see notations

M_{ucw} : moment in windward column

M_{ucL} : moment in leeward column

TABLE 5.5: MOMENTS OF RESISTANCE OF OPEN FRAME MEMBERS

factor, k , for the last open frame, OC2, it is extremely unlikely that k would be greater than 1. The possible explanations may be as follows:

(i) The value of M_{ubc} estimated (column 3 Table 5.5) is incorrect (at least 16% lower). In effect a value of $M_{ubc} = 5.7\text{KN.m}$ would give an efficiency of 100% for the opening corners ($k = 1$).

(ii) For this frame, it was difficult to see from the photographs where the hinges occurred. If the hinges occurred in the columns then $k = 0.94$.

(iii) The equation giving k was derived assuming an efficiency of 100% for the closing corners. Tests carried out by Taylor [58] and by R. L. Yuan et al [74] showed that for some specimens tested the efficiency of closing corners was greater than 1; the highest recorded value being 127%. In the case of OC2, if an efficiency of 100% is assumed for the opening corners, then the efficiency for the closing corners becomes 137%.

5.1.5 Flexural Stiffnesses of Frame Members

The computed values are given in Table 5.6.

infilled frame designation	E_c (KN/mm ²)	I_b (10 ⁴ mm ⁴)	I_c (10 ⁴ mm ⁴)	EI_b (10 ⁶ KN.mm ²)	EI_c (10 ⁶ KN.mm ²)
1	25.8	973	973	251	251
2	27.3	1024	1024	280	280
3	25.7	1127	1127	290	290
4	26.8	8324	968	2231	259
5	24.6	979	8483	241	2087

Notes (i) $I = \frac{bd^3}{12} + 2nA_s \left(\frac{d}{2} - d'\right)^2$ where $n = E_s/E_c$

(ii) E_s see section 3.3.3 Table 3.2

E_c see section 3.3.2 Table 3.1

$E = E_c$

(iii) I_b : second moment of area of beam

I_c : second moment of area of column

TABLE 5.6: FLEXURAL STIFFNESSES OF FRAME MEMBERS

5.2 PHYSICAL PROPERTIES OF INFILL PANELS

The infill properties used in the calculations are given in Table 5.7.

Symbols	VALUE	COMMENTS
l_i	810 mm	width of infill
h_i	810 mm	height of infill
t	35, 57 and 100 mm	weak infill $t = 35$ mm; medium strength infill $t = 57$ mm; strong infill $t = 100$ mm
f_{ci}	7.8 N/mm^2	From tests on three course blockwork assemblies (section 3.4.4 Table 3.5). $f_{ci} = f_{cbw}$ = compressive strength of infill
f_{dci}	6.2 N/mm^2	$f_{dci} = 0.8f_{ci}$ From figure 4 (HAMID and DRYSDALE [75]) diagonal strength = 0.8 vertical strength
E_i	5.2 KN/mm^2	From tests on three course blockwork assemblies (section 3.4.5 Table 3.5) $E_i = E_{bw}$ = static modulus of infill
E_{di}	4.2 KN/mm^2	From figure 6 (HAMID and DRYSDALE [75]) $E_{di} = 0.8E_i$ E_{di} = static modulus along the diagonal
f_{ti}	0.52 N/mm^2	$f_{ti} = \frac{1}{15}f_{ci}$ From Table 3 (HAMID et al [70]) Table 4 (HAMID et al [68]) $f_{ci} = 0.1f_{ci}$ was suggested by MAINSTONE [19] and S. SMITH [36]
f_{dti}	0.52 N/mm^2	$f_{dti} = f_{ti}$ From Table 3 or figure 7 (HAMID et al [70])
f_{bs}	0.34 N/mm^2	From tests on 3 block assemblies (section 3.4.6 fig. 3.12)
μ	0.76	From tests on 3 block assemblies (section 3.4.6 fig. 3.12)
ν	0.2	Rostampour [51] tests on lytag blockwork, ν varied from 0.18 to 0.21
G	2.2 KN/mm^2	$E_i/2(1 + \nu)$
ϵ'_{ci}	3000 μs and 5000 μs	HENDRY [24] suggested a strain at failure of 3000 μs for brickwork HOLMES [15] suggested a strain at failure of 5000 μs for brickwork
c	0.6 to 1	Workmanship factor found to vary from 0.6 to 1 for BENJAMIN and WILLIAMS [14]

Notes (i) a strain at failure of approximately $\epsilon'_{ci} = 3000\mu\text{s}$ was obtained from tests (section 2.4.5 figure 3.10)

(ii) for symbols see list of notations

TABLE 5.7: PHYSICAL PROPERTIES OF INFILL PANELS

5.3 PHYSICAL PROPERTIES OF INFILLED FRAMES

5.3.1 Relative Stiffness Parameters

Two non-dimensional parameters $\lambda_h h$ and $\lambda_\ell \ell$ found appropriate to express the relative stiffness of the infill to the frame members were first introduced by S. Smith [31] who developed the analogy with a beam on an elastic foundation, by which the column of an infilled frame under lateral load may be regarded as one half of a beam on an elastic foundation which under a central concentrated load P , remains in contact with the foundation over a length ℓ_c known as the characteristic length. The general solution for the bending of a beam on an elastic foundation is given by Hetenyi [76] and by Timoshenko [77]. Using Hetenyi's notation, the differential equation for an unloaded section of a beam on a foundation with an elastic modulus k (denoting a reaction ky per unit length of the beam for a deflection y) is

$$EI \frac{d^4 y}{dx^4} = -ky$$

and the general solution is

$$y = e^{\lambda x} (C_1 \cos \lambda x + C_2 \sin \lambda x) + e^{-\lambda x} (C_3 \cos \lambda x + C_4 \sin \lambda x)$$

where

$$\lambda = \sqrt[4]{\frac{k}{EI}}$$

and C_1, C_2, C_3 and C_4 are constants dependent on the loading and end conditions. The characteristic length is defined when $\lambda \ell_c = \pi$ in the general solution and the contact length in the case of the column of an infilled frame is half of this, leading to a parameter

$$\alpha_h = \pi/2\lambda_h$$

where

$$\lambda_h = \sqrt[4]{\frac{E_i t \sin 2\theta}{4EI_c h_i}}$$

Similarly the beam member of the infilled frame may be represented as a beam on an elastic foundation loaded by a moment M, giving rise to a corresponding parameter $\alpha_\ell = \pi/\lambda_\ell$

where

$$\lambda_\ell = \sqrt[4]{\frac{E_i t \sin 2\theta}{4EI_b \ell_i}}$$

The term $\sin 2\theta$ in λ_h and λ_ℓ recognizes the obliquity of the resultant reactions between the infill and the columns and beams. In the above two equations

E_i and E are the elastic modulus of the infill and frame respectively

t is the infill thickness

h_i is the height of the infill

ℓ_i is the width of the infill

I_b and I_c are the second moments of area of the beam and column respectively

θ = slope of diagonal of infill to horizontal.

Three other non-dimensional parameters

$$K_h = 4(\lambda_h h)$$

$$\lambda_h \ell = \ell \sqrt[4]{\frac{E_i t \sin 2\theta}{4EI_c h_i}}$$

and $\lambda_\ell \ell_i = \ell_i \sqrt[4]{\frac{E_i t \sin 2\theta}{4EI_b \ell_i}}$

were used respectively by Mainstone et al [19 - 21], Mallick and Barua [27, 29] and by Kadir and Hendry [22 - 24]. The first two parameters were used in the prediction equations for stiffness and strength. The last parameter was used in the equation giving the shear strength of the infill panel. The computed values of all the relative stiffness parameters for all the infilled frames tested are given in Table 5.8.

Infilled frame designation	K_h	$\lambda_h \frac{1}{mm}$	$\lambda_{\chi} \frac{1}{mm}$	λ_h^h	λ_h^{ℓ}	λ_{χ}^{ℓ}	m_b	m_c	$\frac{E_s/E_c}{E_c/E_i}$	$\frac{I_t}{10^9 mm^4}$	$\frac{E_i I_t}{10^9 KN \cdot mm^2}$	$I_{eb} \cdot 10^6 mm^4$	$I_{ec} \cdot 10^6 mm^4$
IHW1	635	0.0039	0.0039	3.55	3.55	3.16	0.138	0.138	9.3	4.8	1212	196	196
IHM1	964	0.0043	0.0043	3.91	3.91	3.48	0.085	0.085	8.6	5.2	1347	267	267
IHS1	1087	0.0051	0.0051	4.64	4.64	4.13	0.047	0.047	9.4	4.8	1362	419	419
ICM1	1004	0.0044	0.0044	4.00	4.00	3.56	0.082	0.154	9.0	5.0	1305	276	276
ICS1	1640	0.0049	0.0049	4.46	4.46	3.97	0.047	0.084	8.3	5.4	1492	387	387
ICS1**	1807	0.0051	0.0051	4.64	4.64	4.13	0.047	0.084	9.4	4.8	1362	419	419
IHW2	580	0.0038	0.0038	3.46	3.46	3.08	0.192	0.192	7.8	4.9	1279	192	192
IHM2	954	0.0043	0.0042	3.91	3.91	3.40	0.118	0.104	7.2	5.3	1414	262	262
IHM2*	907	0.0043	0.0043	3.91	3.91	3.48	0.118	0.118	7.5	5.2	1399	270	270
ICM2	974	0.0043	0.0043	3.91	3.91	3.48	0.121	0.154	7.4	5.2	1394	268	268
ICM2*	888	0.0042	0.0042	3.82	3.82	3.40	0.118	0.181	7.2	5.3	1414	252	252
IHW3	535	0.0037	0.0037	3.37	3.37	3.00	0.290	0.290	7.6	4.9	1357	193	193
IHM3	870	0.0042	0.0042	3.82	3.82	3.40	0.178	0.178	7.7	4.9	1409	279	279
ICM3	861	0.0042	0.0042	3.82	3.82	3.40	0.178	0.219	7.6	5.0	1430	278	278
ICM4	1472	0.0043	0.0025	4.34	3.91	2.03	0.428	0.143	8.7	5.2	1352	481	269
ICM5	120	0.0026	0.0044	2.37	2.63	3.56	0.085	0.644	8.0	4.7	2907	285	509

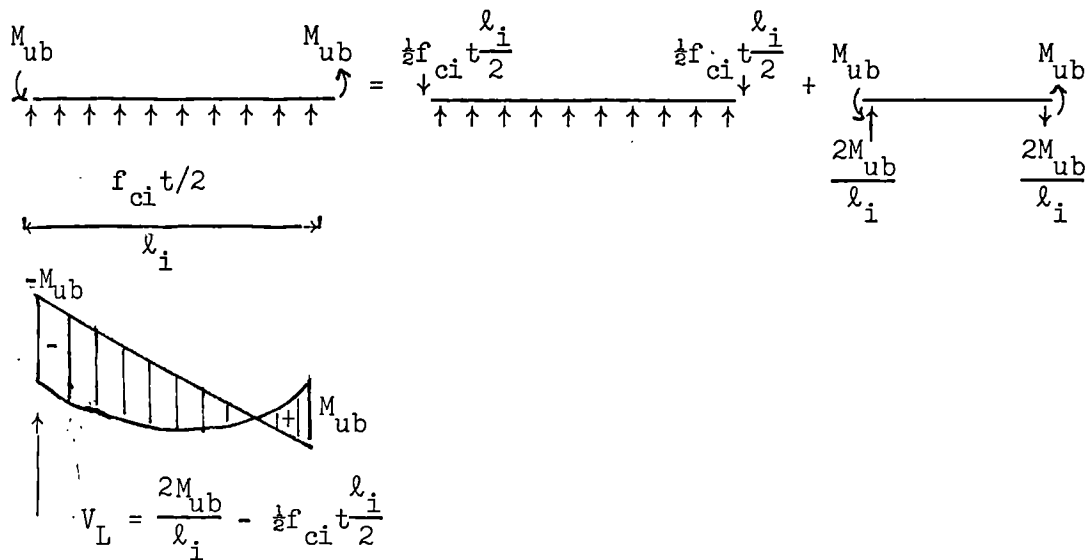
(1) $K_h = 4(\lambda_h^h)^4$

(11) symbols see notations

TALBE 5.8: PHYSICAL PROPERTIES OF INFILLED FRAMES

5.3.2 Relative Strength Parameter

This parameter was first introduced by Wood [44]. In analysing the stronger mode S, where plastic hinges formed at the four corners, Wood [44] assumed that the infill panel exerted a hydrostatic pressure $f_{ci}/2$ on the frame members. The beams would therefore be subjected to ultimate moments (M_{ub}) at both ends (location of plastic hinges) and a uniform loading $f_{ci}t/2$, giving rise to the following bending moments:



From the bending moment diagram shown above, the minimum permissible plastic (ultimate) moment is reached when the shear force V_L at the left-hand end is zero (moment is maximum when shear force is nil).

i.e., when

$$\frac{2M_{ub}}{l_i} - \frac{1}{2}f_{ci}t \frac{l_i}{2} = 0$$

defining m_b as

$$m_b = \frac{8M_{ub}}{f_{ci}tl_i^2}$$

similarly m_c is defined as

$$m_c = \frac{8M_{uc}}{f_{ci}tl_i^2}$$

The computed values for m_b nad m_c are also given in Table 5.8

5.3.3 Moment of Inertia of Transformed Frame-Infill Section

This parameter, I_t , was used in the calculation of the racking stiffness by Fiorato et al [18]. The infilled frame was considered as a vertical cantilever. This parameter is defined as

$$I_t = \frac{t\ell_i^2}{12} + 2 \left[I_c + \frac{E_c}{E_i} \left(\left(bd + \left(\frac{E_s}{E_c} - 1 \right) (A_s + A'_s) \right) \left(\frac{\ell}{2} \right)^2 \right) \right]$$

where

t is the infill thickness

ℓ_i is the width of the infill

I_c is the second moment of area of the column

E_c is the static modulus of concrete

E_i is the static modulus of infill

E_s is the static modulus of steel bars

b is the width of the column

d is the depth of the column

A_s and A'_s are the area of steel in tension and compression respectively

ℓ is the width of the infilled frame between centre lines of columns

The computed values for I_t are also given in Table 5.8

5.3.4 Moment of Inertia of Equivalent Frame Members

Liauw [41] proposed a method based on the equivalent frame method, in which parts of the infill were interpreted to act with adjacent frame members as composite sections in bending. The computed values for I_{eb} (moment of inertia of equivalent beam) and I_{ec} (moment of inertia of equivalent column) are also given in Table 5.8

5.4 PRINCIPAL PARAMETERS FROM THEORETICAL AND EMPIRICAL PREDICTIONS FROM PREVIOUS WORK

5.4.1 Introduction

The equations and charts used in the calculations from previous work giving the lateral racking stiffness, the tensile and shear failure load and the ultimate load are summarized in Table 5.9. The equations from the original papers have been rewritten in a standard notation whenever possible. The abbreviations used in Table 5.9 are as follows:

- B : Brickwork
- B.B: Back to back
- C : Concrete
- D : Diagonal loading
- F : Fixed base
- R : Racking loading
- R.C: Reinforced concrete
- S : Steel

In Table 5.9, the notations used by S. Smith and Carter [36] for calculating the lateral stiffness are as follows:

- R : Diagonal load
- R_c : Diagonal load to cause crushing of the infill
- δ_H : Total horizontal displacement under applied load
- H : Applied load
- Σ_F : Summation of all bars in frame including diagonal struts
- Σ_S : Summation of all diagonal struts only
- F : Force in bars due to unit load replacing H
- U : Force in bars due to unit load only at point where displacement is required
- A_i : Initial cross-sectional area of members, including diagonal struts when $R/R_c = 0$
- A_c : Cross-sectional area of diagonal struts when $R/R_c = 1$ in critical panel, all others proportioned accordingly

- E : Appropriate value for modulus of elasticity for frame members and infill (in the case of the infill this will be the initial tangent modulus)
- H_c : Horizontal load to cause crushing in the critical infill panel determined from the appropriate value of $R_c/f_{ci}h$, for the particular value of λ_h , as given in figure 7 of reference [36].
- L : Length of member

5.4.2 Horizontal Racking Stiffness

The horizontal racking stiffnesses obtained from tests, S_{He} , are compared with the predicted ones from previous work in Table 5.10. None of the existing theoretical or empirical methods seems to be safe to predict the initial horizontal racking stiffness for the type of infilled frames tested. From Table 5.10 it can be seen that the closest are those obtained using Mainstone's equation [46] and S. Smith and Riddington's method [38]. The test results are compared graphically in figure 5.3 with the predictions obtained from these two methods. The choice of the two non-dimensional coordinates was made in order to have Mainstone's equation represented by a straight line. Figure 5.3 shows that even Mainstone's method overestimates the lateral racking stiffness for all infilled frames but one (ICM2*). It also shows the effect of the vertical loads on the lateral racking stiffness. The 'IC' specimens are stiffer than the corresponding 'IH' ones. This has been discussed in section 4.6.3 (see Table 4.4).

Another parameter which is very important in predicting the lateral racking stiffness is the initial modulus of elasticity of the infill material, E_i . If the static modulus of the infill along the diagonal, E_{di} , were used instead of E_i ($E_{di} = 0.8E_i$ see Table 5.7), then S. Smith and Riddington's method would be safe for almost all 'IC' specimens. For this method to be safe for all infilled frames tested, it is either possible to reduce further E_i (use of a penalty

	FRAME	INFILL	SUPPORTS	Lateral racking stiffness $S_H = H/\delta_H$	Tensile failure load H_t	Shear failure load H_s	ultimate load H_u
BENJAMIN & WILLIAMS [14]	R.C	B	F	$S_H = \frac{\lambda_i tG}{1.2h_i}$		$H_s = \frac{f_{bs} c \lambda_i t \lambda_i}{1.5 \lambda_i - \mu c}$	
HOLMES [15]	S	B	D	$S_H = \frac{H_u}{\epsilon_i d \cos \theta}$			$H_{ut} = H_{ui} + H_f$ infill diagonal f_{dei} : comp strength $H_{ui} = \frac{d}{3} f_{dei} \cos \theta$ $H_f = \min \left[\frac{4M_u}{h}, \frac{24EI_c \epsilon_i d}{h^3 \left[1 + \frac{I_c}{I_b} \cot \theta \right] \cos \theta} \right]$
FIORATO et al [18]	R.C	B	F	$S_H = \frac{1}{h^3} \frac{k \lambda_i}{3E_i I_t} + \frac{\lambda_i tG}{\lambda_i}$		$H_s = \frac{f_{bs} \lambda_i t}{1 - \mu \frac{\lambda_i}{h_i}}$	$H_u = \sum \frac{\gamma 2M_u}{l} \frac{\gamma}{ce}$ γ : number of columns $ce = \lambda_i - \lambda_{brace}$; $\lambda_{brace} = \lambda_i/2$ knee braced system: ultimate load = load necessary to develop the yield capacity of the braced columns
MAINSTONE [20, 46]	S	B	D	$S_H = 0.18(K_h) E_i t \sin 2\theta \cos^2 \theta$	$H_t = 0.334(k_h) f_{ci} h_i t \cos^2 \theta$ $H_t = 0.167(k_h) f_{ci} h_i t \cos \sin 2\theta$ f_{ci} : vertical compressive strength of infill		$H_{ut} = H_{ui} + H_f$ $H_{ui} = 0.41(K_h) f_{ci}^{0.125} \sin 2\theta \cos \theta$ $H_{ui} = 0.82(K_h) f_{ci}^{0.125} \cos^2 \theta$ $H_f = \frac{4M_u}{h}$

TABLE 5.9: PREDICTION EQUATIONS FROM PREVIOUS WORK

FRAME	INFILL	SUPPORTS	Lateral racking stiffness $S_H = H/\delta_H$	Tensile failure load H_t	Shear failure load H_s	Ultimate load H_u
S	B	B.B	$S_H = \frac{A+B+C}{C(A+B)}$ $A = \frac{\tan^2 \theta h}{bd_v E}$ $B = \frac{d}{E_1 w \cos^2 \theta}$ $C = \frac{h^3}{12EI_c} \left(\frac{3I_b h + 2I_c \ell}{6I_b h + I_c \ell} \right)$		$H_{st} = H_{si} + H_f$ $H_{si} = \frac{f_{bs} \ell \cdot t}{1 - \mu \tan \theta} \left[\frac{\pi}{\lambda_h \ell_i} \right]$ $H_{st} = \frac{H_{si}}{\psi} \quad \psi = \frac{C}{A+B+C}$ $\psi = f(\lambda_h h, \frac{\ell}{h}) \text{ Chart 7}$	$H_{ut} = H_{ui} + H_{fe}$ $H_{ui} = \lambda' f_{ci} t w \cos \theta;$ $w = \frac{\pi}{2} \sqrt{\left[\frac{I}{\lambda_h} \right]^2 + \left[\frac{I}{2\lambda_h} \right]^2}$ $H_{fe} = \delta_f \frac{12EI_c}{h^3} \left(\frac{6I_b h + I_c \ell}{3I_b h + 2I_c \ell} \right)$ $\delta_f = \delta_i = \Delta_i / \cos \theta \quad \Delta_i = \epsilon'_{ci} d_i$ $\epsilon'_{ci} = 0.003$
R.C	B	B.B	$S_H = 0.1114 E_1 \frac{\ell_i}{h_i} (\lambda_h \ell)^{-0.15}$	$H_t = 0.7018 f_{ti} \ell t (\lambda_h \ell)^{-0.152}$	$H_{st} = H_{si} + H_f$ $H_{st} = 1.1730 f_{bs} \ell t (\lambda_h \ell)^{-0.06}$ in the elastic range $\frac{H_{si}}{H_{st}} = 0.3266 (\lambda_h \ell)^{0.36}$	
R.C	B	R+I vert load on wind ward column	$S_{H_t} = S_{H_i} + S_{H_f}$	$H_t = \frac{3\lambda_i t (\beta - 0.3\beta^2) f_{ti}}{1 + \beta^2 - \sqrt{\beta^4 - 0.8\beta^2 + 1}}$ $\beta = \frac{\ell_i}{h_i}$		
S	B	B.B	$S_H = \frac{H}{\delta_H}$ $\delta_H = H \left[\frac{\sum FUL}{F A_i E} + \frac{H}{2H_u} \left(\frac{\sum FUL}{S E} \left(\frac{A_i - A}{A_i + C} \right) \right) \right]$	$H_t = f\left(\frac{\ell}{h}, \lambda_h h\right) \text{ Chart 9}$	$H_s = f\left(\frac{\ell}{h}, \mu; \lambda_h h\right) \text{ Chart 8}$	$H_u = w t f_{ci} \cos \theta; w = a \sec \theta, a = \frac{\pi}{2\lambda_h}$ $H_u = \frac{\pi}{2\lambda_h h} h f_{ci} t \quad H_u = \frac{\pi}{2\lambda_h h} h f_{ci} t$ $H_u = f\left(\frac{\ell}{h}, \lambda_h\right) \text{ Chart 7}$ suggested chart is for concrete infilling

TABLE 5.9: (Cont)

FRAME	INFILL	SUPPORTS	Lateral racking stiffness $S_H = H/\delta_H$	Tensile failure load H_t	Shear failure load H_s	Ultimate load H_u
S. SMITH & RIDDINGTON [38]	S	R	$\delta_H = H \Sigma \frac{FUL}{EA}$ $w = 0.1d_i$ $S_H = \frac{H}{\delta_H}$		$H_s = \frac{f_{bs} l t}{1.43 - \mu \left(\frac{0.8 l_i}{h_i} - 0.2 \right)}$	$H_u = 1.12(\lambda_h) f_{ci} h_i t \cos^2 \theta$ <p>which is MAINSTONE'S equation [20]</p> $\frac{w'_{ec}}{w'} = 0.56(\lambda_h)^{0.86} = \frac{R_c}{f_{ci}} w' t$ $w' = d_i \sin 2\theta$
SMALLICK & BARUA [29]	S	B.B	$S_H = 0.223 \frac{E_i l_i}{h_i} t \frac{1}{\sqrt{\lambda_h}}$	$H_t = 5.08 f_{ti} l t \frac{1}{\lambda_h}$		$H_{ut} = H_{ui} + H_f$ $H_{ut} = 1.486 f_{ci} l t \frac{1}{\lambda_h}$ $\frac{H_{ui}}{H_{ut}} = 0.3373(\lambda_h)^{0.333}$
LIAW [41]	PERSEX STRIPS (RUBBER AND GELATINE VINAMOLD)	R	eq 11 of reference [41]			
WOOD [44]	S	R				$\text{nominal } m = \frac{8(\text{smaller } M_u)}{f_{ci} l_i^2} = m_n$ $\gamma_p = 2.663 m_n^2 - 1.371 m_n + 0.406$ $\text{effective } m = \text{nominal } \frac{m}{\gamma_p} = m_e$ $f_s = \frac{2\sqrt{m_e}}{m_e + 1} \text{effective } m$ <p>Table 3 gives mode</p> $H_u = f_s \left(\frac{4(\text{smaller } M_u)}{h_i} + \frac{1}{2} \gamma_p f_{ci} l_i \right)$

TABKE 5.9: (Cont)

FRAME	INFILL	SUPPORTS	Lateral racking stiffness $S_H = H/\delta_H$	Tensile failure load H_t	Shear failure load H_s	Ultimate load H_u
						<p>Mode 1 $H_{u1} = f_{ci} \frac{th}{\tan \theta} \sqrt{\frac{2(M_{pi} + M_{pc})}{f_{ci} th^2}}$</p> <p>Mode 2 $H_{u2} = \frac{f_{ci} th}{\tan \theta} \sqrt{\frac{2(M_{pj} + M_{pb})}{f_{ci} th^2}}$</p> <p>Mode 3 $H_{u3} = \frac{4M_{pi}}{h} + f_{ci} th (\frac{2}{3}\beta - \frac{1}{3}\beta^2)$ where β is equal to $\frac{1}{3}$ M_{pj}: smaller value of M_{pb} and M_{pc}</p> <p>$H_u = \min(H_{u1}, H_{u2}, H_{u3})$</p>

LIAW & KWAN [43]

TABLE 5.9: PREDICTION EQUATIONS FROM PREVIOUS WORK

Infilled frame designation	FIORATO et al [18]		BENJAMIN & WILLIAMS [14]		HOLMES [15]		MAINSTONE [20, 46]		S. SMITH & CARTER [36]				S. SMITH & RIDDINGTON [38]		KADIR & HENDRY [22 - 24]		MALLICK S.K. & BARUA [27]		MALLICK S.K. & BARUA [29]		LIAUW [41]		Test results (KN/mm)	
	S_H	w/d	S_H	w/d	$\frac{H}{\Sigma F_{UL}} \frac{F_{UL}}{EA}$	w/d_i	S_H	w/d_i	$R/R_c=0$	$R/R_c=1$	$\ddagger H_{us}$	$\ddagger H_{us}$	w/d_i	$\frac{H}{\Sigma F_{UL}} \frac{F_{UL}}{EA}$	w/d	S_H	$\frac{H}{\Sigma F_{UL}} \frac{F_{UL}}{EA}$	S_H	S_H	S_H	S_H	S_H	S_H	S_{He}
IHW1	69.0	0.33	21.2	0.33	27.5	0.111	10.1	0.360	0.125	21.9	-	18.6	0.1	7.9	0.350	34.0	28.8	16.8	21.6	21.6	109.5	5.3	5.3	
IHW1	105.3	"	32.6	"	42.8	0.108	15.9	0.350	0.120	33.4	-	28.5	"	12.7	0.317	46.4	41.0	26.9	33.5	33.5	184.5	6.3	6.3	
IHS1	161.5	"	54.9	"	67.3	0.103	26.7	0.330	0.120	51.8	-	45.1	"	21.5	0.268	60.9	56.6	46.0	53.9	53.9	347.3	10.4	10.4	
ICM1	104.7	"	32.5	"	42.5	0.107	15.9	0.350	0.120	33.2	50.4	28.4	"	12.7	0.310	45.1	40.0	26.8	33.1	33.1	184.9	12.1	12.1	
ICS1	165.8	"	54.9	"	68.7	0.103	26.9	0.330	0.120	52.7	77.2	45.8	"	21.6	0.278	64.5	59.4	46.3	55.0	55.0	342.2	15.5	15.5	
ICS1**	161.5	"	54.9	"	67.1	0.103	26.7	0.330	0.120	51.7	77.2	45.0	"	21.5	0.268	60.9	56.5	46.0	53.9	53.9	347.3	16.0	16.0	
IHW2	69.5	"	22.4	"	27.7	0.112	10.2	0.360	0.125	22.0	-	18.7	"	7.9	0.359	35.2	29.6	16.8	21.9	21.9	110.0	7.4	7.4	
IHW2	106.3	"	33.0	"	43.2	0.108	15.9	0.350	0.120	33.6	-	28.6	"	12.7	0.323	47.4	42.0	26.9	33.5	33.5	184.7	6.7	6.7	
IHW2*	106.1	"	33.8	"	43.0	0.108	16.0	0.350	0.120	33.5	-	28.5	"	12.7	0.317	46.7	41.2	26.9	33.5	33.5	185.4	9.1	9.1	
ICM2	106.0	"	33.9	"	43.0	0.107	15.9	0.350	0.120	33.5	48.9	28.6	"	12.7	0.317	46.4	41.2	26.9	33.5	33.5	185.0	11.4	11.4	
ICM2*	106.3	"	33.8	"	43.1	0.108	16.0	0.350	0.120	33.6	48.4	28.6	"	12.7	0.325	47.9	42.2	27.0	33.9	33.9	176.8	16.9	16.9	
IHW3	70.1	"	24.5	"	27.6	0.112	10.2	0.360	0.125	22.1	-	18.7	"	7.9	0.369	36.5	30.6	16.9	22.2	22.2	110.5	7.8	7.8	
IHW3	106.3	"	35.9	"	43.2	0.108	16.1	0.350	0.120	33.6	-	28.6	"	12.7	0.325	47.6	42.2	27.0	33.9	33.9	186.5	5.5	5.5	
ICM3	106.6	"	35.9	"	43.1	0.108	16.1	0.350	0.120	33.6	48.2	28.6	"	12.7	0.325	47.7	42.2	27.0	33.9	33.9	186.1	12.0	12.0	
ICM4	98.3	"	34.2	"	42.1	0.104	15.4	0.340	0.120	30.8	45.6	26.4	"	12.0	0.481	55.0	57.2	26.9	33.5	33.5	155.1	14.4	14.4	
ICM5	117.8	"	32.3	"	45.6	0.126	18.6	0.410	0.130	37.8	43.0	31.5	"	12.2	0.344	75.3	47.0	28.6	40.8	40.8	204.2	16.2	16.2	

Notes (i) H_{us} : ultimate load by S. Smith's method } lateral racking stiffness
(ii) \ddagger taking axial loads on columns into account } calculated for H_{us} and $\ddagger H_{us}$

(iii) S_H and $\frac{H}{\Sigma F_{UL}}$ in KN/mm

(iv) $\frac{H}{\Sigma F_{UL}}$: stiffness of structure considered as an equivalent pin-jointed frame

TABLE 5.10: LATERAL RACKING STIFFNESS FROM PREVIOUS WORK

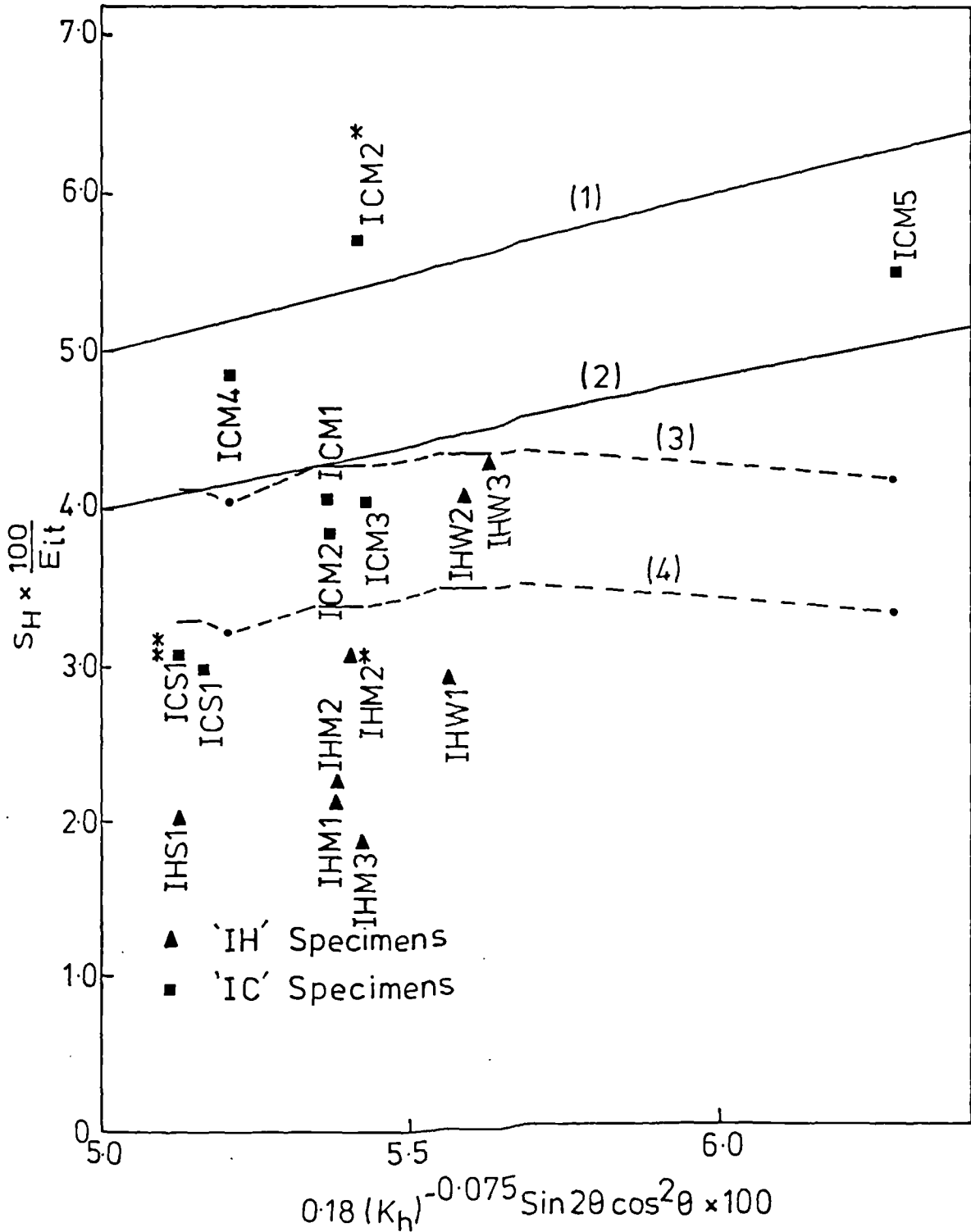


FIG.5.3 COMPARISON OF STIFFNESS TEST RESULTS WITH PREVIOUS WORK

factor for material or to take a width for the diagonal strut less than one tenth of the infill diagonal (i.e., approximately $\frac{1}{10}d_1$).

5.4.3 Infill Cracking Load

5.4.3.1 Tensile failing load

In Table 5.11, the infill cracking loads, H_{CI} , obtained from the tests are compared with both the predicted tensile and shear failing loads. To differentiate between the two modes of infill failure is not an easy task. In this section only the numerical values are considered and compared with the cracking loads obtained from tests. The test results are compared graphically in figure 5.4 with the five methods whose predictions are reported in Table 5.11. As for the lateral racking stiffness, the choice of the two non-dimensional coordinates was made in order to have Mainstone's equation [46] represented by a straight line. Figure 5.4 shows that the safest method for predicting the tensile strength of the infill is that of S. Mallick and Barua [27]. Mainstone's method is not safe for only three infilled frames. The methods which overestimate the tensile strength of the infill are those of Sachanski [28] and S. Smith and Carter [36].

5.4.3.2 Shear failing load

The test results are compared graphically in figure 5.5 with the six methods whose predictions are reported in Table 5.11. Four of the methods are conservative. $H_s/f_{bs}l_i$ varies from 1.76 to 4.72 for the infilled frames tested. The test results lie between the predicted ones by S. Smith and Carter [36] and by Fiorato et al [18].

5.4.4 Ultimate Load

The ultimate loads obtained from the tests are compared with

Infilled frame designation	MAINSTONE [20, 46] w/d _i	MALLICK, S.K. & BARUA [27] H _t (KN)	SACHANSKI [28] H _t (KN)	S. SMITH & CARTER [36] H _t (KN)	MALLICK, S.K. & BARUA [29] H _t (KN)	BENJAMIN & WILLIAMS [14] H _s (KN)	FIORATO et al [18] H _s (KN)	KADIR & HENDRY [22 - 24] H _{st} = $\frac{H_{st}}{\psi}$ (KN)		S. K. MALLICK & BARUA [27] H _{si} (KN) H _{st} (KN)		S. SMITH & CARTER [36] H _s (KN)	S. SMITH & RIDDINGTON [38] H _s (KN)	TEST RESULTS H _{CI}	
								H _{si} (KN)	H _{st} (KN)	H _{si} (KN)	H _{st} (KN)			observed (KN)	graph (KN)
IHW1	0.103	22.8	51.3	49.7	35.6	13.0	40.2	39.4	45.3	6.1	11.8	14.6	9.9	18.0	17.0
IHW1	0.100	35.9	83.6	79.5	52.6	21.2	65.4	50.0	56.2	10.2	19.1	23.3	16.1	47.6	46.0
IHS1	0.095	60.1	146.7	137.0	77.7	37.2	114.8	65.3	70.2	18.8	33.1	40.1	28.3	-	-
ICM1	0.099	35.9	83.6	79.5	51.4	21.2	65.4	47.7	53.0	10.2	19.0	23.3	16.1	45.1	44.6
ICSL	0.096	60.5	146.7	137.0	80.9	37.2	114.8	69.4	75.0	18.6	33.2	40.1	28.3	63.7	63.7
ICSL**	0.095	60.1	146.7	137.0	77.7	37.2	114.8	65.3	70.2	18.8	33.1	40.1	28.3	93.9	-
IHW2	0.104	22.9	51.3	49.7	36.5	13.0	40.2	42.9	48.9	6.0	11.8	14.3	9.9	17.4	17.4
IHM2	0.100	35.9	83.6	79.5	52.6	21.2	65.4	52.7	59.3	10.1	19.1	23.3	16.1	-	-
IHM2*	0.100	36.1	83.6	79.2	52.6	21.2	65.4	50.0	56.2	10.2	19.1	23.3	16.1	59.3	59.3
ICM2	0.100	35.9	83.6	79.5	52.6	21.2	65.4	50.0	56.2	10.2	19.1	23.3	16.1	57.9	57.9
ICM2*	0.100	36.1	83.6	79.5	53.8	21.2	65.4	52.7	59.9	10.1	19.1	23.3	16.1	65.8	65.8
IHW3	0.104	23.1	51.3	49.5	37.5	13.0	40.2	47.2	65.6	6.0	11.8	14.6	9.9	29.7	32.5
IHM3	0.101	36.2	83.6	79.5	53.8	21.2	65.4	53.7	59.9	10.1	19.1	23.3	16.1	36.8	35.8
ICM3	0.101	36.2	83.6	79.5	53.8	21.2	65.4	50.7	59.9	10.1	19.1	23.3	16.1	41.0	-
ICM4	0.097	34.8	83.6	86.4	52.6	21.2	65.4	neg value	-	10.2	19.1	25.5	16.1	55.0	-
ICM5	0.117	42.0	83.6	85.8	86.7	21.2	65.4	47.7	75.7	10.0	21.7	24.4	16.1	74.1	74.1

Shear failing load

Tensile failing load

Note tensile failing load calculated with $f_{ti} = 0.1f_{ci}$

TABLE 5.11: CRACKING LOAD FROM PREVIOUS WORK

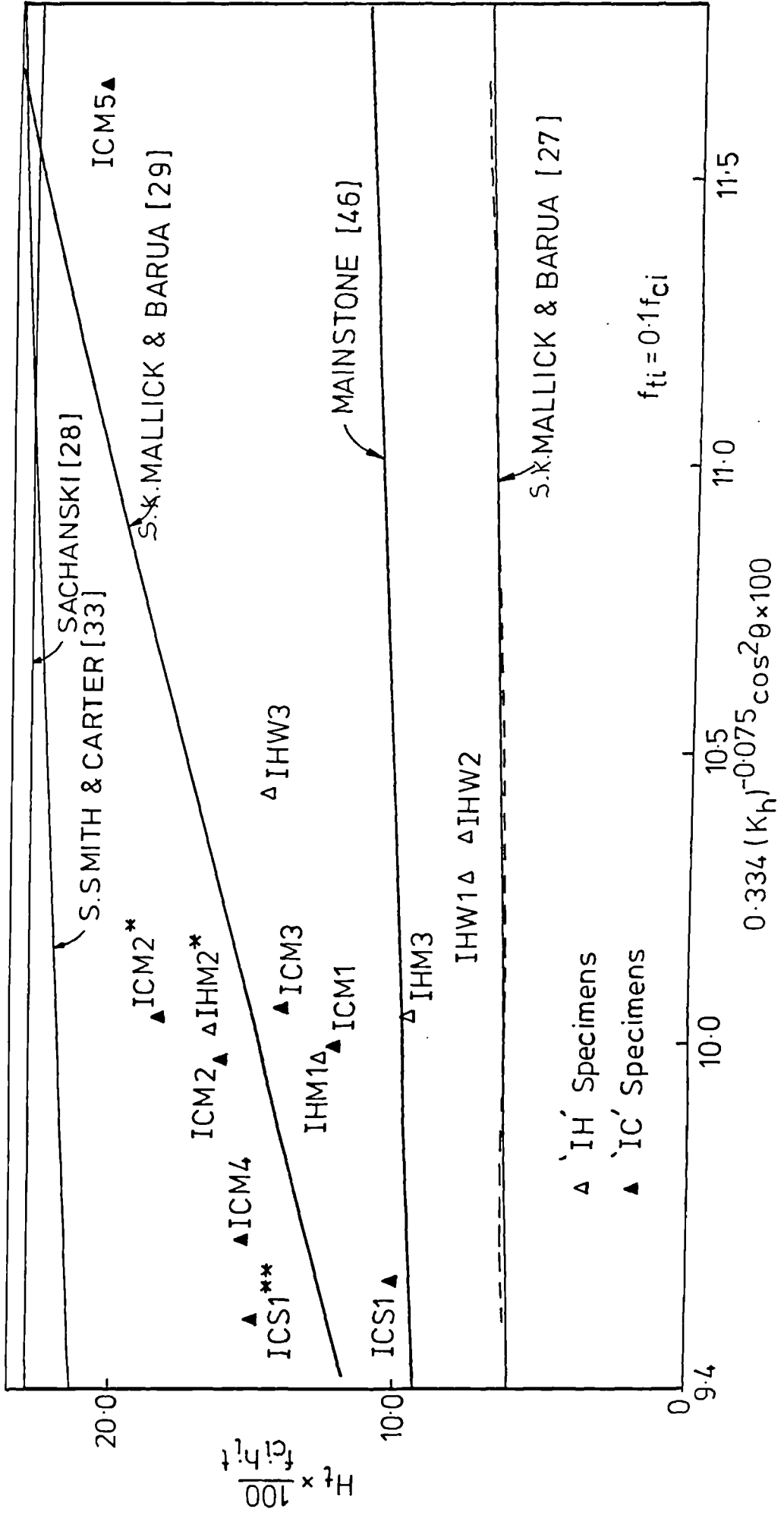


FIG. 5.4 COMPARISON OF INFILL CRACKING LOAD TEST RESULTS WITH TENSILE STRENGTH FROM PREVIOUS WORK

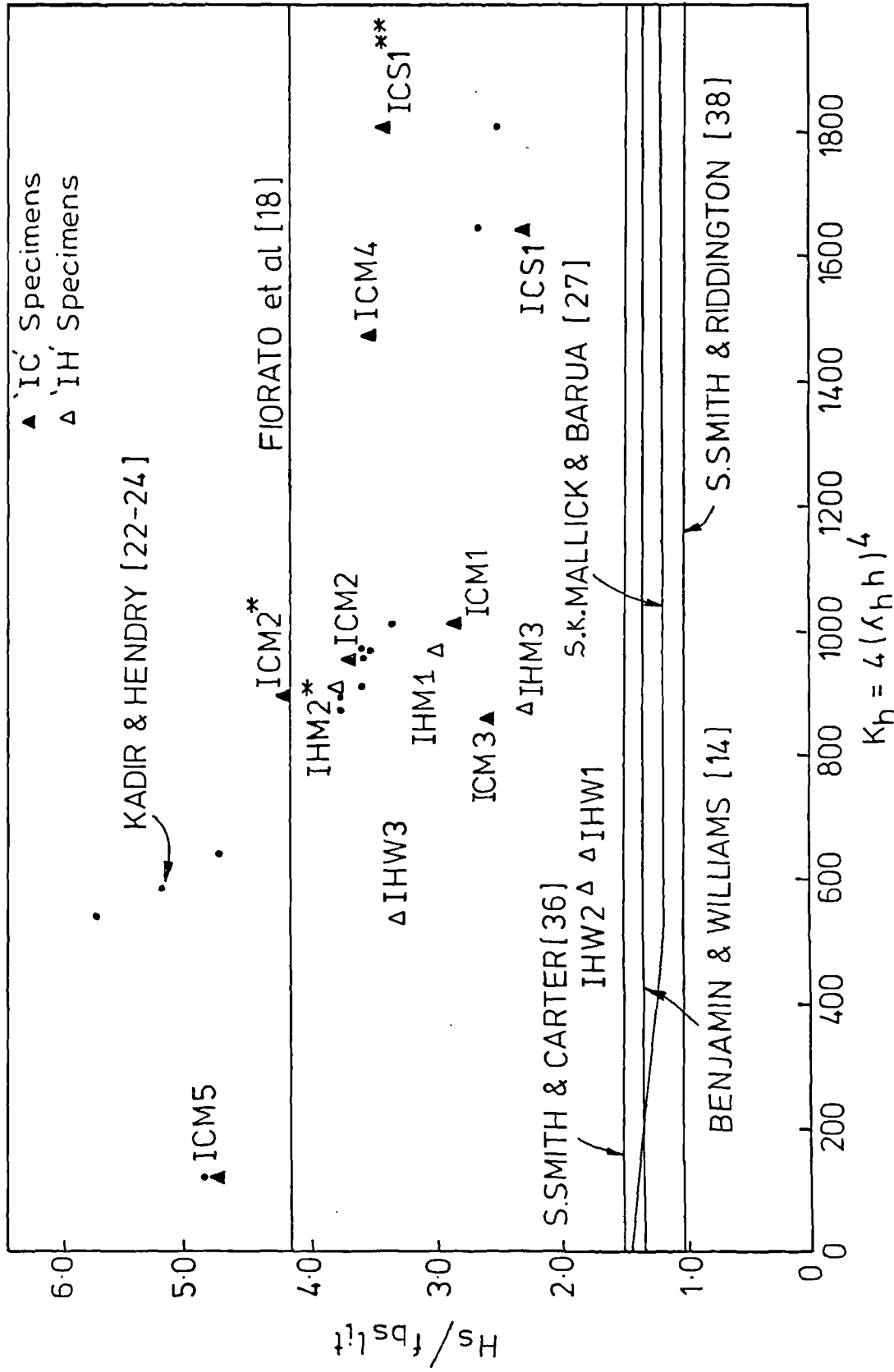


FIG. 5.5 COMPARISON OF INFILL CRACKING LOAD TEST RESULTS WITH SHEAR STRENGTH FROM PREVIOUS WORK

both empirical and theoretical predictions from previous work in Table 5.12. None of the methods seems to be absolutely safe. The method giving the closest predictions to the test results is Wood's method [44].

5.5 WOOD'S METHOD

5.5.1 General

Since Wood's method [44] gives the closest predictions to the test results, it seems important to present the details of the calculations and the different collapse mechanisms predicted for the infilled frames tested by this method. All the results are given in Table 5.13. In this table the separate contributions of the infill and the frame are also given. The way in which f_f and f_i are obtained is given below in section 5.5.2.

5.5.2 Separate Contributions of Infill and Frame for Wood's Method

In the discussion to Wood's method [46], P.A.C.Sims questioned the method used in Wood's design examples [44] concerning the separate contributions of the infill and the frame. He suggested a way to obtain the correct individual contributions by reworking the solutions keeping these contributions separate. In his reply Wood [46] accepted the criticism and agreed with Sim's proposal procedure.

Since the analysis of the collapse mechanisms identified in Chapter 4 is based on the theory of plasticity with the infill and the frame considered separately (this is discussed in Chapter 6), and since Wood's method [44] gives the closest predictions to the test results, it seems important to find the correct separate contributions of infill and frame by this method.

Infilled frame designation	HOLMES [15]		FIORATO et al [18]		MAINSTONE [20, 46]		KADIR & HENDRY [22 - 24]		S. SMITH & CARTER [36]		S. SMITH & RIDDINGTON [38]		S. KHALILICK & BARUA [29]		LIAUW & KWAN [43]		WOOD [44]		Test results	
	w/d	H _{ui} (KN)	H _{ut} (KN)	w/d _i	H _{ui} (KN)	H _{ut} (KN)	w/d _i	H _{ui} (KN)	H _{ut} (KN)	w/d _i	H _u (KN)	w/d _i	H _u (KN)	H _{ui} (KN)	H _{ut} (KN)	H _u (KN)	H _{ut} (KN)	H _{ue} (KN)	H _{pe} (KN)	
IHW1	0.33	82.8	96.4	0.183	40.5	54.1	0.393	43.5	69.7	0.497	109.9	0.184	40.6	53.5	104.0	55.0	42.5	27.6	25.0	
IHM1	"	134.9	148.5	0.174	62.6	76.2	0.357	64.2	92.4	0.451	162.5	0.169	60.7	81.7	153.8	74.2	58.3	53.6	50.5	
IHS1	"	236.6	249.8	0.161	101.5	114.7	0.301	95.0	121.2	0.380	240.3	0.145	91.7	127.8	227.3	96.9	80.6	56.3 [†]	-	
ICM1	"	134.9	148.1	0.173	62.2	75.4	0.348	62.7	89.9	0.441	158.9	0.165	59.5	80.4	150.3	74.2	57.9	61.9	58.6	
IGS1	"	236.6	249.8	0.163	102.7	115.9	0.313	98.8	128.0	0.396	250.0	0.150	94.9	131.2	236.5	96.9	84.7	76.0	73.0	
IGS1**	"	236.6	249.8	0.161	101.5	114.7	0.301	95.0	121.2	0.380	240.3	0.145	91.7	127.8	227.3	96.9	84.7	93.9	82.9	
IHW2	"	82.8	101.7	0.185	40.9	59.8	0.403	44.6	73.8	0.510	112.8	0.188	41.5	54.4	106.7	60.3	47.5	41.0	40.8	
IHM2	"	134.9	151.6	0.174	62.6	79.3	0.363	65.4	94.6	0.451	162.5	0.169	60.7	81.7	153.8	82.1	62.8	50.0 [‡]	-	
IHM2*	"	134.9	153.8	0.175	63.0	81.9	0.357	64.2	94.3	0.451	162.5	0.169	60.7	81.7	153.8	86.3	65.6	63.4	61.5	
ICM2	"	134.9	154.2	0.173	62.5	81.8	0.357	64.2	92.4	0.451	162.5	0.169	60.7	81.7	153.8	86.8	67.9	67.3	62.5	
ICM2*	"	134.9	153.8	0.175	63.2	82.1	0.365	65.7	96.3	0.462	166.4	0.172	62.0	83.0	157.4	86.3	68.7	85.1	81.9	
IHW3	"	82.8	111.4	0.187	41.3	69.9	0.414	45.1	76.2	0.524	115.8	0.192	42.5	55.4	109.4	70.0	57.5	54.3	44.0	
IHM3	"	134.9	163.5	0.176	63.4	92.0	0.365	65.7	96.8	0.462	166.4	0.172	62.0	83.0	157.4	96.0	75.4	51.4	45.0	
ICM3	"	134.9	163.5	0.176	63.4	92.0	0.365	65.7	97.3	0.462	166.4	0.172	62.0	83.0	157.4	96.0	77.6	58.9	55.0	
ICM4	"	134.8	155.4	0.165	59.3	79.9	0.571	102.8	130.5	0.451	162.5	0.154	55.4	81.7	153.8	87.1	77.2	93.7	88.0	
ICM5	"	149.7	163.3	0.225	81.2	94.8	0.408	73.5	186.7	0.746	268.2	0.262	94.4	118.1	253.7	74.2	69.9	92.7	90.9	

Notes (i) † premature failure of windward column extension; the infill remained uncracked (see section 4.4.3)

(ii) ‡ failure of frame without failure of infill (see section 4.4.3)

TABLE 5.1.2: ULTIMATE LOAD FROM PREVIOUS WORK

Infilled frame designation	m _n	Y _p	m _e	mode	f _s = $\frac{2\sqrt{m_e}}{m_e + 1}$	$\frac{M_{ub}}{M_{uc}}$	f = $\frac{f_s + \Delta f}{s}$	$\frac{4M_u}{h_1} + \frac{Y_p f_{ci} t \omega_1}{h_1}$ (KN)	H _{ui} = f _i Σ (KN)		H _f = f _f Σ (KN)		H _{ut} = f _s Σ (KN)		H _{ut} = fΣ (KN)		Test results (KN)		f test		Y _p test	
									(KN)	(KN)	(KN)	(KN)	H _{pe}	H _{ue}	H _{pe} /Σ	H _{ue} /Σ	(a)	(b)				
IHM1	0.138	0.268	0.515	S.R	0.947	1.00	0.947	15.3+29.6=44.9	29.6	12.9	42.5	-	25.0	27.6	0.557	0.615	0.092	0.112				
IHM1	0.085	0.309	0.275	S.R	0.822	1.00	0.822	15.3+55.6=70.9	55.6	2.7	58.3	-	50.5	53.6	0.712	0.756	0.232	0.261				
IHS1	0.047	0.347	0.135	D.C	0.647	1.00	0.647	14.8+109.6=124.4	40.3	40.3	80.6	-	-	56.3 [†]	-	0.453	-	0.170				
ICH1	0.082	0.311	0.264	S.R	0.813	0.54	0.818	14.8+56.0=70.8	56.0	1.5	57.5	57.9	58.6	61.9	0.828	0.874	0.321	0.359				
ICSL	0.047	0.347	0.135	D.C	0.647	0.55	0.681	14.8+109.6=124.4	40.3	40.3	80.6	84.7	73.0	76.0	0.587	0.611	0.286	0.310				
ICSL**	0.047	0.347	0.135	D.C	0.647	0.55	0.681	14.8+109.6=124.4	40.3	40.3	80.6	84.7	82.9	93.9	0.666	0.755	0.369	0.473				
IHM2	0.192	0.241	0.797	S.R	0.994	1.00	0.994	21.2+26.6=47.8	26.6	20.9	47.5	-	40.8	41.0	0.854	0.858	0.178	0.180				
IHM2	0.104	0.292	0.356	S.R	0.880	1.13	0.880	18.8+52.6=71.4	52.6	10.2	62.8	-	-	50.0 [†]	-	0.700	-	0.184				
IHM2*	0.118	0.281	0.420	S.R	0.913	1.00	0.913	21.2+50.6=71.8	50.6	15.0	65.6	-	61.5	63.4	0.857	0.883	0.248	0.264				
ICN2	0.121	0.279	0.434	S.R	0.919	0.79	0.944	21.7+50.2=71.9	50.1	15.9	66.0	67.9	62.5	67.3	0.869	0.936	0.251	0.291				
ICN2*	0.118	0.281	0.420	S.R	0.913	0.65	0.957	21.2+50.6=71.8	50.6	15.0	65.6	68.7	81.9	85.1	1.141	1.185	0.440	0.475				
IHW3	0.290	0.232	1.250	S	0.994	1.00	0.994	32.1+25.7=57.8	25.7	31.8	57.5	-	44.0	54.3	0.761	0.939	0.136	0.207				
IHM3	0.178	0.246	0.724	S.R	0.987	1.00	0.987	32.1+44.3=76.4	44.3	31.1	75.4	-	45.0	51.4	0.589	0.673	0.087	0.114				
ICN3	0.178	0.246	0.724	S.R	0.987	0.81	1.015	32.1+44.3=76.4	44.3	31.1	75.4	77.6	55.0	58.9	0.720	0.771	0.131	0.150				
ICM4	0.143	0.264	0.542	S.R	0.955	3.00	1.055	25.7+47.5=73.2	47.5	22.4	69.9	77.2	88.0	93.7	1.202	1.280	0.419	0.475				
ICM5	0.085	0.309	0.275	S.R	0.822	0.13	0.986	15.3+55.6=70.9	55.6	2.7	58.3	69.9	90.9	92.7	1.282	1.307	0.750	0.780				

Notes 1. (a) $Y_p = \left[\frac{H_{pe}}{4M_u/h_1} \right]^2 \frac{m_n}{4}$ (b) $Y_p = \left[\frac{H_{ue}}{4M_u/h_1} \right]^2 \frac{m_n}{4}$ see section 5.5.3

2. \diamond S.R shear rotation D.C diagonal compression S shear mode

3. f_f and f_i (see section 5.5.2)

4. [†] see section 4.4.3

5. { m_n, Y_p, m_e, f_s etc., see list of notations

TABLE 5.13: ULTIMATE LOAD BY WOOD'S METHOD

Wood [44] introduced a non-dimensional parameter, f , to express the ultimate load

$$H_u = f \left[\frac{4M_u}{h_i} + \frac{1}{2} \gamma_p f_{ci} t \ell_i \right]$$

where M_u is the smaller of M_{pb} and M_{pc} .

For mode S (strong mode)

$$f = 1$$

$$H_{uf} = \frac{4M_u}{h_i}$$

$$\text{and } H_{ui} = \frac{1}{2} \gamma_p f_{ci} t \ell_i$$

The equations quoted below are taken from Wood's paper [44] and reworked as suggested by P.A.C. Sims [46] to find the correct non-dimensional parameters f_f and f_i which are used to find the separate contributions of infill and frame. This being done only for the lower bound solutions for modes SR, DC and CC.

(i) Mode SR

$$X = 1 - \sqrt{\frac{m_n}{2(1 - C)}} \quad (21)$$

where

$$m_n = \frac{8M_u}{f_{ci} t \ell_i^2}$$

$$M_e = -M_u + 8(1 - C)M_u \left(\frac{1}{2} - X\right) / m_n \quad (22)$$

Summation of shear gives

$$H_u = \underbrace{\frac{2(M_u + M_e)}{h_i}}_{H_f} + \underbrace{\sqrt{(C - C)^2} f_{ci} t \ell_i}_{H_i} \quad (25)$$

For a square panel

$$l_i = h_i$$

$$C = \frac{1}{2}$$

and therefore

$$X = 1 - \sqrt{m_n}$$

substituting X in equation (21) gives

$$M_e + M_u = 4M_u \left(\frac{2\sqrt{m_n} - 1}{2m_n} \right) \quad (22')$$

substituting (22') into equation (25)

$$\begin{aligned} H_u &= 2 \frac{4M_u}{h_i} \frac{(2\sqrt{m_n} - 1)}{2m_n} + \frac{1}{2} f_{ci} t l_i \\ &= f \left(\frac{4M_u}{h_i} + \frac{1}{2} f_{ci} t l_i \right) \end{aligned} \quad (25')$$

$$\text{since } l_i = h_i \text{ and } m_n = \frac{8M_u}{f_{ci} t l_i^2}$$

$$\frac{1}{2} f_{ci} t l_i = \frac{4M_u}{m_n h_i}$$

substituting this in equation (25')

$$\begin{aligned} H_u &= \frac{4M_u}{h_i} \left(\frac{2\sqrt{m_n} - 1}{m_n} \right) + \frac{4M_u}{m_n h_i} \\ &= f \left(\frac{4M_u}{h_i} + \frac{4M_u}{m_n h_i} \right) \end{aligned}$$

therefore

$$f = \frac{2\sqrt{m_n} - 1}{m_n} + \frac{1/m_n}{1 + \frac{1}{m_n}}$$

$$f = \frac{2\sqrt{m_n}}{m_n + 1}$$

When the solutions are kept separate

$$H_u = H_f + H_i = \frac{2(M_u + M_e)}{h_i} + \sqrt{C - C^2} f_{ci} t \ell_i$$

with

$$H_f = \frac{2(M_u + M_e)}{h_i}$$

substituting (22') in the equation above gives

$$H_f = \frac{2}{h_i} \left(\frac{4M_u (2\sqrt{m_n} - 1)}{2m_n} \right)$$

H_f is also given by

$$H_f = f_f \left(\frac{4M_u}{h_i} + \frac{1}{2} f_{ci} t \ell_i \right)$$

$$\text{since } \frac{1}{2} f_{ci} t \ell_i = \frac{4M_u}{h_i}$$

therefore

$$f_f = \frac{2\sqrt{m_n} - 1}{m_n + 1}$$

Similarly

$$H_i = f_i \left(\frac{4M_u}{h_i} + \frac{1}{2} f_{ci} t \ell_i \right)$$

from (25) and with $C = \frac{1}{2}$

$$H_i = \frac{1}{2} f_{ci} t \ell_i$$

therefore

$$f_i = \frac{1}{m_n + 1}$$

Remark $f = f_f + f_i$

(ii) Mode DC and CC

Using the same procedure as for mode S.R the following relationships are obtained

$$f = \frac{2\sqrt{m_n}}{m_n + 1}$$

$$f_f = f_i = \frac{\sqrt{m_n}}{m_n + 1}$$

5.5.3 Penalty Factor for Infilled Frames Tested, γ_{pe}

$$H_{uw} = f \left[\frac{4(\text{smaller } M_u)}{h_i} + \frac{1}{2} \gamma_p f_{ci} t \ell_i \right] \quad (1)$$

where H_{uw} is the ultimate load by Wood's method [44] and

$$f = \frac{2\sqrt{m_e}}{m_e + 1} \quad (2)$$

m_e being the effective relative strength parameter and is equal to

$$m_e = \frac{m_n}{\gamma_p}$$

where

$$m_n = \frac{8M_u}{f_{ci} t \ell_i^2} \quad (3)$$

since $\ell_i = h_i$ then

$$\frac{1}{2} f_{ci} t \ell_i = \frac{4M_u}{m_n h_i} \quad (4)$$

In order to get γ_{pe} for the infilled frames tested, H_{uw} should be made equal to H_{ue} (ultimate load from tests).

Substituting (4) in (1) gives

$$H_{ue} = H_{uw} = f \frac{4M_u}{h_i} \left(1 + \frac{\gamma_{pe}}{m_n} \right) \quad (5)$$

substituting (2) in (5) gives

$$\frac{4M_u}{h_i} \frac{\sqrt{\frac{m_n}{\gamma_{pe}}}}{\frac{m_n}{\gamma_{pe}} + 1} \left(1 + \frac{\gamma_{pe}}{m_n} \right) = H_{ue} \quad (6)$$

putting $\frac{4M_u}{h_i} = A$, $\frac{m_n}{\gamma_{pe}} = B$ and $H_{ue} = C$ (6) becomes

$$\frac{2A\sqrt{B}}{B+1} \left(1 + \frac{1}{B} \right) = C \quad (6')$$

$$\frac{2A\sqrt{B}}{(B+1)} \frac{(B+1)}{B} = C \quad (7)$$

$$\frac{B}{B^2} = \frac{C^2}{4A^2} \quad (8)$$

$$B = \frac{4A^2}{C^2} \quad (9)$$

which gives

$$\gamma_{pe} = \frac{m_n}{4} \left(\frac{H_{ue}}{\frac{4M_u}{h_i}} \right)^2$$

if H_{pe} is used instead of H_{ue} then

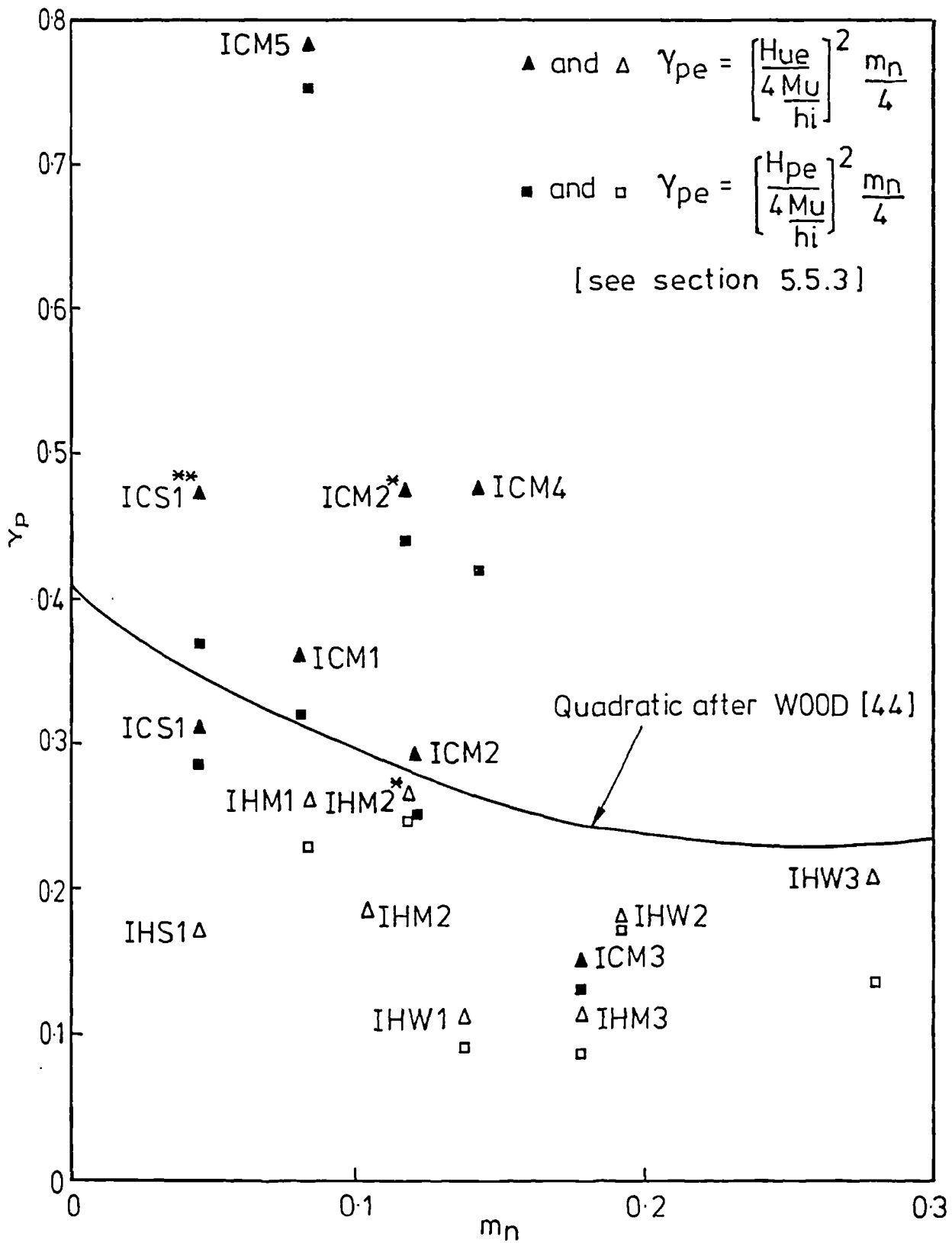
$$\gamma_{pe} = \frac{m_n}{4} \left(\frac{H_{pe}}{\frac{4M_u}{h_i}} \right)^2$$

The values for γ_{pe} using both H_{ue} and H_{pe} are reported in the last two columns of Table 5.13. Wood [44] derived a relationship between the penalty factor, γ_p , and the nominal relative strength parameter, m_n , for steel frames infilled with brickwork. Wood's curve is reproduced

in figure 5.6. The penalty factors obtained from tests, γ_{pe} , for all the infilled frames tested are compared to the curve derived by Wood in the same figure. It can be seen from figure 5.6 that Wood's method is not safe for all the 'IH' specimens and two 'IC' specimens. Figure 5.7 shows the effect, a reduction of 20% of f_{ci} , has on γ_{pe} . The fact that f_{ci} was reduced by 20% made the method safe for an additional four infilled frames. Figure 5.7 shows that the method would be conservative for seven out of eight 'IC' specimens and even over conservative for most of them. Figures 5.6 and 5.7 emphasize the effect the vertical loads on the columns have on the strength of the composite structure. The 'IC' specimens are stronger than the corresponding 'IH' ones. This has been discussed in section 4.6.3 (see Table 4.4).

5.6 MAY'S METHOD

The fact that Wood's method [44] is found not to be safe for all the infilled frames tested might be due to the incorrect estimation of the frame strength. In section 3.3.4 the problem of the efficiency of the opening corners has been discussed. This efficiency is expected to be of the order of 83% for the reinforcement detailing of the corners adopted. From section 5.1.4 (Analysis of Open Frames), the value of k (ratio of plastic (ultimate) moment of joint to plastic (ultimate) moment of beam, or column) has been found to vary between 0.5 and 1. May and Ma [49] extended Wood's method [44] to cover frames in which the joints between beams and columns are weaker than the frame members. The details of the calculations by this method are given in Table 5.14 for three values of k (0.5, 0.75 and 1). Table 5.15 shows the effect a reduction of 20% of the compressive strength of the infill f_{ci} has on the ultimate load. This reduction not only reduces the ultimate load but also it changes the predicted collapse modes for some infilled



\triangle, \square 'IH' Specimens $\blacktriangle, \blacksquare$ 'IC' Specimens

FIG. 5.6 PENALTY FACTOR FROM TESTS FOR f_{ci}

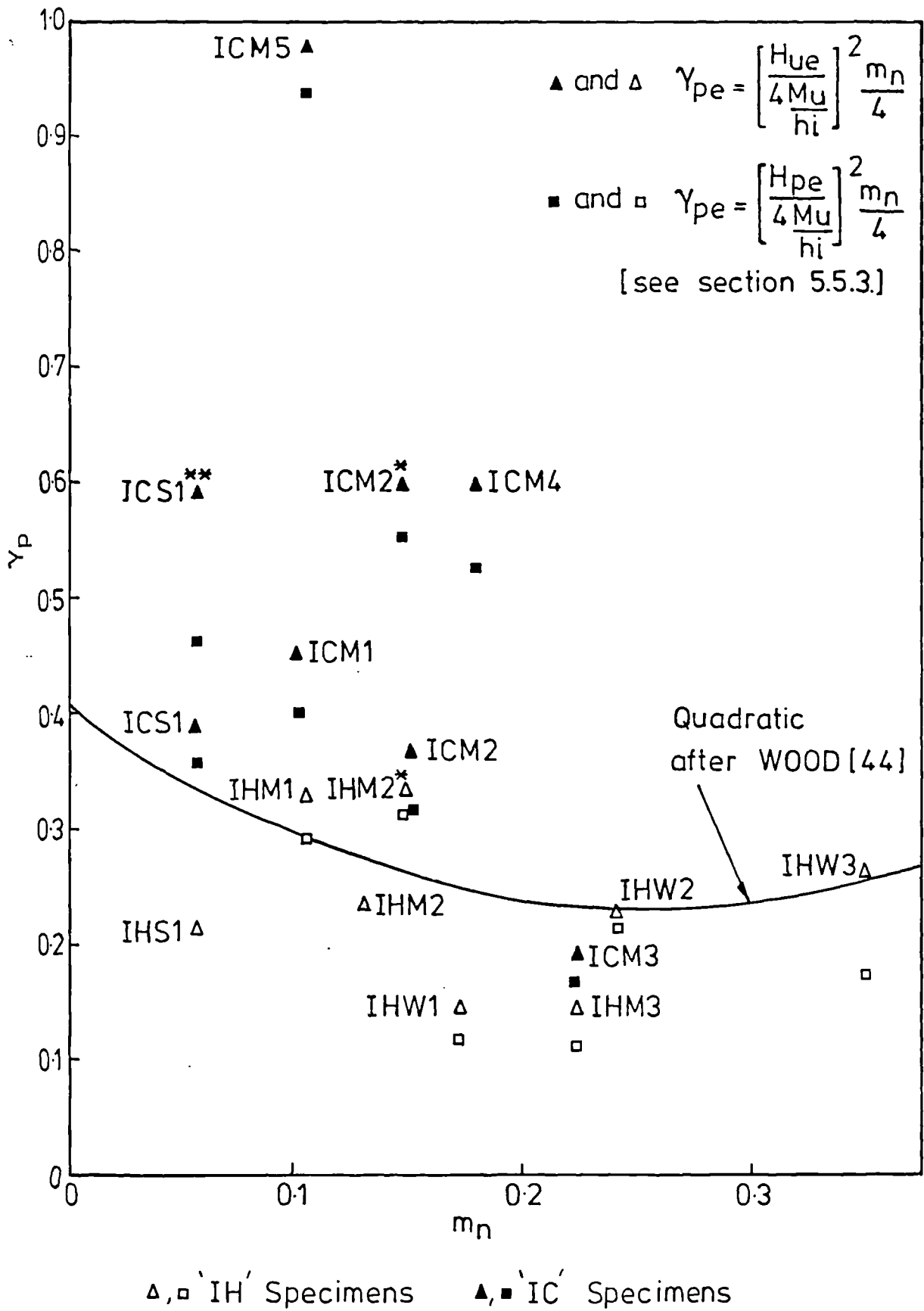


FIG. 5.7 PENALTY FACTOR FROM TESTS FOR 0.8 fci

Infilled frame designation	m_n	γ_p	m_e	mode \diamond	f	$H_{ut} = f \cdot \Sigma$ (KN)	mode \diamond	f	$H_{ut} = f \cdot \Sigma$ (KN)	mode \diamond	f	$H_{ut} = f \cdot \Sigma$ (KN)	mode	f = $f_s + \Delta_f$	$H_{ut} = f \cdot \Sigma$ (KN)
IHW1	0.138	0.268	0.515	S.R. R.S.R	0.816	36.6	S.R. R.S.R	0.886	39.8	S.R. R.S.R	0.947	42.5	S.R	0.947	42.5
IHW1	0.085	0.309	0.275	S.R. R.S.R	0.708	50.2	S.R. R.S.R	0.764	54.2	S.R. R.S.R	0.822	58.3	S.R	0.822	58.3
IHS1	0.047	0.347	0.135	S.R. R.S.R	0.550	68.4	S.R. R.S.R	0.593	73.8	S.R. R.S.R	0.647	80.6	D.C	0.647	80.6
ICM1	0.082	0.311	0.264	S.R. R.S.R	0.701	49.6	S.R. R.S.R	0.757	53.6	S.R. R.S.R	0.813	57.5	S.R	0.818	57.9
IGS1	0.047	0.347	0.135	S.R. R.S.R	0.550	68.4	S.R. R.S.R	0.593	73.8	S.R. R.S.R	0.647	80.6	D.C	0.681	84.7
IGS1**	0.047	0.347	0.135	S.R. R.S.R	0.550	68.4	S.R. R.S.R	0.593	73.8	S.R. R.S.R	0.647	80.6	D.C	0.681	84.7
IHW2	0.192	0.241	0.797	S	0.778	37.2	S	0.889	42.5	S.R. R.S.R	0.994	47.5	S.R	0.994	47.5
IHM2	0.104	0.292	0.356	S.R. R.S.R	0.757	54.1	S.R. R.S.R	0.817	58.3	S.R. R.S.R	0.880	62.8	S.R	0.880	62.8
IHM2*	0.118	0.281	0.420	S.R. R.S.R	0.790	56.7	S.R. R.S.R	0.852	61.2	S.R. R.S.R	0.913	65.6	S.R	0.913	65.6
ICM2	0.121	0.279	0.434	S.R. R.S.R	0.795	57.2	S.R. R.S.R	0.858	61.7	S.R. R.S.R	0.919	66.0	S.R	0.944	67.9
ICM2*	0.118	0.281	0.420	S.R. R.S.R	0.790	56.7	S.R. R.S.R	0.852	61.2	S.R. R.S.R	0.913	65.6	S.R	0.957	68.7
IHW3	0.290	0.232	1.250	S	0.722	41.7	S	0.861	49.8	S	0.994	57.5	S	0.994	57.5
IHM3	0.178	0.246	0.724	S	0.791	60.4	S	0.895	68.4	S.R. R.S.R	0.987	75.4	S.R	0.987	75.4
ICM3	0.178	0.246	0.724	S	0.791	60.4	S.R. R.S.R	0.895	68.4	S.R. R.S.R	0.987	75.4	S.R	1.015	77.6
ICM4	0.143	0.264	0.542	S	0.815	59.7	S.R. R.S.R	0.892	65.3	S.R. R.S.R	0.955	69.9	S.R	1.055	77.2
ICM5	0.085	0.309	0.275	S.R. R.S.R	0.708	50.2	S.R. R.S.R	0.764	54.2	S.R. R.S.R	0.822	58.3	S.R	0.986	69.9
				k = 0.5 mode S for $m_e \geq 0.536$			k = 0.75 mode S for $m_e \geq 0.602$			k = 1 mode S for $m_e \geq 1$				Wood's method	

Notes 1. \diamond R.S.R = Revised shear rotation

S = Shear mode

D.C = Diagonal compression mode

(see sections 2.4.5 and 2.4.7)

2. k: ratio of plastic moment of joint to plastic moment of beam or column

$$3. f_s = \frac{2\sqrt{m_e}}{m_e + 1}$$

4. Δ_f : increment for f_s when the plastic moments in beams and columns are not equal

$$5. \Sigma = \frac{4M}{h_i} + k\gamma_c f_{ci} l_i$$

TABLE 5.1.4: ULTIMATE LOAD BY MAY'S METHOD FOR k = 0.50, 0.75 AND 1.0 AND f_{ci}

Infilled frame designation	m_h	γ_p	m_e	mode \diamond	f	$H_{ut} = f\Sigma'$ (KN)	mode \diamond	f	$H_{ut} = f\Sigma'$ (KN)	mode	f = $f_s + \Delta_f$	$H_{ut} = f\Sigma'$ (KN)
IHW1	0.173	0.249	0.696	S	0.796	29.7	S	0.898	33.5	S.R.	0.984	36.7
IHW1	0.106	0.291	0.365	R.S.R. S.R.	0.762	43.6	R.S.R.	0.822	47.0	S.R.	0.885	50.6
IHS1	0.059	0.334	0.176	R.S.R. S.R.	0.610	63.5	S.R.	0.659	65.4	R.S.R.	0.714	70.8
ICH1	0.103	0.293	0.352	R.S.R. S.R.	0.754	43.0	R.S.R.	0.814	46.4	S.R.	0.882	50.3
IGS1	0.059	0.334	0.176	R.S.R. S.R.	0.610	60.5	R.S.R.	0.659	65.4	D.C	0.748	74.2
IGS1**	0.059	0.334	0.176	R.S.R. S.R.	0.610	60.5	R.S.R.	0.659	65.4	D.C	0.748	74.2
IHW2	0.240	0.230	1.042	S	0.744	33.9	S	0.872	36.2	S	1.000	41.5
IHW2	0.130	0.273	0.477	R.S.R. S.R.	0.809	47.0	R.S.R.	0.873	50.7	S.R.	0.935	54.3
IHW2*	0.148	0.261	0.567	S	0.814	47.9	R.S.R.	0.898	52.8	S.R.	0.961	56.5
ICH2	0.151	0.260	0.581	S	0.814	48.1	R.S.R.	0.901	53.2	S.R.	0.989	58.5
ICH2*	0.148	0.261	0.567	S	0.814	47.9	R.S.R.	0.898	52.8	S.R.	1.005	59.1
IHW3	0.363	0.258	1.406	S	0.693	38.1	S	0.847	46.6	S	0.986	54.2
IHW3	0.223	0.232	0.961	S	0.755	49.5	S	0.878	57.5	S.R.	1.000	65.5
ICH3	0.223	0.232	0.961	S	0.755	49.5	S	0.878	57.5	S.R.	1.028	67.3
ICH4	0.179	0.246	0.729	S	0.790	48.3	S	0.895	54.7	S.R.	1.087	66.4
ICH5	0.106	0.291	0.365	R.S.R. S.R.	0.762	43.6	R.S.R.	0.822	47.0	S.R.	1.049	60.0
					k = 0.5	mode S for $m_e \geq 0.536$		k = 0.75	mode S for $m_e \geq 0.602$		k = 1	mode S for $m_e \geq 1$
												Wood's method

Notes 1. \diamond R.S.R = Revised shear rotation

S = Shear mode

D.C = Diagonal compression mode

(see section 2.4.5 and 2.4.7)

2. k: ratio of plastic moment of joint to plastic moment of beam or column

$$3. f_s = \frac{2\sqrt{m_e}}{m_e + 1}$$

4. Δ_f : increment for f_s when the plastic moments in beams and columns are not equal

$$5. \Sigma' = \frac{4M_u}{h_i} + \frac{1}{2}\gamma_p \times 0.8f_{ci} \times t l_i$$

TABLE 5.15: ULTIMATE LOAD BY MAY'S METHOD FOR k = 0.50, 0.75 AND 1.0 AND 0.8f_{ci}

frames by both methods [44, 49].

From Tables 5.12 and 5.14, it can be seen that the closest predictions to the test results are those obtained by Wood's and May's methods [44, 49]. Three other methods, (Mainstone [20, 46], Kadir and Hendry [22-24] and S.K. Mallick and Barua [29]) however, give relatively close predictions to the test results when only the infill contribution, H_{ui} , is considered (Table 5.12, columns 6, 9 and 15). In figures 5.8 to 5.11, the ultimate and plastic loads, H_{ue} and H_{pe} , obtained from the tests are compared graphically to the predicted ultimate loads by Wood's and May's methods [44, 49].

The choice of the two non-dimensional parameters, f and m_e , as coordinates in figures 5.8 to 5.11 was made in order to have Wood's predicted loads [44] represented by the curve.

$$f = \frac{\sqrt{m_e}}{m_e + 1}$$

where

$$f = \frac{H_{ut}}{\frac{4M_u}{h_i} + \frac{1}{2}\gamma_p f_{ci} t l_i}$$

$$= \frac{H_{ut}}{\Sigma}$$

and

$$m_e = \frac{8M_u}{\gamma_p f_{ci} t l_i^2}$$

M_u being the smaller of M_{pb} and M_{pc} and H_{ut} the total ultimate predicted load.

All the other loads, H_{ue} , H_{pe} and H_{ut} are put in a non-dimensional form $f = \frac{H}{\Sigma}$ and plotted against m_e .

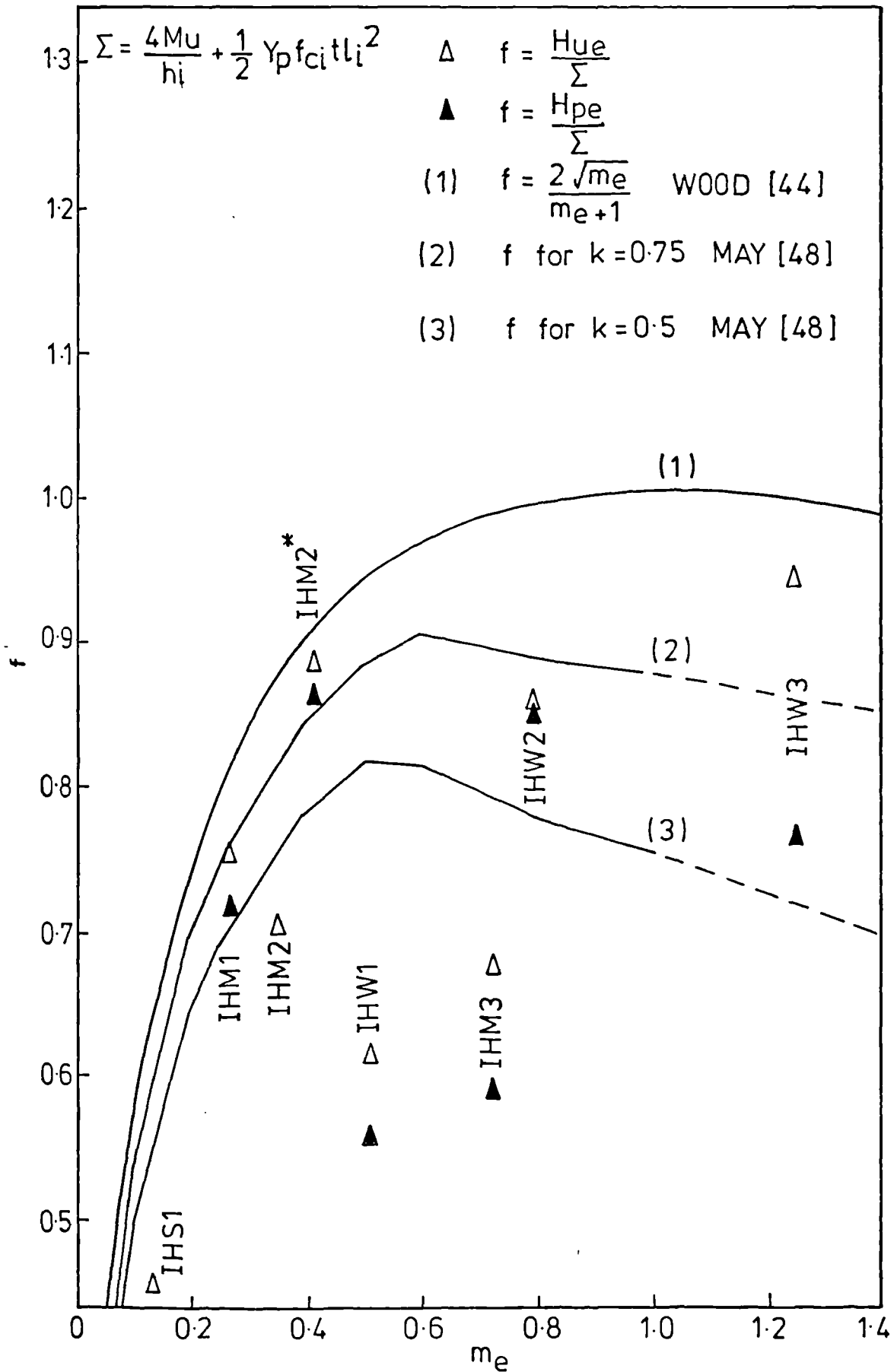


FIG.5.8 COMPARISON OF ULTIMATE AND PLASTIC LOAD TEST RESULTS FOR 'IH' SPECIMENS WITH PREVIOUS WORK FOR f_{ci}

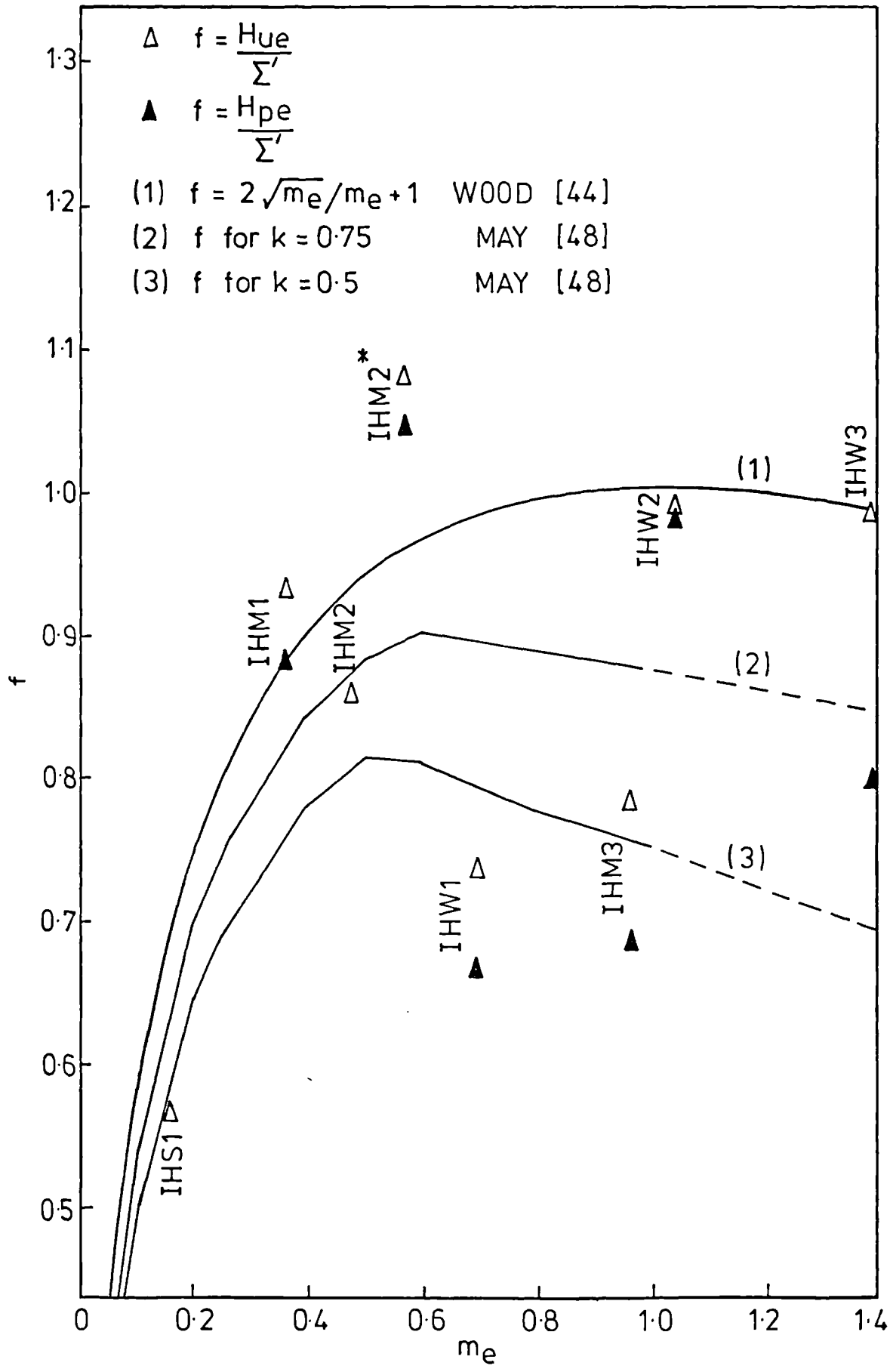


FIG. 5-9 COMPARISON OF ULTIMATE AND PLASTIC LOAD TEST RESULTS FOR 'IH' SPECIMENS WITH PREVIOUS WORK FOR $0.8f_{ci}$

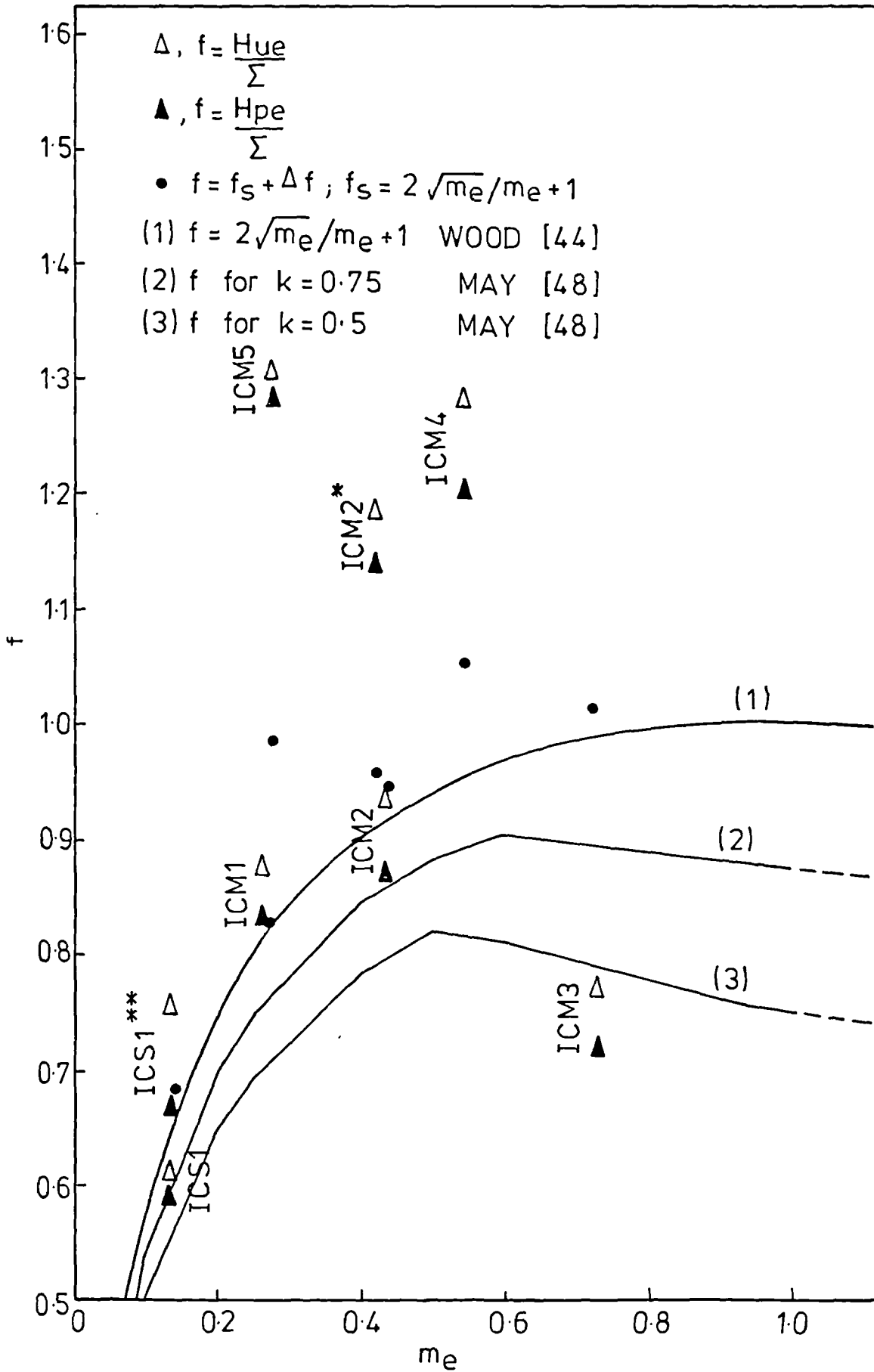


FIG.5.10 COMPARISON OF ULTIMATE AND PLASTIC LOAD TEST RESULTS FOR 'IC' SPECIMENS WITH PREVIOUS WORK FOR f_{ci}

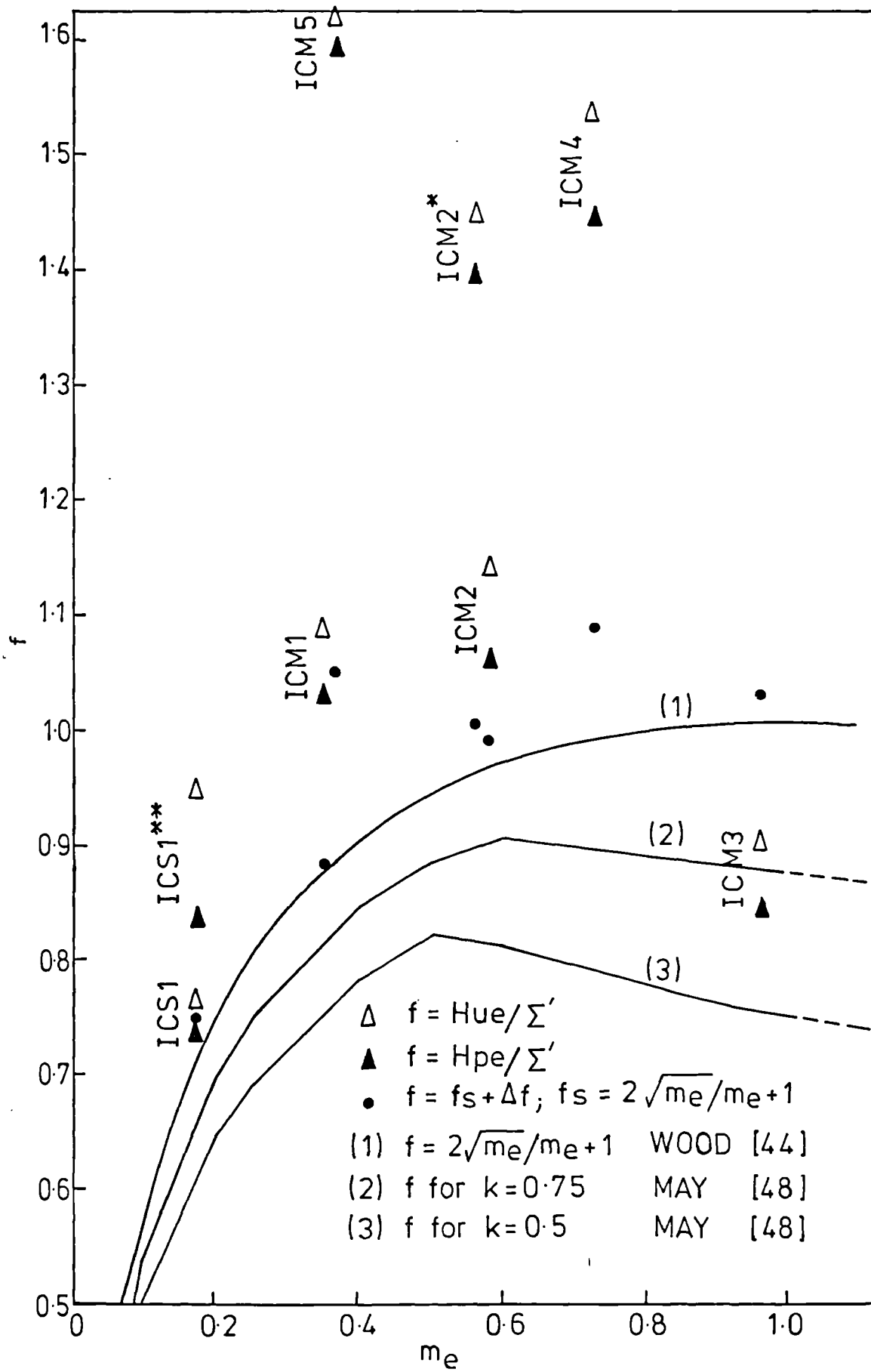


FIG.5.11 COMPARISON OF ULTIMATE AND PLASTIC LOAD TEST RESULTS FOR 'IC' SPECIMENS WITH PREVIOUS WORK FOR 0.8 f_{ci}

Figures 5.9 to 5.11 show the effect a reduction of 20% of f_{ci} has on the predicted results. This reduced strength of infill represents in fact the diagonal infill strength, f_{dci} , as defined in Table 5.7. The use of f_{dci} may be more appropriate than that of f_{ci} for the methods based on the diagonal strut concept.

It also must be pointed out that in Wood's method [44], the infill was assumed to exert a hydrostatic pressure against the frame members of an intensity, $\gamma_p f_{ci}$. But from tests on assemblies of blockwork (section 3.4.4, Table 3.5) it was shown that the compressive strength for $\theta = 90^\circ$ (θ being the angle between the bed joint and the line of application of load) was 35% higher than that for $\theta = 0$. Thus a reduction of 20% for f_{ci} may be thought to be realistic for this method.

CHAPTER 6

ANALYSIS OF THE TWO IDENTIFIED PLASTIC COLLAPSE MECHANISMS

6.1 GENERAL

The two collapse mechanisms which have been identified and discussed in Chapter 4 are analysed in this chapter. The analysis is based on the theory of plasticity. The frame and the infill are considered separately. The dissipation of energy in the infilled frame is taken as the sum of the separate dissipations of energy in the idealized tapered diagonal strut and in the frame. The geometry of the two collapse mechanisms is given in figure 6.1.

6.2 ANALYSIS OF MECHANISM 1

6.2.1. Determination of Angles of Rotation

From figure 6.1(a), if β is small then $\Delta' = \Delta$;

$$\theta = \frac{\Delta}{h},$$

$$\alpha = \frac{\Delta}{h'} = \frac{h\theta}{h'},$$

$$l'\beta = (l - l')\theta, \text{ giving } \beta = \frac{(l - l')\theta}{l'}$$

These angles can also be obtained using instantaneous centres as shown in figure 6.2.

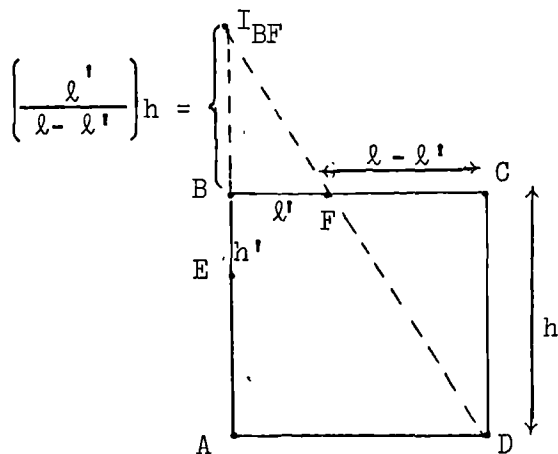
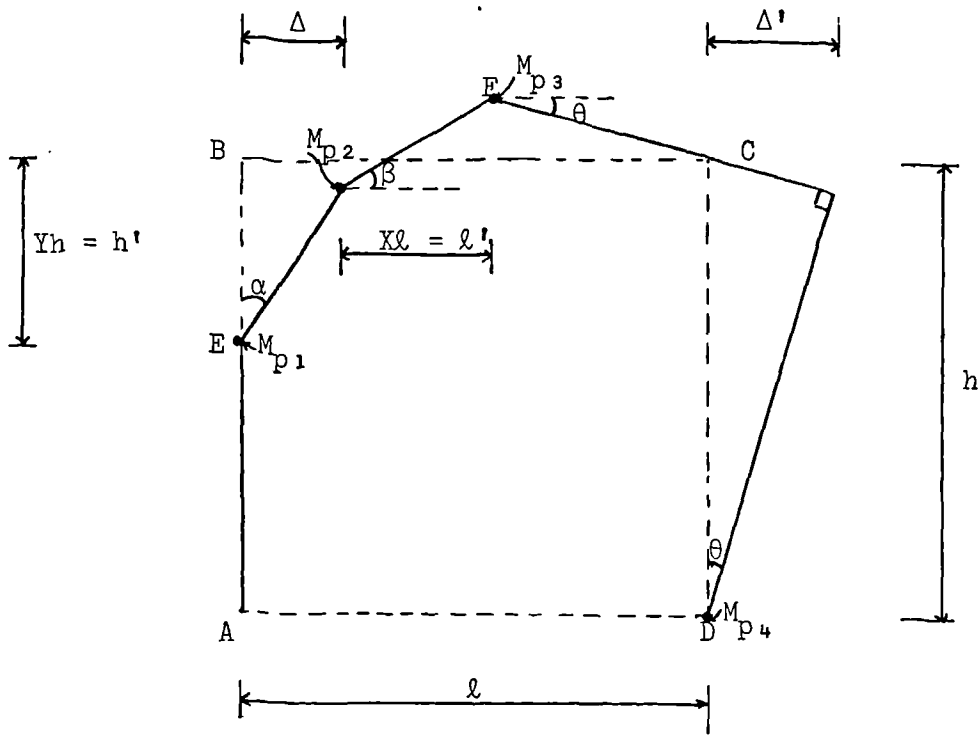
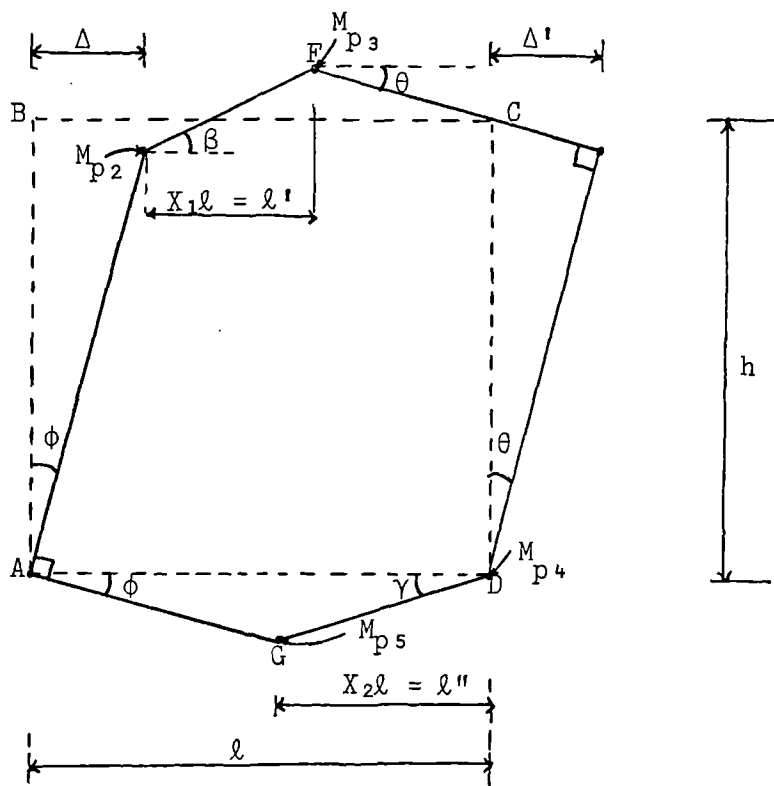


FIGURE 6.2: INSTANTANEOUS CENTRE FOR MECHANISM 1



(a) Mechanism 1



(b) Mechanism 2

FIGURE 6.1: GEOMETRY OF COLLAPSE MECHANISMS

$$h'\alpha = \frac{l'}{l - l'} h\beta$$

$$l'\beta = (l - l')\theta, \text{ giving } \beta = \frac{(l - l')}{l'}\theta$$

$$\alpha = \frac{l'}{l - l'} \cdot \frac{h}{h'} \frac{(l - l')}{l'}\theta, \text{ giving } \alpha = \frac{h}{h'}\theta$$

The hinge rotations are as follows:

at D, θ

at E, $\alpha = \frac{h}{h'}\theta$

at B, $\alpha + \beta = \left[\frac{h}{h'} + \frac{(l - l')}{l'} \right] \theta$

and at F, $\beta + \theta = \left[1 + \frac{(l - l')}{l'} \right] \theta$

6.2.2 Dissipation of Energy in Infilled Frame

The work done on the infilled frame is taken as the sum of the work done on the frame and that done on the idealized tapered diagonal strut. Having expressed the different angles of rotation in relation to θ the frame plastic work can be simply expressed as

$$W_f = M_{p_1} \cdot \frac{h}{h'} \theta + M_{p_2} \left[\frac{h}{h'} + \frac{l - l'}{l'} \right] \theta + M_{p_3} \left[1 + \frac{l - l'}{l'} \right] \theta + M_{p_4} \theta$$

putting $h' = Yh$ and $l' = Xl$ then the work done on the frame is given by

$$W_f = M_{p_1} \frac{\theta}{Y} + M_{p_2} \left(\frac{1}{Y} + \frac{1}{X} - 1 \right) \theta + M_{p_3} \frac{\theta}{X} + M_{p_4} \theta \quad (1)$$

To find the work done on the diagonal strut, a uniform plastic pressure against the frame is assumed as shown in figure 6.3. Along

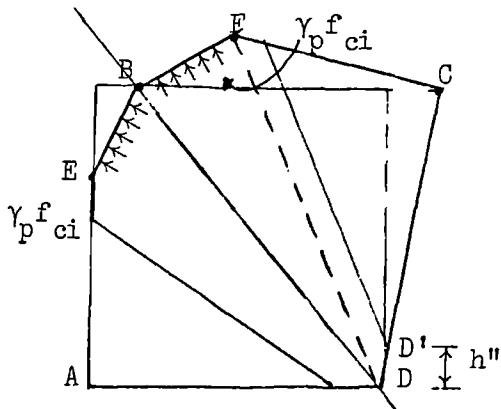


FIGURE 6.3: 'PLASTIC' DIAGONAL STRUT

the lengths EB and BF, the pressure is $\gamma_p f_{ci}$ (effective compressive strength) where γ_p is a penalty factor to allow for idealization of plasticity as suggested by Wood [44]. The work done on the diagonal strut may be split as follows:

a) that part of the strut below the diagonal BD.

There is movement only on length EB and the plastic work below the diagonal is equal to

$$W_{i_1} = h' \times \gamma_p f_{ci} \times t \times \frac{h'}{2} \times \alpha \quad (2)$$

b) that part of the strut above diagonal BD.

If the part to the right of line FD (figure 6.3) can be treated separately from the part to the left of this line, then the work done above the diagonal is equal to the work done on the part to the left of FD only. This is because the part to the right of FD does not change in length; since \widehat{FCD} remains 90° , and therefore no work is done on this part. Thus, the plastic work above the diagonal is equal to:

$$W_{i_2} = l' \times \gamma_p f_{ci} \times t \times \frac{l'}{2} \times \beta \quad (3)$$

If the 'dividing line' is not FD but FD' , where D' is some distance, h'' , above D on the leeward column. In this case some work will be done on the frame by the contact forces along the length DD' . This will be negative plastic work and would be given by

$$W_{i_3} = -h'' \times \gamma_p f_{ci} \times t \times \frac{h''}{2} \times \theta \quad (4)$$

In this case the work done on the part to the left of FD' would be

$$W_{i_2} + W_{i_3} = \frac{1}{2} \gamma_p f_{ci} t (l'^2 \beta - h''^2 \theta) \quad (5)$$

For the specimens tested it appears that h'' is very small compared to l' , thus, h''^2 is negligibly small and the work done above the diagonal would be equal to W_{i_2} . The total strut work is therefore

$$W_{it} = W_{i1} + W_{i2} \approx \frac{1}{2} \gamma_p f_{ci} t (h'^2 \alpha + \ell'^2 \beta) \quad (6)$$

The work done by the external load is

$$H_p \Delta = H_p h' \alpha = H_p h \theta \quad (7)$$

Thus the final work equation is

$$\begin{aligned} H_p h \theta &= W_f + W_{it} \\ &= M_{p1} \frac{\theta}{Y} + M_{p2} \left(\frac{1}{Y} + \frac{1}{X} - 1 \right) \theta + M_{p3} \frac{\theta}{X} + M_{p4} \theta \\ &\quad + \frac{1}{2} \gamma_p f_{ci} t \left(h'^2 \frac{h}{h'} \theta + \ell'^2 \frac{(\ell - \ell')}{\ell'} \theta \right) \end{aligned} \quad (8)$$

giving

$$H_p = \left(\frac{M_{p1}}{Y} + \left(\frac{1}{Y} + \frac{1}{X} - 1 \right) M_{p2} + \frac{M_{p3}}{X} + M_{p4} \right) \frac{1}{h} + \frac{1}{2} \gamma_p f_{ci} t \left(h' + \frac{\ell'}{h} (\ell - \ell') \right) \quad (9)$$

Putting $X = aY$, $h' = Yh$ and $\ell' = X\ell = aY\ell$ and since for the square frames tested $\ell = h$, we obtain

$$H_p = \frac{aM_{p1} + (a + 1 - aY)M_{p2} + M_{p3} + aYM_{p4} + \frac{1}{2} \gamma_p f_{ci} t h Y (1 + a - a^2 Y)}{aYh} \quad (9b)$$

6.2.3 Minimization of H_p

In equation (9b) if the penalty factor, γ_p , is taken as a variable in order to evaluate it as part of the solution rather than taking it from an empirical curve such as that proposed by Wood [44], then H_p is expressed in terms of three unknowns, a , Y and γ_p . The determination of the extrema of H_p consists of differentiating partially the relation (9b) with respect to a , Y and γ_p and setting the derivatives equal to

zero. This yields a system of three equations in three unknowns whose solution (a_0, Y_0, γ_{p_0}) is to be substituted in relation (9b). This gives either a maximum or a minimum for the function $H_p = f(a, Y, \gamma_p)$ depending on the sign of the determinant of the Hessian matrix. The mathematical procedure to check whether the solution yields a maximum or a minimum is as follows:

- (i) form the Hessian matrix (i.e., the matrix of second derivatives)
- (ii) evaluate the second derivatives for the solution (a_0, Y_0, γ_{p_0})
- (iii) determine the sign of the determinant of the matrix computed in (i).

If the determinant is positive (negative) the solution (a_0, Y_0, γ_{p_0}) yields a minimum (maximum). When the determinant is nil, $H_p(a_0, Y_0, \gamma_{p_0})$ is not an extremum. If, however, γ_p is taken as a constant, then H_p is given in terms of two variables only a and Y . The procedure of minimizing H_p is similar to that described above. These two cases are treated separately.

(a) Case 1. Penalty factor, γ_p , taken as a variable

Differentiating equation (9b) with respect to a , Y and γ_p gives

$$\left\{ \begin{array}{l} \frac{\partial H_p}{\partial a} = \frac{-M_{p_2} - M_{p_3}}{a^2 Y h} + \frac{1}{2} \gamma_p f_{ci} \operatorname{th} Y (1 - 2aY) \end{array} \right. \quad (10)$$

$$\left\{ \begin{array}{l} \frac{\partial H_p}{\partial Y} = \frac{-aM_{p_1} - (a+1)M_{p_2} - M_{p_3}}{aY^2 h} + \frac{1}{2} \gamma_p f_{ci} \operatorname{th} (1 + a - 2a^2 Y) \end{array} \right. \quad (11)$$

$$\left\{ \begin{array}{l} \frac{\partial H_p}{\partial \gamma_p} = \frac{1}{2} f_{ci} \operatorname{th} Y (1 + a - a^2 Y) \end{array} \right. \quad (12)$$

Setting the above three equations equal to zero yields

$$\left\{ \begin{array}{l} Y^2(1 - 2aY) = \frac{2(M_{p2} + M_{p3})}{a^2 \gamma_p f_{ci} t h^2} \end{array} \right. \quad (10a)$$

$$\left\{ \begin{array}{l} Y^2(1 + a - 2a^2Y) = \frac{2(aM_{p1} + (a+1)M_{p2} + M_{p3})}{a \gamma_p f_{ci} t h^2} \end{array} \right. \quad (11a)$$

$$\left\{ \begin{array}{l} Y(1 + a - a^2Y) = 0 \end{array} \right. \quad (12a)$$

setting equation (12) equal to zero yields (12a) because f_{ci} , t and h are all different from zero. Dividing (11a) by (10a) yields

$$\frac{1 + a - 2a^2Y}{1 - 2aY} = \frac{a[a(M_{p1} + M_{p2}) + M_{p2} + M_{p3}]}{M_{p2} + M_{p3}} \quad (13)$$

From equation (12a)

$$Y = \frac{1 + a}{a^2}$$

$$\text{and } Y = 0$$

But for $Y = 0$ there is no mechanism, so only the first solution (equation (12b)) is considered.

Substituting (12b) in equation (13) gives

$$\frac{-a(1 + a)}{-(2 + a)} = a \frac{[a(M_{p1} + M_{p2}) + M_{p2} + M_{p3}]}{M_{p2} + M_{p3}} \quad (14)$$

which gives when rearranged

$$(M_{p1} + M_{p2})a^2 + 2(M_{p1} + M_{p2})a + M_{p2} + M_{p3} = 0 \quad (15)$$

The solutions of this equation are

$$a = -1 \pm \sqrt{\frac{M_{p1}^2 + M_{p2}(M_{p1} - M_{p3}) - M_{p1}M_{p3}}{M_{p1} + M_{p2}}} \quad (16)$$

But for the infilled frames tested which developed this mechanism,

M_{p1} and M_{p3} are equal when the axial forces in frame members are ignored. Thus, putting $M_{p1} = M_{p3}$ in equation (16) yields a negative value for a (i.e., $a = -1$). This indicates that if H_p (equation (9b)) admits any minima or maxima, they all should be in the plane $a = -1$.

Thus for other values of a , the function has no turning point.

(b) Case 2. Penalty factor, γ_p , taken as a constant

In this case $\frac{\partial H_p}{\partial \gamma_p} = 0$ and the solution of the problem would consist of solving the system of equations (10a) and (11a). This being a non-linear system could not easily be solved explicitly. Putting in equation (9) $h' = Yh$ and $l' = Xl$ and since for square frames tested $l = h$, we obtain

$$H_p = \left(\frac{M_{p1}}{Y} + \left(\frac{1}{Y} + \frac{1}{X} - 1 \right) M_{p2} + \frac{M_{p3}}{X} + M_{p4} \right) \frac{1}{h} + \frac{1}{2} \gamma_p f_{ci} t l (Y + X (1 - X)) \quad (9c)$$

Differentiating equation (9c) with respect to X and Y gives

$$\frac{\partial H_p}{\partial X} = \frac{-(M_{p2} + M_{p3})}{hX^2} + \frac{1}{2} \gamma_p f_{ci} t l (1 - 2X) \quad (17)$$

$$\frac{\partial H_p}{\partial Y} = \frac{-(M_{p1} + M_{p2})}{hY^2} + \frac{1}{2} \gamma_p f_{ci} t l \quad (18)$$

setting the above two equations equal to zero and putting $h = l$, we obtain

$$X^2(1 - 2X) = \frac{2(M_{p2} + M_{p3})}{\gamma_p f_{ci} t l^2} \quad (17a)$$

$$Y^2 = \frac{2(M_{p1} + M_{p2})}{\gamma_p f_{ci} t l^2} \quad (18a)$$

For a fixed value of γ_p , the right hand sides of the above two equations are known quantities. Thus X and Y may be determined directly. Hence H_p is also determined and it only remains to check whether these values of X and Y give H_p minimum. In the case where $M_{p1} = M_{p3}$ are equal, which is the case for the infilled frames which developed this mechanism, then from (17a) and (18a)

$$X^2(1 - X) = Y^2 \quad (19)$$

The solution of this equality may be found either numerically or graphically. This equality is satisfied when $Y^2 = 0.037$ giving

$$X = 0.33$$

and $Y = 0.19$

Thus from either equation (17a) or (18a)

$$\gamma_p = \frac{2(M_{p1} + M_{p2})}{0.037 f_{ci} t l^2} \quad (20)$$

For the infilled frames which developed mechanism 1, the penalty factor, γ_p , evaluated from equation (20) ranges from 1.24 for IHW1 to 2.56 for IHW3. Thus, the mathematical procedure yields solutions incompatible with the physical limitations ($0 < \gamma_p \leq 1$).

6.2.4 Comments

From the previous section, it has been shown that the mathematical or analytical method produced results incompatible with the physical limitations ($0 < X \leq 1$, $0 < Y \leq 1$ and $0 < \gamma_p \leq 1$). In the first case (γ_p taken as a variable) the mathematical procedure yielded a negative value for a (i.e., $a = X/Y = -1$). This means that any minima or maxima which the function $H_p = f(a, Y, \gamma_p)$ (equation (9b)) might have should be in the plane $a = -1$. Thus outside this plane the function has no turning point. In the second case (γ_p taken as a constant) the yielded values for X and Y were within the physical limitations but that of the penalty factor, γ_p , was outside (i.e. $\gamma_p > 1$).

Since $H_p = f(a, Y, \gamma_p)$ has no turning point outside the plane $a = -1$, an alternative numerical procedure limiting the range of the variables to the physical limits could be appropriate to find a local minimum. The solution of the problem would be to find the two limiting values of the parameter, a , in the range of physical limitations. The minimum would occur at one of the borders.

6.2.5 Numerical Procedure for Mechanism 1

The method for minimizing H_p (equation 9(b)) within the physical limitations is as follows:

Step 1: Differentiate H_p with respect to Y only and setting this partial derivative to zero yields

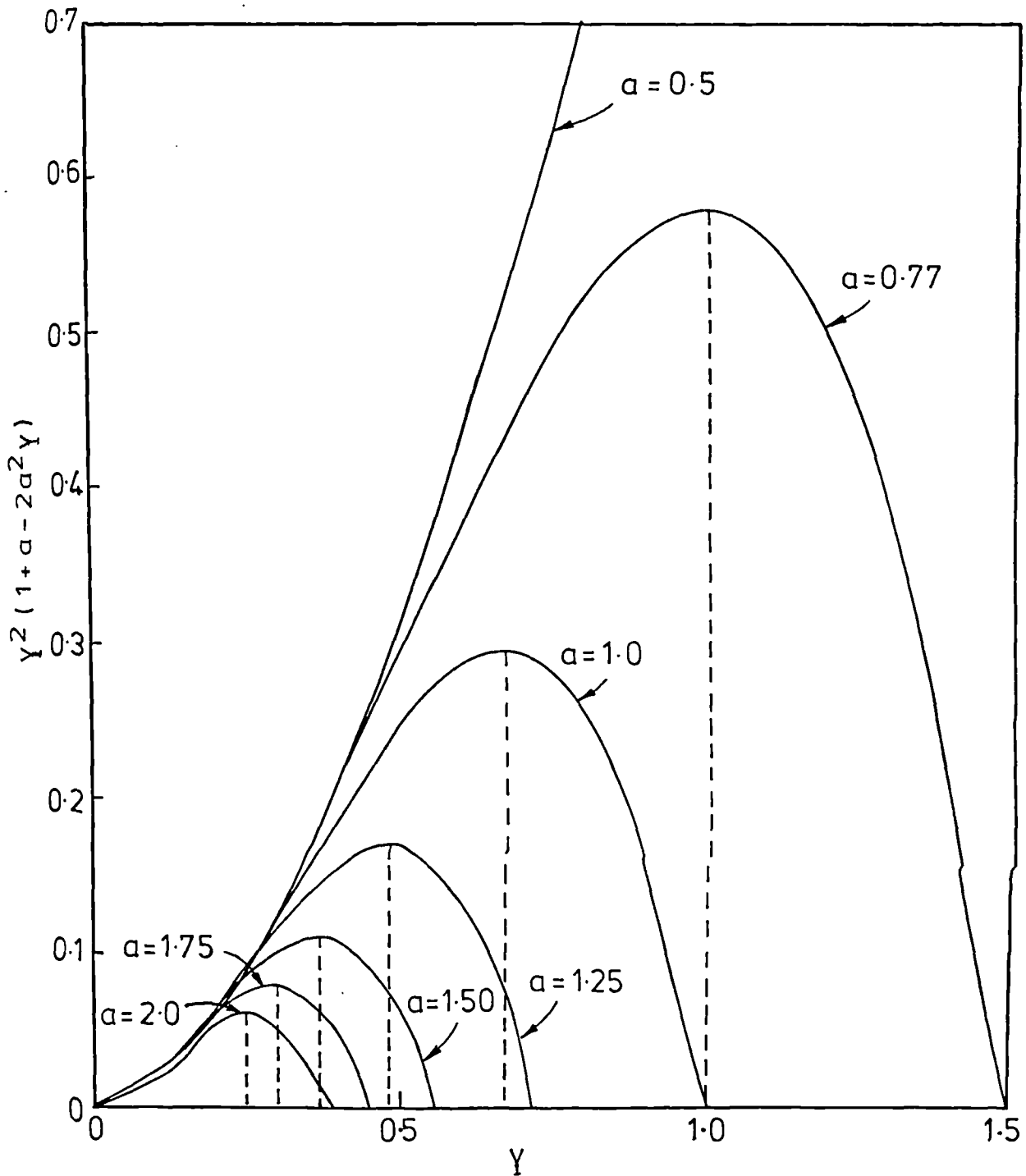
$$Y^2(1 + a - 2a^2Y) = \frac{2[aM_{p1} + (a+1)M_{p2} + M_{p3}]}{a\gamma_p f_{ci} th^2} \quad (11a)$$

Step 2: Fix a value for the parameter, a .

A realistic range may be taken as $0.5 \leq a \leq 2$ (from observations of photographs)

Step 3: Vary the penalty factor, γ_p , between its limits 0 and 1. A value of 0 for γ_p gives an indeterminate result, so a realistic increment of 0.1, starting from 0.1, up to 1 is reasonable.

Step 4: The left hand side of equation (11a), being a polynomial of the third degree in Y , may be plotted graphically for values of Y between 0 and 1 and for different values of the parameter, a , (i.e., $a = 0.5, 0.75, 1, 1.25, 1.5, 1.75$ and 2.0). The graphical representation of this family of curves is shown in figure 6.4. For each value of γ_p , the right hand side of equation (11a) is a constant for each value of a , and may be represented by a horizontal line in figure 6.4. This line may or may not intersect the curve plotted for a given value of the parameter, a . (Thus for different values of γ_p , there is a series of parallel lines). When the line and the curve do not intersect there is no solution for equation (11a). When they intersect, there are either one or two solutions. The unique solution is for the case when the line is tangential to the curve.



Note: for $\alpha=0.5$ the maximum occurs at $\gamma=2$

FIG. 6.4 GRAPHICAL REPRESENTATION OF LEFT HAND SIDE OF EQUATION (11a)

Step 5: Having a set of values for a , Y_p and one or two values of Y , these may be substituted in equation (9b) to yield either one or two values for H_p .

The trial and error analysis was conducted for different values of Y_p (between 0.1 and 1) and different values of a ($0.5 \leq a \leq 2$). The minimum value for H_p was found to occur in all cases for the maximum of $Y^2(1 + a - 2a^2Y)$ which is the left hand side of equation (11a). This corresponds to the case where there is one unique solution for equation (11a) and the horizontal line obtained in Step 4 is tangential to the curve in figure 6.4. The detailed calculations are given in Appendix E. These calculations showed that H_p (equation 9b) increases with increasing values of the parameter, a , and decreases with increasing values of Y . The value of the parameter, a , giving the lowest value for H_p may be determined by differentiating the left hand side of equation (11a) with respect to Y and setting the derivative equal to zero. Thus

$$2Y + 2aY - 6a^2Y^2 = 0$$

giving

$$Y = \frac{2 + 2a}{6a^2} \quad (21)$$

The highest possible maximum for $Y^2(1 + a - 2a^2Y)$, which is the left hand side of equation (11a), for the permissible range $0 < Y \leq 1$ occurs for $Y = 1$ (figure 6.4). Hence putting $Y = 1$ in equation (21) yields

$$6a^2 - 2a - 2 = 0 \quad (22)$$

and therefore

$a = 0.77$

In conclusion, for the specimens developing this mechanism, the

set of values of Y , a and γ_p giving the lowest value for H_p are respectively

$$a = 0.77$$

$$Y = 1 \quad \text{and from equation (11a)}$$

$$\gamma_p = \frac{2(aM_{p1} + (a+1)M_{p2} + M_{p3})}{af_{ci}tl^2[Y^2(1+a-2a^2Y)]}$$

The value of γ_p giving the lowest value for H_p is that when the maximum of $Y^2(1+a-2a^2Y)$ is reached within the physical limitations. Thus γ_p may be simply expressed for this mechanism as

$$\gamma_p = \frac{1.54M_{p1} + 3.54M_{p2} + 2M_{p3}}{0.45f_{ci}tl^2} \quad (23)$$

and is part of the solution.

Calculating γ_p from equation (23) and substituting its value and those of a and Y (i.e., $a = 0.77$ and $Y = 1$) in equation (9b) will give the minimum plastic loads for the infilled frames which developed this mechanism.

6.3 ANALYSIS OF MECHANISM 2

6.3.1 Determination of Angles of Rotation

From figure 6.1(b), if β and γ are small then $\Delta' = \Delta$;

$$\theta = \frac{\Delta}{h} = \phi,$$

$$l'\beta = (l - l')\theta, \text{ giving } \beta = \frac{(l - l')}{l'}\theta,$$

$$\text{and } l''\gamma = (l - l'')\theta, \text{ giving } \gamma = \frac{(l - l'')}{l''}\theta$$

The hinge rotations are as follows

at B, $\theta + \beta$
 at F, $\beta + \theta$
 at D, $\theta + \gamma$
 and at G, $\theta + \gamma$

6.3.2 Dissipation of Energy in Infilled Frame

As for the previous mechanism, the work done on the infilled frame is taken as the sum of the work done on the frame and that done on the idealized tapered diagonal strut. The frame plastic work can be expressed as

$$W_f = M_{p2} (\theta + \beta) + M_{p3} (\theta + \beta) + M_{p4} (\theta + \gamma) + M_{p5} (\theta + \gamma)$$

$$= (M_{p2} + M_{p3}) \left[1 + \frac{(\ell - \ell')}{\ell'} \right] \theta + (M_{p4} + M_{p5}) \left[1 + \frac{(\ell - \ell'')}{\ell''} \right] \theta$$

Putting $\ell' = X_1 \ell$ and $\ell'' = X_2 \ell$ gives

$$W_f = \left(\frac{M_{p2} + M_{p3}}{X_1} + \frac{M_{p4} + M_{p5}}{X_2} \right) \theta \quad (24)$$

To find the work done on the diagonal strut, a uniform plastic pressure against the frame is assumed as shown in figure 6.5.

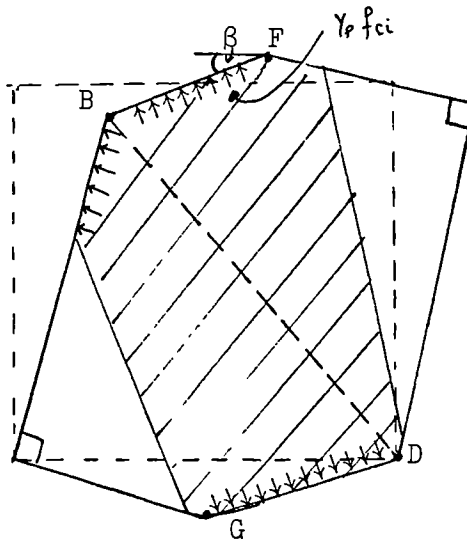


FIGURE 6.5: 'PLASTIC' DIAGONAL STRUT FOR MECHANISM 2

Along the lengths BF and DG, the pressure is taken as $\gamma_p f_{ci}$. The work done on the diagonal strut may be split as follows:

(a) movement on length BF

$$\begin{aligned} W_{i1} &= \gamma_p f_{ci} \times l' t \times \frac{l'}{2} \times \beta \\ &= \frac{1}{2} \gamma_p f_{ci} t l'^2 X_1 (1 - X_1) \theta \end{aligned} \quad (25)$$

(b) movement on length DG

$$\begin{aligned} W_{i2} &= \gamma_p f_{ci} \times l'' t \times \frac{l''}{2} \times \gamma \\ &= \frac{1}{2} \gamma_p f_{ci} t l''^2 X_2 (1 - X_2) \theta \end{aligned} \quad (26)$$

Thus the total strut work is

$$W_{it} = W_{i1} + W_{i2} = \frac{1}{2} \gamma_p f_{ci} t l^2 (X_1 - X_1^2 + X_2 - X_2^2) \theta \quad (27)$$

The work done by the external load is

$$H_p \Delta = H_p h \theta \quad (28)$$

Thus the final work equation is

$$\begin{aligned} H_p h \theta &= W_f + W_{it} \\ &= \left(\frac{M_{p2} + M_{p3}}{X_1} + \frac{M_{p4} + M_{p5}}{X_2} \right) \theta \\ &\quad + \frac{1}{2} \gamma_p f_{ci} t l^2 (X_1 - X_1^2 + X_2 - X_2^2) \theta \end{aligned} \quad (29)$$

giving

$$H_p = \left(\frac{M_{p2} + M_{p3}}{X_1} + \frac{M_{p4} + M_{p5}}{X_2} \right) \frac{1}{h} + \frac{1}{2} \gamma_p f_{ci} t \frac{l^2}{h} (X_1 - X_1^2 + X_2 - X_2^2) \quad (30)$$

Putting $X_1 = X_2 = X$ (justifiable from photographs) in equation (30) we obtain

$$H_p = \frac{M_{p2} + M_{p3} + M_{p4} + M_{p5}}{Xh} + \gamma_p f_{ci} t \frac{\ell^2}{h} X(1 - X) \quad (30a)$$

6.3.3 Minimization of H_p

As for mechanism 1, the penalty factor, γ_p , may be taken as a variable in equation (30a) or as a constant (i.e., from Wood's curve).

(a) Case 1. Penalty factor, γ_p , taken as a variable

Equation (30a) is thus expressed in terms of two variables X and γ_p .

The procedure to minimize H_p is as previously described in section 6.2.3.

$$\left\{ \begin{aligned} \frac{\partial H_p}{\partial X} &= \frac{-(M_{p2} + M_{p3} + M_{p4} + M_{p5})}{hX^2} + \gamma_p f_{ci} t \frac{\ell^2}{h} (1 - 2X) \end{aligned} \right. \quad (31)$$

$$\left\{ \begin{aligned} \frac{\partial H}{\partial \gamma_p} &= f_{ci} t \frac{\ell^2}{h} (X^2 - X) \end{aligned} \right. \quad (32)$$

setting the two equations above equal to zero gives

$$\left\{ \begin{aligned} X^2(1 - 2X) &= \frac{M_{p2} + M_{p3} + M_{p4} + M_{p5}}{\gamma_p f_{ci} t \ell^2} \end{aligned} \right. \quad (31a)$$

$$\left\{ \begin{aligned} X^2 - X &= 0 \end{aligned} \right. \quad (32a)$$

setting (32) equal to zero yields (32a) because f_{ci} , t , ℓ , and h are all different from zero. The solutions for (32a) are $X = 0$ and $X = 1$. The first one is outside the permissible range ($0 < X \leq 1$). The second one yields a negative value for γ_p which is a physical impossibility ($0 < \gamma_p \leq 1$).

(b) Case 2. Penalty factor, γ_p , taken as a constant

In this case $\frac{\partial H_p}{\partial \gamma_p} = 0$ and only equation (31a) remains. If γ_p is taken from Wood's curve [44] for instance, this may be substituted in

equation (31a) to yield a value for X. The left hand side of equation (31a) is plotted graphically against X in figure 6.6. The right hand side of equation (31a), for a fixed value of γ_p , is a constant and may be represented by a horizontal line in figure 6.6. The intersection of the curve with the line will give the solution for equation (31a). There may be one, two or no solution for equation (31a) depending on whether the line intersects the curve or not. If the line is tangential to the curve then there is one unique solution which may be substituted in equation (30a). So for a fixed value of γ_p there may or may not be a corresponding value for H_p . In the affirmative this solution may not yield the minimum value for H_p . So recourse should be made, as for mechanism 1, to a trial and error analysis where γ_p is made to vary between 0.1 and 1.

6.3.4 Numerical Procedure for Mechanism 2

Since for a fixed value of γ_p , equation (31a) may not have a solution or even when this exists it may not yield the lowest value for H_p then it would be appropriate to vary γ_p from 0.1 up to 1 and proceed as in the previous section (Case b). Thus for different values of γ_p , there is a series of parallel lines which may be represented in figure 6.6. The minimum value of H_p is found to occur when the maximum of the left hand side of equation (31a) is reached. This corresponds to the case where there is one unique solution for equation (31a) (line is tangential to the curve in figure 6.6). The detailed calculations are given in Appendix E. The value of X giving the maximum of the left hand side of equation (31a) is thus obtained by differentiating $X^2(1 - 2X)$ with respect to X and setting the derivative equal to zero.

$$2X - 6X^2 = 0 \implies \boxed{X = \frac{1}{3}}$$

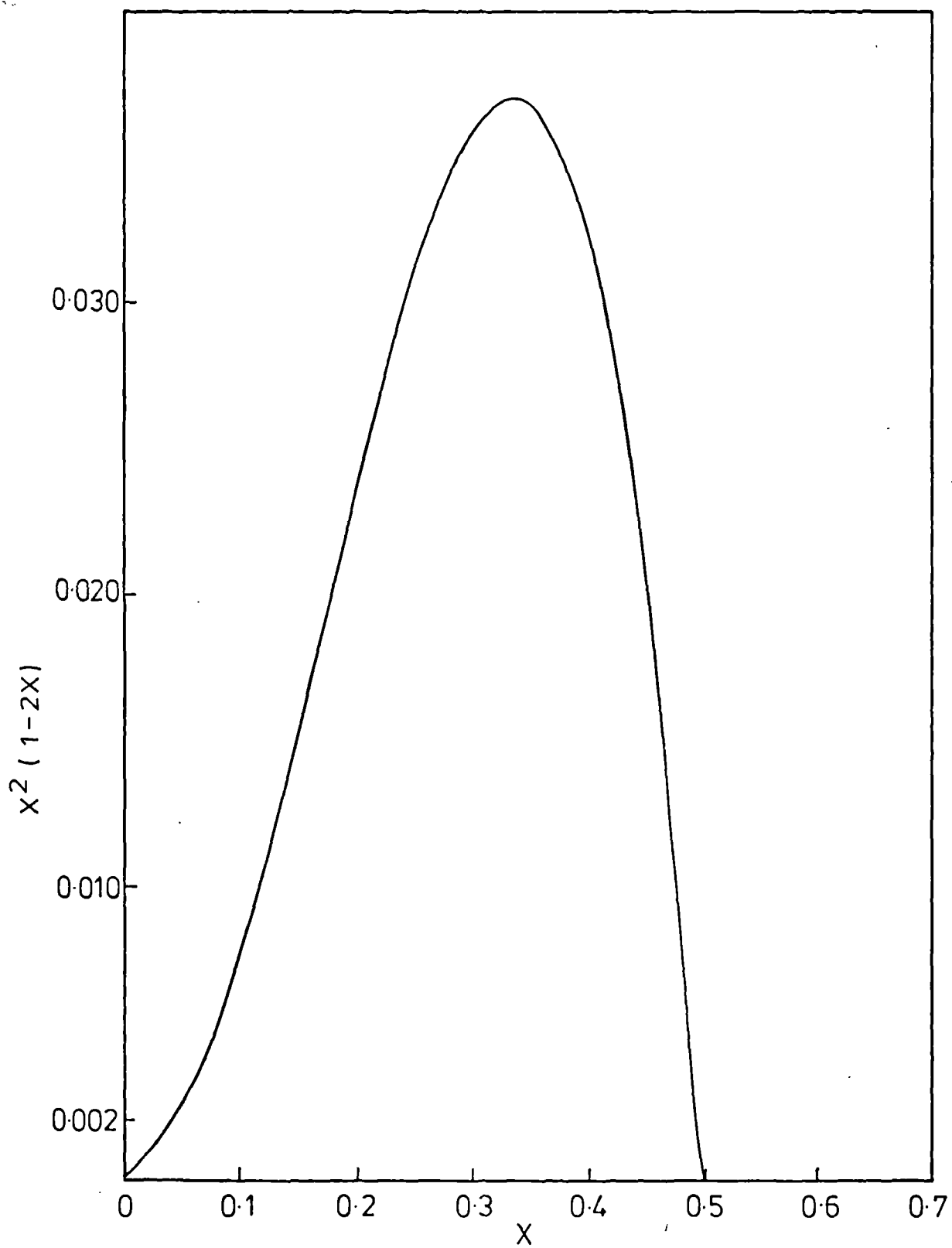


FIG.6.6 GRAPHICAL REPRESENTATION OF LEFT HAND SIDE OF EQUATION (31a)

Putting $X = \frac{1}{3}$ in equation (31a) yields

$$\gamma_p = \frac{27(M_{p2} + M_{p3} + M_{p4} + M_{p5})}{f_{ci} t l^2} \quad (33)$$

6.4 COMPARISON WITH TEST RESULTS

Substituting $a = 0.77$ and $Y = 1$ in equation (9b) and $X = 0.33$ in equation (30a) yields the predicted plastic loads for the two mechanisms. These are given by

$$H_{pa1} = \frac{0.77(M_{p1} + M_{p2}) + M_{p3} + M_{p4}}{0.77h} + 0.58\gamma_{pi1} f_{ci} t h \quad (34)$$

and

$$H_{pa2} = \frac{3(M_{p2} + M_{p3} + M_{p4} + M_{p5})}{h} + \frac{2}{9}\gamma_{pi2} f_{ci} t \frac{l^2}{h} \quad (35)$$

where

H_{pa1} and H_{pa2} are the plastic loads obtained from the numerical analysis and γ_{pi1} and γ_{pi2} the penalty factors to allow for the idealization of plasticity in the infill for mechanisms 1 and 2 respectively. The latter are given by equations (23) and (33) respectively.

$$\gamma_{pi1} = \frac{1.54M_{p1} + 3.54M_{p2} + 2M_{p3}}{0.45f_{ci} t l^2} \quad (23)$$

$$\gamma_{pi_2} = \frac{27(M_{p_2} + M_{p_3} + M_{p_4} + M_{p_5})}{f_{ci} t l^2} \quad (33)$$

The predicted plastic loads are compared to the test results in Table 6.1. From this table, it can be seen that the ratio of the plastic load obtained from experiment, H_{pe} , to the one obtained from analysis, H_{pa} , varies from 0.48 to 1.70 for mechanism 1 and from 0.48 to 0.87 for mechanism 2. But for the specimens which actually developed mechanism 1, this ratio varies from 0.48 to 1.28 and for those which developed mechanism 2, it varies from 0.56 to 0.87. From the same table, it can also be seen that for some specimens, the analysis fails to predict the plastic load for mechanism 2 because the value of the penalty factor, γ_{pa} , is outside the permissible range ($0 < \gamma_{pa} \leq 1$). The reasons for the discrepancy between the analysis and the experiment might be attributed to the following factors:

(i) The plastic analysis assumes full ultimate moments of resistance for frame members whereas in the tests most of the hinges which formed failed to develop this full capacity because of the limited ductility of reinforced concrete frames.

(ii) The strength of the joints particularly for IHM3 and ICM3 is low because of the disposition of reinforcement in the opening corners as discussed in section 4.7. This strength should be around 20% that of the adjacent members according to Taylor's tests [57] on opening corners.

(iii) The calculations of the ultimate moments of resistance, M_p , did not take into account the axial loads in frame members because these are not known a priori. This overestimates particularly the plastic

Infilled Frame Designation	◇				□				◇				□				Identified mechanism from tests	
	γ_{pa}	H_{fa} (KN)	H_{ia} (KN)	H_{pa} (KN)	H_{pe}/H_{pa}	γ_{pa}	H_{pa} (KN)	H_{pe}/H_{pa}	γ_{pa}	H_{fa} (KN)	H_{ia} (KN)	H_{pa} (KN)	H_{pe}/H_{pa}	γ_{pa}	H_{pa} (KN)	H_{pe}/H_{pa}		
IHW1	0.18	13.1	26.3	39.4	0.63	0.13	27.6	0.90	1.24	-	-	-	1.24	72.0	0.35	1		
IHW1	0.11	13.4	26.2	39.6	1.28	0.08	27.7	1.83	0.78	34.9	70.1	105.0	0.48	0.55	73.5	0.69		
IHS1	0.06	12.9	25.1	38.0	-	0.04	26.6	-	0.43	33.6	67.8	101.4	-	0.30	71.0	-		
ICM1	0.14	16.0	33.3	49.3	1.19	0.10	34.5	1.70	0.78	34.3	70.1	104.4	0.56	0.55	73.1	0.80	2	
ICM1	0.08	15.5	33.4	48.9	1.49	0.06	34.2	2.13	0.43	33.6	67.8	101.4	0.72	0.30	71.0	1.03		
ICM1**	0.08	15.5	33.4	48.9	1.70	0.06	34.2	2.43	0.43	33.6	67.8	101.4	0.82	0.30	71.0	1.17		
IHW2	0.25	18.4	36.6	55.0	0.74	0.18	38.5	1.06	1.74	-	-	-	-	1.22	-	-	1	
IHW2	0.16	18.9	38.1	57.0	-	0.11	39.9	-	1.13	-	-	-	-	0.79	106.7	-		
IHW2*	0.16	18.4	38.1	56.5	1.09	0.11	39.6	1.56	1.07	-	-	-	-	0.75	101.0	0.61		
ICM2	0.18	24.3	42.9	67.2	0.93	0.13	47.0	1.33	1.16	-	-	-	-	0.81	109.5	0.57		
ICM2*	0.18	21.0	42.9	63.9	1.28	0.13	44.7	1.83	1.07	-	-	-	-	0.75	101.0	0.81		
IHW3	0.37	27.0	54.1	81.1	0.54	0.26	56.8	0.77	2.56	-	-	-	-	1.79	-	-	1	
IHW3	0.23	26.8	54.8	81.6	0.55	0.16	57.1	0.79	1.55	-	-	-	-	1.09	-	-	1	
ICM3	0.24	28.4	57.1	85.5	0.64	0.17	59.9	0.91	1.55	-	-	-	-	1.09	-	-	2	
ICM4	0.49	52.1	129.5	181.6	0.48	0.34	127.1	0.69	4.02	-	-	-	-	2.81	-	-	1	
ICM5	0.25	35.8	59.5	95.3	0.95	0.18	66.7	1.36	0.63	34.9	69.8	104.7	0.87	0.44	73.3	1.24	2	
MECHANISM 1												MECHANISM 2				$\bar{x}_a = 0.77$	$\bar{x}_a = 0.33$	
																$\bar{y}_a = 1.00$		

- Notes: 1. ◇ taking full capacity of plastic moments 4. suffix e indicates experiment 7. H_{ia} : load carried by the infill
2. □ taking 70% of plastic moments 5. $H_{pa} = H_{fa} + H_{ia}$ 8. ▲ Failure of frame without failure of infill
3. suffix a indicates analysis 6. H_{fa} : load carried by the frame 9. - no value for $\gamma_{pa} > 1$

TABLE 6.1: COMPARISON OF PLASTIC LOAD TEST RESULTS WITH ANALYSIS

moment, M_{p1} , in the windward (tension) column.

(iv) The limited ductility of the frame was particularly pronounced for the specimen with deep beams, ICM4. Its beams remained almost straight and only minor flexural cracks occurred. This would explain why the analysis predicted such a high plastic load.

(v) The effect of workmanship is also very important as discussed in section 4.7 and has a direct influence on the strength of the infilled frame.

Thus for design purposes, the method would be reliable if the following changes are operated:

(i) The plastic moments of resistance of frame members should be taken as 70% of the calculated ultimate moments. This effectively introduces a penalty factor, γ_{pf} , to allow for the limited ductility of reinforced concrete frames.

(ii) The use of the appropriate moment of resistance of the joints.

(iii) Since the analysis assumes an idealized tapered diagonal strut, the compressive strength of the infill to be used is that appropriate to diagonal loading, f_{dci} . This may be taken as 80% of the value for vertical loading, f_{ci} (see Table 5.7).

(iv) If the value of γ_{pi2} is still greater than 1 then it would be safe to estimate the plastic load using equation (34), with γ_{pi1} obtained from equation (23).

CHAPTER 7

CONCLUSIONS

7.1 OVERALL BEHAVIOUR OF REINFORCED CONCRETE FRAMES WITH BLOCKWORK INFILLS

7.1.1 General Influence of Infill Panels

The use of even a low strength and low modulus infill material (i.e., blockwork infill) inside a reinforced concrete frame was found not only to increase both the initial racking stiffness and the strength of the open frame but also to delay the occurrence of cracks in the frame and to reduce the sidesway at peak load and at the onset of plastic collapse. For the 100 mm square section frames tested, the initial racking stiffness increased by a factor ranging from 5.9 to 14.0, the increase in strength by a factor ranging from 2.2 to 7.8 when the plastic loads are compared and by a factor ranging from 2.4 to 8.6 when the peak loads are compared. The cracking strength of the open frame increased by a factor ranging from 2.5 to 12.3. For the specimens tested the frame cracking load for the infilled frames was found to be higher than the peak load of the corresponding open frame. For the specimens subjected to racking load only the ratio of the two loads varied from 1.1 to 2.4. For the specimens subjected to combined loading this ratio varied from 1.9 to 5.5. The reduction in sidesway deflection when the plastic stage was reached ranged from 25 to 73%.

7.1.2 Load/deflection Response

The general load/deflection response of infilled frames of this type may be characterised as follows:

The response is linear elastic until the frame cracks. This is

generally accompanied by a drop in stiffness. In the meantime peripheral cracks will have occurred in the unloaded corners. For some infilled frames, however, these cracks occur at the same time as those which develop in the frame. Following the cracking of the frame, the response remains linear until the infill cracks. The cracking of the infill is accompanied by a further drop in stiffness. The response becomes slightly non-linear due to increasing amounts of cracking both in the frame and the infill until the peak load is reached. Peak load frequently represents an unstable condition and may be followed by a sudden drop in load. Provided the column strength is such that tensile failure does not occur, the load then stabilizes to yield a plastic plateau. The length of the plateau is governed by the behaviour of the frame at large deflections. For those frames in which ultimate failure was due to shear in the windward column, the length of the plastic plateau was relatively short, whereas in the frames in which flexural failure occurred there was a long plateau. For the frames tested, the ratio of the plastic load to the peak load ranged from 0.81 to 0.99.

7.1.3 Modes of Collapse

A number of different modes of failure have been identified on the basis of the behaviour of the bounding frame. Most of the infilled frame failures involved the formation of a mechanism in which flexural failure of the reinforced concrete frame occurred at various locations. In addition to these modes of failure some frames failed either in shear or due to tension in the windward column. Two plastic collapse mechanisms have been identified as representing the normal behaviour of the majority of the frames. The first is associated with the frames subjected to racking load only and the second with combined vertical

and horizontal loading. For the two mechanisms, the infill appears to behave as an idealized tapered diagonal strut with the maximum width at the windward end.

7.1.4 Comparison with Steel Frames

The response of a reinforced concrete infilled frame differs from that of a steel infilled frame for the following reasons:

- (a) Limited ductility of reinforced concrete frames.
- (b) High sensitivity of reinforced concrete frame due to tension, and to shear stress in the frame due to the exerted pressure by the infill.
- (c) Existence of a relatively better bond between the infill and the frame, thus only peripheral or boundary cracks developed in the unloaded corners instead of the neat separation described by investigators who tested steel infilled frames. There was also no evidence of slip between the frame and the infill.

7.2 PARAMETERS AFFECTING BEHAVIOUR

7.2.1 Vertical Loads on Columns

The application of vertical loads on columns results in a substantial increase in stiffness and strength and can lead to a different collapse mechanism. The effect of the vertical load is to suppress the cracking and formation of hinges in the windward column.

7.2.2 Infill Thickness

The infill thickness has a direct effect on both stiffness and strength. The thicker the infill, the stiffer and the stronger is the infilled frame. The use of a thicker infill also delays the occurrence

of cracks both in the infill and the frame.

7.2.3 Workmanship

The quality of the workmanship used in the construction of the infill walls can have a great influence on the stiffness, cracking load and strength of this type of infilled frame. This influence may be great enough to negate expected increases in strength and stiffness when thicker infill panels or stronger frames are used.

7.2.4 Frame Member Sizes and Reinforcement

The effect of amount of reinforcement in frame members may be pronounced only when the frames are used in combination with thin infill panels. A substantial increase in the strength and stiffness of either the beams or the columns may result in a considerable increase in strength. The stiffness of the infilled frame, however, depends to a large extent on the stiffness of the infill rather than that of the frame.

7.2.5 Reinforcement Detailing

The results for the two specimens without diagonal links in the opening corners show that the detailing of the reinforcement can have a significant influence on strength. This confirms the work of Taylor et al [57-59] on the importance of disposition of reinforcement on the strength of frame joints. Thus, for these two specimens the frames contributed less to the overall strength. The effect of reinforcement detailing combined with that of workmanship may produce results well outside the general trend.

7.3 METHODS OF ANALYSIS

7.3.1 Initial Racking Stiffness

For this type of structure, a conservative but reasonable method of predicting the initial racking stiffness is to treat the infilled frame as an equivalent pin-jointed frame with the infill replaced by a diagonal strut whose width is equal to $\frac{1}{15}$ of its length. The modulus of elasticity should be that relevant to diagonal loading and this may be assumed to be 80% of the value for vertical loading.

7.3.2 Cracking Strength of the Infill

The tensile and shear strength of the infill may be as above predicted respectively by Mainstone's method [20, 46] and that due to S. Smith and Carter [36]. The cracking strength would be the smaller of the two predicted values.

7.3.3 Ultimate Strength

The ultimate strength may be predicted using the proposed method based on a plastic analysis for the frame and an idealized tapered diagonal strut. The following factors are important:

(i) The plastic moments of resistance for frame members should be taken as 70% of the calculated ultimate moments. This effectively introduces a penalty factor, γ_{pf} , to allow for the limited ductility of reinforced concrete frames.

(ii) The compressive strength of the infill to be used is that appropriate to the diagonal loading. This may be taken as 80% of the value for vertical loading. The penalty factor, γ_p , introduced to allow for the idealization of plasticity in the infill, is found as part of the solution and its value is determined analytically.

7.4 FURTHER WORK

Investigations can be carried out to cover

- multistorey infilled frames
- multibay infilled frames
- infilled frames subjected to combined loading for different values of vertical loads
- infilled frames covering an important range of variation in frame member stiffnesses and strengths
- infilled frames with different infill strengths
- study of masonry failure.

APPENDIX A

SCHEDULE OF REINFORCEMENT

The details of the different arrangements of the reinforcement used are given in figures A.1 to A.4. The reinforcement details for frame type 5 have been given in figure 3.6. The changes operated in the disposition of reinforcement were necessary to ease the construction of the reinforcing cage and to avoid the problem which occurred in the windward column extension of IHM2. The fact that the reinforcing cage was not welded to the tube led to a premature failure of the frame as discussed in section 4.4.3.

Scale 1:10 Dimensions in mm

• welding

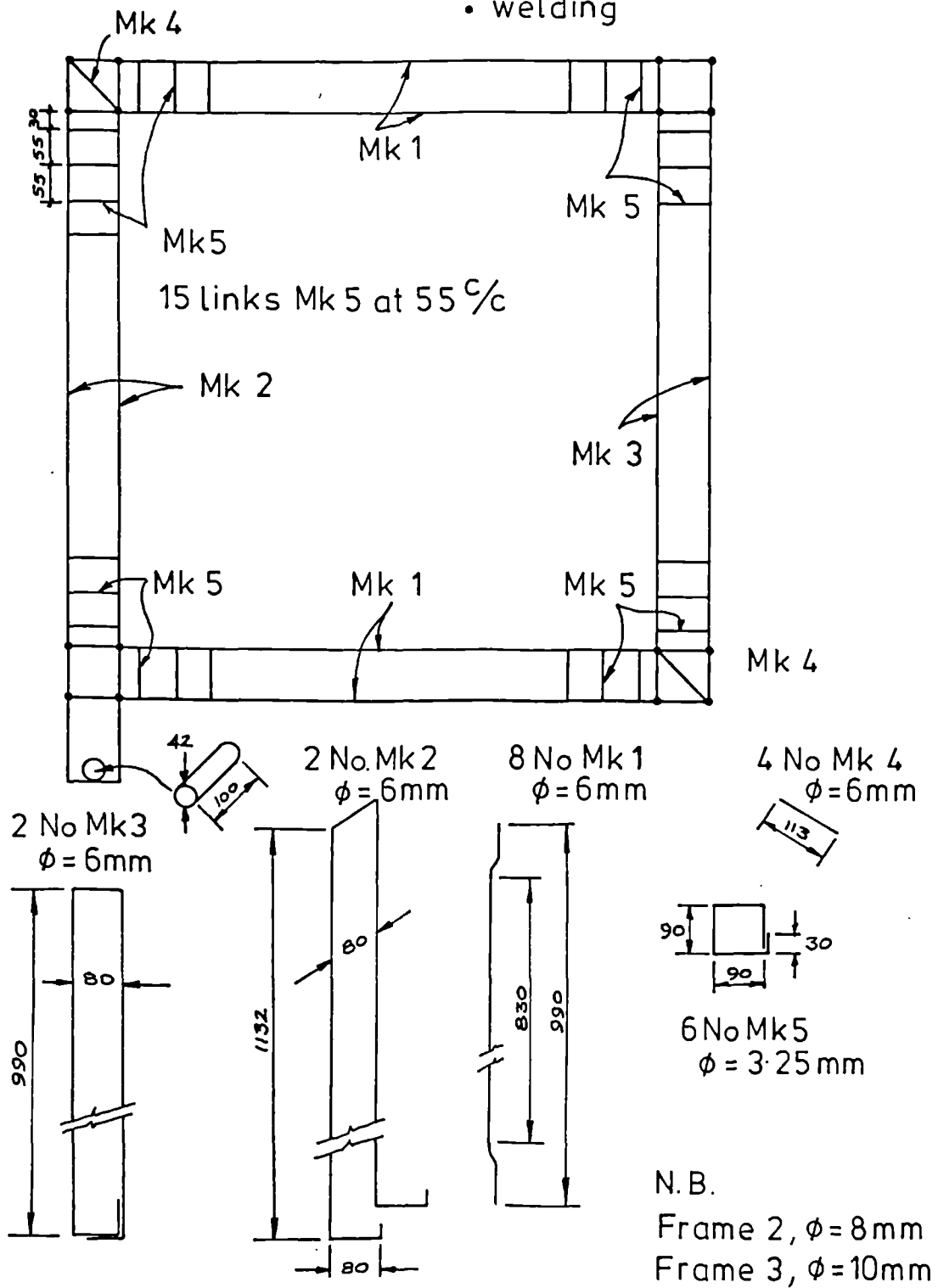
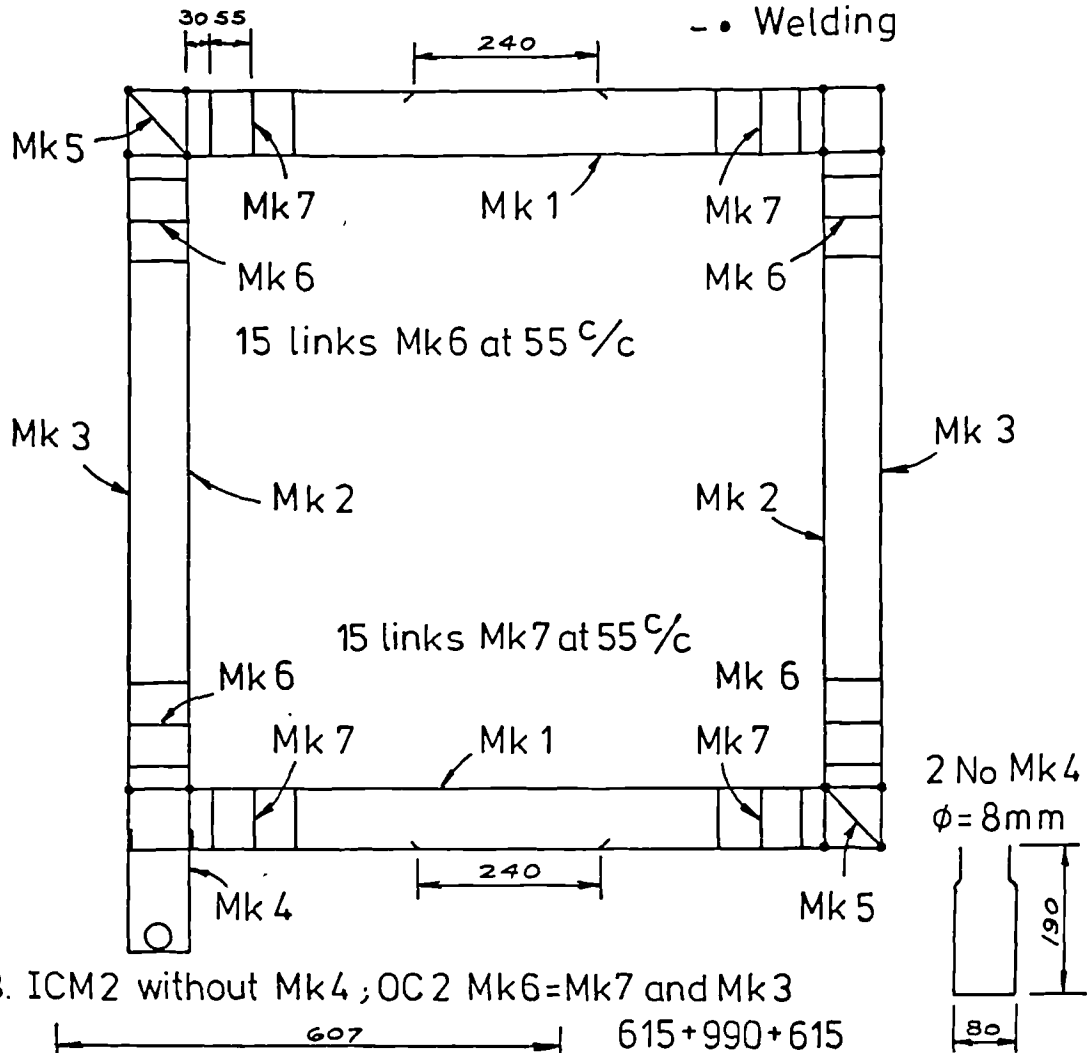


FIG.A1 REINFORCEMENT DETAILS FOR FRAMES 1,2 & 3

Scale 1:10 Dimensions in mm

- • Welding



NB. ICM2 without Mk4 ; OC 2 Mk6=Mk7 and Mk3

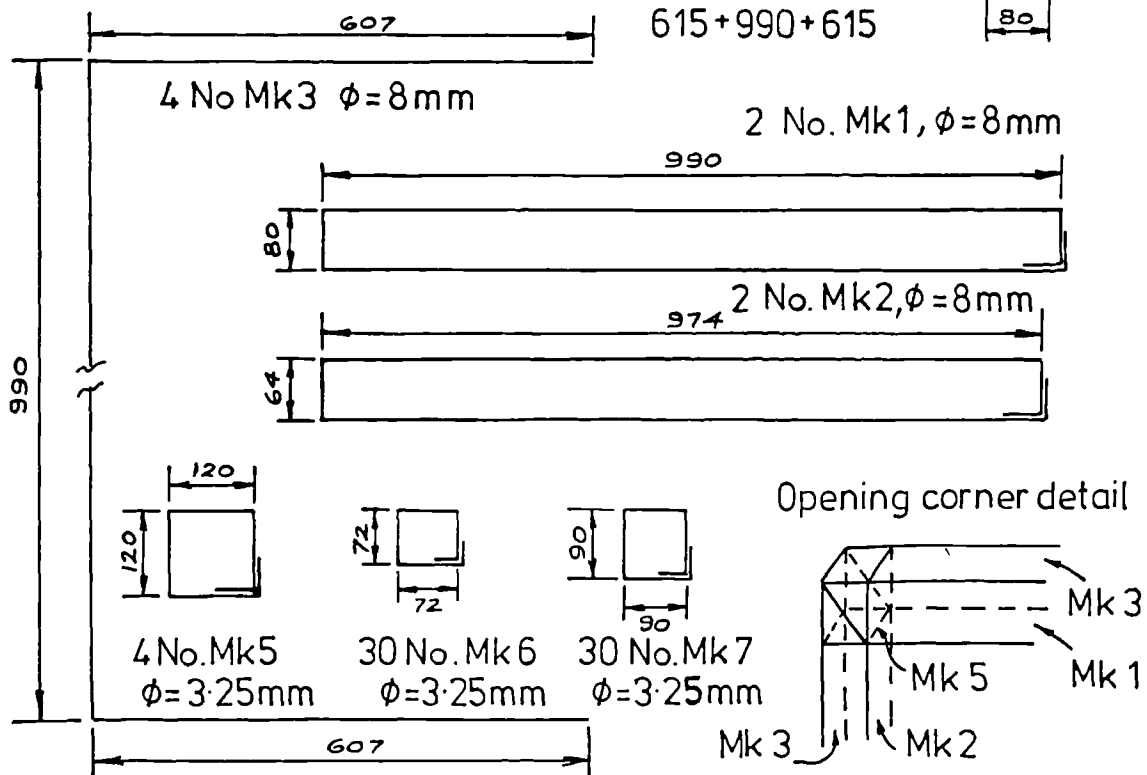
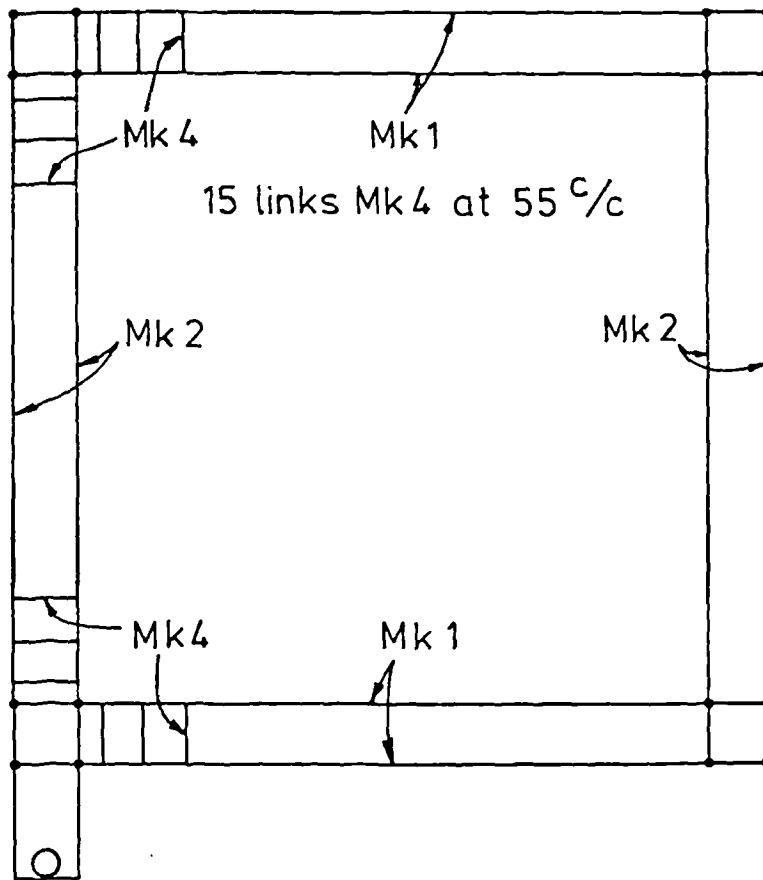


FIG.A2 REINFORCEMENT DETAILS FOR EARLY FRAMES 2

Scale 1:10 Dimensions in mm

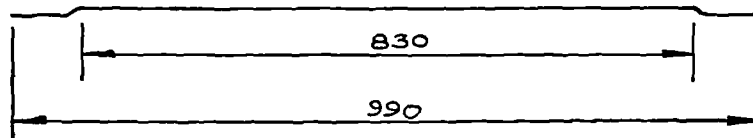
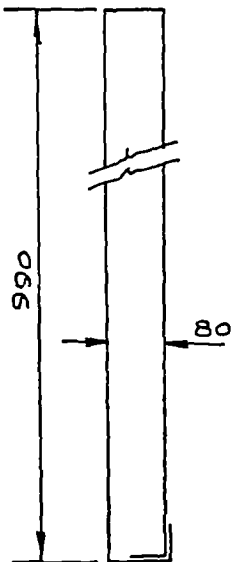
• Welding



4 No. Mk 2

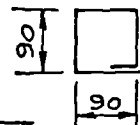
$\phi = 10\text{mm}$

8 No. Mk 1 $\phi = 10\text{mm}$



60 No. Mk 4

$\phi = 3.25\text{mm}$



Opening corner detail

2 No. Mk 3

$\phi = 10\text{mm}$

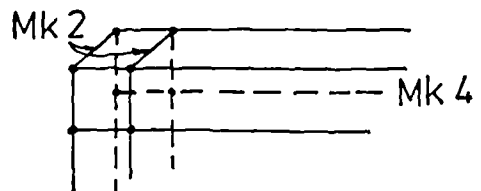
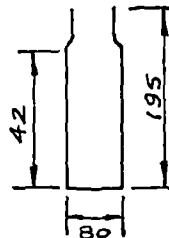


FIG.A3 REINFORCEMENT DETAILS FOR IHM3 AND ICM3

Scale 1:10 Dimensions in mm

• Welding

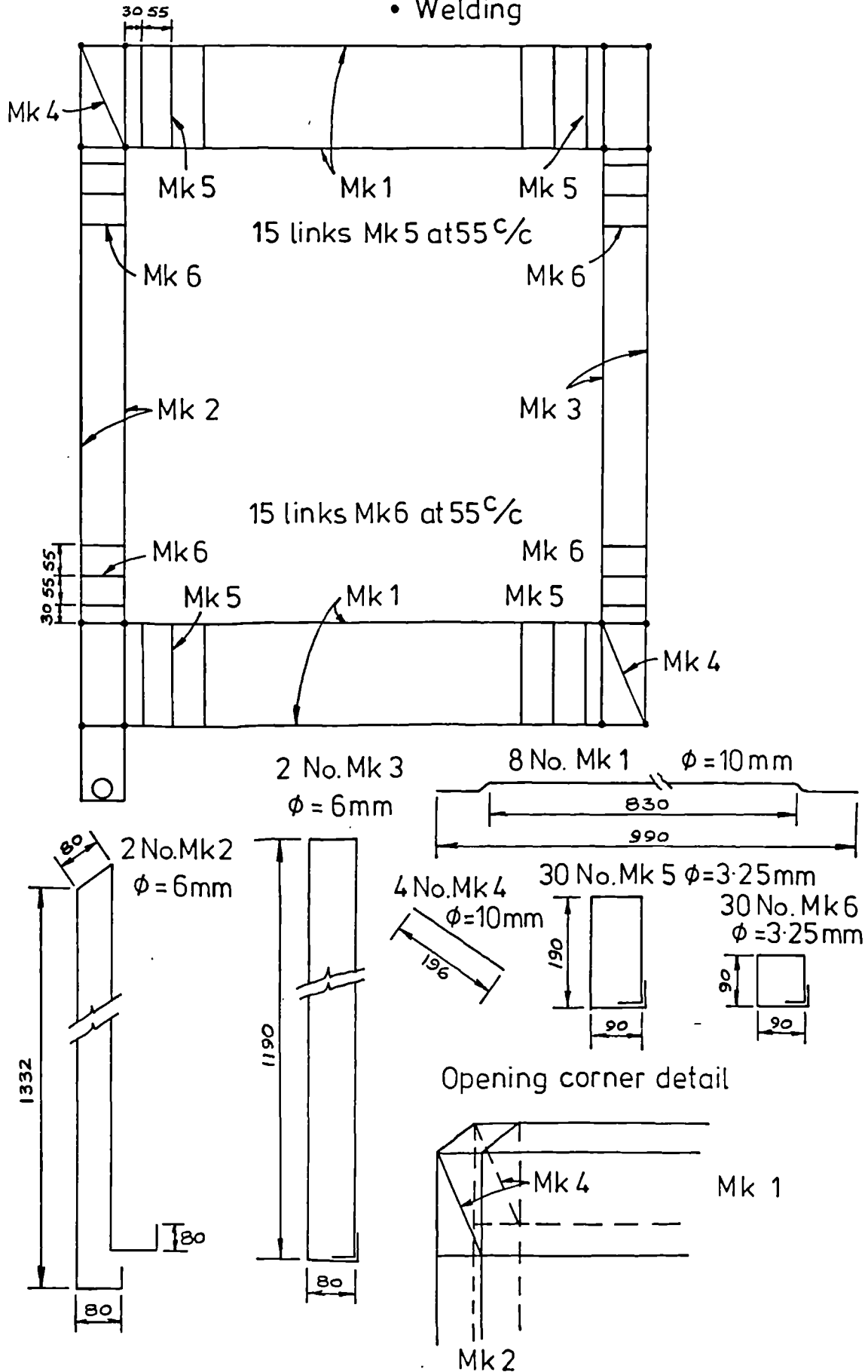


FIG. A4 REINFORCEMENT DETAILS FOR FRAME 4

APPENDIX B

ACCURACY OF READINGS

B.1 ACCURACY OF INSTRUMENTS

The accuracy of the load-cell readings has been estimated by four methods. That of the jack, the two L.V.D.T's and the electrical demec gauge by two methods. These methods are summarized below:

(1) If n is the reading in millivolt, division or microstrain and K is the calibration factor of the instrument and $S.D_c$ the standard deviation of the calibration factor then the accuracy may be expressed as

$$A = (K \pm SD_c) \times n$$

Thus each reading is given to \pm the standard deviation of the calibration factor.

(2) If the output for the same load, deflection or strain is taken n times, then the accuracy may be expressed as

$$A = K \times SD_n$$

where SD_n is the standard deviation of n readings.

(3) The data-logger output is given to the hundredth of a millivolt but for the purpose of this calculation, ΔV is taken as 0.5μ volt.

The output formula for full wheatstone bridge is

$$\Delta V = \frac{(1 + \mu)}{2} K \varepsilon E$$

where E is the input

$$\varepsilon : \text{strain} = \frac{\Delta l}{l} = \frac{\sigma}{E_s} = \frac{N}{AE_s}$$

A : area of load-cell

E_s : Young's modulus for load-cell

K : gauge factor

μ : Poisson's ratio

and N : axial load

For the two load-cells used

E = 5 volts

A = 491 mm²

K = 1.78

$E_s = 200 \text{ KN/mm}^2$

$\mu = 0.3$

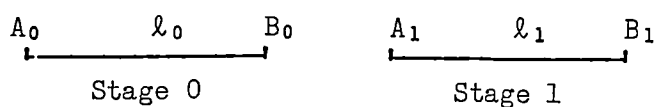
$\Delta V = 0.5 \times 10^{-6}$ volts

Thus N is given to $\pm 9N$

(4) Using the same procedure as in (3) but with ΔV equal to the standard deviation of n readings for the same load. This standard deviation was of 2μ volts for load-cell 1 and 1.2μ volts for load-cell 2. The accuracy of the readings for all the instruments used and the different calibration factors have been given in Table 3.7.

B.2 ACCURACY OF STRAIN MEASUREMENTS FROM PHOTOGRAMMETRY

The way to measure the strains using photogrammetry techniques is to compare the photographs taken at different stages of loading with that taken before the load is applied. For the specimens tested, the scale of the plates was 1 : 24.7 and each coordinate was given to ± 5 microns. Thus each length on the plate is given to $\pm 10\mu$.



The actual strain is given by

$$\epsilon_a = \frac{l_1 - l_0}{l_0} = \frac{\Delta l}{l} \quad (1)$$

The estimated strain is given by

$$\epsilon_{es} = \frac{(l_{1p} \pm 10\mu) - (l_{0p} \pm 10\mu)}{(l_{0p} \pm 10\mu)} \quad (2)$$

where l_{op} and l_{ip} are the lengths on the plate. The actual length l_0 is 100 mm and since the plate scale is 1 : 24.7 then $l_{op} = 4048\mu$.

Equation (2) can be rewritten as

$$\epsilon_{es} = \frac{(l_{ip} - l_{op}) \pm 20\mu}{l_{op} \pm 10\mu} \quad (3)$$

dividing both the numerator and the denominator by l_{op} and since

$$\frac{l_{ip} - l_{op}}{l_{op}} = \frac{l_1 - l_0}{l_0} = \epsilon_a$$

then

$$\epsilon_{es} = \frac{\epsilon_a \pm 49.4 \times 10^{-4}}{1 \pm 24.7 \times 10^{-4}} \quad (4)$$

Thus the possible values for ϵ_{es} are

$$0.99\epsilon_a + 49.3 \times 10^{-4}$$

$$0.99\epsilon_a - 49.3 \times 10^{-4}$$

$$1.00\epsilon_a + 49.5 \times 10^{-4}$$

$$1.00\epsilon_a - 49.5 \times 10^{-4}$$

Thus the strain measurements from photogrammetry are given to $\pm 4900\mu$ strain. These measurements were recorded from Carl Zeiss Iena 1818 stereocomparator using one component.

APPENDIX C

LOAD-DEFLECTION GRAPHS IN THE INITIAL STAGES AT AN ENLARGED SCALE

These load-deflection diagrams are given in figures C.1 to C.3. These large scale plots eased the calculations of the different racking stiffness values, prior to cracking of the frame, after cracking of the frame and after cracking of the infill.

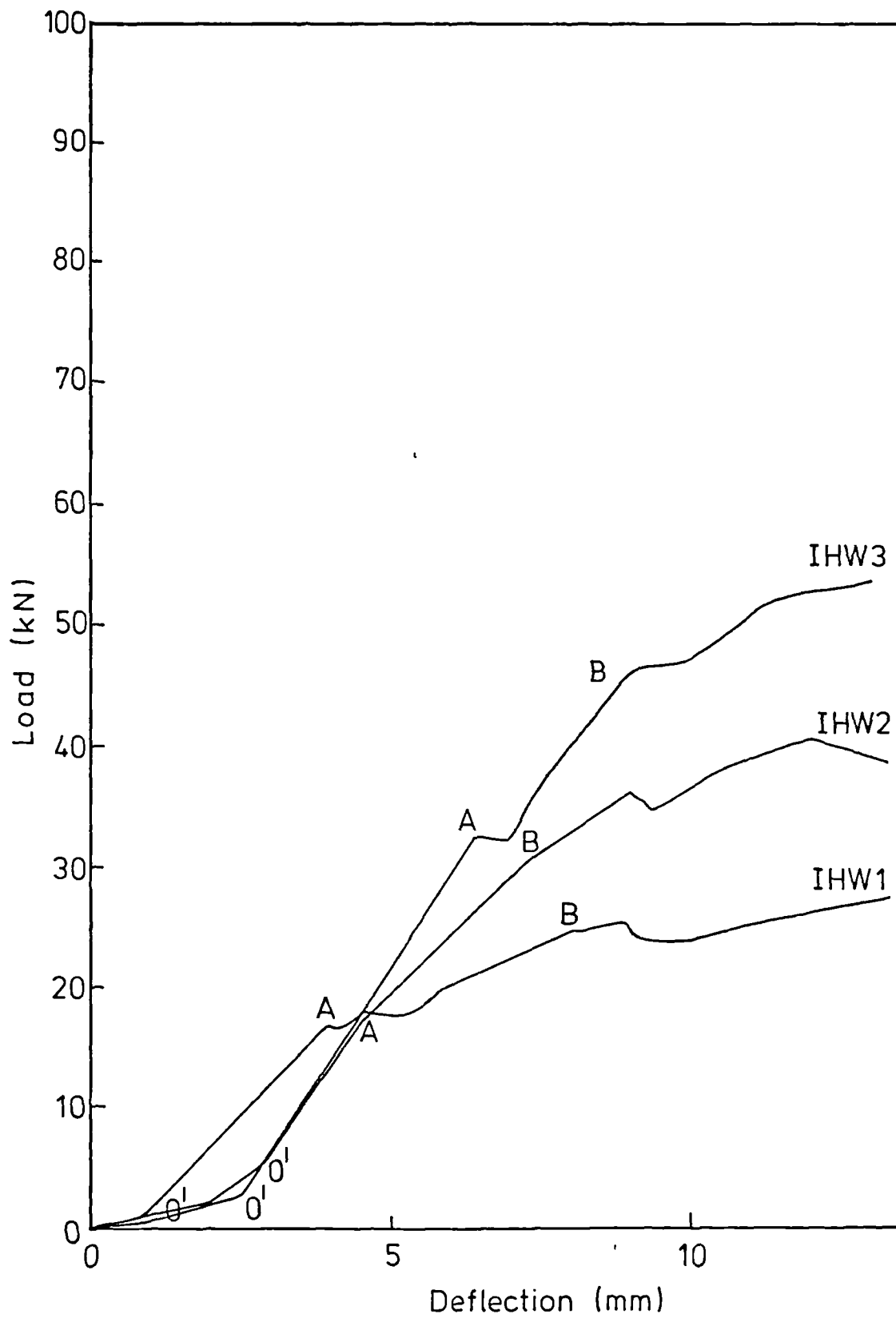


FIG.C1 LOAD - DEFLECTION DIAGRAMS FOR WEAK INFILLS AT AN ENLARGED SCALE

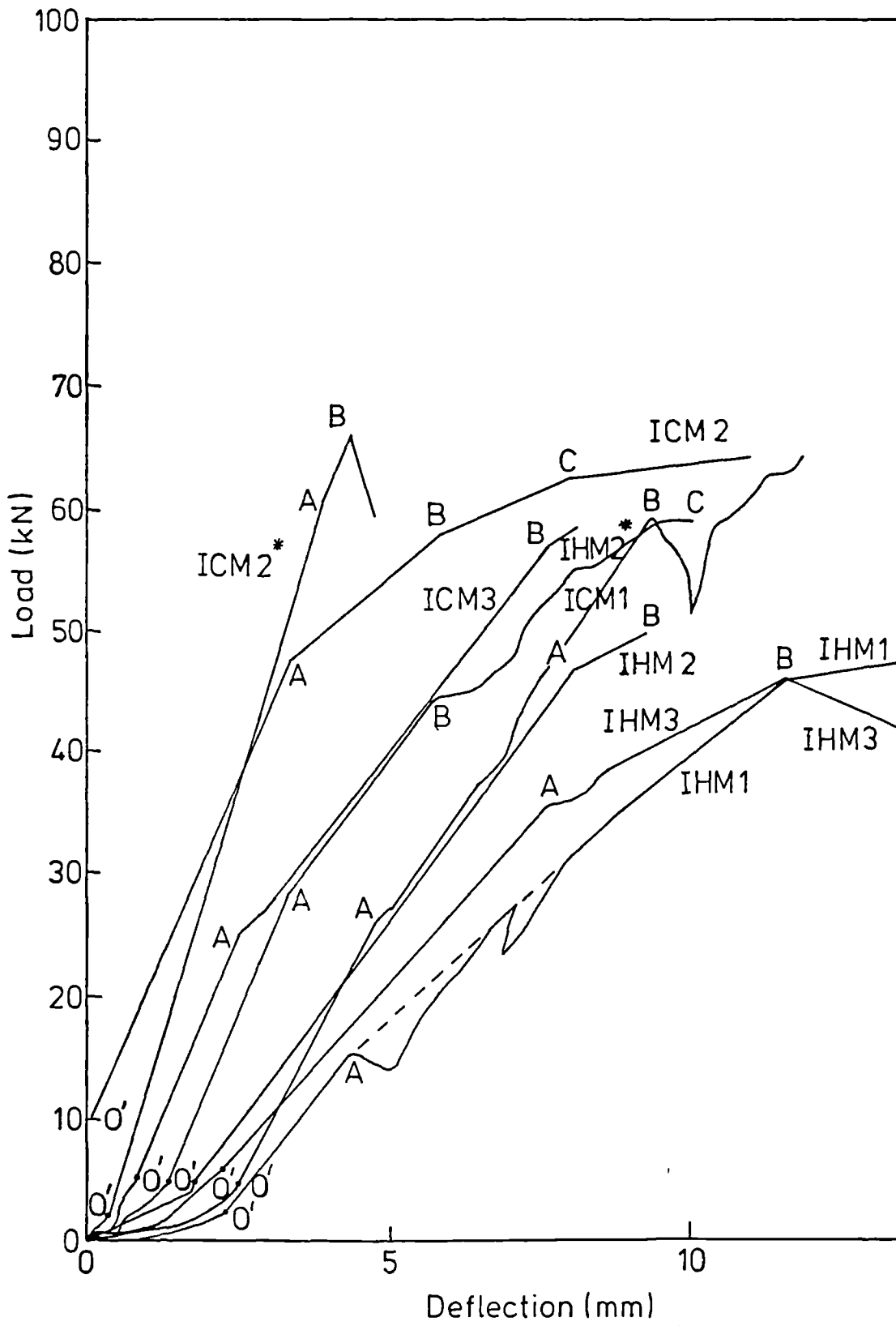


FIG.C.2 LOAD - DEFLECTION DIAGRAMS FOR MEDIUM STRENGTH INFILL AT AN ENLARGED SCALE

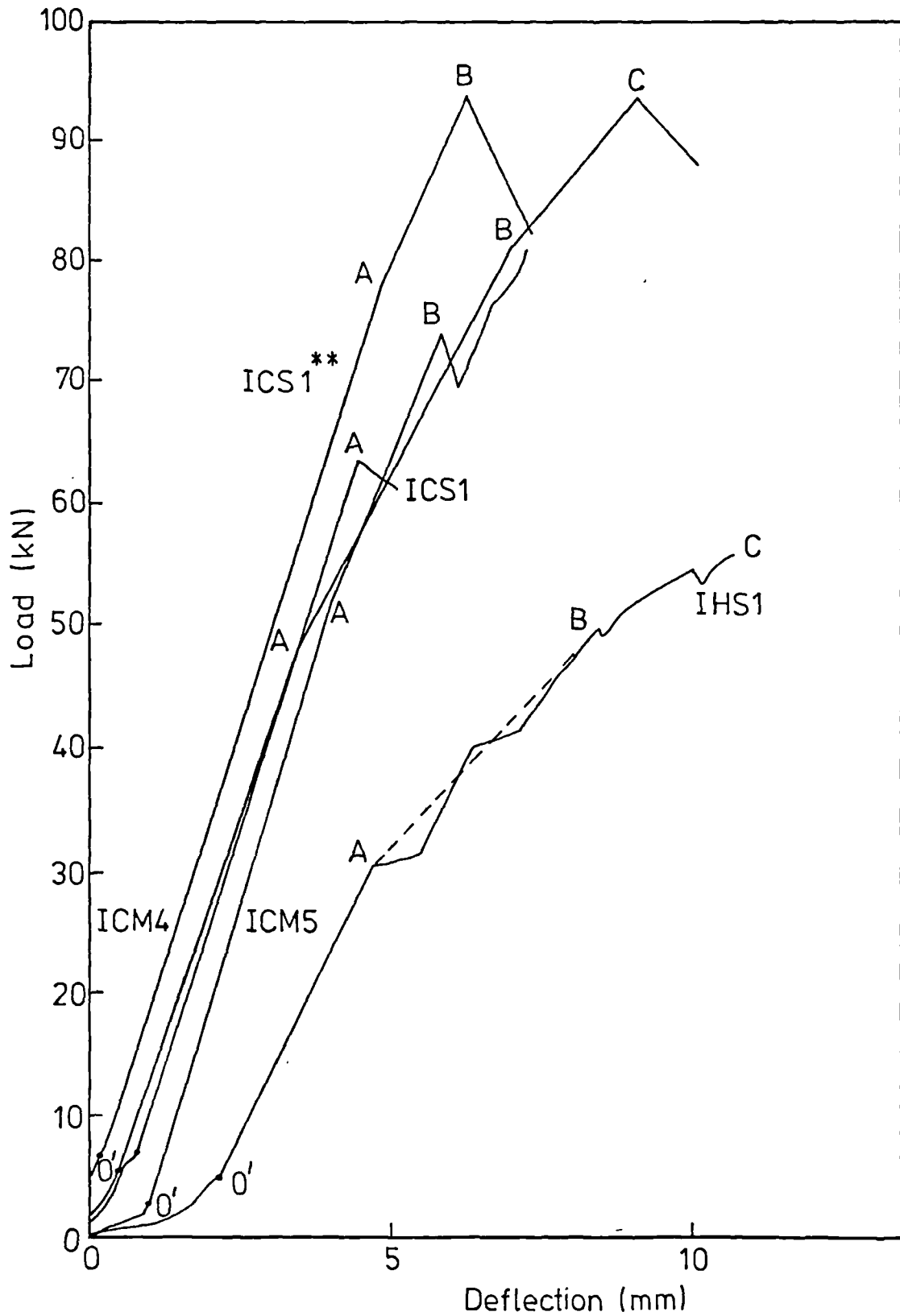
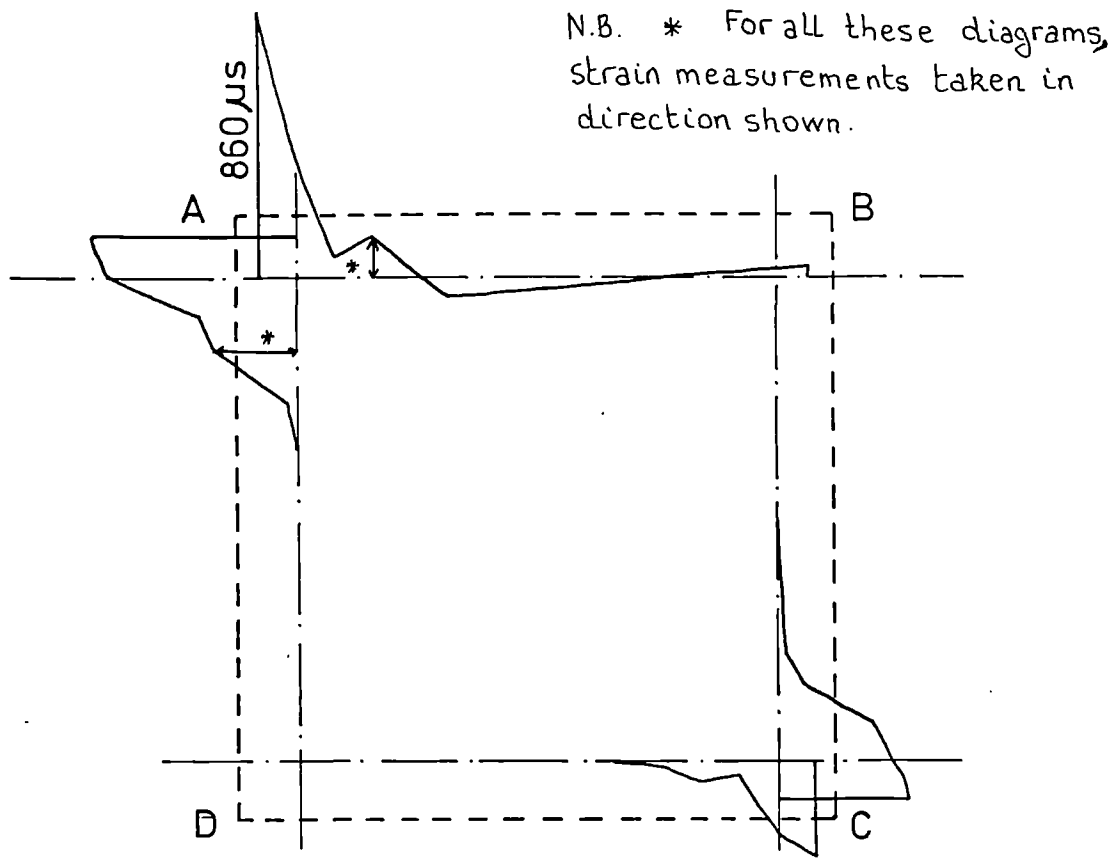


FIG.C3 LOAD-DEFLECTION DIAGRAMS FOR STRONG INFILL AND FOR FRAMES WITH DEEP BEAMS OR DEEP COLUMNS AT AN ENLARGED SCALE

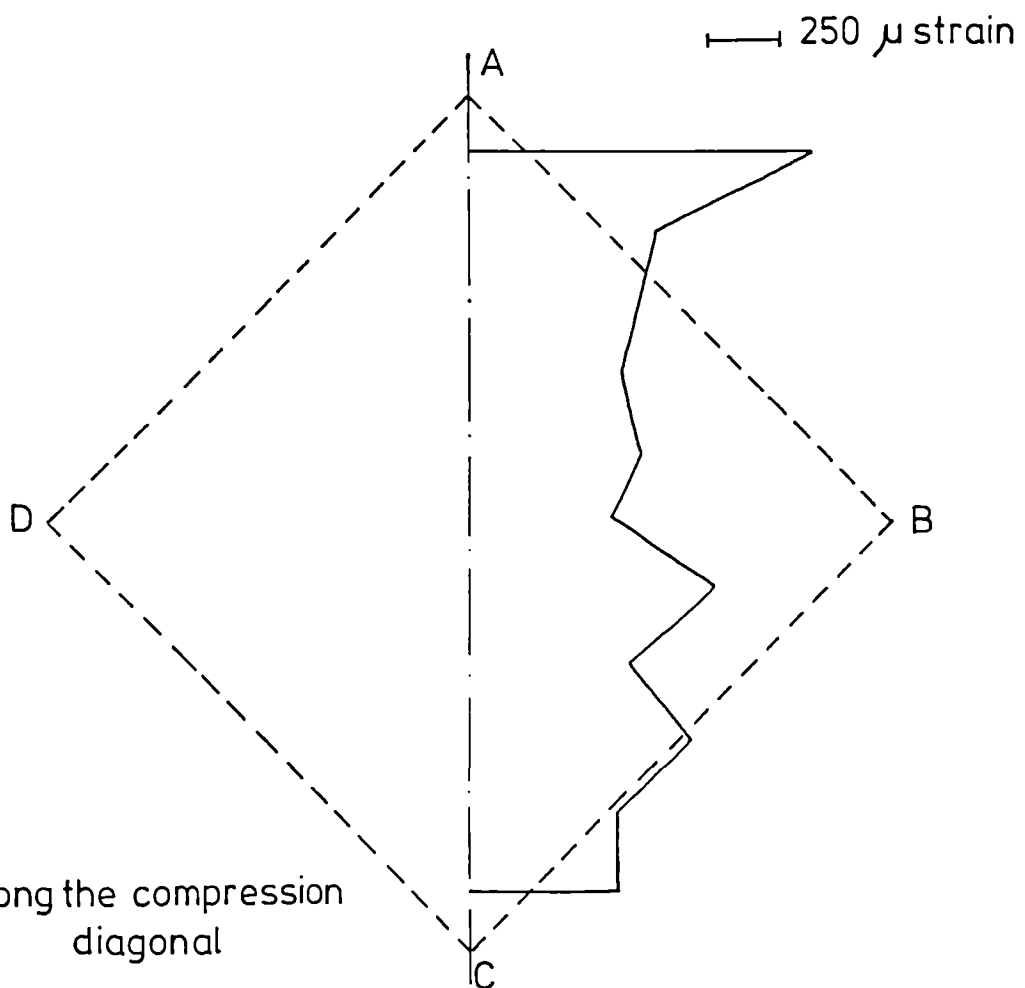
APPENDIX D

STRAIN DISTRIBUTION OVER THE INFILL

The strain distribution for the three types of infill, W, M and S used in combination with the weakest frame type 1 are given in figures D.1, D.2 and D.4. Figures D.3 and D.5 show the strain distribution over the infill after application of vertical loads.

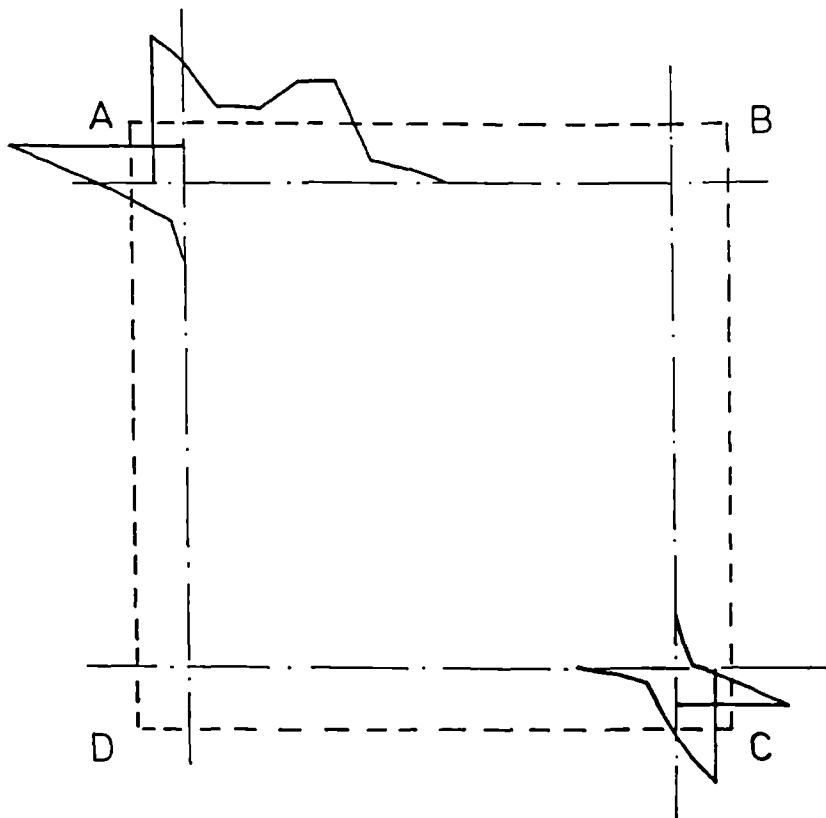


a) Along the periphery



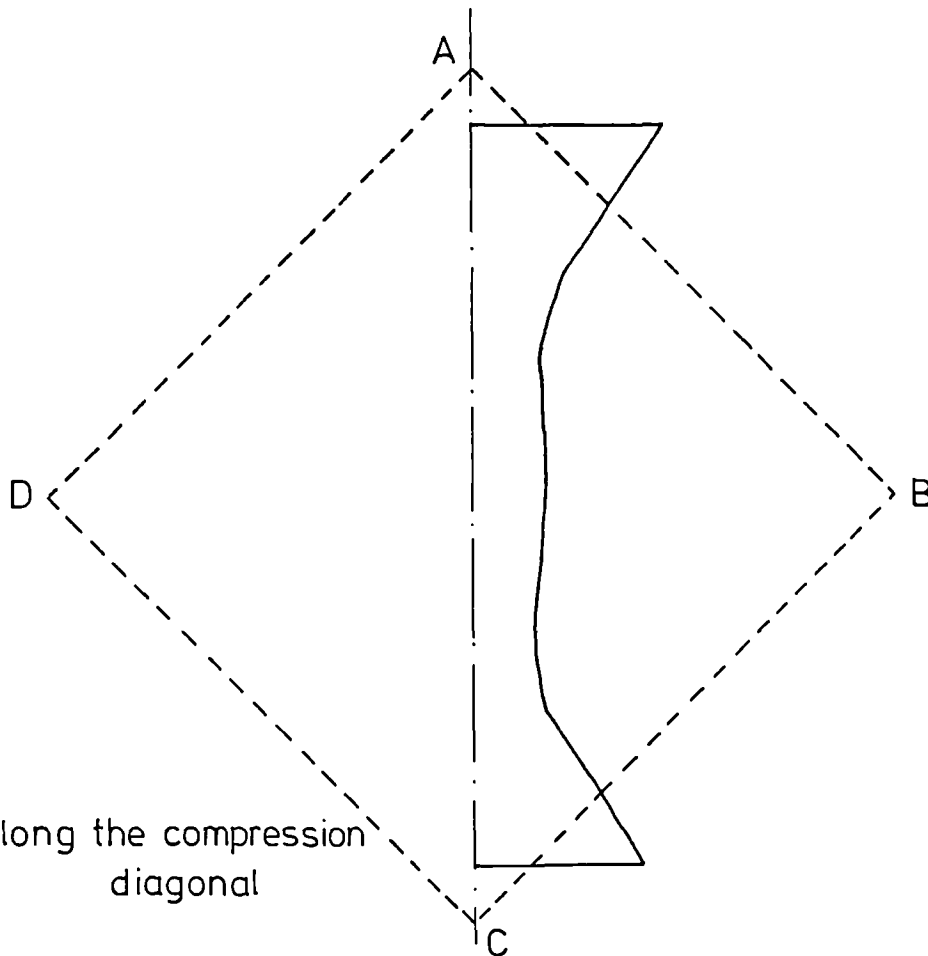
b) Along the compression diagonal

FIG.D1 STRAIN DISTRIBUTION OVER THE INFILL FOR IHW1 AT A LOAD OF 17.3 KN



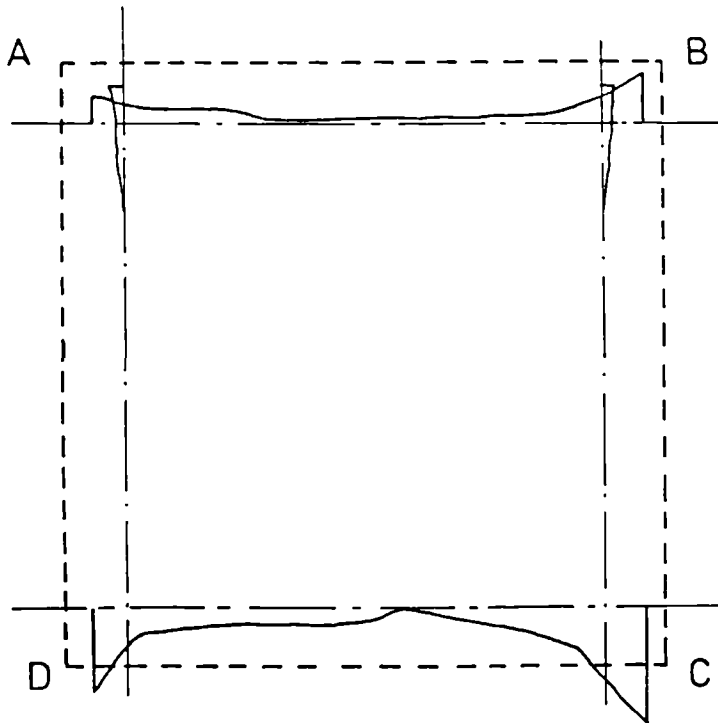
a) Along the periphery

250 μ strain



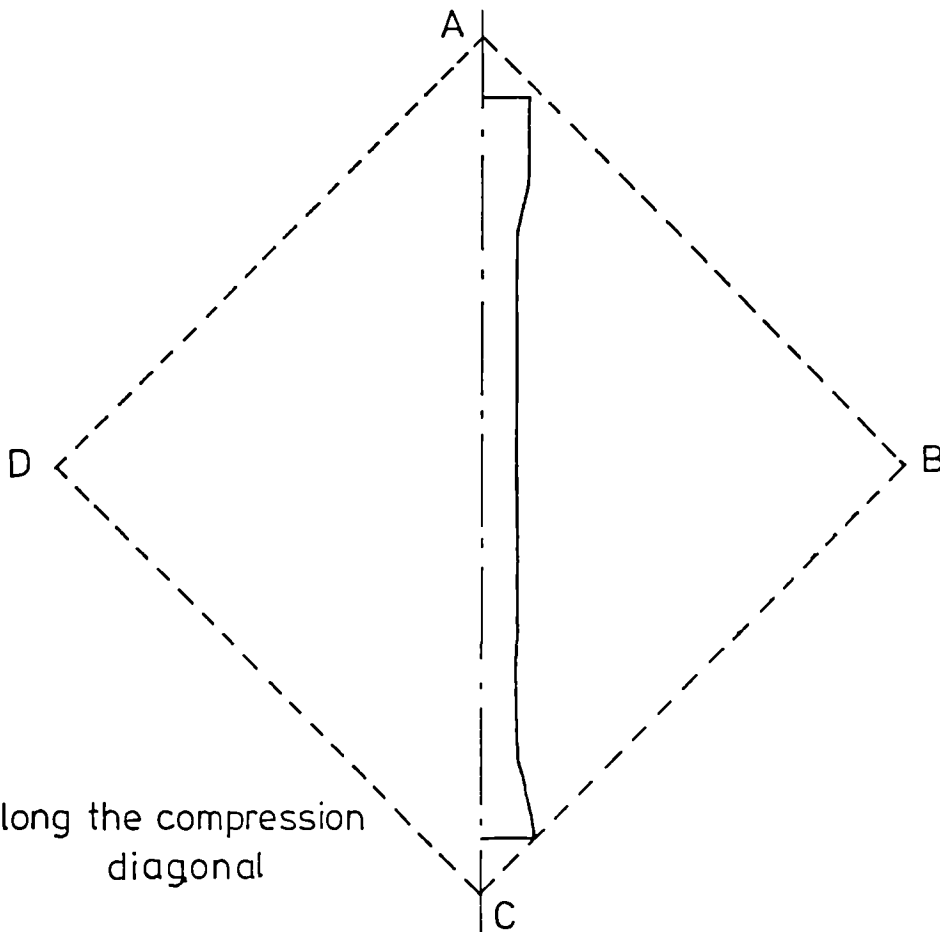
a) Along the compression diagonal

FIG.D2 STRAIN DISTRIBUTION OVER THE INFILL FOR IHM1
AT A LOAD OF 23.5 KN



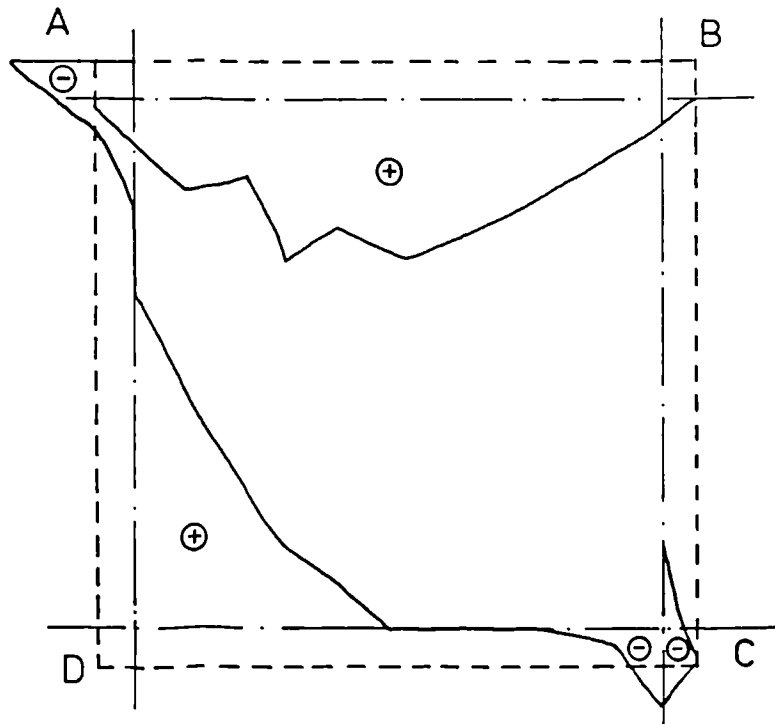
a) Along the periphery

— 250 μ strain



b) Along the compression diagonal

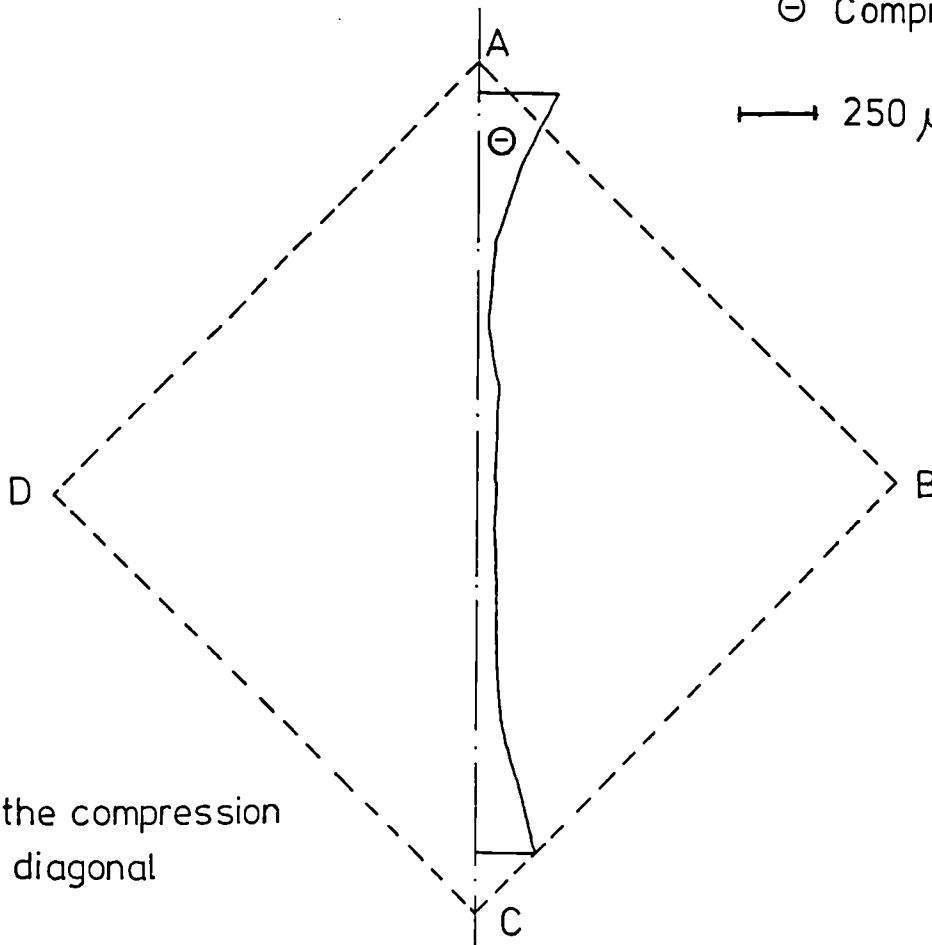
FIG.D3 STRAIN DISTRIBUTION OVER THE INFILL FOR ICM1 AFTER APPLICATION OF VERTICAL LOADS



a) Along the periphery

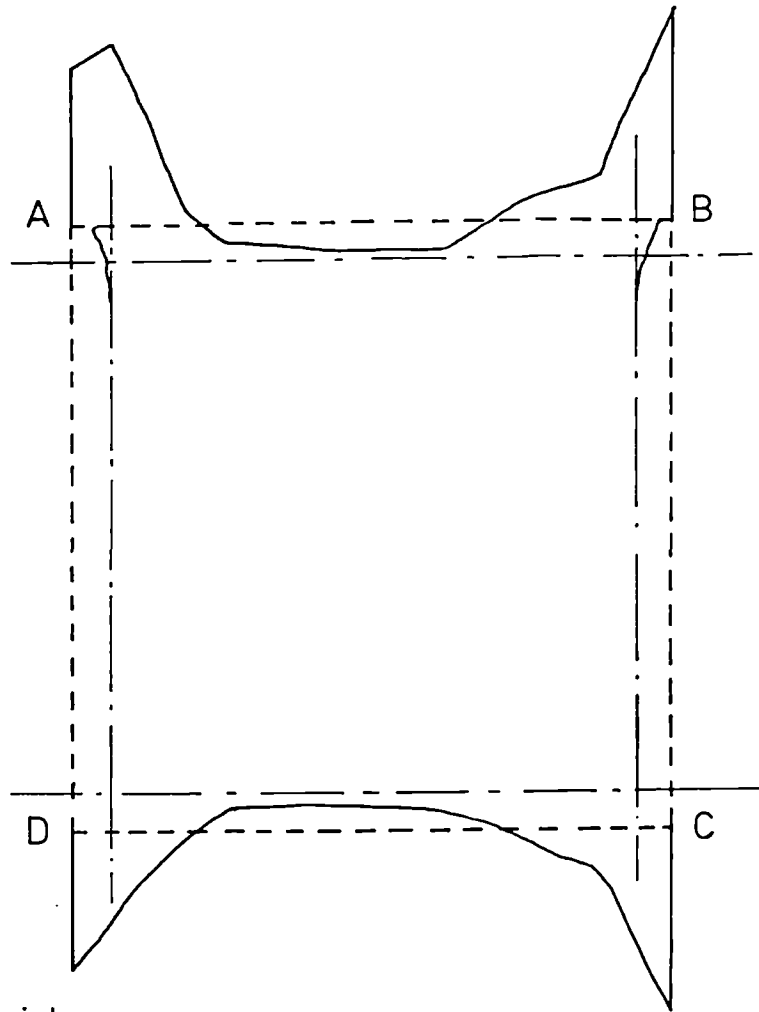
⊕ Tension
 ⊖ Compression

→ 250 μ strain

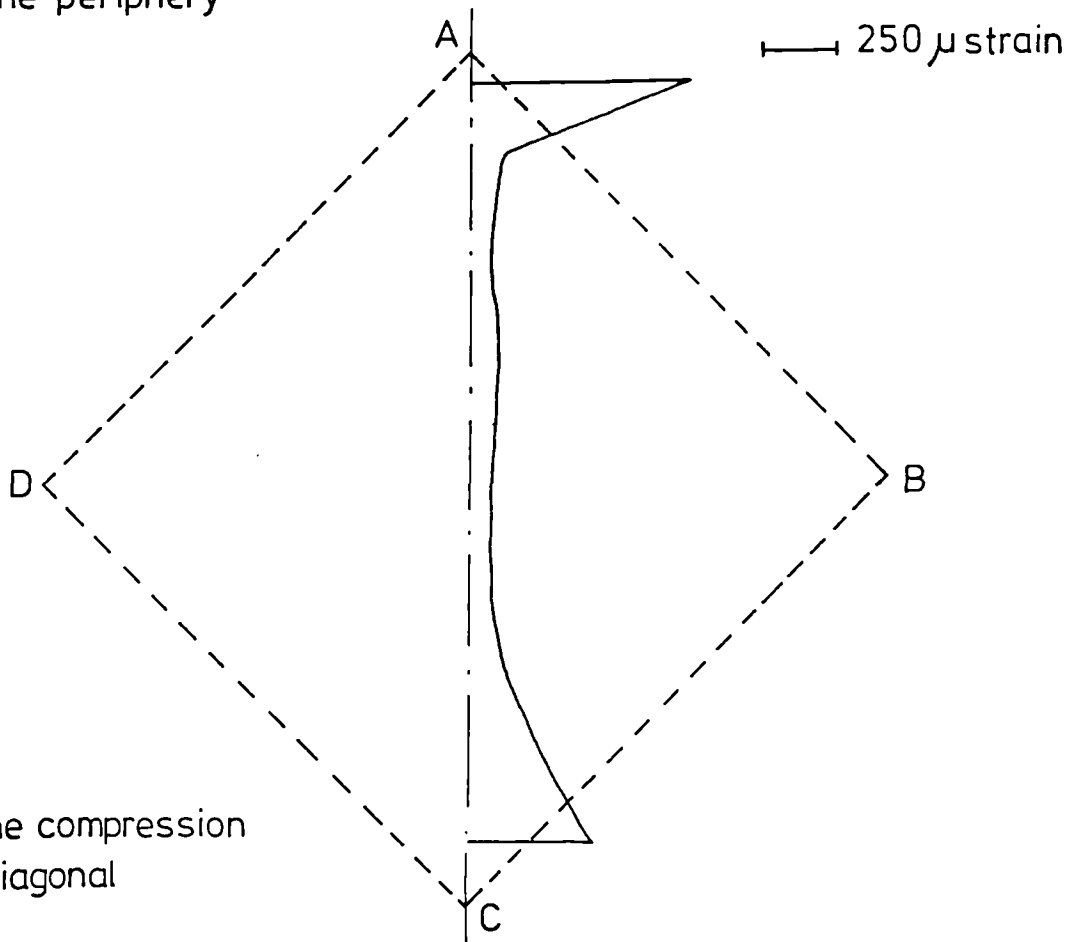


b) Along the compression diagonal

FIG. D4 STRAIN DISTRIBUTION OVER THE INFILL FOR IHS1
 AT A LOAD OF 27.1 KN



a) Along the periphery



b) Along the compression diagonal

FIG. D5 STRAIN DISTRIBUTION OVER THE INFILL FOR ICS1 AFTER APPLICATION OF VERTICAL LOADS

APPENDIX E

NUMERICAL ANALYSIS

E.1 MECHANISM 1

Table E.1 gives the detailed calculations for a specific value of $a = 1$ for a typical infilled frame, IHW1, which developed mechanism 1. This worked example is necessary to illustrate the way of proceeding.

The values for the different moments of resistance are respectively

$$M_{p1} = M_{p3} = 3.1 \text{KN.m}$$

$$M_{p2} = M_{p4} = 0.8 \times 2.6 = 2.1 \text{KN.m}$$

The values of M_{p2} and M_{p3} have been reduced by 20% because there are the moments in the opening corners. The effect of axial loads on frame members is not taken into account when estimating the plastic moments of resistance of frame members because these axial loads are not known a priori.

The compressive strength of the infill material is

$$f_{ci} = 7.8 \text{N/mm}^2 \text{ (Table 5.7)}$$

For $a = 1$ (i.e., $X = Y$), equation (11a)

$$Y^2(1 - Y) = M_{p1} + M_{p3} + 2M_{p2} / \gamma_p f_{ci} t l^2$$

The left hand side of this equation is plotted graphically in figure 6.4 and the right hand side is given in the second column of Table E.1 for different values of γ_p .

The procedure used for the case of $a = 1$ is repeated for different values of a . The results are summarized in Table E.2 and these are plotted against a in figure E.1.

γ_p	R.H.S. of Eq(11a)			For Y_1			For Y_2		
		Y_1	Y_2	H_f (KN)	H_i (KN)	H_p (KN)	H_f (KN)	H_i (KN)	H_p (KN)
0.1	0.460	-	-	-	-	-	-	-	-
0.2	0.230	-	-	-	-	-	-	-	-
0.3	0.153	-	-	-	-	-	-	-	-
0.31	0.148*	0.67	0.67	15.4	34.3	49.7	15.4	34.3	49.7
0.4	0.115	0.46	0.83	24.8	35.2	60.0	13.8	48.2	62.0
0.5	0.092	0.39	0.87	29.3	39.0	68.3	13.1	61.1	74.2
0.6	0.077	0.35	0.89	32.7	43.0	75.7	12.8	73.6	86.4
0.7	0.066	0.31	0.91	36.9	45.6	82.5	12.6	86.2	98.8
0.8	0.058	0.28	0.91	40.8	47.9	88.7	12.6	98.6	111.2
0.9	0.051	0.26	0.92	44.0	50.6	94.6	12.4	98.9	111.3
1.0	0.046	0.25	0.93	45.7	54.3	100.0	12.3	123.6	135.9

Notes: (i) Y_1 and Y_2 obtained from intersection of right hand side of Eq(11a) and curve in figure 6.4.

(ii) - The horizontal line and the curve in figure 6.4 do not intersect

(iii) * The horizontal line is tangential to the curve in figure 6.4

(iv) $H_p = H_f + H_i$ equation (9b)

TABLE E.1: H_p FOR TEST PANEL IHW1 FOR $a = 1$

a	\bar{y}	γ_p	H_f (KN)	H_i (KN)	$H_p = H_f + H_i$ (KN)
0.50	2.00	-	-	-	-
0.75	1.04	-	-	-	-
0.77	1.00	0.18	13.1	26.3	39.4
0.80	0.94	0.20	13.7	28.0	41.7
0.90	0.78	0.25	15.5	30.7	46.2
1.00	0.67	0.31	15.4	34.3	49.7
1.25	0.48	0.48	21.4	42.9	64.3
1.50	0.37	0.67	25.7	51.3	77.0
1.75	0.30	0.88	29.9	60.1	90.0
1.90	0.27	1.00	32.3	64.6	96.9
2.00	0.25	1.10	-	-	-

Note: - values outside the permissible ranges for \bar{y} and γ_p , $0 < \bar{y} \leq 1$, and $0 < \gamma_p \leq 1$

TABLE E.2: PREDICTED PLASTIC LOAD FOR TEST PANEL IHWL FOR DIFFERENT VALUES OF a

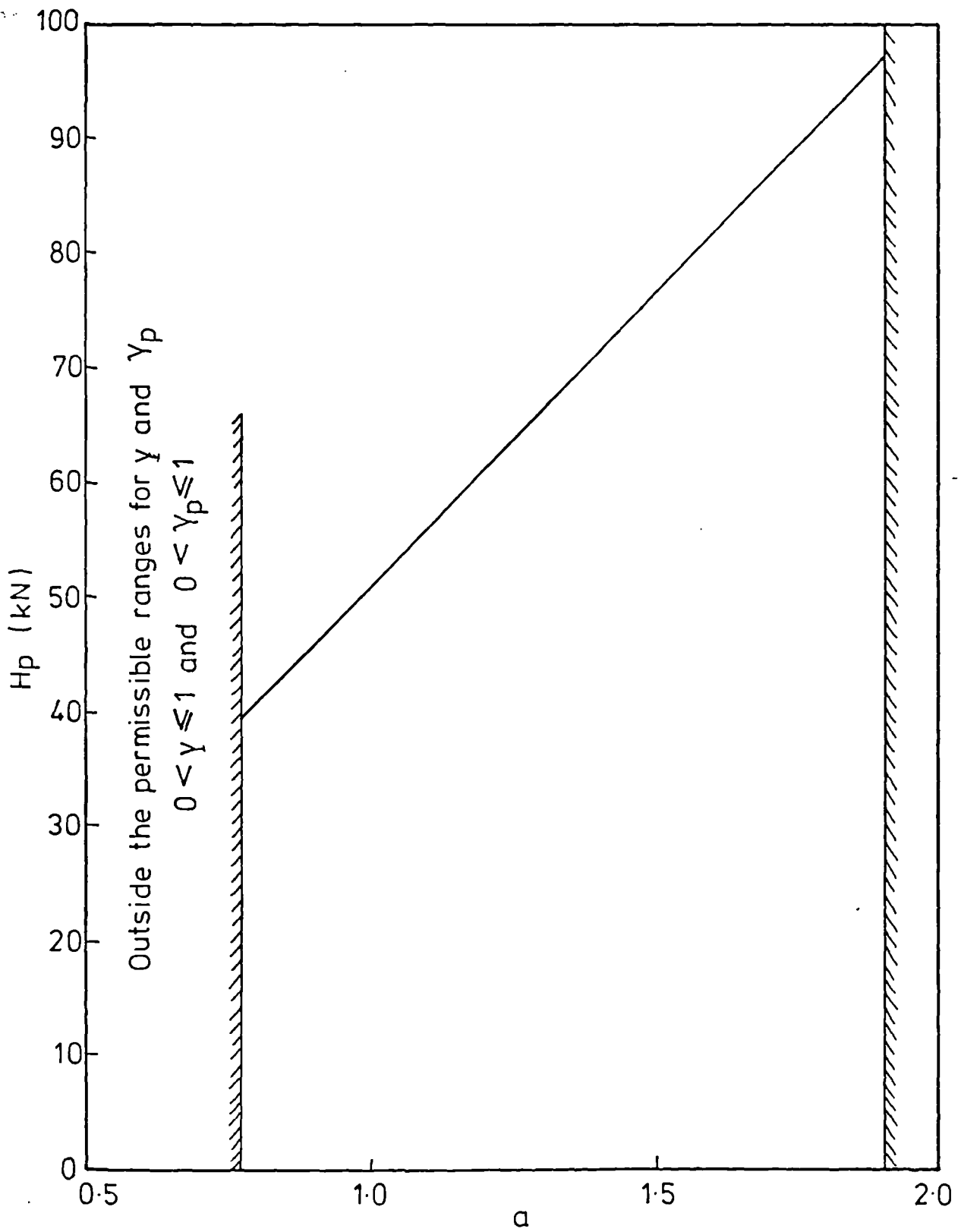


FIG.E1 PREDICTED PLASTIC LOAD FOR IHW1 FOR DIFFERENT VALUES OF a

E.2 MECHANISM 2

Table E.3 gives the detailed calculations for a typical infilled frame, ICMI, which developed mechanism 2.

γ_p	R.H.S. of Eq31(a)			For X_1			For X_2		
		X_1	X_2	H_f (KN)	H_i (KN)	H_p (KN)	H_f (KN)	H_i (KN)	H_p (KN)
0.1	0.282	-	-	-	-	-	-	-	-
0.2	0.141	-	-	-	-	-	-	-	-
0.3 [†]	0.094	-	-	-	-	-	-	-	-
0.4	0.071	-	-	-	-	-	-	-	-
0.5	0.056	-	-	-	-	-	-	-	-
0.6	0.047	-	-	-	-	-	-	-	-
0.7	0.040	-	-	-	-	-	-	-	-
0.76	0.037*	0.330	0.330	34.3	68.3	102.6	34.3	68.3	102.6
0.8	0.035	0.285	0.375	40.1	66.0	106.1	30.5	75.9	106.4
0.9	0.031	0.250	0.405	45.7	68.3	114.0	28.2	87.7	115.9
1.0	0.028	0.225	0.420	50.8	70.5	121.3	27.2	98.6	125.8

- Notes:
- (i) X_1 and X_2 obtained from intersection of R.H.S. of Equation (31a) and curve in figure 6.6
 - (ii) - The horizontal line and the curve in figure 6.6 do not intersect
 - (iii) * The horizontal line is tangential to the curve in figure 6.6
 - (iv) $H_p = H_f + H_i$ equation (30a)
 - (v) [†] For value of $\gamma_p = 0.31$ from Wood's curve [44]. There is no solution for equation (30a)

TABLE E.3: H_p FOR TEST PANEL ICMI

REFERENCES

- [1] POLYAKOV, S.V., "Masonry in Framed Buildings",
G.L. Cairns, Trans, National Lending Library for Science
and Technology, Boston Spa, Yorkshire, England, 1963.
- [2] POLYAKOV, S.V., "On the Interaction Between Masonry Filler Walls
and Enclosing Frame when Loaded in the Plane of the Wall",
Translation in earthquake engineering, E.E.R.I., San Francisco,
1960 ,pp 36-42.
- [3] THOMAS, F.G., "The Strength of Brickwork",
The Structural Engineer, pp 35-46, Feb , 53.
- [4] OCKLESTON, A.J., "Load Tests on a Three-Storey Reinforced
Concrete Building in Johannesburg",
Struc Eng, 1955, 33, Oct , pp 304-322.
- [5] COHEN, J. and OZELL, A.M., "Discussion on Paper by Benjamin and
Williams [14]",
Jnl A.C.I., V 30, pp 1409-12, 1959.
- [6] READ, J.B., "Testing to Destruction of Full Size Portal Frames",
Technical report TRA/390, Cement and Concrete Association,
August, 1965.
- [7] SIMMS, L.G., "The Behaviour of No-Fines Concrete Panels as the
Infill in Reinforced Concrete Frames",
Civ Engineer and Pub Works Review, Nov, 1967, pp 1245-1250.
- [8] COULL, A., "The Influence of Concrete Infilling on the Strength
and Stiffness of Steel Frames",
Cement and Concrete, Oct-Dec, 1966, pp 162-169.
- [9] MALLICK, S.K., BARUA, H.K. and RAO, M.B., "Behaviour of One-
Storey Reinforced Concrete Frame with Brick Masonry Infill
Under Lateral Loads",
Jnl Str Eng, V 3, No 2, July, 1975, pp 81-88.
- [10] "Discussion on Mallick et al [9]",
Jnl of Str Eng, V 3, No 2, July, 1975, pp 81-88,
Journal of Structural Engineering, V 4, No 1, April, 1976,
pp 49-61.
- [11] IRWIN, A.W. and AFSHAR, A.B., "Performance of Reinforced Concrete
Frames with Various Infills Subject to Cyclic Loading",
Proc I.C.E., Part 2, 1979, 67, June, pp 509-520.
- [12] SANEINEJAD, A., "The Behaviour of Model Infilled Frames",
M. Eng Thesis, Sheffield University, Sept, 1981.
- [13] BENJAMIN, J.R., and WILLIAMS, H.A., "The Behaviour of One-
Storey Reinforced Concrete Shear Walls",
Proc A.S.C.E., V 83, No ST3, 1957, Paper 1254, 49pp .
- [14] BENJAMIN, J.R., and WILLIAMS, H.A., "The Behaviour of One-
Storey Brick Shear Walls",
Proc A.S.C.E., V 84, ST4, 1958, Paper 1723, 29pp .

- [15] HOLMES, M., "Steel Frames with Brickwork and Concrete Infilling",
Proc of I.C.E., August, 1961, V 19, pp 473-478.
- [16] WOOD, R.H., "The Stability of Tall Buildings",
Proc I.C.E., V 11, pp 69-102, 1958.
- [17] HOLMES, M., "Combined Loading on Infilled Frames",
Proc I.C.E., May, 1963, V 25, pp 31-38.
- [18] FIORATO, A.E., et al, "An Investigation of the Interaction of
Reinforced Concrete Frames with Masonry Filled Walls",
University of Illinois, Nov, 1970.
- [19] MAINSTONE, R.J. and WEEKS, G.A., "The Influence of a Bounding
Frame on the Racking Stiffnesses and Strengths of Brick
Walls",
Proc 2nd Int brick masonry conf, Stoke-on-Trent, April, 1970,
pp 165-171, also BRS current paper CP3/72.
- [20] MAINSTONE, R.J., "On the Stiffnesses and Strengths of Infilled
Frames",
Proc I.C.E., Supplement IV, paper 73605, 1971, pp 57-90.
- [21] MAINSTONE, R.J., "Supplementary Note on the Stiffnesses and
Strengths of Infilled Frames",
Current paper 13/74, Feb, 74, BRE.
- [22] KADIR, M.R.A., "The Structural Behaviour of Masonry Infill
Panels in Frame Structures",
PhD Thesis, Edinburgh University, 1974.
- [23] KADIR, M.R.A. and HENDRY, A.W., "The Behaviour of Brickwork
Infilled Frames Under Racking Load",
Proc 5th Int Symp load bearing brickwork British Ceramic
Research Association, London, 1975, No 24, Sept, 1975,
pp 65-77.
- [24] HENDRY, A.W. "Structural Brickwork",
London, MacMillan, 1981.
- [25] SEDDON, A.E., "The Strength of Concrete Walls Under Axial and
Eccentric loads",
Sym Strength Conc Strc, Session D, paper No 1, 1956 .
- [26] SIMMS, L.G. and WOOD, R.H., "A Tentative Design Method for
the Composite Action of Heavily Loaded Brick Panel Walls
Supported on R.C. Beams",
BRS, CP26/69, Building Research Station, Watford, Herts,
1969.
- [27] MALLICK, S.K., and BARUA, H.K., "Behaviour of Single Storey
Reinforced Concrete Frame Infilled with Brickwork Under
Lateral Loads",
Proc of the 6th World Conf on Earthquake engineering,
New Delhi, Jan, 1977.

- [28] SACHANSKI, S , "Analysis of the Earthquake Resistance of Frame Buildings Taking into Consideration the Carrying Capacity of the Filling Masonry",
Proc 2nd World Conf in Earthquake engineering, Tokyo, 1960, 3, pp 2127-2141.
- [29] MALLICK, S.K., and BARUA, H.K., "Behaviour of Mortar Infilled Steel Frames Under Lateral Load",
Building and Environment, V 12, Pergamon Press, 1977, pp 263-272.
- [30] STAFFORD SMITH, B., "Lateral Stiffness and Strength of Infilled Frames",
J.S.D., ASCE, 88, ST6 , 1962, pp 183-199.
- [31] STAFFORD SMITH, B., "Behaviour of Square Infilled Frames",
J.S.D. ASCE, 92, ST1 1966 ,pp 381-403.
- [32] STAFFORD SMITH, B., "Methods of Predicting the Lateral Stiffness and Strength of Multi-Storey Infilled Frames",
Building Science, V 2, pp 247-257 , 1967 .
- [33] STAFFORD SMITH, B., and CARTER, C., "On the Structural Behaviour of Masonry Infilled Frames Subjected to Racking Loads",
Int conf str masonry systems, Austin, Texas, University of Texas at Austin, 1967, ed JOHNSON, F.B., Gulf, Houston, Texas, 1969, pp 226-233.
- [34] SIMMS, L.G., "The Shear Strength of Some Storey-Height Brickwork and Blockwork Walls",
Technical note, C.P.T.B., 1964.
- [35] STAFFORD SMITH, B., "Model Test Results of Vertical and Horizontal Loading of Infilled Frames",
Jnl ACI, pp 618-624, Aug, 1968.
- [36] STAFFORD SMITH, B., and CARTER, C., "A Method of Analysis for Infilled Frames",
Proc I.C.E., V 44, pp 31-49, Sep, 1969.
- [37] STAFFORD SMITH, B., and RIDDINGTON, J.R., "Analysis of Infilled Frames Subject to Racking with Design Recommendations",
The Struc Engineer, June, 1977, No 6, V 55.
- [38] STAFFORD SMITH, B., and RIDDINGTON, J.R., "The Design of Masonry Infilled Steel Frames for Bracing Structures",
The Structural Engineer, March, 1978, No 1, V 56B, pp 1-6.
- [39] MALLICK, D.V., and SEVERN, R.T., "The Behaviour of Infilled Frames Under Static Loading",
Proc of I.C.E., Dec, 1967, V 38, pp 639-656.
- [40] LIAUW, T.C., "Elastic Behaviour of Infilled Frames",
Proc I.C.E., 46 , 1970, 343-349.
- [41] LIAUW, T.C., "An Approximate Method of Analysis for Infilled Frames With and Without Openings",
Building Science, 7, 1972 , pp 233-238.

- [42] LIAUW, T.C., "Stress Analysis for Panel of Infilled Frames",
Building Science, V 8, pp 105-112, Pergamon Press, 1973.
- [43] LIAUW, T.C., and KWAN, K.H., "Plastic Theory of Non-Integral
Infilled Frames",
Paper 8635, proc I.C.E., Part 2, 1983, 75, Sept, pp 379-396.
- [44] WOOD, R.H., "Plasticity, Composite Action and Collapse Design
of Unreinforced Shear Wall Panels in Frames",
Proc Instit. Civ. Eng., Part 2, 1978, 65, June, pp 381-411.
- [45] NIELSEN, M.P., "On the Strength of Reinforced Concrete Discs",
Acta Polytechnic Second Series, 70, Copenhagen, 1971,
Bulletin 2.
- [46] "Discussion on WOOD'S Paper [44]
Proc I.C.E., Part 2, 1979, 67, Mar, pp 237-245.
- [47] SIMS, P.A.C., "Plastic Analysis of Reinforced Concrete Panels
in Frames",
I.A.S.B.E., Colloquium Copenhagen, 1979, pp 95-102.
- [48] MAY, I.M., "Determination of Collapse Loads for Unreinforced
Panels With and Without Openings",
Proc I.C.E., Part 2, 1981, 71, Mar, pp 215-233.
- [49] MAY, I.M. and MA, S.Y.A., "Collapse Loads for Unreinforced Panels
With Weak Joints",
Int Jnl of Masonry Construction, V 2, No 3, 1982, pp 109-114.
- [50] HENDRY, A.W. and MURTHY, C.K., "Comparative Tests on $\frac{1}{3}$ and
 $\frac{1}{6}$ Scale Model Brickwork, Piers and Walls",
Proc B.C.Soc, 4, 1965, pp 45-66.
- [51] ROSTAMPOUR, M., "Aspects of the Design of the Multi-Storey
Buildings in Lightweight Concrete Blockwork",
PhD Thesis, University of Edinburgh, 1973.
- [52] BS 12: 1978 "Specification for Ordinary and Rapid-Hardening
Portland Cement".
- [53] BS 882: Part 2: 1973 "Aggregates from Natural Sources for
Concrete".
- [54] BS 1881: 1970
Part 1: "Methods of Sampling Fresh Concrete",
Part 2: "Methods of Testing Fresh Concrete",
Part 3: "Methods of Making and Curing Test Specimens",
Part 4: "Methods of Testing Concrete for Strength",
Part 5: "Methods of Testing Hardened Concrete for Other
than Strength".
- [55] BS 4461: 1978 "Specification for Cold Worked Steel Bars for
the Reinforcement of Concrete".
- [56] BS 18: Part 2: 1971 "Methods for Tensile Testing of Metals".

- [57] TAYLOR, H.P.J. and BALINT, P.S., "Reinforcement Detailing of Frame Corner Joints with Particular Reference to Opening Corners",
Technical report 42.462, Feb, 1972, Cement and Concrete Ass.
- [58] TAYLOR, H.P.J. and SOMERVILLE, G., "The Influence of Reinforcement Detailing on the Strength of Concrete Structures",
The Structural Engineer, Jan, 1972, No 1, V 50, pp 7-19.
- [59] TAYLOR, H.P.J. and CLARKE, J.L., "Some Detailing Problems in Concrete Frame Structures",
The Structural Engineer, Jan, 1976, No 1, V 54, pp 19-32.
- [60] DAVIES, J.M., "The Design of Multi-Storey Buildings Stiffened by Diaphragm Action",
University of Salford, Dept of Civ Eng, Report Ref 77/95, Aug, 1978.
A state of the art report prepared for committee 11 of the European convention for constructional steelwork.
- [61] BS 5628: Part 1: 1978, "Code of Practice for the Structural Use of Unreinforced Masonry".
- [62] Lytag Concrete Block Manual
Part 1: Sep, 1979: Thermal Block Range,
Part 2: Sep, 1979: Basic Design Data,
Part 3: May, 1979: Thermal and Structural Design.
- [63] BS 4551: Part 1: 1970, "Methods of Testing Mortars".
- [64] BS 890: 1972, "Building Limes".
- [65] BS 1200: 1976, "Sands for Mortar for Plain and Reinforced Brickwork, Blockwalling and Masonry".
- [66] BS 2028, 1364: 1968, "Precast Concrete Blocks".
- [67] BS 1142: Part 3: 1972, "Insulating Board".
- [68] HAMID, A.A. and DRYSDALE, R.G., "Behaviour of Concrete Block Masonry Under Axial Compression",
A.C.I. Jnl, June, 1979, 76, No 6, pp 707-721.
- [69] HERRMANN, M., Tonindustrie Zeitung,
1943 (11/12)
- [70] HAMID, A.A., et al "Shear Strength of Concrete Masonry Joints",
J Str Div, A.S.C.E., V 105, ST7, July, 1979, pp 1227-1240.
- [71] BS 1610: 1964, "Methods for the Load Verification of Testing Machines".
- [72] KONG, F.K. and EVANS, R.H., "Reinforced and Prestressed Concrete",
London, Nelson, 1975.

- [73] CP 110: Part 1: 1972, "The Structural Use of Concrete".
- [74] YUAN, R.L., et al "Experiments on Closing Reinforced Concrete Corners",
Proc of the A.S.C.E., V 108, No ST4, April, 1982, pp 771-779.
- [75] HAMID, A.A. and DRYSDALE, R.G., "Concrete Masonry Under Combined Shear and Compression Along the Mortar Joints",
Jnl A.C.I., Sept/Oct, 1980, No 5, V 77, pp 314-320.
- [76] HETENYI, M., "Beams on Elastic Foundations",
University of Michigan Press, Ann Arbor, 1946, 2-4.
- [77] TIMOSHENKO, S., "Strength of Materials, Part II",
Van Nostrand, Princeton, 1956, 3rd Ed, 1-2.